CONDENSING ANNULAR FLOW INSIDE TUBES

by

Emilio Guevara M.

A Thesis

submitted for the Degree of
Doctor of Philosophy to
The City University
Department of Mechanical Engineering

August, 1980.

CONTENTS

Page

LIST OF TABLES

LIST OF FIGURES

Figure 70 : Difference between calculated and tabulated values for v_f.

Figure 71 : Difference between calculated and tabulated values for v_g.

ACKNOWLEDGEMENTS

I wish to express my sincerest gratitude to my supervisor, Dr.D.H.T. Gotham, of The City University, for his unfailing encouragement, help and guidance throughout the period which this research has taken.

I gratefully acknowledge the [redacted] for their grant which enabled me to carry out this investigation.

I would like to express my gratitude to all the members of the staff and workshops of The City University for the help that they have given me. In particular, I would like to express my special thanks to [redacted] without whom the experimental part of this investigation would not have been possible.

My thanks also go to [redacted] for the excellent, and speedy, job she has made of typing this thesis.

Finally, I express my deepest thanks to all my family for the help and support that they have given me over the years and to [redacted], who has helped and supported me in so many ways throughout this work.

ABSTRACT

The problem of condensing annular flow inside a horizontal tube was studied experimentally and theoretically.

In the experimental investigation measurements of the local heat transfer coefficient and pressure drop were made for condensing steam inside a 38.1 mm I.D. and 3.0 m long horizontal tube.

The range of conditions covered during the experimental study was:

1. Condensing pressure, 0.4 - 0.6 Bar (abs)
2. Inlet superheat, 0 - 1.0°C
3. Coolant flow rate, 5342 - 9687 kg/hr
4. Inlet quality, 0.55 - 1.0
5. Exit quality, 0.30 - 0.68
6. Vapour mass velocity, 134200 - 620497 kg/hr-m^2
7. Inlet velocity, 97 - 186 m/s

A wall suction device was used to measure the liquid film flow rate at the end of the test section. The liquid entrainment at this point was evaluated from these measurements.

The experimental entrainment results were plotted on a basis of existing correlating parameters for adiabatic two-phase flow and the data points were reasonably well represented by a single curve.

The local heat transfer coefficient was found to increase and decrease along the condenser tube. A correlation equation is presented for the pressure drop based on the Martinelli pressure parameters.

The theoretical analysis was based on the assumption that during condensation, the flow pattern was annular. The flow was divided into a droplets-vapour core and an axisymmetric liquid film. The resulting set of six non-linear partial differential equations were solved numerically with the use of a digital computer. Good agreement was found between the theoretical and experimental values of pressure drop, vapour quality and liquid film flow rate.

NOMENCLATURE

Ac, dAc	Core and differential core flow area, m^2
A_E, A_E^*	area and non-dimensional area occupied by the entrained droplets, m^2
A_G, A_G^*	area and non-dimensional area occupied by the vapour, m^2
A_I, dA_I	interfacial and differential interfacial element area, m^2
A_T, dA_T	total and differential total flow area, m^2
A_Z, dA_Z	liquid and differential liquid element flow area in the axial (Z-) direction, m^2
A_W, dA_W	contact and differential contact element flow area, m^2
A_ϕ, dA_ϕ	liquid and differential liquid element flow area in the circumferential (ϕ-) direction, m^2
$C_{p_{CW}}$	specific heat of cooling water, KJ/kg ^oK
D_i	tube diameter, m.
g	gravitational acceleration, m/s^2
h	local heat transfer coefficient, $kW/m^2\ ^oK$
h_L	enthalpy of saturated liquid, KJ/kg
h_G	enthalpy of saturated vapour, KJ/kg
h_{fg}	latent heat of vapourization, KJ/kg
h_{GO}	inlet enthalpy of saturated vapour, KJ/kg
H_L	non-dimensional enthalpy of saturated liquid
H_G	non-dimensional enthalpy of saturated vapour
H_{FG}	non-dimensional latent heat of vapourization
$\dot{m}''_C$	condensation rate, kg/m^2-s
$\dot{m}''_I$	interchange rate, kg/m^2-s
p	static pressure, N/m^2
p_o	inlet static pressure, N/m^2
p^*	non-dimensional static pressure

Q	total radial heat rate, Watt
R	Tube radius, m
R_{e_ℓ}	Liquid Reynolds number
R_{eG}	Vapour Reynolds number
S_E	entrainment slip ratio
t	parametric variable in the entrainment correlation
V_Z^*	non-dimensional axial liquid film velocity
V_ϕ^*	non-dimensional circumferential liquid film velocity
V_{CZ}^*	non-dimensional axial velocity component of condensate particles at the interface
$V_{C\phi}^*$	non-dimensional circumferential velocity component of condensate particles at the interface
V_{IZ}^*	non-dimensional axial velocity component of the interchange flow at the interface
$V_{I\phi}^*$	non-dimensional circumferential velocity component of the interchange flow at the interface
V_G	vapour velocity, m/s
V_E	entrained droplet velocity, m/s
V_Z	axial liquid film velocity, m/s
V_ϕ	circumferential liquid film velocity, m/s
V_o	inlet vapour velocity, m/s
V_{CZ}	axial velocity component of condensate particles at the interface, m/s
$V_{C\phi}$	circumferential velocity component of condensate particles at the interface, m/s
V_{IZ}	axial velocity component of the interchange flow at the interface, m/s
$V_{I\phi}$	circumferential velocity component of the interchange flow at the interface, m/s
W_E	entrainment mass flow rate, kg/s
W_G	vapour mass flow rate, kg/s
W_L	liquid film mass flow rate, kg/s
W_T	total mass flow rate, kg/s

x	mass vapour quality
x_C	mass core quality
Z	axial distance along the condenser tube

GREEK LETTERS

α_c	core mean void fraction
β	liquid to vapour density ratio
$\bar{\beta}$	angle between the interface and the tube wall
γ	constant as defined by Eqn.(61)
$\bar{\gamma}$	angle as defined in Fig.57a
δ	liquid film thickness, m
δ^*	non-dimensional liquid film thickness
η	non-dimensional axial distance along the condenser
μ_ℓ	liquid viscosity, kg/m-s
μ_G	vapour viscosity, kg/m-s
ν_ℓ	liquid kinematic viscosity, m^2/s
ν_G	vapour kinematic viscosity, m^2/s
ρ_G	vapour density, kg/m^3
ρ_ℓ	liquid density, kg/m^3
ρ_o	inlet vapour density, kg/m^3
ρ^*	non-dimensional vapour density
ϕ	angular co-ordinate, radians
ψ	non-dimensional vapour velocity
τ_W	axial wall shear stress, N/m^2
$\tau_{W\phi}$	circumferential wall shear stress, N/m^2
τ_I	interfacial shear stress, N/m^2

CHAPTER 1

INTRODUCTION

Condensation is a process of phase transformation from the vapour to liquid phase. In many engineering systems, for example, power generation, condensation inside a tube is an integral component of the basic cycle. Also one method of desalination depends exclusively on the condensation process. A fundamental understanding of this process in all its various forms is therefore an essential prerequisite for the design of plant.

In condensation the local quality of the vapour-liquid mixture changes along the tube due to the progressive change from vapour to liquid. As a result of these changes in quality the vapour and liquid phases may assume different geometrical configurations at different locations along the same condenser tube. Such flow configurations are usually termed two-phase flow patterns or flow regimes. A change of flow pattern usually means a change in the mode of transport of momentum and heat.

It is certainly to be expected that the rates of heat, mass and momentum transfer obey different quantitative laws according to which flow regime prevails, whether the transfer in question is from one fluid phase to the other, or between a fluid phase and the walls of the duct through which it flows. Therefore, the performance of a condenser is strongly dependent on these two-phase flow patterns which exist along the tube and hence a knowledge of the flow pattern becomes important when producing a model on which a theoretical analysis can be based.

Although several comprehensive studies have been made of the flow patterns in adiabatic two-phase flow of air/water mixtures and in boiling little information is available for condensation. For practical purposes, it needs to be recognised, that there is no reliable method available for predicting the flow regime which is likely to exist in condensation under the conditions of engineering operation, still less is there quantitative information about the associated friction and heat transfer laws.

Among the several flow patterns that have been identified during two-phase flow with or without heat addition, annular flow has been found to be one of the utmost importance in practical applications. Common to almost all analyses of vapour condensation inside a tube is the explicit assumption of ideal annular flow. In ideal annular flow the condensate forms a film of liquid on the tube walls and the vapour flows in the interior core. However, in practice, it is known that this flow pattern does not truly exist very often because, among other effects, travelling waves will form at the liquid-vapour interface due to the shearing action of the high speed vapour core. Eventually, the liquid along the tube walls begins to break up into small droplets and enter the vapour core region of the pipe. The droplets formed in this manner are carried along in the vapour and subsequently redeposited on the wavy liquid film. The amount of entrainment in the vapour core being the balance between the droplets entrained from and deposited onto the liquid film. This process, called interchange, continues as long as the annular flow regime is present.

In systems of this kind, the prediction of pressure drop and heat transfer coefficients are of primary concern, and depend on both the wall and interfacial shear stress. These, on the other hand, are influenced by the losses involved with the formation of droplets from the waves and their subsequent deposition. Consequently, in order to describe this problem fully, it is necessary to have knowledge of the shape and unsteady behaviour of the waves at the vapour-liquid interface together with the accompanying mass, momentum, and energy transfer across the interface due to both droplet interchange and condensation.

A wide range of experimental and theoretical work has been carried out in the past years on the characteristics and transport phenomena of wavy films without heat addition. Statistical methods were employed to explore the structure of the gas-liquid interface of thin films. The interface was shown to be random and to possess a relatively infrequent large-wave structure and a secondary pattern of small ripples. But, in spite of the above, there seems to be no definite approach to the problem and more experimental work is needed to test the applicability of these results to the case of condensation.

The literature survey revealed that measurements of entrainment rates during condensation were not given the attention they deserve by researchers in the field. Most analytical studies on condensation, reported in literature, were based on the assumption that entrainment did not occur. Due to the lack of such information, correlations,which were developed from adiabatic two-phase flow studies, have been used during condensation. The applicability of these correlations has not yet been proven.

The first objective of this investigation was to study experimentally the use of porous-wall suction method to measure the liquid film flow-rate and, thus, the entrainment rate during condensation inside a horizontal tube. An experimental study of the pressure drop, local heat transfer coefficient and liquid film thickness was also to be undertaken. The second objective was to develop a theoretical analysis for the annular flow condensation inside a horizontal tube.

CHAPTER 2

LITERATURE SURVEY

2.1. Introduction

The subject of condensation heat transfer in process applications may be variously classified with respect to the mode (dropwise or filmwise), geometry (in-tube or on-tube), the substance condensed (pure component, multicomponent, or vapour with a noncondensible gas), and whether or not vapour shear on the liquid film affects the rate of heat transfer and the flow of the liquid.

This chapter is restricted to a discussion of previous studies of forced flow filmwise condensation of a pure vapour inside a straight tube. Two different types of mechanisms can be distinguished: laminar and turbulent.

Prior to any detailed work being carried out on the theoretical or experimental side a comprehensive literature survey on this subject was undertaken and a report subsequently produced (Guevara,1977). This survey indicated that there had been very few investigations of entrainment during condensation inside a tube.

Since, as mentioned previously, a literature survey on condensation inside tubes has been carried out only the major points in that survey will be restated here. Recourse should be made to this literature survey (Guevara, 1977) for details of references wherever appropriate.

2.2. Condensation Inside tubes

Condensation inside tubes is important because of its many industrial applications, for example, refrigeration plant, steam power plant, desalination plant and condenser design. This has called the attention of many investigators who have carried out a considerable amount of research with the aim of obtaining correlations for predicting the overall or mean heat transfer coefficient and pressure drop during condensation.

In the early stages, the general approach to the problem was to equate the shear stress in the condensate flow to the gravity force. The increasing rate of condensate was then related to the heat transfer rate. The latter, in addition,

was reduced to a heat transfer coefficient with the assumption of a linear temperature distribution in the condensate layer.

During condensation the rate of heat transfer is closely coupled to the hydrodynamic characteristics of the condenser. An improved knowledge of the local condensing heat transfer coefficient is therefore an essential prerequisite for predicting the performance of an inside-tube condenser and optimizing its design. Therefore, local temperature and static pressure measurements together with the development of more reliable correlations for predicting pressure drop and heat transfer coefficients are required.

2.2.1. Flow Patterns During Condensation Inside Tubes

The flow pattern is a very important subject of study and a great deal of work has been done to determine characteristics of various patterns and the boundary between the regimes. Flow-patterns maps, of the kind proposed by Baker (1954) for flow in horizontal pipes, by Hewitt and Roberts (1969) for flow in vertical pipes,and recently, by Weisman et al (1979) for flow in horizontal lines, represent attempts to systematise this knowledge, such as it is.

Although extensive research on flow patterns has been conducted, most of this research has been concentrated on two-phase gas-liquid flow adiabatic systems. Some investigations have been carried out for two-phase flow with boiling, but very little has been published on flow patterns of condensing fluids. Most analytical studies on condensation were based on the assumption that a certain flow pattern existed, without reference to the conditions under which such a pattern can exist. In a few other cases, the flow pattern was assumed on the basis of a criteria developed for adiabatic flow.

So far, to the author's knowledge, no successful flow pattern analysis on developing condensation two-phase flow has been available. Some experimental results, such as those by Soliman and Azer (1971), Traviss and Rohsenow (1973), Soliman (1973) and Keshock et al (1974) point out the following qualitative trends:

1. The pressure of the condensing fluid, tube diameter, rate of cooling water and inlet superheat were found to be important parameters that affect the development of the flow patterns inside the condenser tube.
2. According to Soliman and Azer (1971) and Soliman (1973) the Baker's map (1954) is not suitable for predicting flow patterns during condensation inside tubes while Traviss and Rohsenow (1973) concluded that the Baker's map can be used for predicting flow patterns during condensation inside tubes. This has been substantiated by Keshock et al (1974). Soliman (1973) proposed a new modified Baker's map.
3. Attempts have also been made to find a simple criteria for the transition from one flow regime to another. For example, the following criteria describes the transition from spray to annular flow (Soliman, 1973):

$$N_{WE}/N_{RE}^{0.275} < 163 \qquad \text{annular}$$

$$N_{WE}/N_{RE}^{0.275} > 163 \qquad \text{spray}$$

where N_{WE} and N_{RE} are the Weber and Reynolds number respectively. Traviss and Rohsenow (1973) postulated that the transition from annular to stratified flow occurs at a constant value of the liquid Fronde number. This constant value was determined to be $F_{RL} = 45$ from their flow regime data. Recently, Jaster and Kosky (1976) suggested that the development of the flow regimes along the condenser is dominated by the shear ratio "F" and from their experimental data the following criteria was obtained:

$F > 29$ annular

$29 > F > 5$ transition

$F < 5$ stratified

where

$$F \equiv \frac{\text{Axial Shear Force}}{\text{Gravitational body Force}} \equiv \frac{\tau_W}{\rho_\ell g \delta}$$

and τ_W: wall shear stress, δ : liquid film thickness, ρ_ℓ and g are the liquid density and gravitational acceleration respectively.

2.2.2. Heat Transfer Coefficients

From the references reviewed (Guevara, 1977) it was evident that the problem of condensation inside tubes is extremely complicated to solve theoretically and that the experimental results to date seem to be quite inconsistent and incomplete. This can be attributed to the theoretical and experimental difficulties in defining and controlling the numerous parameters involved. These facts have today precluded the use of all but very simple analytical model which in turn are valid under very restricted conditions of tube condensation. Thus, for predicting local heat transfer coefficients a very large number of techniques have been proposed and indeed, almost all the references reviewed contain a new correlation. These range from very arbitrary ones to highly sophisticated treatments of the mechanic of the flow. Boyko and Kruzhiling (1967), Soliman et al (1968), Kosky and Staub (1971) and Traviss et al (1973) are examples.

While many of these have been valuables as practical design tools and have added to our understanding of the phenomena involved, there does not appear to be any general predictive technique which has been verified over a wide range of parameters. Narayama and Sarma (1972) considered the flow phenomena to be a homogeneous mixture of liquid and vapour. The principle of analogy between the momentum and energy was made use of to predict the condensation heat transfer coefficient. They compared their correlation with data obtained by other investigators for different fluids (Freon-12, propane and steam) and oreientations (horizontal and vertical). The deviation was less than ±15%. Cavallini and Zecchin (1971) and Cavallini and Zecchin (1972) presented a correlation which was successful in drawing together within ±15% the experimental data concerning the condensation of various refrigerants (11, 12, 22, 113 and 114) obtained from different sources (Goodykoontz and Brown, 1967; Traviss et al, 1971; Altman et al, 1960). In a recent publication, Shah (1979) presented a simple correlation for predicting heat transfer coefficients during condensation inside pipes. It has been verified by comparison with a wide variety of experimental data. These include fluids water, R-11, R-12, R-22, R-113, methanol, ethanol, benzene, toluene, and trichloroethylene condensing in

horizontal, vertical and inclined pipes of diameters ranging from 7 to 40 mm. The mean deviation was found to be 15.4%.

In spite of the various attempts for obtaining general correlations for predicting heat transfer coefficients during condensation inside pipes, no analysis studied has taken into account the effects on heat transfer coefficients due to entrainment and turbulent transport mechanisms. Entrainment may become important at high qualities, i.e. 100 to 85%, while the latter at intermediate qualities or during condensation in the wavy/stratified flow regime for example.

Isachenko and Salonzoda (1972) measured the local heat transfer coefficient during the condensation of steam in a vertical pipe. They found that at high Reynolds number, the local heat transfer coefficient may increase and decrease along the condensing length. They called this behaviour "surges" of heat transfer and suggested that they correspond to "stripping" of the condensate. Hilding (1967) obtained similar behaviour for the local heat transfer coefficient.

Connell et al (1974) conducted an experimental study within the wavy/stratified flow regime using water and methanol as condensing fluids inside a 38.1 mm I.D., 2.44 m long copper tube. It was found that the heat transfer coefficient inside a horizontal tube condenser is strongly dependent upon the axial and circumferential location. Like Isachenko and Salonzoda (1972) and Hilding (1967), Connell et al found that the local heat transfer coefficient increased and decreased along the condenser tube. It was suggested that the decrease in resistance to heat transfer was due to an increasing contribution to the heat transfer by turbulent transport mechanisms. These may be associated with surface instabilities, as well as rapid eddy transport directly to the interface, but these mechanisms are not as well understood at this time.

Brunfield and Theofarious (1976) conducted an analytical study of the turbulent liquid film in which the results of wavy falling liquid film adiabatic flow of Telles and Dukler (1970), Chu and Dukler (1974) and Chu and Dulker (1975) were incorporated. The result was compared with data of Ueda et al (1974) obtained during condensation inside a vertical tube. The predicted

value agreed fairly well with the experimental data. However to substantiate analyses of this kind, extensive experimental studies have to be carried out towards the understanding of the very complicated wavy structure at the vapour-liquid interface. The associated transport and mass transfer phenomena need to be understood as well.

2.2.3. Pressure Drop

Knowing the pressure drop in a two-phase flow system is of primary interest to the designer in order to establish the pumping load and prescribe the longitudinal variation in pressure necessary to compute the fluid properties along a channel.

A number of methods have been proposed for predicting pressure drop in two-phase flow. The method which has been most commonly used is that of Lockhart and Martinelli. It has been successfully used for all flow patterns, although the assumptions made associate it closer with the separate flow model. The method consists of an empirically determined relationship between the square root of the ratio of the two-phase pressure drop to that if only vapour alone were flowing in the duct, ϕ_G, and the ratio of the pressure gradient of the liquid to that of the vapour phases flowing alone in single-phase flow, X. Different relationships exist between ϕ_G and X depending on whether the liquid and vapour flows are laminar or turbulent.

A great number of investigators compared their experimental determined values of pressure drop with those predicted by the Lockhart and Martinelli correlation. Many of them found fair to good agreement for a great variety of fluids and conditions. Others found poor agreement with additional effects of flow rate, quality, tube diameter, flow patterns and liquid-film characteristics being found. Modifications have been proposed to account for these effects and to apply to a specific problem. During condensation, the Martinelli parameters have been

correlated by the following expression:

$$\phi_G = 1 + a\, X_{tt}^{b}$$

where ϕ_G is the modified parameter based on an experimentally measured pressure drop during annular flow condensation, X_{tt} is the Martinelli parameter when the flow of both the liquid and vapour phases are turbulent, a and b are constant and have to be determined for the range of parameters being tested.

A number of other methods attempt to approach the problem of pressure drop during condensation from a more fundamental theoretical viewpoint. However, since the liquid-vapour interface is complicated by the presence of waves, these approaches fall short of providing an improved method for predicting pressure drop. These studies do, however, add to the knowledge concerning interfaces and may lead to a better technique for predicting pressure drop.

CHAPTER 3

EXPERIMENTAL RIG, INSTRUMENTATION AND EXPERIMENTAL TECHNIQUES

3.1. Introduction

As discussed earlier there is a need for further research in the field of condensation inside tubes. Thus it was necessary to design the test apparatus so that it was capable of supporting a general research programme in condensation as well as satisfying the requirements for the present project.

The objectives of the experimental part of this investigation were to study the pressure drop, liquid film thickness and flow rate in condensing annular flow inside a horizontal tube. An experimental study was made of the local heat transfer coefficent. Droplet deposition and entrainment could also be measured.

The condensing fluid used was steam.

3.2. Description of the Experimental Rig

Fig.1 shows the experimental apparatus used in this work, which is also shown diagrammatically in Fig.2. It consists of three major sections: section A, a precondenser, where the quality at inlet to the test section was controlled by partial condensation, section B where the condensing experiments were carried out, and the third one C, where the deposition of liquid droplets could be studied.

For ease of description the experimental rig is described under five sub-headings.

(i) Steam supply system
(ii) Precondenser
(iii) Test condenser
(iv) Deposition section
(v) Water circulating system.

3.3. Steam Supply System

Steam from an existing Stone Platt Fired Boiler at 13.8 bar was reduced to the rig pressure. A safety valve limited this pressure to about 2.8 bar. After this throttling process which resulted in a few degrees of superheat a portion of the inlet steam was diverted and passed through a desuperheater E before entering the steam jacket of section C.

The steam used for the experimental work passed through a steam flow control valve, an orifice plate, a strainer and a desuperheater D in which the conditions at the entry of section A can be accurately determined. After the steam had passed through the rig and the liquid film, formed as a result of condensation in the test condenser, been drawn off through the porous sinter bush B2, the remaining uncondensed steam was passed through the main condenser and then to a measuring tank. A constant rate was held by observation of the pressure drop across the orifice plate.

The orifice plate facility was designed and manufactured to comply with B.S.S. 1042. It was fitted with D and D/2 taps and condensation chambers, one in each pressure pipe, were installed to ensure that the pressure pipes were filled with liquid. The pressure differential across the orifice plate was measured by using a 0.5 m long glass, mercury filled, manometer, fitted with a plexiglass safety screen in case of rupture. The calibration of the orifice plate was checked by collecting the condensate from the main condenser in measuring tanks.

The steam supply system was instrumented to measure the pressure downstream of the reducing valve, upstream of the orifice plate and at the inlet of the desuperheater D. Pressures were measured by calibrated Bourdon tubes gauges. Temperature upstream of the orifice plate and at the desuperheater D inlet were measured. Inlet and outlet cooling water temperatures and the condensate temperature at the exit of the main condenser were also measured. All the temperatures were measured by using calibrated copper-constantan thermocouples. The cooling water flow rate to the main condenser was measured by a rotameter type flow meter.

3.4. The Precondenser

The precondenser was used to provide established conditions at entry to section B. It consisted of a 5.0 m long horizontal stainless steel tube, 38.1 mm I.D., surrounded by a 76 mm O.D. 5 mm wall, ordinary steel tube, with the cooling water passing counter currently through the annular space. This was followed by a film removal unit (porous sinter bush B1). Care was taken to minimise discontinuities between the precondenser and the film removal unit and between the film removal unit and the test condenser. A bell-shaped entry was provided to ensure smooth entry of the vapour stream. Supporting spacers were included to prevent section A from sagging. Fig.3 shows the constructional details of the precondenser and the deposition section C, which were mounted individually on supports and checked by a spirit level to ensure that they were all mounted horizontally and were co-axially aligned before being coupled together. To accommodate any expansion, due to heating during operation, flanges a,b, c and d were allowed to slide along the respective outer tubes. A pulley arrangement was fitted to flange d so as to support a vertical weight to counterbalance the thrust induced by the steam flowing through the rig. It also helped the entire section back to its original position. Several O rings were used at different positions to stop any possible leaking.

Section A was instrumented to measure the inlet and outlet temperatures of the cooling water. The inlet and outlet temperatures of the vapour stream through the precondenser, were also measured. All temperatures were measured by calibrated copper-constantan thermocouples of 30 st gauge wire. Inlet and outlet pressures together with the pressure drop were also measured as illustrated in Fig.7. Typical calibration curves are shown in Appendix D.

3.5. Test Condenser

The test condenser was provided with instrumentation to measure the tube wall temperature at several stations in the axial direction, cooling water temperature at several stations in the axial direction, static pressures at different axial positions along the tube condenser and condensate mass flow rate withdrawn from porous sintered section. Facilities for measuring the liquid film thickness were also provided.

The tube condenser consisted of a thick walled stainless steel tube inside which the condensation occurs. This tube was jacketed with a single larger tube in which the cooling water flowed countercurrently. The condenser tube dimensions were 38.1 mm I.D., with 5.08 mm wall thickness and a length of 3.0 m. The cooling water jacket was made of stainless steel 304S schedule 40 62.71 mm I.D., with 5.16 mm wall thickness. Supporting spacers were included to prevent sagging on the condenser tube. Fig.4 and Fig.5 show construction details and a photographic view respectively of the test condenser.

3.5.1. Pressure and Temperature measurement

Fig.6 shows the location of the tappings for the static pressure measurement along the condenser. Eight pressure taps of 1.0 mm inside diameter were drilled perpendicularly to the tube wall at the bottom of the tube condenser. The end of a stainless steel tubing 316S 0.79 mm I.D. with 0.41 mm wall thickness was soldered into each pressure tap and the other end extending 60 mm before it was connected to the manometer tube by means of a 6.35 mm O.D. transparent tubing. Placing the taps at the bottom of the section allowed condensed liquid to completely fill the lines, however, an extra precaution was taken to prevent steam from entering the pipes connecting the pressure tappings to the manometers by placing small steam separation vessels in the connecting pipes. The lines for the eight pressure taps were connected by a valving arrangement so that pressure differentials could be measured between any two taps. The pressure differentials were measured with

carbontetrachloride-filled U-tube manometers. The static pressure at a position of 0.04 m from the beginning of the cooling section was measured with a mercury-filled U-tube manometer allowing the calculation of the static pressure at any pressure tap by subtracting the accumulative pressure drop from this value. The knowledge of the static pressure distribution allowed the determination of the saturation temperature, T_s, all along the condenser tube with the assumption of equilibrium between the vapour and liquid phases. Fig.7 shows a schematic diagram for pressure drop measurement.

Copper-constantan thermocouples were installed to measure the temperature in the test condenser. Thermocouple stations for measuring condenser tube wall temperature were spaced 0.340 m apart, and each station consisted of four thermocouples equally spaced around the circumference starting at the top. The bare physical junction of the thermocouple was placed 3 mm from the outer surface of the condenser tube. A total of 32 wall thermocouple probes were constructed and calibrated before installation. Thermocouple stations for measuring cooling water temperature were spaced 0.335 m apart. Each cooling water temperature measuring thermocouple station consisted of two thermocouple probes placed symmetrically opposite each other on a vertical plane. The thermocouples were mounted such that the hot junctions were placed within the middle annular space through which water flowed. The inlet and outlet cooling water temperatures were also measured. Fig.6 and Fig.8 show wall and cooling water thermocouple station spacings and a photographic view of the test condenser assembly details respectively.

Fig.10 and Fig.9 show a photographic view of the assembly and different thermocouple arrangements. As can be seen, a copper-constantan pair was insulated within a 2.11 mm O.D. stainless steel sheath and a copper disc, with a hole through the centre, was soldered to the end of the thermocouple sheath

to hold in place the thermocouple junction. In addition, brass discs were soldered around the sheath to compress a rubber washer. This, in addition to preventing leaking, helped to obtain good contact between the thermocouple and the wall surface.

All thermocouple outputs in the test condenser and those in the system were measured by a Dynamic code 6600 Data logger with an accuracy of ±0.025% of reading. Fig.11 shows a photographic view of the thermocouple wire connection arrangement.

3.5.2. Condensate Mass Flow Rate

One of the commonest methods for measuring the amount of condensed vapour during studies of condensation inside tubes has been the use of a vapour-liquid separator. The liquid from the separator was collected and measured and the uncondensed vapour was then passed through and condensed in a main condenser where it was measured. The sum of these two values represented the total mass flow rate.

It is very well known that when high velocity steam is condensing inside a tube, only a fraction of the condensate flows as a liquid film on the wall of the tube, the remaining liquid forms entrained droplets in the gas core. In this case, if one is interested in measuring the fraction of liquid entrained, the above mentioned method alone will not be suitable since the vapour-liquid separator does not discriminate between the two fractions, it just measures the sum of them.

Entrainment can be measured directly by using sampling or isokinetic probes and integrating the data, from these, over the gas core. Liquid film flow-rate and, thus, entrainment rate, can be measured directly by extracting the liquid film and determining the extracted flow. Hewitt and Lovegrove (1976) surveyed the methods for measuring film flow-rate. They concluded that measurements of liquid film flow by the porous wall suction method are far more likely to give the true film flow.

In this experimental study the liquid film flow-rate was measured by extracting the liquid film formed as a result of condensation through a porous sinter. The sinter whose internal diameter was the same as that of the test section, was located at the exit of the test section. Care was taken to ensure that the bore was continuous and that there were no ridges at the various joints as illustrated in Fig.4. Suction was then applied to the outside of the sinter to remove the liquid flowing along the tube wall. The extracted liquid, together with small amount of steam from the main core, passed through a heat exchanger HE2. The condensate from the HE2 was then passed through a measuring vessel MV2 before returning to the main condenser. The heat exchanger which was designed and constructed for this experimental study, consisted of a 17.46 mm O.D. stainless steel coiled pipe in an annular bath of cooling water. Fig.2 and Fig.12 show the connecting lines of this arrangement and a close up of the device respectively.

Calibrated copper-constantan thermocouples were used to measure the temperature of the extracted mixture, outlet temperature of the condensate from the heat exchanger and inlet and outlet temperatures of the cooling water. The mass flow rate of condensate from the heat exchanger was measured by measuring the time taken to collect a known volume of liquid.

3.6. Deposition Section

The deposition section consisted of a horizontal stainless steel tube, 38.1 mm I.D. and 4.0 m long, surrounded by a somewhat larger 76 mm O.D., 5 mm wall ordinary steel tube, with steam passing through the annular space. This was followed by a film removal unit. No condensation will take place in this section and the liquid film formed as a result of droplet deposition will be drawn off through a sintered bush B3 and measured as described in section (3.5.2.). Care was taken to ensure that there were no ridges at the various joints as

shown in Fig.13. Supporting spacers were included to prevent section C fromsagging.

Temperature and pressure measurements facilities to measure the temperature and pressure of the vapour-droplets mixture were provided and the arrangements were as described in section (3.4). The pressure of the vapour in the jacket was also measured by a calibrated pressure gauge. Good control of the vapour conditions in the jacket could be achieved by using the desuperheater E and the appropriate control valve as illustrated in Fig.2.

3.7. The Water Circulating System

3.7.1. Cooling Water

The cooling water circuit was designed to permit the control of the water flow rate to the test condenser and precondenser. The control of the water flow rate was achieved by adjusting the opening of the valves in the circuit, in this way, the water flow through the test condenser could be varied while the water flow through the precondenser was kept constant and vice versa.

In addition to the cooling water requirements for the test condenser and precondenser, the circuit also provided facilities for each of the water cooled heat exchangers, HE1, HE2 and HE3 connected to the extraction lines of the liquid film removal units B1, B2 and B3. Water flow rates to the test condenser, precondenser and heat exchangers were measured by rotameter type flow meters. All rotameters were calibrated by a weighting tank and stop watch before installation. A typical calibration curve is shown in Appendix D. All the connections from the cooling water circuit to the rig were made from flexible tubing so that it could be adjusted for expansion, and also insulated the test section from external vibration.

3.7.2. Desuperheating Water

Water from the Boiler feed water was used for desuperheating purpose as shown in Fig.2. It was constructed to provide the right combination flow pressure for an efficient performance of the industrial nozzle fitted at the end of the injection line. This could be achieved by adjusting the opening of the appropriate control valves and pressure regulator. The inlet temperature was measured by a calibrated copper-constantan thermocouple. The amount of desuperheating water was measured by a calibrated rotameter.

3.8. Test Procedure

Before any test was carried out the rig was pressure tested and leak checked. Once all the appropriate measures to stop the leaks were followed, the rig was opened to the steam supply and final checks for leaks were made.

The test started by putting the main condenser into operation and allowing the cooling water to circulate through it. The boiler was then started and allowed to build up pressure for a period of 20 to 30 mins. At the same time the cooling water main to the rig was opened and the cooling water allowed to circulate through the test condenser, precondenser and heat exchanger HE2. Once the boiler pressure was reached, the pressure reducing valve was adjusted to keep this pressure at a value of 2.8 bar and the steam allowed to flow through the rig. The system was allowed to run while necessary adjustments were being made to get the required operating conditions, such as steam flow rate, condensing pressure, and cooling water flow-rate. Once the operating conditions had been obtained, the film removal unit B2 was put into operation by applying suction to the porous sinter. The control valve controlling the rate of extraction was then opened. When suction was applied the inlet pressure to the test condenser dropped due to the reduction in the resistance of the system. The operation was then completed by readjusting the inlet pressure to its original value. The pressure lines were finally purged.

After this initial starting up operation the rig was run until steady state conditions were obtained. They were established when the readings of all pressure, temperature and flow rate measuring instruments remained steady for at least half an hour. Steady state conditions could be reached in any run within two hours, however, the system was run for a period of 2½ hours before any readings were made.

During each run the following measurements were taken after reaching the steady state:

1. Steam mass flow rate to the rig.
2. Manometer readings at the precondenser inlet, inlet and exit of the test condenser, and the pressure differentials between each pressure tap along the test condenser.
3. Temperatures in the test condenser and those in the system in millivolts.
4. Water flow rates to the test condenser, precondenser and heat exchanger.
5. The amount of condensate leaving the heat exchanger HE2.

In addition to the above readings the ambient temperature and the barometric pressure were recorded during each run. Also, for each run the inlet and exit cooling water temperature, condensate temperature and water flow rate at the main condenser were recorded.

CHAPTER 4

DISCUSSION OF THE EXPERIMENTAL RESULTS

4.1. Introduction

In high velocity vapour condensing annular flow, part of the condensate phase is often entrained as small droplets in the vapour core. Determination of the split of the liquid flow between the film and the vapour core is of vital importance in understanding and calculating systems of this type.

In this chapter the entrainment experimental results obtained during condensation inside a horizontal tube are discussed together with local heat transfer coefficients results.

The total axial pressure distribution results, although not the main objective of the investigation, are presented and discussed as they are of considerable interest since existing correlations and theories still do not give predictions to within the desired engineering tolerances.

4.2. Experimental Results

Forty sets of experimental data were taken during the present investigation. The range of conditions covered can be summarized as follows:

1. Condensing pressure, 0.4. - 1.6 bar (abs)
2. Inlet superheat, $0^{o}C$ - $1^{o}C$
3. Coolant flow rate, 5342 - 9687 kg/hr
4. Inlet quality, 0.55 - 1.0
5. Exit quality, 0.30 - 0.68
6. Steam mass velocity, 134200 - 620497 $kg/hr\text{-}m^2$
7. Inlet velocity, 97 - 186 m/s.

All thermodynamic and transport properties for the vapour were based on the vapour static pressure and were calculated from empirical equations which were obtained especially for the present investigation (Appendix C). Satisfactory accuracy of representation of these properties (within ±0.02 per cent of the tabulated values) was achieved.

The raw experimental data for all the runs, such as temperatures in millivolts obtained from the data logger, manometer and pressure gauge readings, and scale flow rate readings were fed into a digital computer program. The computer programe reduced the data into a useful form, and computed the operating conditions and thermophysical properties of vapour as output. Appendix B gives details of the calculation procedure.

Table 1 includes a summary of the reduced experimental steady-state data taken for the forty runs. The coolant temperature at a given station was taken from the average of two thermocouples readings at that particular station. The wall temperature at a given station was taken as the average of the four wall thermocouple readings at different circumferential locations at that particular station.

The static pressure variation along the test condenser was obtained from the static pressure at the inlet of the test condenser, which was measured with a mercury-filled U-tube manometer, and the pressure drop between any two stations, which was measured with carbontetrachloride-filled U-tube manometer. The saturation temperature variation was obtained from the temperature corresponding to the measured static pressure.

The local vapour mass flow rate, liquid mass flow rate and quality were obtained from a stepwise heat-balance. The details of all heat transfer calculations are given in Appendix B. Table 2 summarizes the computed data for the forty runs.

The pressure and temperature of the vapour were measured at three locations upstream of the test condenser. The first location was at the inlet of the desuperheater E, the second and third locations at which the vapour's pressure and temperature were measured, were at the inlet and exit of the precondenser. The latter was located at a position 0.14 m upstream of the test condenser entry. The amount of superheat at these locations was estimated by comparing the

measured temperature with the saturation temperature corresponding to the measured pressure.

During the preliminary testing of the test facility, contrary to expectation, it was found that the vapour entering the precondenser had lost most of its superheat which had resulted from the throttling process. In addition, the boiler superheating unit was not operational during the time this investigation was carried out. On account of this the desuperheater E was never used as such and control over the amount of inlet superheat was not required during the course of the present experimental study. Consequently, the vapour's inlet quality was an unknown variable and had to be estimated by performing a heat-balance analysis on the rig starting from the exit of the main condenser and working backwards towards the inlet of the test condenser or precondenser as appropriate. To check the accuracy of the heat balance run 40 (Table 1) was specially designed for this purpose. During this particular run the cooling water rate of the main condenser which was 300 litres/minute for the majority of the experimental test, was reduced to 100 litres/minute. This was done to provide a larger temperature difference on the cooling water side of the main condenser so that an accurate measurement of this temperature difference could be made. In addition, the mass flow rate of vapour was kept low (inlet pressure of 0.6 bar abs.) with the result that the vapour was slightly superheated at the inlet to the precondenser. Furthermore, those experimental runs (run 33, 34 and 39: Table 1) which showed a slight superheat ($1^{o}C$) were used for comparison as well. Agreement with the heat balance was obtained within 5%. Other experimental tests, for example, run 14, 15 and 16, which also showed a slight amount of superheat at the inlet of the test condenser, were also used for comparison, but they gave a somewhat larger error. This was attributed to the fact that the temperature rise on the cooling water side of the main condenser was small, i.e. $3^{o}C$. This resulted in the

rate of heat gained by the cooling water in the main condenser being underestimated, and as a consequence the overall rate of heat transferred to the cooling water in the rig and the inlet enthalpy to the test condenser being underestimated.

It is to be recalled that during high velocity condensation inside a horizontal tube,the flow pattern was expected to be annular flow over the whole length of the condenser tube. In order to check this, two methods for predicting the type of flow regime, were used to indicate the probable flow regime present in the test condenser for each of the forty runs. The first was the Baker's map (Baker, 1954) and the second, the modified Baker's map (Soliman, 1973). The results are shown in Fig.14 and Fig.15. From these results, one can see that according to the Baker's map the flow pattern was annular over the whole length of the condenser tube for all the forty runs. It was also found that different runs occupied similar pattern areas in Fig.14 and Fig.15. It was then decided not to include all the data to avoid overcrowding the figures.

On the other hand, according to the modified Baker's map the spray flow regime was predicted for all the forty runs of this investigation. It is worth pointing out that the modified Baker's map was the first attempt to establish a flow pattern map based on experimental condensation data. As such, its application was limited to the conditions covered by the experimental tests (Soliman, 1973). Any attempt then to use this map to predict a flow pattern for a different range of conditions may produce results which are misleading. By definition (Soliman, 1973), spray flow is that in which all liquid condensate is carried in the direction of the flow by the vapour as a mist. The possibility of the existence of this type of flow pattern was ruled out by reference to the results on liquid film flow rate measurements. These results showed (Fig.16) that a portion of the condensate was flowing as a liquid film while the remainder as entrained droplets in the vapour core. This supported the flow pattern predictions on the Baker's map. However, Baker's map was based on adiabatic flow of two-phase systems and the actual

results could deviate very significantly from it. The literature survey (Guevara, 1977) showed that the experimental evidences on flow patterns during condensation were contradictory. On one side, Soliman (1973) concluded the Baker's map can not be used for predicting flow pattern during condensation inside tubes while on the other side, Traviss and Rohsenow (1973) concluded that the Baker's map can be used for predicting flow pattern during condensation inside tubes. Since the Baker's map has been accepted universally as a useful guide to indicate the type of flow during condensation inside tubes and based on the results on the liquid film flow rate measurement, it was concluded that the flow pattern present in the test condenser during the present experimental tests was annular.

4.2.1. Liquid Film Flow Measurements

As mentioned previously, the flow rate in the condensate film at the end of the test condenser was determined by sucking it off at that point, but the measured value had to be corrected to allow for any vapour withdrawn simultaneously. This was done by carrying out a heat balance on the heat exchanger HE2 (See Fig.2) using the following equation:

$$W_{EXT}(h_{\ell_1} - h_{\ell_2}) + W_{GEXT}\,\lambda = W_{CWHE}(h_{\ell_4} - h_{\ell_3})$$

where W_{EXT} is the extracted mixture mass flow rate, kg/s

W_{GEXT} is the amount of vapour extracted, kg/s

W_{CWHE} is the cooling water mass flow rate, kg/s

h_{ℓ_1}, h_{ℓ_2} are the liquid enthalpies at the exit and inlet of the heat exchanger respectively, kJ/kg

h_{ℓ_3}, h_{ℓ_4} are the enthalpies of the cooling water at the inlet and outlet respectively, kJ/kg

λ is the latent heat, kJ/kg.

The method basically consisted of removing variable amounts of vapour by changing the pressure differential across the sinter. By the use of the above equation, the liquid flow rate through the sinter was calculated. Vapour flow rates through the sinter were then plotted against the liquid flow rates. The curve so obtained was termed the take-off characteristic of the sinter. Provided this take-off characteristic has a straight line portion, it may be extrapolated back to zero vapour take-off rate. The liquid flow thus obtained at zero vapour take-off was assumed to be the undisturbed film flow.

Unfortunately, it was found during the preliminary testing of the device, that this simple procedure could not be used to determine the take-off characteristic. This was due to the fact that when suction was applied to the sinter, the conditions along the rig changed. The main effect was to reduce the pressures along the rig and consequently the temperatures. Since the boiler driving force (i.e. the pressure drop between the pressure downstream of the pressure reducing valve and the vacuum in the main condenser) remained constant, physically what happened was that by opening the extraction line, which was connected to the main condenser via the vacuum line (Fig.2), the resistance of the system was reduced. This resulted in a slight increase in the vapour mass flow rate followed by a decrease in the pressure along the rig. The decrease in pressure was found to vary between 0.15 to 0.25 bar (g). Therefore there was an uncertainty on whether all the points on the take-off characteristic corresponded to the same flow conditions. It was then decided, for the sake of comparability between the various tests, to run the rig with the extraction operational for the duration of any particular test. The procedure, as mentioned in section (3.8) of Chapter 3, was basically as follows: once the operating conditions in the rig were obtained, the film removal unit B2 was put into operation by applying suction on the porous sinter. The control valve controlling the rate of extraction was fully opened. As the test condenser inlet pressure dropped, as discussed previously,

it was then restored to its original value by further opening the flow control valve, i.e. the vapour mass flow rate in the test condenser was increased slightly.

A further uncertainty arose when using the film removal device as to whether the liquid film had been completely withdrawn. One way of ensuring this was to obtain the take-off characteristic of the sinter. Provided this take-off characteristic had a horizontal line portion, i.e. the liquid film flow is independent of the amount of vapour extracted, the liquid film flow may be considered to be completely removed. This criteria could not be used during this investigation for the reasons already discussed. This problem was pursued by an undergraduate student using an air-water test facility. The problem was approached by firstly investigating the effect of the porous sinter length on the film flow rate accompanied by visual observations. No quantitative information was obtained by the time the present investigation was concluded, but from the visual observations it was found that there was always a very thin liquid film overshooting the sinter. However, the suction applied in that case was considerably smaller than the one used for the current condensing tests.

The measured film flow rate was obtained as follows: as it was mentioned earlier the extraction device was kept operational for the duration of any experimental test. The amount of liquid together with any vapour extracted through the porous sinter bush was continuously passed through the heat exchanger HE2 (Fig.2) where any trace of uncondensed vapour was condensed. A two-way valve connected to the measuring vessel MV1, allowed measurements to be made without disturbing the flow conditions in the test condenser. This was possible because the pressure differential across the sinter remained constant while the collection and timing of a known volume of condensate, was in progress. Once the rate of condensate had been measured it was then corrected for the amount of vapour present by using the expression referred to earlier in this section. The value so obtained

was the fraction of liquid condensate flowing as a liquid film. This procedure was repeated for most of the tests. The values of the amount of condensate based on a step-wise heat balance on the test condenser were then plotted versus the experimentally measured liquid film flow rates. In this graph points on the equal line which is represented by the continuous line, would represent conditions of no entrainment since it means that the extracted flow rates equalled those based on a heat balance analysis. On the other hand, if a fraction of the total liquid flow was in the form of droplets entrained in the vapour-core the experimentally measured liquid film flow rates were expected to be less than the corresponding calculated values based on a heat balance. The amount of entrainment for any experimental test was obtained by subtracting the experimentally measured liquid film flow rate from that calculated from a heat balance.

Unfortunately, there were no other experimental values on entrainment during condensation inside tubes available in the literature which could be used for comparison with the results of the present experimental study. To the author's knowledge this represents the first attempt to use the porous-wall suction method to determine the liquid film flow rate and, thus, the entrainment for condensation inside tubes.

It can be seen from Fig.16 that most of the data points were positioned close to a smooth curve drawn through them although the scatter of the experimental data is occasionally rather large. It may be supposed that this comes mainly from the complexity of the experiments in which a partially blocked porous sinter may have been responsible for these inconsistencies. The time factor precluded the repetition of the experiments for these particular points.

Thus, in spite of the scatter observed, it can be seen that there is a general tendency for the amount of entrainment to be higher for tests with larger rates of condensation. For these tests the liquid film became thicker together with an increase of the roughness at the interface. This reduced the vapour-core flow cross-sectional area, giving as a

consequence a higher vapour velocity, followed by an increase in the shear action at the interface due to the higher relative velocity between the vapour and liquid in the film. The high relative velocity at the interface created more favourable conditions for entrainment giving, as a result, the increase in entrainment observed. As condensation progressed along the condenser tube, the mass flow rate of the vapour was reduced due to condensation and the vapour velocity then decreased towards the end of the condenser tube whereas the pressure, and therefore the vapour density, decreased at a rate slower than the vapour flow rate while the vapour cross-sectional area still remains relatively constant. However, the vapour velocity remained high enough to maintain the generation of droplets by entrainment from the surface of the liquid film. This was true when only a fraction of the vapour was condensed in the test condenser as was the case in the present condensation experimental tests.

Ishii and Grolmes (1975) developed an inception criteria for droplet entrainment based on the shearing off of roll-wave crest. This criteria was incorporated in the data reduction analysis and could be checked at any location in the tube condenser. Calculation for a few experimental tests showed that the conditions for entrainment were present over the whole length of the test condenser.

It is of significant interest to consider some of the means which are currently available, and are at present being developed, for the calculation of entrained fraction. The majority of the available entrainment correlations are based on two-phase, annular mist flow data of two components flowing adiabatically in a tube, usually air and water. The need for taking additional experimental data has been pointed out by the different authors to further check and improve the correlations. Correlations of the type put forward by Hughmark (1973), Hutchinson and Whalley (1973) and Paleev and Filippovich (1966) were chosen for the purpose of comparison. Instead of trying to predict the entrainment experimental data by using those correlations it was decided to use the proposed

correlating parameters to see if they could be used for correlating entrainment data obtained during condensation inside a tube. This was done chiefly because these correlations were based on two component, two-phase annular mist flow data,for air-water systems. Moreover, the data were mainly taken after equilibrium conditions had been assumed to occur (i.e. at a distance away from the inlet where the rate of entrainment equals the redeposition rate). However, the correlation proposed by Hutchinson and Whalley (1973) had been used with reasonably good results to calculate critical heat flux in forced convection boiling, Whalley et al (1974).

Hughmark (1973) plotted the volumetric ratio ($=W_E\rho_G/W_G\rho_\ell$) against the dimensionless film thickness corresponding to the vapour phase y_G^+ which is defined as

$$y_G^+ = yV_G^*/\nu_G$$

where

V_G^* is the shear velocity $\left[(\tau_W+\tau_I)/2\rho_G\right]^{0.5}$, m/s

y is the film thickness, m

ν_G is the vapour kinematic viscosity, m^2/s

The wall and interfacial shear stresses together with the liquid film thickness required in the above correlation were those calculated from the experimental data by the method shown in Appendix B. The properties were calculated at the measured pressure 0.04 m upstream of the porous sinter bush.

The results of the comparison is shown in Fig.17. The first point to note is that entrainment appears to begin at a minimum y_G^+ of about 15, and this is immediately inconsistent with the correlation of Hughmark which suggested a value of 35 for the onset of entrainment. Hewitt and Taylor (1970) pointed out that, even at very high gas velocities, the fraction of liquid entrained can be zero if the liquid flow rate is below the limit of the onset of entrainment. On the other hand, calculations based on an inception criteria (Ishii and Grolmes, 1975) showed that conditions for entrainment were

presented over the whole length of the test condenser. This inconsistency may be due to the fact that for two-phase air-water (for example) the liquid film thickness presumably resulted from the combined effects of droplet deposition and entrainment, i.e. there was not contribution from condensation. Thus, if considerable entrainment was occurring in the case of air-water system the liquid film thickness may decrease along a tube, while with condensation it may increase. Unfortunately, no simultaneous measurements of entrainments and liquid film thickness were made during condensation to substantiate this statement. Ueda et al (1972) measured the liquid film thickness at three locations for steam condensing in down-flow inside a vertical tube. It was found that the thickness of the film increased along the tube condenser. Since the maximum value of the liquid film thickness measured was approximately 0.3 mm, the separation of liquid droplets from the condensate film - droplet entrainment - was considered insignificant. However, entrainment from the liquid film reduces the amount of liquid and thus the film thickness. This could have been the case in their experiments although the film thickness may still have continued to increase at a lower rate along the tube condenser due to condensation. It is significant to point out that the liquid film thickness predicted by the theoretical analysis, which accounts for entrainment, showed a similar trend to the experiments of Ueda et al.

From the above discussion it can be concluded that in order to have a better assessment of this problem, simultaneous measurements of entrainment and liquid film thickness should be made.

Also, it can be observed from Fig.17, that there is some agreement between the results of the present study and Hughmark's correlation for values of $y_G^+ > 46$. This merely implies consistency, since this range is similar with the range of y_G^+ covered by the correlation. In general the trend of the experimental results is somewhat consistent with the correlation. The experimental data could be represented by a second order relation as follows:

$$(W_E/W_G)(\rho_G/\rho_\ell) = 1.0878 \times 10^{-8}(y_G^+)^{3.1421-0.326 \log_{10}(y_G^+)}$$

In Fig.18, the Paleev and Filippovich correlation is illustrated with the inclusion of the experimental data obtained in this study, and is represented analytically by the following equation.

$$\frac{G_f}{G_\ell} = 0.985 - 0.44 \log_{10}\left[\frac{\bar{\rho}}{\rho_\ell}\left(\frac{\mu_\ell V_G}{\sigma}\right)^2 \times 10^4\right]$$

where $$\bar{\rho} = \rho_G\left[1 + G_\ell\ (1 - G_f/G_\ell)/A_T\rho_G V_G\right]$$

and

G_f is the mass liquid flow in a film, kg/s
G_ℓ is the total mass liquid flow, kg/s
μ_ℓ is the viscosity of the liquid, kg/m-s
σ is the surface tension of the liquid, N/m
V_G is the mean gas velocity, m/s
A_T is the cross-sectional area of the duct
ρ_ℓ, ρ_G are the liquid and gas densities

The experimental data lie very considerably below the Paleev and Filippovich correlating line. This was expected since the Paleev and Filippovich's data were taken after equilibrium conditions had been assumed to occur, (i.e. the entrainment rate equals the redeposition rate). In the case of a condensing flow where the conditions are continually changing, the attainment of equilibrium conditions is highly unlikely, thus the entrained liquid flow rate with condensation might very well be less than would be attained at the equilibrium state, though the deviations in condensation systems are not likely to be as significant as they are in evaporating systems. On the other hand, condensation may tend to prevent entrainment due to the transverse liquid flow at the vapour-liquid interface. Furthermore, there may be a diameter effect which is not taken account of by the correlation. In general, plotting the experimental data on the basis of the parameters suggested by Paleev and Filippovich showed these parameters could be useful when correlating entrainment rate during condensation.

Hutchinson and Whalley (1973) related the concentration of droplets in the vapour core at hydrodynamic equilibrium C_E to the group $(\tau_I \delta/\sigma)$ where τ_I is the interfacial shear stress, δ the film thickness and σ the surface tension. Since as discussed previously, equilibrium was not likely to occur during condensation C_E could not be used. Instead the concentration of droplets in the vapour core defined as

$$C = W_L / (W_L / \rho_\ell + W_G / \rho_G)$$

was used. The results are illustrated in Fig.19. As can be seen there is some scatter around the line drawn through the data, however they show a similar trend to the correlation given by Hutchinson and Whalley but based on C_E. It appears that a correlation based on $(\tau_I \delta/\sigma)$ and C could give a better representation of the data when comparison is made with the results of the other two correlations tried in this study. The results of Fig.19 could be represented as follows

$$C = 3.47 \times 10^{-4} (\tau_I \delta/\sigma)^{-6.99-3.85 \log_{10}(\tau_I \delta/\sigma)}$$

Although the results shown in Figs.17 to 19 are encouraging and might form the first step to study experimentally entrainment during condensation inside tubes, there is much work to be done and more experimental data is needed before a final correlation can be developed.

4.2.2. Local Heat Transfer Coefficient

Typical variation of the local heat transfer coefficient, local heat flux and cooling water temperature along the condenser is shown in Fig.20 through 24. The local heat flux was obtained from the knowledge of the cooling water mass flow rate, the specific heat of coolant and the cooling water temperature gradient. The cooling water temperature gradient was determined graphically from the plot of the cooling water temperature as a function of length. The local heat transfer coefficient was obtained by dividing the local heat flux by the temperature difference between the local saturation temperature and the inner

wall temperatures. The inner wall temperature was computed from the wall temperature measurements which were corrected for conduction between the wall thermocouple junction location and the inner wall.

The literature survey (Guevara, 1977) found that in some previous works the local heat transfer coefficient decreased along the condenser as condensation progressed. Contrary to this Fig.20 through 24, shows that the local heat transfer coefficient decreased and increased along the condenser tube. As can be seen these variations in the local heat transfer coefficient correspond to changes in the slope of the cooling water temperature curve.

However, previous experimental studies (Hilding, 1967; Isachenko and Salonzoda, 1972) of high velocity vapour condensation inside a tube have shown a similar pattern for the variation of the local heat transfer coefficient along the condenser tube. It had been suggested that these changes corresponded to variations in the value of the interfacial shear stress between the vapour and the condensate film. At a very high interfacial shear stress, a considerable amount of entrainment may occur. As a result, the liquid film thickness decreases. Eventually the condensate may be stripped from the surface of the film at some locations inside the tube condenser. This results in a very high value for the heat flux and a decrease in the temperature difference between saturation and inner wall temperature at those locations and as a consequence, the observed high value in the local heat transfer coefficient.

Following the above statement one should expect that the peaks on the axial distribution for the local heat transfer coefficient should correspond directly with the peaks observed on the axial distribution for the interfacial shear stress. In order to verify this, comparisons were made for five experimental tests. Referring to Fig.23 and Fig.46 corresponding to run 1 it can be seen that at a location of approximately $Z/L = 0.6$ the peaks for both the interfacial shear stress and the local heat transfer coefficient correspond; however this was not the case at a Z/L of about 0.2. For test 4, Fig.22 and Fig.45, the lowest value for the interfacial shear stress

occurred at the lowest value of the local heat transfer coefficient at about Z/L = 0.2. Similar observations apply to Fig.24 and Fig.47. A better correspondence was observed by comparing Fig.21 and Fig.44 for the experimental test 12, at approximately the same places Z/L = 0.2 and Z/L = 0.6. The comparison shows that the increases in the interfacial shear stress do not always correspond directly to the increases in heat transfer coefficient. This may be due to the fact that entrainment was occurring with the rate of droplets generation being higher at some locations than at others. It is suggested then that there is a region of change in the behaviour of the heat transfer which is consistent with a system in which both the interfacial shear and entrainment are significant. Enhancement in the heat transfer are also known to be due to turbulent mechanisms in the liquid film. However, quantification of these effects was not possible from the present experimental data. A more complete discussion of this topic would require a more comprehensive experimental study on waves and the way in which they are affected by entrainment and condensation.

An attempt was made to compare the experimental heat transfer coefficient with the predictions of existing correlations. For this purpose, Shah's correlation (Shah, 1979) was used. It was chosen because it is based on a wide range of experimental conditions and its simplicity. The results of this comparison are shown in Figs. 25 and 26 for different tests. These showed that the correlation does not predict the observed variations in the local heat transfer coefficient. In general the correlation overpredicts the experimental data.

These variations on the heat transfer coefficient could be predicted if the effect due to turbulent transport mechanisms, wave instability and entrainment were incorporated. The literature survey showed that of the available correlations recommended for predicting local heat transfer coefficient during condensation inside tubes, none incorporated these features. The work of Brumfield and Theofarious (1976) in adiabatic turbulent falling liquid films could be taken as a first step to approach the problem. However, considerable

experimental information on wave parameters during condensation is needed but this is not yet available.

During the course of the present experimental investigation it was observed that some air was being extracted through the porous sinter bush together with the small amount of vapour and the liquid drawn off. It is very well known that the presence of a noncondensible gas during condensation has a detrimental effect on the heat transfer. It was then necessary to estimate the amount of air present. First of all, since suction was applied continuously to the sinter, checks for leaks were made. It was found that this was not the case and that the air was present in the boiler feed water and then released when vapour was generated. In order to estimate the amount of air present, the air extracted through the porous sinter bush was collected in the measuring vessel MV1 (Fig.2) over a period of time (i.e. the duration of a test). It was found that the amount so collected was too small to be measured. It was thought that with the high vapour velocities in the condenser there was no possibility of a substantial build-up of air at the vapour liquid interface as could arise in some other condensing situations.

4.2.3. Axial Pressure results

Figs.29 and 30 show the effect of the inlet static pressure on the axial static pressure distribution for typical runs and two different cooling water flow rates. These runs were chosen so that they have nearly the same inlet quality and cooling water temperature. It is important to point out that these two variables could not be controlled precisely during the present experimental investigation. However, it was thought that the variations in the inlet quality and cooling water temperature were not large enough to mask the effect induced by the variations of the inlet pressure. Bearing this in mind it can be concluded from Figs.27-28 that increasing the inlet static pressure to the test condenser while keeping the cooling water flow rate constant produced an increase in the overall pressure drop along the test condenser. As the inlet static pressure was increased the total

steam mass flow rate increased and the temperature difference between the steam and the cooling water increased since the condensing temperature became higher. This led to an increase in the temperature rise on the cooling water side together with a higher heat rate gained by the cooling water which resulted in an increase in the amount of condensate in the film. As the amount of condensate increases, the liquid film becomes more wavy and thus increasing the friction loss of both phases, and thus the overall pressure drop along the test condenser.

The negative slope of the static pressure axial distribution indicated that the local frictional pressure gradient ($=2\tau_w/R$) was larger than the local momentum pressure gradient over a large portion of the condenser tube. The local frictional pressure gradient was calculated by subtracting the momentum term from the total pressure gradient. Estimation of the momentum term in two-phase flows are somewhat arbitrary in that the velocity and the phase distribution are not usually known in sufficient detail to compute with certainty the momentum change in the flow. Appendix B shows details of this calculation and the results shown in Figs.32-42. It can be seen from these figures that the major contribution to the total pressure gradient was due to friction as expected for higher to intermediate qualities. Similar conclusions can be drawn from Figs.43-47 for the interfacial frictional pressure gradient for the vapour core. For the experimental tests of this study the frictional pressure gradient due to friction on the wall of the tube was almost equal to the frictional pressure gradient due to friction on the vapour-liquid interface. That is to say, that the wall shear stress was almost equal to the interfacial shear stress which means that the momentum changes in the liquid film were negligibly small. However, it is to be remembered that the wall and interfacial shear stress were inferred from the experimental total pressure gradient by subtracting the momentum term from it as outlined in Appendix B.

Figs.29-31 show the effect of the inlet quality on the axial static pressure distribution. It can be seen that for the same inlet pressure and cooling water rates, the overall pressure drop along the test condenser increases as the inlet quality decreases. The quality at the inlet of the test condenser was varied by independently controlling the cooling water flow rate through the precondenser. Reducing the inlet quality while keeping the inlet pressure and cooling water flow rate in the test condenser constants, resulted in an increase in the vapour mass flow rate.

For the test with lower inlet quality the liquid film became thicker, and the interfacial roughness presented by the film to the vapour core increased and this augmented the friction loss affecting in this way the pressure drop. This fact also explains the effect of the inlet quality on the wall shear stress distribution (Figs.48-50). However, contrary to expectations, the wall shear stress did not remain higher over the whole length of the condenser tube for the smaller inlet quality, instead, as can be seen from Figs.48-50, the wall shear stress remained higher over a certain length from the test condenser's entry. This might be due to the presence of entrainment in the vapour core affecting the momentum term. In addition, entrainment reduces the amount of liquid flowing in the annular film and this may affect the wall shear stress. A better understanding of this behaviour could be obtained by measuring the annular liquid film thickness along the condenser tube, but, although facilities for doing this were provided at the end of the test condenser, such measurements were not performed during the course of this experimental study. Similar reasoning may be followed to explain the variations observed in the wall and interfacial friction factors as shown in Figs.51-52. The wall and interfacial friction factors were calculated from the experimental total pressure distribution by the method shown in Appendix B.

The usual way of correlating frictional pressure drop results during condensation inside a tube has been in terms of the modified Lockhart-Martinelli pressure parameters, ϕ_G and X_{tt} as follows:

$$\phi_G = 1 + a\, X_{tt}^{b}$$

The modified parameter ϕ_G was based on an experimentally measured total pressure distribution during annular condensation of steam inside a horizontal tube. The parameters ϕ_G and X_{tt} were computed as shown in Appendix B.

An attempt was made to correlate the calculated values of ϕ_G and X_{tt} based on the above relation. It was found that they could not be correlated in that simple form. This was mainly due to the variations observed in the wall shear stress.

The results of Chain and Ibele (1964) showed that the ϕ_G versus X_{tt} plots were a function of both the gas and liquid Reynolds numbers. Chain and Ibele proposed a modification to the Martinelli correlation to take into account the effective liquid Reynolds number and gas Reynolds number for annular and annular mist flow regimes.

An attempt was then made to account for the variations in both the vapour and liquid Reynolds numbers. It was found in this study that a better correlation of the data could be obtained when the effects of the vapour and liquid Reynolds numbers were incorporated. Results of Fig.53 reveals the possibility of such correlation. It was found that for high velocity vapour condensing inside a horizontal tube

$$\left(\frac{1 + \phi_G}{\phi_G}\right) \frac{R_{e_\ell}}{R_{e_G}} = 3.11 \times 10^{-4} + 1.89576\, X_{tt}$$

This result shows that the ratio (R_{e_ℓ}/R_{e_G}) could be an important parameter to consider when correlating wall and

interfacial shear stresses during high velocity condensation inside a tube at high vapour mass flow rate. The literature review on condensation inside tubes showed that no data have been obtained at vapour mass flow rates as high as those reached during the present experimental study.

CHAPTER 5

ANALYSIS

5.1. Introduction

Condensation flow modelling is extremely difficult due to the complex thermo-hydrodynamic coupling between phases, i.e. the exchange of mass, momentum and energy between phases.

This coupling is significantly more pronounced in the internal than in the external flow and this is very much so when the gravitational effect becomes important, i.e. horizontal flow. Furthermore, the presence of a moving internal interface makes predictions of flow behaviour even much more difficult than in single phase flow. This is because the shape and movement of the interface is not known a priori, but form part of the problem being solved. In addition, they affect the structure of the flow field profoundly and may dominate transport processes between phases.

The objectives of this analysis are:

1) To develop a mathematical model for annular flow pattern during condensation inside horizontal tubes.
2) To solve numerically the governing equations, to predict the changes in pressure, vapour quality, velocities and geometry of the liquid film in the direction of the flow.

5.2. Physical Model for Condensation Annular Flow Inside Tubes

For the current experimental investigation it was expected that the flow pattern, during high velocity condensation inside a horizontal tube, would be predominantly annular over the whole portion of the condenser tube. During annular flow some of the liquid is entrained as droplets in the vapour core while the remaining liquid is distributed as a thin film around the tube wall. The vapour phase usually flows at a much higher velocity than the liquid droplets and the film velocity, and, as a result, exerts a drag force on the droplets and liquid film interface. The momentum transfer from the vapour to the droplets through the drag force is accompanied by a corresponding decrease in momentum in the vapour, which, in turn, produces changes

in the droplets' trajectories. On the other side, the momentum transfer from the vapour to the liquid film, due to the shearing action, is accompanied by an additional momentum flux due to interfacial mass transfer. A part of the total interfacial momentum flux is consumed at the interface to generate surface waves, while another part is used to overcome axial wall friction, and also to accelerate the liquid film. These coupling phenomena, schematically illustrated in Fig.[54], comprise a very complex interaction which affects both the vapour and liquid phases.

The literature survey on condensation inside tubes, showed that information on drag coefficient was not presently available. Moeck and Stachiewicz (1972) found that this information for accelerating particles was inconsistent although good approximation of the data could be obtained. This fact explains why several authors have assumed that either the vapour core was free of entrainment or that the vapour and droplets velocities were equal. The former has enjoyed wider usage when modelling annular flow condensation inside tubes.

Jacowitz and Brodkey (1964) studied the stability of the liquid film during adiabatic annular two-phase flow inside horizontal tubes. They considered four models and concluded that a steady-state dynamic model with minor circumferential motion was the only possible one. The existence of a small circumferential downward velocity inside the liquid film was proved experimentally by Anderson and Russell (1970), Butterworth (1972) and Butterworth and Pulling (1974). Visual observations of the annular flow pattern during condensation inside tubes (Soliman, 1973) revealed that the liquid annulus was eccentric with the centre-line of the tube, and the liquid film appeared always thicker at the bottom than at the top of the tube. These facts were taken into consideration in constructing the present model.

Thus, the model (Fig.55) on which the analysis is based, is assumed annular, where a portion of the liquid flows in a low velocity annular film in contact with the tube wall, while the remainder of the liquid flows as entrained droplets in a relatively high velocity vapour core. A fluid element within the film has two velocity components; a small, but not negligible, circumferential velocity component caused by the gravitational force, and a high axial velocity component caused by the vapour on the film at the interface.

5.3. Mathematical Model

The analysis involves the following assumptions:

1. Portion of the liquid flows in an asymetric annulus and the entrained droplets and vapour flow in the core with a smooth interface.
2. A wedge shaped differential flow element is divided in two regions - a two-dimensional liquid film of thickness δ and a one-dimensional entrained droplet vapour core. Any differential liquid film element has two velocity components, V_Z in the axial (Z-) direction and V_ϕ in the circumferential (ϕ-) direction. Both V_Z and V_ϕ as well as δ, vary with the axial and circumferential location in the tube. The value of the circumferential velocity vanishes at both the top and the bottom of the tube. Any differential entrained droplet-vapour core element has one velocity component in the axial (Z-) direction for both the vapour, V_G, and the entrained droplets, V_E.
3. The core is a homogeneous mixture of liquid droplets at the saturation temperature together with saturated vapour.
4. The ratio of the local entrained liquid velocity to the local vapour velocity (S_E) is assumed constant throughout the core. As a matter of fact, this is not the situation and S_E varies in both the radial and axial direction, but at the present time, this variation is not known. Through the lack of knowledge on this matter a value of S_E equal to one is assumed.

5. The flow is steady.
6. The liquid and vapour transport and thermal properties are constant across the film and the core respectively.
7. The liquid subcooling in the film is negligible.
8. The momentum fluxes can be evaluated using flow average velocities.
9. The mass transfer of liquid crossing the interface is assumed to be made up of two processes: the transfer of liquid from the vapour to the liquid due to condensation, and the interchange which includes the effects of entrainment and deposition.
10. The heat flux is constant around the duct periphery.
11. The effect of the presence of a non-condensible gas is neglected.

5.3.1. Geometry Considerations (Appendix A)

The elemental liquid film flow area in the axial (Z-) direction, dA_Z is

$$dA_Z = \frac{1}{2} (2R - \delta) \tag{1}$$

and, in the circumferential (ϕ-) direction, dA_ϕ

$$dA_\phi = \delta dZ \tag{2}$$

The elemental flow area at the interface, dA_I, is

$$dA_I = (R - \delta)\, dZ d\phi \tag{3}$$

The elemental contact area between the liquid and the wall is:

$$dA_W = RdZd\phi \tag{4}$$

The elemental flow area for the core is

$$dA_c = \frac{1}{2} (R - \delta)^2\, d\phi \tag{5}$$

and for the elemental total flow area

$$dA_T = \frac{1}{2} R^2\, d\phi \tag{6}$$

5.3.2. Development of Equations

i. Continuity Equation

The continuity equation applied to the control volume occupied by the liquid film differential element shown in

Fig.56 states that the sum of the mass flow rates entering the control volume must be equal to the sum of the flow rates leaving the control volume, therefore we can write:

$$\rho_\ell dA_Z V_Z - \frac{\partial}{\partial Z}(\rho_\ell dA_Z V_Z)\frac{dZ}{2} + \rho_\ell dA_\phi V_\phi - \frac{\partial}{\partial \phi}(\rho_\ell dA_\phi V_\phi)\frac{d\phi}{2} + \dot{m}_c'' dA_I = \rho_\ell dA_Z V_Z + \frac{\partial}{\partial Z}(\rho_\ell dA_Z V_Z)\frac{dZ}{2} + \rho_\ell dA_\phi V_\phi + \frac{\partial}{\partial \phi}(\rho_\ell dA_\phi V_\phi)\frac{d\phi}{2} + \dot{m}_I'' dA_I \quad (7)$$

Making use of the relations given by Eqns.(1),(2) and (3), Eqn.(7) reduces to:

$$-\frac{\partial}{\partial Z}(\frac{1}{2}\delta(2R-\delta)\rho_\ell V_Z) - \frac{\partial}{\partial \phi}(\delta\rho_\ell V_\phi) + \dot{m}_c''(R-\delta) = \dot{m}_I''(R-\delta) \quad (8)$$

It is easily shown that $\dot{m}_c''$ and $\dot{m}_I''$ are related to the vapour and entrained droplets mass flow rates respectively, by the following expressions:

$$\frac{dW_G}{dZ} = -2\pi(R-\delta)\dot{m}_c'' \quad (9)$$

and

$$\frac{dW_E}{dZ} = 2\pi(R-\delta)\dot{m}_I'' \quad (10)$$

substituting back Eqns.(9) and (10) into Eqn.(8) we obtain:

$$\frac{\partial}{\partial Z}(\frac{1}{2}\delta(2R-\delta)\rho_\ell V_Z) + \frac{\partial}{\partial \phi}(\delta\rho_\ell V_\phi) + \frac{1}{2\pi}\frac{dW_G}{dZ} + \frac{1}{2\pi}\frac{dW_E}{dZ} = 0 \quad (11)$$

In order to non-dimensionalize Eqn.(11) and the succeeding governing equations, the following dimensional parameters are defined:

$$\psi = V_G/V_o \qquad V_E^* = V_E/(V_o\psi)$$

$$V_Z^* = V_Z/(V_o\psi) \qquad V_{C\phi}^* = V_{C\phi}/(V_o\psi)$$

$$V_\phi^* = V_\phi/(V_o\psi) \qquad V_{I\phi}^* = V_{I\phi}/(V_o\psi)$$

$$V^*_{CZ} = V_{CZ}/(V_o\psi) \qquad \delta^* = \delta/2R$$

$$V^*_{IZ} = V_{IZ}/(V_o\psi) \qquad \eta = Z/2R$$

$$\rho^* = \rho_G/\rho_o \qquad x = W_G/W_T$$

$$\beta = \rho_\ell/\rho_G \qquad x_C = W_G/(W_G+W_E)$$

$$p^* = p/p_o$$

also from the definition of x and x_C it may be shown that

$$\frac{W_L}{W_T} = (1 - \frac{x}{x_C}) \quad \text{and} \quad \frac{W_E}{W_T} = x(\frac{1 - x_C}{x_C})$$

Upon substituting the appropriated non-dimensional parameters into Eqn.(11) it also may be written as:

$$\frac{\partial}{\partial\eta}(\frac{1}{2}\,\delta^*(1 - \delta^*)V^*_Z\psi) + \frac{\partial}{\partial\phi}(\delta^* V^*_\phi\psi) + \frac{W^*_T}{\beta\rho^*}\left[\frac{1}{x_C}(1 - \frac{x}{x_C}\frac{\partial x_C}{\partial x})\right]\frac{dx}{d\eta} = 0 \qquad (12)$$

Eqn.(12) can be expanded to yield:

$$\frac{1}{2}\,\delta^*(1 - \delta^*)\psi\,\frac{\partial V_Z}{\partial\eta} + \frac{1}{2}\,(1 - 2\delta^*)\psi V^*_Z\frac{\partial\delta^*}{\partial\eta} + \frac{1}{2}\delta^*(1 - \delta^*)V^*_Z\frac{\partial\psi}{\partial\eta}$$

$$+ \frac{W_T^*}{\beta\rho^*}\left[\frac{1}{x_C}(1 - \frac{x}{x_C}\frac{\partial x_C}{\partial x})\right]\frac{dx}{d\eta} = \Gamma^*_{1\phi} \qquad (13)$$

where

$$\Gamma^*_{1\phi} = \psi(\delta^*\frac{\partial V^*_\phi}{\partial\phi} + V^*_\phi\frac{\partial\delta^*}{\partial\phi})$$

and

$$W^*_T = W_T/(8A_T V_o\rho_o)$$

ii. Conservation of Momentum Equation

The main forces to be considered in obtaining the pertinents momentum equations are shown in Fig.57a and Fig.57b. Any other force such as surface tension, hydrostatic lift force and drag force on droplets are neglected.

ii.-1 Momentum Equation for the liquid film differential element in the axial (Z-) direction

Applying the principle of conservation of momentum to the control volume occupied by the liquid, Fig.56, and with reference to Fig.57b, in the axial (Z-) direction, one can write

$$\Sigma dF_Z = (\Sigma M_{out})_Z - (\Sigma M_{in})_Z \qquad (14)$$

where $(\Sigma M_{out})_Z$ and $(\Sigma M_{in})_Z$ are the summations of the rates of momentum transfer out and in of the differential liquid film element, respectively in the axial (Z-) direction. ΣdF_Z is the summation of forces acting on the differential liquid film element in the axial (Z-) direction.

The various terms in the momentum balance, equation (14), will be evaluated as follows:

$$\Sigma dF_Z = dF_{sp} + dF_{Ip} + dF_{IT}\cos\bar{\beta} - dF_{WZ} \qquad (15)$$

where dF_{sp} = static pressure force

$$= (p - \frac{dp}{dZ}\frac{dZ}{2})(dA_Z - \frac{\partial dA_Z}{dZ}\frac{dZ}{2}) - (p + \frac{dp}{dZ}\frac{dZ}{2})(dA_Z + \frac{\partial dA_Z}{\partial Z}\frac{dZ}{2})$$

dF_{Ip} = interfacial pressure force

$$= p\frac{\partial dA_Z}{\partial Z}dZ$$

dF_{IT} = interfacial shear force

$$= \tau_I dA_I$$

dF_{WZ} = wall shear force

$$= \tau_W dA_W$$

Substituting back and making use of Eqns.(1),(3) and (4), Eqn.(15) reduces to

$$\Sigma dF_Z = \frac{-1}{2}\,\delta(2R - \delta)\,\frac{dp}{dZ}\,d\phi dZ + (R - \delta)\tau_I d\phi dZ - R\tau_W d\phi dZ \tag{16}$$

Making reference to Fig.56 one can write

$$(\Sigma M_{out})_Z = \rho_\ell V_Z^2 dA_Z + \frac{\partial}{\partial Z}(\rho_\ell V_Z^2 dA_Z)\,\frac{dZ}{2} + \rho_\ell V_Z V_\phi dA_\phi$$

$$+ \frac{\partial}{\partial \phi}(\rho_\ell V_Z V_\phi dA_\phi)\,\frac{d\phi}{2} + V_{EZ}\dot{m}''_I dA_I \tag{17}$$

and

$$(\Sigma M_{in}) = \rho_\ell V_Z^2 dA_Z - \frac{\partial}{\partial Z}(\rho_\ell V_Z^2 dA_Z)\,\frac{dZ}{2} + \rho_\ell V_Z V_\phi dA_\phi$$

$$- \frac{\partial}{\partial \phi}(\rho_\ell V_Z V_\phi d_\phi)\,\frac{d\phi}{2} + V_{CZ}\dot{m}''_C dA_I \tag{18}$$

Substituting Eqn.(17) and Eqn.(18) together with Eqn.(16) into Eqn.(14) and after making use of the expression given by Eqns.(1), (2), (3), (9), and (10) we get

$$\frac{\partial}{\partial Z}\left(\frac{1}{2}\,\delta(2R - \delta)V_Z^2\right) + \frac{\partial}{\partial \phi}(V_Z V_\phi \delta) + \frac{V_{EZ}}{2\pi\rho_\ell}\frac{dW_E}{dZ}$$

$$+ \frac{V_{CZ}}{2\pi\rho_\ell}\frac{dW_G}{dZ} = \frac{-1}{2\rho_\ell}\,\delta(2R - \delta)\,\frac{dp}{dZ} - \frac{R}{\rho_\ell}\,\tau_W + \frac{(R-\delta)}{\rho_\ell}\,\tau_I \tag{19}$$

which can also be written in a non-dimensional form as follows:

$$\frac{\partial}{\partial \eta}\left[\frac{1}{2}\,\delta^*(1-\delta^*)(V_Z^*\psi)^2 + \frac{\partial}{\partial \phi}(\psi^2 V_\phi^* V_Z^* \delta^*) + \frac{\psi W_T^*}{\beta\rho^*}\cdot\right.$$

$$\left.\left\{V_{CZ}^* + V_{EZ}^*\left[\frac{1}{x_C}\left(1 - \frac{x}{x_C}\,\frac{\partial x_C}{\partial x}\right) - 1\right]\right\}\frac{dx}{d\eta}\right] =$$

$$- \frac{\tau_W^*}{2\beta\rho^*} + \frac{1}{2}\,(1 - 2\delta^*)\,\frac{\tau_I}{\beta\rho^*}^* - \frac{1}{2}\,\delta^*(1 - \delta^*)\,\frac{P_o^*}{\beta\rho^*}\,\frac{dp^*}{d\eta} \tag{20}$$

Eqn.(20) may be expanded to yield

$$\delta^*(1-\delta^*)V_Z^*\psi^2\frac{\partial V_Z^*}{\partial\eta}+\frac{1}{2}(1-2\delta^*)(V_Z^*\psi)^2\frac{\partial\delta^*}{\partial\eta}+\delta^*(1-\delta^*)\psi V_Z^{*2}\frac{d\psi}{d\eta}$$

$$+\frac{\psi W_T^*}{\beta\rho^*}\left\{V_{CZ}^*+V_{EZ}^*\left[\frac{1}{x_C}(1-\frac{x}{x_C}\frac{\partial x_C}{\partial x})-1\right]\right\}\frac{dx}{d\eta}$$

$$+\frac{1}{2}\delta^*(1-\delta^*)\frac{P_o^*}{\beta\rho^*}\frac{dp^*}{d\eta}=-\frac{\tau_W^*}{2\beta\rho^*}\left[1-(1-2\delta^*)\right]\frac{\tau_I^*}{\tau_W^*}+\Gamma_{2\phi}^* \qquad (21)$$

where

$$\Gamma_{2\phi}^*=\psi^2\frac{\partial}{\partial\phi}(V_Z^*V_\phi^*\delta^*)$$

and

$$\tau_I^*=\tau_I/(U_o{}^2\rho_o)$$

$$\tau_W^*=\tau_W/(U_o{}^2\rho_o)$$

$$P_o^*=p_o/(U_o{}^2\rho_o)$$

ii.-2 Momentum Equation for the liquid film differential element in the circumferential (ϕ-) direction

Applying the principle of conservation of momentum to the control volume occupied by the liquid, Fig.56, and with reference to Fig.57a, in the circumferential (ϕ-) direction, one can write

$$\Sigma dF_\phi=(\Sigma M_{out})_\phi-(\Sigma M_{in})_\phi \qquad (22)$$

where $(\Sigma M_{out})_\phi$ and $(\Sigma M_{in})_\phi$ are the summation of the rates of momentum transfer out and in of the differential liquid film element, respectively in the circumferential (ϕ-) direction. ΣF_ϕ is the summation of the forces acting on the differential liquid film element, in the circumferential (ϕ-) direction.

The various terms in the momentum balance, Eqn.(22) will be evaluated as follows:

$$\Sigma dF_\phi=dF_{g\phi}-dF_{I\phi}-dF_{W\phi} \qquad (23)$$

where

$dF_{g\phi}$ = gravity force component in the circumferential (ϕ-) direction

$= dF_g \sin\phi = g\rho_\ell dA_Z dZ \sin\phi$

$dF_{I\phi}$ = Interfacial shearing force component in the circumferential (ϕ-) direction

$= dF_I \sin\bar{\beta}\sin\bar{\gamma} = \tau_I dA_I \sin\bar{\beta}\sin\bar{\gamma}$

$dF_{W\phi}$ = circumferential wall shearing force

$= \tau_{W\phi} dA_W$

Substituting back, Eqn.(23) becomes

$$\Sigma dF_\phi = g\rho_\ell dA_Z dZ\sin\phi - \tau_I dA_I \sin\bar{\beta}\sin\bar{\gamma} - \tau_{W\phi} dA_W \qquad (24)$$

With reference to Fig.56 , one can write

$$(\Sigma M_{out})_\phi = \rho_\ell V_\phi^2 dA_\phi + \frac{\partial}{\partial\phi}(\rho_\ell V_\phi^2 dA_\phi)\frac{d\phi}{2} + \rho_\ell V_\phi V_Z dA_Z + \frac{\partial}{\partial Z}(\rho_\ell V_\phi V_Z dA_Z)\frac{dZ}{2} + V_{I\phi}\dot{m}''_I\, dA_I \qquad (25)$$

$$(\Sigma M_{in})_\phi = \rho_\ell V_\phi^2 dA_\phi - \frac{\partial}{\partial\phi}(\rho_\ell V_\phi^2 dA_\phi)\frac{d\phi}{2} + \rho_\ell V_\phi V_Z dA_Z - \frac{\partial}{\partial Z}(\rho_\ell V_\phi V_Z dA_Z)\frac{dZ}{2} + V_{C\phi}\dot{m}''_C\, dA_I \qquad (26)$$

Substituting Eqns.(25),(26) and (24) together with the expression given by Eqns.(1),(2),(3),(4),(9) and (10), and after dividing throughout by $\rho_\ell dZ d\phi$, we finally obtain

$$\frac{\partial}{\partial Z}\left(\frac{1}{2}\delta(2R-\delta)V_Z V_\phi\right) + \frac{\partial}{\partial\phi}(V_\phi^2\delta) + \frac{V_{E\phi}}{2\pi\rho_\ell}\frac{dW_E}{dZ} + \frac{V_{C\phi}}{2\pi\rho_\ell}\frac{dW_G}{dZ} = \frac{1}{2}g\delta(2R-\delta)\sin\phi - \frac{(R-\delta)}{\rho_\ell}\tau_I\sin\bar{\beta}\sin\bar{\gamma} - \frac{R}{\rho_\ell}\tau_{W\phi} \qquad (27)$$

which can also be written in a non-dimensional form as follows

$$\frac{\partial}{\partial\eta}\left(\frac{1}{2}\delta^*(1-\delta^*)\psi^2 V_Z^* V_\phi^*\right) + \frac{\partial}{\partial\phi}\left(\delta^*(\psi V_\phi^*)^2\right) + \frac{\psi W_T^*}{\beta\rho^*}\cdot$$

$$\left\{ V_{C\phi}^* + V_{I\phi}^* \left[\frac{1}{x_C}\left(1 - \frac{x}{x_C}\frac{\partial x_C}{\partial x}\right) - 1\right]\right\}\frac{dx}{d\eta}$$

$$= \frac{1}{2F_r}\delta^*(1-\delta^*)\sin\phi - \frac{(1-2\delta^*)\tau_I^*}{2\beta\rho^*}\sin\bar{\beta}\sin\bar{\gamma} - \frac{\tau_{W\phi}^*}{2\beta\rho^*} \qquad (28)$$

Eqn. (28) may be expanded to yield

$$\frac{1}{2}\delta^*(1-\delta^*)\psi^2 V_\phi^*\frac{\partial V_Z^*}{\partial\eta} + \frac{1}{2}\delta^*(1-\delta^*)\psi^2 V_Z^*\frac{\partial V^*}{\partial\eta}$$

$$+ \frac{1}{2}(1-2\delta^*)\psi^2 V_\phi^* V_Z^*\frac{\partial\delta^*}{\partial\eta} + \delta^*(1-\delta^*)\psi V_\phi^* V_Z^*\frac{d\psi}{d\eta}$$

$$+ \frac{\psi W_T^*}{\beta\rho^*}\left\{V_{C\phi}^* + V_{I\phi}^*\left[\frac{1}{x_C}\left(1 - \frac{x}{x_C}\frac{\partial x_C}{\partial x}\right) - 1\right]\right\}\frac{dx}{d\eta}$$

$$= \frac{1}{2F_r}\delta^*(1-\delta^*)\sin\phi - \frac{1}{2}(1-2\delta^*)\frac{\tau_I^*}{\beta\rho^*}\sin\bar{\beta}\sin\bar{\gamma}$$

$$- \frac{\tau_{W\phi}^*}{2\beta\rho^*} + \Gamma_{3\phi}^* \qquad (29)$$

where

$$\Gamma_{3\phi}^* = -\psi^2\frac{\partial}{\partial\phi}\left(\delta^* V_\phi^{*2}\right)$$

and

$$F_r = 2gR/V_o^2$$

ii.3 Momentum Equation for the vapour core differential element in the axial (Z-) direction

Before deriving this equation it will be useful to define the core mean void fraction as

$$\alpha_C = A_G/(A_G + A_E) \qquad (30)$$

which can easily be expressed as a function of the core dryness fraction, x_C, as follows:

$$\alpha_C = \beta S_E x_C/(1 + \beta S_E x_C - x_C) \tag{31}$$

The derivative of the core mean void fraction with respect to the axial location, in a non-dimensional form, is found to be:

$$\frac{d\alpha_C}{d\eta} = \frac{\beta S_E}{(1+\beta S_E x_C - x_C)^2}\left[\left(\frac{\partial x_C}{\partial x}\right)\frac{dX}{d\eta} - \frac{x_C(1-x_C)}{\rho^*}\left(\frac{d\rho^*}{dp^*}\right)\frac{dp^*}{d\eta}\right] \tag{32}$$

Now, by following the same steps in deriving the previous momentum equations, and by referring to Fig.58, we can write

$$\Sigma dF_Z = (\Sigma M_{out})_Z - (\Sigma M_{in})_Z \tag{33}$$

where

$$(\Sigma M_{out})_Z = dA_C\,\alpha_C\rho_G V_G^2 + \frac{\partial}{\partial Z}(dA_C\alpha_C\rho_G V_G^2)\frac{dZ}{2} + dA_C(1-\alpha_C)\rho_\ell V_E^2$$

$$+ \frac{\partial}{\partial Z}(dA_C(1-\alpha_C)\rho_\ell V_E^2)\frac{dZ}{2} + V_{CZ}\dot{m}_C''' dA_I \tag{34}$$

$$(\Sigma M_{in})_Z = dA_C\alpha_C\rho_G V_G^2 - \frac{\partial}{\partial Z}(dA_C\alpha_C\rho_G V_G^2)\frac{dZ}{2} + dA_C(1-\alpha_C)\rho_\ell V_E^2$$

$$- \frac{\partial}{\partial Z}(dA_C(1-\alpha_C)\rho_\ell V_E^2)\frac{dZ}{2} + V_{EZ}\dot{m}_I''' dA_I \tag{35}$$

$$\Sigma dF_Z = -dA_C\frac{dp}{dZ}dZ - \tau_I dA_I \tag{36}$$

Eqns.(34),(35) and (36) may be replaced into Eqn.(33), together with Eqns.(3),(5),(9), and (10), to yield

$$\frac{\partial}{\partial Z}\left(\frac{1}{2}(R-\delta)^2\alpha_C\rho_G V_G^2\right) + \frac{\partial}{\partial Z}\left(\frac{1}{2}(R-\delta)^2(1-\alpha_C)\rho_\ell V_E^2\right)$$

$$- \frac{V_{CZ}}{2\pi}\frac{dW_G}{dZ} - \frac{V_{EZ}}{2\pi}\frac{dW_E}{dZ} = \frac{-1}{2}(R-\delta)^2\frac{dp}{dZ} - (R-\delta)\tau_I \tag{37}$$

which can be written in a non-dimensional form as

$$\frac{\partial}{\partial\eta}\left(\frac{1}{2}(1-2\delta^*)^2\alpha_C\rho^*\psi^2\right)+\beta\rho^*\frac{\partial}{\partial\eta}\left(\frac{1}{2}(1-2\delta^*)^2(1-\alpha_C)(S_E\psi)^2\right)$$
$$-4\psi W_T^*\left\{V_{CZ}+V_{IZ}^*\left[\frac{1}{x_C}\left(1-\frac{x}{x_C}\frac{\partial x_C}{\partial x}\right)-1\right]\right\}\frac{dx}{d\eta}$$
$$+\frac{1}{2}(1-2\delta^*)^2 P_o^*\frac{dp^*}{d\eta}=-2(1-2\delta^*)\tau_I^* \qquad (38)$$

By performing derivatives and making use of the relations from equations (31) and (32) and after rearranging we finally get

$$-2(1-2\delta^*)\alpha_C\psi^2\left[1+\left(\frac{1-x_C}{x_C}\right)S_E\right]\frac{\partial\delta^*}{\partial\eta}+(1-2\delta^*)^2\alpha_C\psi$$
$$\left[1+\left(\frac{1-x_C}{d_C}\right)S_E\right]\cdot\frac{d\psi}{d\eta}+\frac{4\psi W_T^*}{\rho^*}\left\{(1-2\delta^*)^2\psi(1-\beta S_E^2)\right.$$
$$\left.\frac{(\alpha_C/x_C)^2}{\beta S_E}\left(\frac{\partial x_C}{\partial x}\right)\frac{\rho^*}{8W_T^*}-V_{CZ}^*-V_{IZ}^*\left[\frac{1}{x_C}\left(1-\frac{x}{x_C}\frac{\partial x_C}{\partial x}\right)-1\right]\right\}\cdot$$
$$\frac{dx}{d\eta}+\frac{1}{2\rho^*}(1-2\delta^*)^2\left[\psi^2\alpha_C\left(\frac{d\rho^*}{dp^*}\right)\cdot(\alpha_c+(1-\alpha_C)\beta S_E^2)\right.$$
$$\left.+P_o^*\right]\frac{dp^*}{d\eta}=-2(1-2\delta^*)\frac{\tau_I^*}{\rho^*} \qquad (39)$$

iii. Conservation of Energy Equation

iii.-1 For the liquid Film Differential Element

The conservation of energy applied to the control volume occupied by the liquid (Fig.56) gives:

$$\rho_\ell V_Z dA_Z\left(h_\ell+\frac{V_Z^2}{2}\right)+\frac{\partial}{\partial Z}\left[\rho_\ell V_Z dA_Z\left(h_\ell+\frac{V_Z^2}{2}\right)\right]\frac{dZ}{2}$$
$$-\rho_\ell V_Z dA_Z\left(h_\ell+\frac{V_Z^2}{2}\right)+\frac{\partial}{\partial Z}\left[\rho_\ell V_Z dA_Z\left(h_\ell+\frac{V_Z^2}{2}\right)\right]\frac{dZ}{2}-h_{fg}\dot{m}_C'''\,dA_I$$
$$-\dot{m}_C'''\,dA_I\left(h_\ell+\frac{V_i^2}{2}\right)=-\frac{dQ}{2\pi RdZ}\,dA_W \qquad (40)$$

Eqns.(1),(3),(4), and (9) may be replaced into Eqn.(40) to give

$$\frac{\partial}{\partial Z}\left[\frac{1}{2}\,\delta(2R-\delta)\,V_Z\left(h_\ell+\frac{V_Z^2}{2}\right)\right]+\frac{h_{fg}}{2\pi\rho_\ell}\frac{dW_G}{dZ}+\frac{1}{2\pi\rho_\ell}\left(h_\ell+\frac{V_i^2}{2}\right)\cdot\frac{dW_G}{dZ}=-\frac{1}{2\pi\rho_\ell}\frac{dQ}{dZ} \tag{41}$$

which can be written in a non-dimensional form as follows:

$$\frac{\partial}{\partial\eta}\left[\frac{1}{2}\,\delta^*(1-\delta^*)\psi^3V_Z^*\left(\frac{H_{Go}}{\psi^2}H_L+\frac{V_Z^{*2}}{2}\right)\right]+\frac{W_T^{*\,2}}{\beta\rho^*}\left(\frac{H_{Go}}{\psi^2}H_G+\frac{V_i^{*2}}{2}\right)\frac{dX}{d\eta}=-\frac{W_T^*}{\beta\rho^*}\frac{dQ^*}{d\eta} \tag{42}$$

Eqn.(42) may also be written as

$$\frac{1}{2}\,\delta^*(1-\delta^*)\psi^3\left(\frac{H_{Go}}{\psi^2}H_L+3\,\frac{V_Z^{*2}}{2}\right)\frac{\partial V_Z^*}{\partial\eta}+\frac{1}{2}(1-2\delta^*)\psi^3V_Z^*\left(\frac{H_{Go}}{\psi^2}H_L+\frac{V_Z^{*2}}{2}\right)\frac{\partial\delta^*}{\partial\eta}+\frac{1}{2}\,\delta^*(1-\delta^*)V_Z^*\psi^2\left(\frac{H_{Go}}{\psi^2}H_L+3\,\frac{V_Z^{*2}}{2}\right)\cdot\frac{d\psi}{d\eta}+\frac{W_T^*\psi^2}{\beta\rho^*}\left(\frac{H_{Go}}{\psi^2}H_G+\frac{V_i^{*2}}{2}\right)\frac{dX}{d\eta}+\frac{1}{2}\delta^*(1-\delta^*)\psi\,V_Z^*H_{Go}\left(\frac{dH_L}{dp^*}\right)\frac{dp^*}{d\eta}=\frac{-W_T^*}{\beta\rho^*}\frac{dQ^*}{d\eta} \tag{43}$$

where

$$Q^* = Q/(V_o^{\,2}W_T)$$

$$H_G = h_G/h_{Go}$$

$$H_{Go} = h_{Go}/V_o^{\,2}$$

and

$$H_L = h_\ell/h_{Go}$$

iii.-2 For the total wedge shaped differential element

The conservation of energy applied to the control volume occupied by the entrained droplets vapour core and the liquid in the film, Fig.55, gives

$$\alpha_C dA_C \rho_G V_G (h_G + V_G^2/2) + \frac{\partial}{\partial Z}(\alpha_C dA_C \rho_G V_G (h_G + V_G^2/2))\frac{dZ}{2}$$

$$+ (1-\alpha_C) dA_C \rho_\ell V_E (h_\ell + V_E^2/2) + \frac{\partial}{\partial Z}((1-\alpha_C) dA_C \rho_\ell V_E (h_\ell + V_E^2/2))\frac{dZ}{2}$$

$$+ dA_Z \rho_\ell V_Z (h_\ell + V_Z^2/2) + \frac{\partial}{\partial Z}(dA_Z \rho_\ell V_Z (h_\ell + V_Z^2/2))\frac{dZ}{2}$$

$$- \alpha_c dA_C \rho_G V_G (h_G + V_G^2/2) + \frac{\partial}{\partial Z}(\alpha_c dA_C \rho_G V_G (h_G + V_G^2/2))\frac{dZ}{2}$$

$$- (1-\alpha_C) dA_C \rho_\ell V_E (h_\ell + V_E^2/2) + \frac{\partial}{\partial Z}((1-\alpha_C) dA_C \rho_\ell V_E (h_\ell + V_E^2/2))\frac{dZ}{2}$$

$$- dA_Z \rho_\ell V_Z (h_\ell + V_Z^2/2) + \frac{\partial}{\partial Z}(dA_Z \rho_\ell V_Z (h_\ell + V_Z^2/2))\frac{dZ}{2}$$

$$= -\frac{dQ}{2\pi R dZ} dA_W \qquad (44)$$

Simplifying and after making use of Eqns.(1),(4), and (5), Eqn.(44) reduces to:

$$\frac{\partial}{\partial Z}\left[\frac{1}{2}(R-\delta)^2 \alpha_C \rho_G V_G (h_G + V_G^2/2)\right] + \frac{\partial}{\partial Z}\left[\frac{1}{2}(R-\delta)^2 (1-\alpha_C)\rho_\ell V_E (h_\ell + V_E^2/2)\right] + \frac{\partial}{\partial Z}\left[\frac{1}{2}\delta(2R-\delta)\rho_\ell V_Z (h_\ell + V_z^2/2)\right]$$

$$= -\frac{1}{2\pi}\frac{dQ}{dZ} \qquad (45)$$

which can also be written in a non-dimensional form as follows:

$$\frac{\partial}{\partial \eta}\left[\frac{1}{2}(1-2\delta^*)^2 \alpha_C \rho^* \psi (H_{Go} H_G + \psi^2/2)\right] + \beta\rho^* \frac{\partial}{\partial \eta}\left[\frac{1}{2}(1-2\delta^*)^2 \cdot (1-\alpha_C) S_E \psi^3 \left(\frac{H_{Go}}{\psi^2} H_L + S_E^2/2\right)\right] + \beta\rho^* \frac{\partial}{\partial \eta}\left[2\delta^*(1-\delta^*) V_Z^* \psi^3 \cdot \left(\frac{H_{Go}}{\psi^2} H_L + V_Z^{*2}/2\right)\right] = -4 W_T^* \frac{dQ^*}{d\eta} \qquad (46)$$

Making use of the relations from Eqns.(31) and (32), and after expanding the differentials and rearranging, we get

$$\delta^*(1-\delta^*)\psi^3\left(\frac{H_{Go}}{\psi^2}H_L+3\frac{V_Z^{*2}}{2}\right)\frac{dV_Z^*}{d\eta}-(1-2\delta^*)\frac{\psi}{\beta}\left\{H_{Go}\left[\alpha_C H_G-(V_Z^*-(1-\alpha_C)S_E)\beta H_L\right]+\frac{\psi^2}{2}\left[\alpha_C-(V_Z^{*3}-(1-\alpha_c)S_E^{\,3})\beta\right]\right\}\frac{\partial\delta^*}{\partial\eta}$$

$$+\frac{1}{2\beta}\left\{\frac{1}{2}(1-2\delta^*)^2\left[H_{Go}(\alpha_C H_G+(1-\alpha_C)\beta S_E H_L)+3\frac{\psi^2}{2}(\alpha_C+(1-\alpha_c)\beta S_E^{\,3})\right]+2\delta^*(1-\delta^*)\beta V_Z^*\psi^2\left(\frac{H_{Go}}{\psi^2}H_L+3\frac{V_Z^{*2}}{2}\right)\right\}\frac{d\psi}{d\eta}$$

$$\frac{1}{2\beta}\left\{\frac{1}{2}(1-2\delta^*)^2\frac{\psi}{\beta S_E}\left(\frac{\alpha_C}{x_C}\right)^2\left[H_{Go}(H_G-\beta S_E H_L)+\frac{\psi^2}{2}(1-\beta S_E^{\,3})\right]\cdot\left(\frac{\partial x_C}{\partial x}\right)\right\}\frac{dX}{d\eta}+\frac{1}{2\beta}\left\{\frac{1}{2}(1-2\delta^*)^2\psi\left[H_{Go}(\alpha_C H_G+(1-\alpha_C)\beta S_E H_L)+\frac{\psi^2}{2}(\alpha_C+(1-\alpha_C)\beta S_E^{\,3})\right]\frac{\alpha_C}{\rho^*}\left(\frac{d\rho^*}{dp^*}\right)+\frac{1}{2}(1-2\delta^*)^2 H_{Go}\psi\left(\alpha_C\frac{dH_G}{dp^*}+(1-\alpha_C)\beta S_E\frac{dH_L}{dp^*}\right)+2\delta^*(1-\delta^*)\beta V_Z^*\psi H_{Go}\left(\frac{dH_L}{dp^*}\right)\right\}\cdot\frac{dp^*}{d\eta}=\frac{-2W_T^*}{\beta\rho^*}\frac{dQ^*}{d\eta} \qquad (47)$$

Equations (13),(21),(29),(39),(43) and (47) describe the characteristics of the liquid film and vapour core during annular condensing flow inside a horizontal tube. These equations constitute a set of six non linear partial differential equations which include six unknowns, namely, the axial velocity V_Z^*, the circumferential velocity V_ϕ^*, the liquid film thickness δ^*, the vapour velocity ψ, the quality for the total flow x, and the static pressure along the condenser tube p^*, and have to be solved simultaneously and numerically. The necessary condition is that the system of equations is closed, i.e. the number of unknowns being the same as that of equations. We see that this condition is not satisfied and that there are certain parameters that need to be determined before a solution can be sought. These parameters are: the core quality $x_C=x_C(x)$,

both the axial and circumferential wall shear stress, τ_W and $\tau_{W\phi}$, the interfacial shear stress, τ_I, the velocities V^*_{CZ}, V^*_{IZ}, $V^*_{C\phi}$ and $V^*_{I\phi}$ and the heat transfer distribution $dQ^*/d\eta$. These parameters will be determined in a later section.

5.3.3. Liquid Film Symmetry

There is experimental evidence (Jacowitz and Brodkey, 1964) suggesting that during horizontal, adiabatic annular flow of gas-liquid mixtures, a vertical plane passing through the centre line of the tube divides the liquid film into two identical halves. The same observation was reported by Soliman (1973). This fact was used in this analysis.

Considering the fact that the angle ϕ is measured from the top most position in the clockwise direction, Fig.55 , the symmetry criterion can be expressed mathematically as follows:-

$$\delta^*(\eta,\phi) = \delta^*(\eta,2\pi-\phi) \qquad (48a)$$

$$V_Z^*(\eta,\phi) = V_Z^*(\eta,2\pi-\phi) \qquad (48b)$$

and

$$V^*_\phi(\eta,\phi) = V^*_\phi(\eta,2\pi-\phi) \qquad (48c)$$

Differentiating Eqns.(48a) and (48b) w.r.t. ϕ, we get

$$\frac{\partial\delta^*}{\partial\phi}(\eta,\phi) = -\frac{\partial\delta^*}{\partial\phi}(\eta,2\pi-\phi) \qquad (49a)$$

and

$$\frac{\partial V_Z^*}{\partial\phi}(\eta,\phi) = -\frac{\partial V_Z^*}{\partial\phi}(\eta,2\pi-\phi) \qquad (49b)$$

Substituting $\phi = 0$ (top of the tube) and $\phi=\pi$ (bottom of the tube) into Eqns.(49a) and (49b), the following symmetry conditions results

$$\frac{\partial\delta^*}{\partial\phi}(\eta,0) = -\frac{\partial\delta^*}{\partial\phi}(\eta,\pi) \qquad (50)$$

and

$$\frac{\partial V_Z^*}{\partial\phi}(\eta,0) = -\frac{\partial V_Z^*}{\partial\phi}(\eta,\pi) \qquad (51)$$

the third symmetry condition can be deduced from Eqn.(48c) as,

$$V_\phi^*(\eta,0) = V_\phi^*(\eta,\pi) = 0 \qquad (52)$$

The implications of Eqns.(50),(51) and (52) will be discussed in more detail in a later chapter dealing with the analytical solution.

5.3.4. Evaluation of the Core Dryness Fraction

It has long been recognised that the entrained droplets considerably affect the transport phenomena in annular flow. It is also generally agreed that droplets are formed from wave instability on the film and thus entrained in the gas stream. Thus, to really understand the highly complex entrainment phenomena, it is necessary to have information on the wave motion, drop generation, drop movement, and the rate of drop deposition. In this way, information on the amount of liquid droplets entrained in the core may be obtained since it is the balance between the droplets formed and the droplets deposited.

There are essentially two descriptions of droplet deposition which have been incorporated into mathematical models of annular two-phase flow. The first of these assumes that droplet deposition is a mass transfer process in which the flux of droplets onto the film is proportional to the mean concentration of droplets in the gas core. The constant of proportionality, called the mass transfer coefficient, has been shown experimentally to be fairly insensitive to the flow rates of gas and liquid for a given system pressure in a round tube geometry (Hewitt and Taylor, 1970). In addition a model of heated annular flow, due to Whalley et al (1974), which incorporated the above description of droplet deposition gives acceptable predictions of the liquid flow distribution. The weak link in this approach is that the mass transfer coefficient must be known beforehand and at present is chosen by reference to a correlation developed by Whalley et al (1974). The correlation relates the mass transfer coefficient to the surface tension and has little, if any, theoretical basis.

The second description is due to Hutchinson et al (1971) and assumes that the droplets in the gas core interact with the turbulent eddies in such a way that the deposition process is essentially diffusive. The predictions of this theory agree well with experimental data and at first sight the second approach would appear preferable to the first in that it is more soundly based. However, it too suffers from a weak link in that it requires specification of a diffusion coefficient. A calculation procedure for the diffusion coefficient is detailed in Hutchinson et al (1971) but requires the mean value of the droplet size, which is also unknown beforehand. Such information is not available during forced convection condensation (McCoy and Hanratty, 1977).

The majority of the available entrainment correlations (Paleev and Filippovich, 1966; Moeck and Stachiewicz, 1972; Hughmark, 1973, Whalley et al, 1974) are based on two-phase annular-mist flow data of two components flowing adiabatically in a tube, usually air and water. Berry and Goss (1972) used an empirical correlation which expresses the relation between the core dryness fraction and the quality for the total flow as required in the present analysis.

Thus, due to the question of applying air-water data, taken under adiabatic conditions, to condensing flow, the correlation used by Berry and Goss (1972) is used in this analysis. The correlation is given in a parametric form as:

$$x = k\left[(1 - a_1)t - a_2t^2 - a_3t^3 - a_4t^4\right] \qquad (53)$$

$$x_c = 2kt - x \qquad (54)$$

where

$$k = 0.707107$$
$$a_1 = 0.638377\lambda$$
$$a_2 = 1.137108\lambda$$
$$a_3 = 2.24691\lambda$$
$$a_4 = 0.794244\lambda$$

and λ is a correlation parameter which account for the variation in entrainment. Basically this correlation allows to obtain a value of x_c for a known value of x. An iterative process is involved.

5.3.5. Evaluation of the Wall Shear Stress

Analytical predictions of the wall shear stress are very complicated, since it is quite dependent on the entrainment momentum transfer and on the wavy motion at the interface. Zanelly and Hanratty (1973) reported instantaneous and simultaneous measurements of shear stress and liquid film thickness in horizontal film flow. It was shown that the shear stress and the wavy amplitude were in phase under the conditions for which no entrainment occurred, and the opposite when entrainment occurred. Pimsner and Toma (1977) showed that the shear stress ratio was a unique function of the fraction of liquid in waves as defined by Telles and Dukler (1970).

It can be concluded from the above discussion that any correlation to be used in this analysis should account for the entrainment momentum transfer and wavy motion. Pimsner and Toma (1977) presented a correlation for the shear stress at the wetted wall as a linear function of the fraction of liquid in waves (Telles and Dukler, 1970) based on air-water flow. However, it is not known how this parameter could be affected by condensation at the interface.

The method which has had the most general success is that of Lockhart and Martinelli. This method consists of an empirically determined relationship between the Lockhart and Martinelli pressure parameters, ϕ_G and X_{tt}. Since relations to calculate the wall shear stress for the vapour flow alone are well established, the two-phase wall shear stress is readily found. However, when the wall shear stress increases and decreases along the condenser tube, the relation between ϕ_G and X_{tt} is not obvious as it was found for some of the experimental runs during the present investigation. It was then decided to use the wall shear stress calculated as a by-product from the experimental data.

5.3.6. Evaluation of the Interfacial Shear Stress

The interfacial shear stress correlation used in this analysis is the one proposed by Berry and Goss (1972). This correlation is based on values of interfacial shear stress which were derived from experimental data for high velocity condensing steam flowing in a horizontal tube. The correlation is expressed as follows:

for $1.0 > x > 0.745$

$$\tau_I = \frac{\tau_W}{x}(2.0x^{0.589}-1) \tag{55}$$

for $0.745 > x > 0.1$

$$\tau_I = \frac{\tau_W}{x}(1.734x^{0.111}-1) \tag{56}$$

5.3.7. Evaluation of the Circumferential Wall Shear Stress

Soliman (1973) established that the circumferential downward flow due to gravity which exists in the liquid was very small. It can then be assumed that conventional analytical methods for laminar flow may be employed to obtain an expression for $\tau_{W\phi}$. Since the liquid film thickness is very small compared to the radius of the tube, the circumferential flow can be treated as the flow over a flat plate. Consequently, the wall shear stress can be expressed by:

$$\tau_{W\phi} = \frac{1}{2} f_\phi \rho_\ell V_\phi^2 \tag{57}$$

The friction factor can be calculated from the analogy suggested by Jacowitz and Brodkey (1964) as follows:

$$f_\phi = \frac{5.4\mu_\ell}{\delta\rho_\ell V_\phi} \tag{58}$$

Equn.(58) can be substituted into Eqn.(57) to give

$$\tau_{W\phi} = 2.7\mu_L(V_\phi/\delta) \tag{59}$$

which in the notation used in this analysis can be written as:

$$\tau^*_{W\phi} = 1.35\ \mu_\ell{}^* \frac{\psi V^*_\phi}{\delta^*} \tag{60}$$

where

$$\mu_\ell{}^* = \mu_\ell/(V_\sigma \rho_o R)$$

5.3.8. Evaluation of the Velocities V^*_{CZ}, $V^*_{C\phi}$, V^*_{IZ} and $V^*_{I\phi}$

In condensation it is generally assumed that V_{CZ} (the axial component of the velocity at which the condensate particles leave the vapour stream and enter the liquid film) has a value of the same order of magnitude of the liquid velocity at the vapour-liquid interface, V_Z. Soliman (1973) assumed the following relationship between V_{CZ} and the mean liquid film velocity:

$$V_{CZ} = \gamma V_Z \tag{61}$$

where γ is a constant having a value of 1.25 for turbulent flow, and the value of 2.0 for laminar flow in the liquid film. The calculated Reynolds number for the present investigation showed that the flow in the liquid film was turbulent over the complete length of the condenser tube. Therefore,

$$V_{CZ} = 1.25\ V_Z \tag{62}$$

which may also be written as:

$$V^*_{CZ} = 1.25\ V^*_Z \tag{63}$$

Little is known about the velocity V_{IZ}. It should be at least of the same order of magnitude as the liquid velocity at the tip of the waves. Through the lack of knowledge in this matter, it is assumed that:

$$V^*_{IZ} = 1.25\ V^*_Z \tag{64}$$

Since the circumferential flow is assumed laminar, then for the circumferential components we have:

$$V^*_{C\phi} = 2.0\ V^*_\phi \tag{65}$$

and

$$V^*_{I\phi} = 2.0\ V^*_\phi \tag{66}$$

5.3.9. Evaluation of $dQ^*/d\eta$

Two different methods for calculating the derivative of the total radial heat rate with respect to Z may be used in this study. The first method used values of dQ/dZ obtained experimentally for a given data point. The following procedure was used: (i) The measured axial cooling water temperature distribution $T_{CW}(Z)$ was approximated with a polynomial of order fifth, (ii) assuming that the total radial heat rate out of the two-phase flow stream was absorbed by the cooling water, a heat balance on the cooling water side from the inlet up to some position Z gives:

$$Q(Z) = W_{CW} C_{\rho CW} (T_{CW}(Z) - T_{CW}(0)) \tag{67}$$

(iii) the above expression was differentiated to obtain

$$\frac{dQ(Z)}{dZ} = W_{CW} C_{\rho CW} \frac{dT_{CW}(Z)}{dZ} \tag{68}$$

which may be expressed in non-dimensional form as

$$\frac{dQ(\eta)}{d\eta} = W_{CW} C_{\rho CW} \frac{dT_{CW}(\eta)}{d\eta} \tag{69}$$

The value of $dQ^*/d\eta$ can be calculated from the following relation

$$\frac{dQ^*}{d\eta} = \frac{1}{V_o^2 W_T} \frac{dQ}{d\eta} \tag{70}$$

The second method was by making a local heat transfer balance in the radial direction in order to determine the total radial heat transfer rate. In doing so the local liquid film heat transfer coefficient should be known as a function of the local parameters. A suitable heat transfer correlation for the local heat transfer coefficient may be used.

By the determination of $x_C, \tau_W, \tau_{W\phi}, \tau_I, V^*_{CZ}, V^*_{C\phi}, V^*_{IZ}, V^*_{I\phi}$ and $dQ^*/d\eta$, the formulation of the problem is completed. Only the numerical procedure used in solving the governing equations needs to be discussed. This is the subject of the following chapter.

CHAPTER 6

NUMERICAL SOLUTION AND RESULTS

6.1. Introduction

An analysis of condensing annular flow inside a horizontal tube, was developed in the previous chapter in which the flow was modelled as a two-dimensional liquid film and a one-dimensional droplet-vapour core. According to this analysis the governing equations were: the continuity equation for the liquid film, (Eqn.13), the momentum equations for the liquid film in the axial and circumferential directions, (Eqns.21 and 29), the momentum equation for the vapour-core (Eqn.39), and the energy equations for the liquid film and the total flow, (Eqn.43 and 47).

Equations (13),(21),(29),(39),(43) and (47) represent a set of six nonlinear, first order, partial differential equations with six unknowns, namely; V_Z^*, V_ϕ^*, δ^*,ψ, x and p^*. Of these V_Z^*, V_ϕ^* and δ^* are functions of two independent variables: Z (axial location) and ϕ(circumferential location) while the remaining three ψ, x and p^* are only a function of Z. They can be written in index notation as follows:

$$A_{i,j} \frac{\partial \bar{X}_i}{\partial \eta} = C_i - B_{i,j} \frac{\partial \bar{X}_i}{\partial \phi} \qquad (71)$$

substituting

$$D_i^* = C_i - B_{i,j} \frac{\partial \bar{X}_i}{\partial \phi} \qquad (72)$$

Eqn.71 reduces to

$$A_{i,j} \frac{\partial \bar{X}_i}{\partial \eta} = D_i^* \qquad i = 1,2.....6 \quad j=1,2.....6 \qquad (73)$$

where

$$A_{i,j} = A_{i,j}(V_Z^*, V_\phi^*, \delta^*, \psi, x, p^*)$$

$$D_i^* = D_i^* (V_Z^*, V_\phi^*, \delta^*, \psi, x, p^*, \frac{\partial \bar{X}_i}{\partial \phi})$$

and

$$\bar{X}_1 = V_Z^* \qquad \bar{X}_4 = \psi$$

$$\bar{X}_2 = V_\phi^* \qquad \bar{X}_5 = x$$

$$\bar{X}_3 = \delta^* \qquad \bar{X}_6 = p^*$$

Due to the complex form of these equations it was impossible to obtain an independent equation for each of the variables. Therefore the mathematical solution of these equations appeared to be possible or practical only by a numerical approach.

The nature of the problem constituted an initial value problem, i.e. in addition to the governing equations, initial conditions were needed to solve this problem. This particular aspect was discussed in an earlier report (Guevara, 1979) and will be dealt with in the next section.

Therefore if particular values of the fundamental variables are known at the entrance to the condenser tube, the set of differential equations may be solved to determine the local values of the six derivatives at that location. The values of the derivatives so determined may then be applied over a small increment of Z to determine new values for the six fundamental dependent variables at the end of the increment. Proceeding forward along the condenser tube the above process is continued until either the total length of the condenser is reached or complete condensation occurs.

6.2. Inlet Conditions

As mentioned previously, in addition to the governing equations, initial conditions were needed to initiate the calculation procedure. These conditions were the dimensionless static pressure p^*, the dimensionless vapour and liquid velocities ψ, V_Z^*, and V_ϕ^*, the dimensionless liquid film thickness δ^*, and the quality for the total flow x, at the entrance to the condenser tube. Of these, p^* and x are usually known before-hand.

Thus, if it is assumed that the liquid film has formed at the entrance to the condenser tube the problem presents no difficulty since by choosing a suitable correlation; i.e. the void fraction, the problem could be solved provided the total mass flow rate, inlet static pressure and inlet quality are known. This has been a common practice in other analyses of condensation, i.e. the calculation procedure was assumed to begin at a location inside the condenser where a value for the liquid film thickness was assumed.

If, on the other hand, it is assumed that the liquid film has not formed at the entrance to the condenser tube, i.e. $\delta^* = 0$, it is not possible to obtain a solution for the six derivatives at this location because equation (21) reduces to zero identity and a coefficient singularity appears in equation (29). Since the necessary condition was that the system of equations was closed, it was necessary to develop a set of equations which apply over a short length (0.1 D_i or less) from the entrance to the condenser tube.

The same fundamental laws used to derive the governing equations (13,21,29,39,43,and 47) were used (Guevara, 1979) and a set of four non-linear algebraic equations which may be applied to the inlet of the condenser, provided an annular liquid film has not formed, were obtained. The assumptions made in developing this set of equations were:

1. The liquid film thickness is circumferently uniform. This appears to be reasonable since for the high dryness fraction likely to be encountered at the entrance, the gravitational force in the liquid film is negligible.
2. Because of the very low liquid film flow rate, any contribution due to entrainment of liquid from the film to the vapour core, is negligible. Consequently, if any amount of entrained droplets enter the condenser tube, its mass flow rate is assumed constant over the increment.
3. The liquid film flow is laminar.
4. Heat transfer rate is known.
5. The circumferential velocity in the liquid film is zero.

In attempting to solve this set of four non-linear algebraic equations, various iterative techniques were used. Most of these techniques, either did not converge to a realistic solution, or needed long computer time to converge to a solution.

The major difficulty encountered in solving the system of equations was the non-linearity of the algebraic equations. Solving a system of non-linear algebraic equations usually consumes much more computation time than a linear system. It was then necessary to use a much simpler set of equations which, while converging to a realistic solution, consumes very little computation time. This simplification will be outlined in the next section.

6.2.1. Simplification of the Equations

Since a set of four non-linear algebraic equations which may be applied over a very short length from the condenser inlet was obtained, only the simplified version of these equations will be stated here. For details of the original equations recourse should be made to Guevara (1979).

In order to establish finite values of the dependent variables at the start of the numerical solution process, it was further assumed that the transport and thermal properties of each phase remain constant over the increment. Consequently the mass conservation equation reduced to:

$$\psi = (1 - A_E^*)/(A_G^* + \beta V_Z^* (1 - A_G^* - A_E^*)) \qquad (74)$$

where A_E^* and A_G^* are the dimensionless areas occupied by the entrained droplets and the vapour phase respectively.

The momentum equation for the whole flow becomes:

$$p^* = 1 - 4(\bar{\tau}_W^*/P_o^*)\Delta\eta - (\psi^2/P_o^*)\left[A_G^* + \beta(A_E^* S_E^2 + V_Z^* (1 - A_G^* - A_E^*)) - (1 - A_E^*(1 - \beta S_E^2))/\psi^2\right] \qquad (75)$$

where $\bar{\tau}_W^*$ is the average wall shear stress over the small increment ΔZ.

It follows from assumption (2) that the amount of liquid in the liquid film over the increment is only due to condensation. The energy equation may then be expressed as:

$$\Delta W_L = \Delta\eta (dQ/d\eta)/h_{fg} \tag{76}$$

where ΔW_L is the amount of liquid condensed over the increment, $\Delta\eta$ is the dimensionless length of the increment ($=\Delta Z/2R$), h_{fg} is the latent heat of condensation taken at the inlet saturation pressure, and $dQ/d\eta$ is the heat transfer rate.

For a developing laminar liquid layer (assumption (3)) and with the assumption of a linear velocity distribution in the liquid layer of thickness δ, we have

$$\tau_W = \mu_\ell \frac{2V_Z}{\delta} \tag{77}$$

If it is further assumed that a laminar vapour layer begins to develop from the leading edge of the tube entrance, the local interfacial shear stress can be expressed, from boundary layer theory (Schlichting, 1968), as:

$$\tau_I = 0.332\ \rho_G V_o^2 \left(\frac{\nu_G}{V_o \Delta Z}\right)^{0.5} \tag{78}$$

where it has been assumed that the mean vapour velocity changes very little over the short increment ΔZ.

At the beginning of vapour condensation the total liquid flow ΔW_L is a very small quantity with virtually negligible momentum. In this region, it may therefore be assumed that $\tau_I = \tau_W$. Using this in Eqn.(78) and substituting into Eqn.(77) the liquid velocity may be expressed in non-dimensional from, as:

$$V_Z^* = \frac{1}{\psi}\left[0.166\ M^*(\mu_G/\mu_\ell)\sqrt{N^*/(\Delta\eta\beta)}\right]^{\frac{1}{2}} \tag{79}$$

where

$$M^* = \Delta W_L/\pi D_i^2 \rho_\ell$$

and

$$N^* = \rho_\ell D_i/V_o \mu_G$$

It can easily be shown that the dimensionless liquid film thickness is given by:

$$\delta^* = 0.5 \left(1 - \sqrt{A_G^* + A_E^*} \right) \qquad (80)$$

the quality for the whole flow as:

$$x = (\rho_G A_T V_o / W_T) A_G^* \psi \qquad (81)$$

and the core dryness fraction

$$x_C = 1/(1 + \beta S_E A_E^* / A_G^*) \qquad (82)$$

It is necessary to evaluate $\bar{\tau}_W^*$, to find a numerical value for Eqn.(75). By definition, $\bar{\tau}_W^*$ may be calculated from the following expression:

$$\bar{\tau}_W^* = \frac{1}{\Delta Z} \int_0^{\Delta Z} \tau_W^* dZ$$

substituting Eqn.(78) in the above expression and integrating gives

$$\bar{\tau}_W^* = 0.644 \, (\mu_G^* / \Delta\eta)^{0.5} \qquad (83)$$

where

$$\mu_G^* = \mu_G / \rho_G V_o D$$

The set of equations (Eqns.74,75,76,79,80,81,82 and 83) may be solved by an iterative method for a very short, finite initial increment ΔZ to obtain finite values of the dependent variables δ^*, V_Z^*, ψ, p^* and x necessary for digital computation. The procedure is as follows:-

1. The values of ΔW_L and $\bar{\tau}_W^*$ are calculated from Eqns.(76) and (83) respectively.
2. Assume an initial value for the dimensionless vapour velocity ψ, i.e.$\psi = 1.0$.
3. Set iteration counter equal to zero.

4. Calculate the dimensionless liquid velocity V_Z^* from Eqn.(79).
5. From Eqn.(74) determine a new value for the dimensionless vapour velocity ψ.
6. Check for convergence. When the difference between two successive approximations is less than some reference value go to step 7, otherwise go back to step 3.
7. The dimensionless static pressure p^*, liquid film thickness δ^*, vapour quality x, and the core dryness fraction x_c are determined from Eqns.(75),(80), (81) and (82) respectively.

In practice it was found that convergence could be achieved in no more than six iterations.

6.3. Computational Procedure

Once all the correlations and starting condition equations have been developed for a two-phase system in annular condensing flow, they were then used in a numerical solution of the analysis represented by Eqns.(13),(29),(39),(43) and (47). These equations were written in a compact form as:

$$A_{i,j} \frac{\partial \bar{X}_i}{\partial \eta} = D_i^* \qquad (73)$$

where $A_{i,j}$ is a (6 x 6) square matrix and D_i^* a column vector.

By referring to Fig.59, the whole cross-sectional area of the tube was divided into a number of similar small wedge shaped elements with their apex at the centre of the tube. Each element was bounded by a wedge angle $\Delta\phi$ and a dimensionless length $\Delta\eta$. Within each wedge a portion of the volume adjacent to the base was filled with a flowing liquid, and the remainder with a flowing vapour-droplets homogeneous mixture. Due to symmetry of the liquid film in the ϕ-direction, the solution domain was bounded between $\phi=0$ and $\phi=\pi$, and $\Delta\phi=$ 3 degrees. The solution along the axial direction η was started from the condenser's entrance and proceeded until the end of the tube was reached.

During the present study a value of $\Delta\eta = 0.25$ was used.

To solve the equations numerically, the following steps were carried out:

1. The derivative of the dependent variables were determined at all mesh points of tube cross-section I, I >1, starting from the top of the tube ($\phi = 0$, J = 1) and proceeding towards the bottom of the tube ($\phi = \pi$, J = N+1), where N is the number of subdivisions. At the top of the tube $V_\phi^*(I,0)=0$, therefore only five of the governing equations were solved simultaneously at that location. Since, at any tube cross-section I, the values of the dependent variables p^*, x and ψ are independent of the circumferential location ϕ only Eqns.(13),(21) and (29) were solved simultaneously at all the mesh points for $1 < J < N+1$. Furthermore, at the bottom of the tube $V_\phi^*(I,\pi)=0$, and the governing equations were reduced to Eqns.(13) and (21). The method used to solve numerically a set of simultaneous linear equations was the Gauss's technique. Values of $\partial\delta^*(I,J)/\partial\phi$, $\partial V_Z^*(I,J)/\partial\phi$ and $\partial V^*(I,J)/\mu\phi$ appearing in equation (13),(21) amd (29) were calculated from the following formulae.

$$\frac{\partial\delta^*}{\partial\phi}(I,J) = \frac{\delta^*(I,J+1) - \delta^*(I,J-1)}{2(\Delta\phi)} \qquad (84)$$

$$\frac{\partial V_Z^*}{\partial\phi}(I,J) = \frac{V_Z^*(I,J+1) - V_Z^*(I,J-1)}{2(\Delta\phi)} \qquad (85)$$

and

$$\frac{\partial V_\phi^*}{\partial\phi}(I,J) = \frac{V_\phi^*(I,J+1) - V_\phi^*(I,J-1)}{2(\Delta\phi)} \qquad (86)$$

Due to the symmetry of the flow of the liquid film around a vertical plane passing through the centre line of the tube, Eqns.(84),(85) and (86) reduce to the following form at the top and bottom of the tube,

$$\frac{\partial \delta^*}{\partial \phi}(I,J) = 0 \qquad \text{at } \phi = 0,\pi \qquad (87)$$

$$\frac{\partial V_Z^*}{\partial \phi}(I,J) = 0 \qquad \text{at } \phi = 0,\pi \qquad (88)$$

$$\frac{\partial V_\phi^*}{\partial \phi}(I,J) = \frac{V_\phi^*(I,J+1)}{\Delta\phi} \qquad \text{at } \phi = 0 \qquad (89)$$

and

$$\frac{\partial V_\phi^*}{\partial \phi}(I,J) = \frac{-V_\phi^*(I,J-1)}{\Delta\phi} \qquad \text{at } \phi = \pi \qquad (90)$$

2. Once the derivative of the dependent variables have been calculated, Euler's method of numerical integration was then utilized to determine values of the dependent variables at a position $\eta+\Delta\eta$.

$$(\bar{X}_i)_{\eta+\Delta\eta} = (\bar{X}_i)_{\eta} + \left(\frac{\partial \bar{X}_i}{\partial \eta}\right)_{\eta} \cdot \Delta\eta \qquad (91)$$

It was decided to use Euler's method even though it was a first order procedure (i.e. the error is a linear function of $\Delta\eta$) since most higher order methods require several recalculations of the derivatives $\partial \bar{X}_i(I,J)/\partial\eta$. Inasmuch as the calculations in step (1) were rather complex, the use of Euler's method along with a very small increment $\Delta\eta$ is actually more feasible.

3. With the new values of the dependent variables at $\eta+\Delta\eta$ the matrix $A_{i,j}$ and the column vector D_i^* are again determined and steps (1) and (2) are repeated until the end of the condenser tube.

6.4. Numerical Results

The analysis and the correlations together with the inlet condition equations presented in the theoretical analysis and in section (6.2) of this chapter were programmed in Fortran IV language to run on The City University Computer Centre's Honeywell digital computer.

It is to be recalled that the analysis should be able to predict both the axial and circumferential liquid velocities together with the liquid film thickness at any axial and circumferential location. During the course of the present study it was found that when the calculations of the circumferential velocity were included, they yielded meaningless results for the distribution of V_ϕ^*. The solution later went unstable with wildly fluctuating circumferential and axial velocities. Several attempts were made to avoid this instability in the solution, but they did not produce the desired results.

In previous works some authors have preferred to specify limits to this velocity component. Jacowtiz and Brodkey (1964) suggested, based on experimental observations, that the circumferential velocity should be limited to the maximum value $(V_\phi)_{MAX}$ = 0.00122 m/s (0.004 ft/s). Coney (1973) suggested that the velocity in the circumferential direction should be limited to the maximum velocity that the liquid could attain by free fall under gravity from the top of the tube. Coney (1973) arrived at an expression for the liquid film thickness at which the surface velocity in the circumferential direction reaches the free fall velocity. This expression can be written as follows:

$$\delta_M = \left[\frac{8}{(1+\cos\phi)} \frac{R\rho_\ell \nu_\ell^2}{\Delta\rho g} \right]^{0.25}$$

where ϕ represent the angle from the top of the tube. As can be seen the above expression leads to a singularity when the bottom of the tube is approached. The values of δ_M become excessively large for $\phi > \pi/2$ giving solutions which could not be physically possible, i.e. values for $\delta_M > R$. This in fact was not a serious problem for Coney (1973) since he was interested in the solution at the top of the tube (ϕ = 0) giving a value for δ_M of

$$\delta_M = \left[\frac{4R\rho_\ell \nu_\ell^2}{\Delta\rho\, g} \right]^{0.25}$$

i.e. δ_M changes slightly with variations in the liquid and vapour densities and the liquid kinematic viscosity.

This criteria was used in the current analysis in order to obtain solutions for the circumferential velocity but it did not succeed in producing the desired result. Initially a stable solution was obtained along the condenser in which the circumferential velocity increased while the axial velocity decreased. At some distance from the inlet,the circumferential velocity reached values of the same order of magnitude as the axial velocity. After this the solution became unstable and was terminated.

Following these unsuccessful attempts to obtain a satisfactory solution the program was run with the circumferential velocity equal to zero. Although this represented a departure from the original aim of the analysis to produce a general solution for condensation in a tube the consequences for this project were not as serious as might be expected. The high vapour core velocity produced in the working section during the present experimental tests resulted in a high interfacial shear stress which led to a thin liquid film whose circumferential velocity was considerably less than the axial velocity of the vapour core. A theoretical solution in which the circumferential velocity was equal to zero represented a limiting case which would be approached by the experimental results.

The introduction of this modification into the program produced a stable solution. The immediate effect in the solution was to induce a constant liquid film thickness and axial velocity around the circumference in the annular liquid film at any axial location along the condenser. However, it is recognised that if the geometry of the annular liquid film is to be studied, this velocity component has to be included.

The analytical results were then compared with data from two experimental runs for the condensation of high velocity vapour inside a tube. The specific runs were number 14 and 15 of the present experimental investigation. They were selected due to the fact that the inlet quality was one ($X_{inlet} = 1.0$). For other runs in which the liquid film had formed due to condensation in the precondenser, there was uncertainty on the amount of liquid flowing as entrained droplets leaving the precondenser, making it difficult to establish the inlet

conditions necessary for the analytical solution. However, although facilities for extracting the liquid film at the end of the precondenser were provided, these measurements were not performed during the course of the experimental investigation.

The parameters needed for the analytical solution were selected to correspond closely to their respective values used in the experimental investigation. These parameters were:

1. Total mass flow rate of the condensing vapour, W_T in kg/s
2. The coolant mass flow rate, W_{CW} in kg/s
3. The coolant axial temperature distribution, T_{CW} in ^{o}C
4. The absolute inlet pressure, P_o in Bar
5. The inlet quality of the condensing fluid, x
6. The condenser inside diameter, D_i in m.

Fig.60 through 65, illustrated the comparison between the analytical results and the experimental data for these two experimental runs. The only parameters compared were the total axial static pressure distribution, p, the quality for the whole flow, x, and the liquid film mass flow rate W_L, since these were the parameters which were known experimentally. The experimental total axial static pressure distribution was obtained from the observations from the manometers. The quality for the whole flow and the liquid film mass flow rate were obtained by the method shown in Appendix B.

The comparison between the analytical and experimental total axial static pressure distribution shows that the theoretical analysis predicted a slightly larger overall total pressure drop than the experimental values, but there was a general agreement along the condenser. This moderate discrepancy might be due to the fact that the total static pressure was primarily determined in the theoretical analysis from the momentum equations for the liquid film and the droplet-vapour core, which require predictions of the wall and interfacial shear stresses. These values of the wall and interfacial

shear stresses were required as input data in the analytical solution. They were chosen so as to coincide with their computed values from the experimental total axial pressure distribution. It was assumed that the total pressure distribution p(Z) could be expressed as a fifth or less order function of the length Z, and constants for the function p(Z) were determined by applying the least square method to the eight static pressure readings obtained in each test. Then $(dp/dZ)_{Total}$ was obtained by differentiating p(Z). The frictional pressure gradient was calculated by subtracting the momentum term from the total pressure gradient so obtained.

In the data reduction analysis (Appendix B) in order to compute the momentum effects, a knowledge of the vapour and liquid axial velocity distributions was required. Inasmuch as these measurements were not made, a void fraction correlation (Smith, 1969-70) was used. Therefore, any disagreement between the analytical and experimental total pressure distribution may be due to inaccuracies in estimating the momentum effects when calculating both the wall and interfacial shear stresses.

In the case of the quality for the whole flow, the analytical results, although slightly higher, were in fairly good agreement with the experimental value.

For the final parameter compared, the liquid film mass flow rate, the analytical results generally underpredicted the experimental values. It is important to point out that in the data reduction analysis (Appendix B) the computation of the liquid film mass flow rate along the condenser tube was carried out by assuming that all the condensed liquid was flowing as a annular film around the tube wall. This was a necessary assumption since the vapour distribution along the condenser tube was not known before-hand. Therefore, the fact that the theoretical analysis accounted for the presence of entrainment in the vapour core, resulted in the analysis predicting a lower liquid film mass flow rate.

CHAPTER 7

CONCLUSIONS

The results of an experimental and an analytical investigation of the liquid film flow rates, local heat transfer coefficient and total pressure distribution during condensation inside a horizontal tube, were presented. In the experimental investigation, a porous wall suction device was used to measure the liquid film flow at the end of the test condenser. The entrainment flow was the difference between the total liquid flow and the film flow. The entrainment results were compared with existing entrainment correlations based on two-phase, annular mist flow data of two components flowing adiabatically in a duct. It was found that entrainment data obtained during condensation inside a horizontal tube, could be correlated on the basis of existing parameters currently used for correlating entrainment data in adiabatic systems. The results were found to correlate fairly closely about the lines given by the equations.

$$(W_E/W_G)(\rho_G/\rho_\ell) = 1.0878 \times 10^{-8}(y_G^+)^{\left[3.1421-0.326 \log_{10}(y_G^+)\right]}$$

and

$$C = 3.47 \times 10^{-4}(\tau_I \delta/\sigma)^{\left[-6.99-3.85 \log_{10}(\tau_I \delta/\sigma)\right]}$$

For the range of conditions covered in this study it was found that the local heat transfer coefficient may increase and decrease along the condenser tube.

From the total pressure distribution results it was found that the local frictional pressure drop could be better correlated in terms of the Martinelli pressure parameters if the liquid to vapour Reynolds number ratio is incorporated as follows:

$$\left(\frac{1+\phi_G}{\phi_G}\right)\frac{R_{e_\ell}}{R_{e_G}} = 3.11 \times 10^{-4} + 1.89576\, X_{tt}$$

In the analytical investigation, a mathematical model was developed for annular flow during condensation inside horizontal tubes. The governing equations were solved numerically to predict the changes in the static pressure vapour quality and liquid film flow rate. Good agreement was found between the theoretical predictions of the pressure drop, and the experimental data of the present investigations.

REFERENCES

ALTMAN, M., F.W. STAUB and R.H. NORRIS (1960) Local heat transfer and pressure drop for R-22 condensing in horizontal tubes. AICHE Chem.Eng.Prog.Symp.Ser.,Vol.56, No.30, pp.151-159.

ANDERSON, R.J. and RUSSELL, W.F. (1970) Film formation in two-phase annular flow. AICHE J., Vol.16, No.4, pp.626-633.

BAKER, O. (1954) Simultaneous flow of oil and gas. Oil and Gas J., V.53, pp.185-195.

BOYKO, L.B. and KRUZHILIN, G.N. (1967) Heat transfer and hydraulic resistance during condensation of steam in horizontal tube and in bend of tubes. Int.J. Heat and Mass Transfer, No.30, V.13, pp.361-373, Mar.

BRUMFIELD, L.K. and THEOFANOUS, T.G. (1976) On the prediction of heat transfer across turbulent liquid films. J.of Heat Transfer. Trans.ASME, pp.496-502, Aug.

BUTTERWORTH, D. and PULLING, D.J. (1972). A visual study of mechanisms in horizontal annular, air-water flow. AERE-M2556, Oct.

BUTTERWORTH, D. and PULLING, D.J. (1974) Mechanisms in horizontal annular air-water flow. Symp.on Multiphase flow System., University of Strathclyde, Glasgow, APril.

CONNEL, M.P., BICKINGHAM, P.and WOOD, D.G. (1974) Condensation inside a horizontal tube. I.Chem.E.Symp.Ser.No.38 Paper D2.

CAVALLINI, A. and ZECCHIN, R.F. (1971) Proc.of 13th Internl Congress of Refrig., 2, 193, Aug.

CAVALLINI, A. and ZECCHIN, R.F. (1972) La Termotechnica, XXVI, 199.

CONEY, M.W.E. (1974) The analysis of a mechanism of liquid replenishment and draining in horizontal two-phase flow. Int.J. Multiphase Flow, Vol.1, pp.647-449.

CHIEN, S.F. and IBELE, W. (1964) Pressure drop and liquid film thickness of two-phase annular and annular mist flow. J.Heat Transfer, 86C, pp.89-96.

CHU, K.J. and DUKLER, A.E. (1974) Statistical characteristics of thin, wavy, films: Part II Studies of the substrate and its wavy structure. AICHE J.Vol.20, No.4, pp.695-706, July.

CHU, K.J. and DUKLER, A.E. (1975) Statistical characteristics of thin, wavy, films : Part III Structure of the large waves and their resistance to gas flow. AICHE J., Vol.21, No.3, pp.583-593, May.

GOODYKOONTZ, I.H. and BROWN, W.F. (1967) Local heat transfer and pressure drop distribution for Freon-113 condensing in downward flow in a vertical tube. NASA-TN-D-3952, May.

GUEVARA, E. (1977) Condensation inside tubes: A survey.Research Memo. ML95, Dept.of Mech.Eng., The City University.

GUEVARA, E. (1979) Condensation inside tubes: Inlet conditions problem. Research Memo. No.114, Dept.of Mech.Eng., The City University.

HILDING, W.E. (1967) An analytical and experimental investigation of the two-phase flow of a high velocity vapour condensing in a tube. Report NASA-CR-78653.

HEWITT, G.F. and ROBERTS, D.N. (1969a) Studies of two-phase flow patterns by simultaneous X-ray and flash photography. AERE-M2159.

HEWITT, G.F. and HALL-TAYLOR, N.S. (1970) Annular two-phase flow. Pergamon Press, Oxford.

HEWITT, G.F. and LOVEGROVE, P.C. (1976) Experimental methods in two-phase flow studies. EPRI NP18 Final Report, March.

HUTCHINSON, P., HEWITT, G.F. and DUKLER, A.E. (1971) Deposition of liquid and solid dispersions from turbulent gas streams : a stochastic model. Chem.Engng.Sci.26, pp.419-439.

HUTCHINSON, P. and WHALLEY, P.P. (1973) A possible characterisation of entrainment in annular flow. Chem.Engng.Sci.28, pp.974-975.

HUGHMARK, G.A. (1973) Film thickness, entrainment, and pressure drop in upward annular and dispersed flow. AICHE J., Vol.19, p.1062.

ISACHENKO, V.P. and SALONZODA, F. (1972) Local heat transfer during condensation of water vapour in a vertical pipe. Heat Transfer Sov.Res. V4 n4 pp.142-47, July-Aug.

ISHII, M. and GROLMES, M.A. (1975) Inception criteria for droplet entrainment in two-phase concurrent film flow. AICHE J., Vol.21, No.2., pp.308-318.

JACOWITZ, L.A. and BRODKEY, R.S. (1964) An analysis of geometry and pressure drop for the horizontal annular, two-phase flow of water and air in the entrance region of a pipe. Chem.Eng.Sci., 19, pp.261-274.

JASTER, H. and KOSKY, P.G. (1976) Condensation heat transfer in a mixed flow regime. Int.J.Heat Mass Transfer, V19, pp.95-99.

KESHOCK, E.G. SPENCER, G., FRENCH, B.L. and WILLIAMS, J.L. (1974) A photographic study of flow condensation in 1-g and zero-g environments. Int.Heat Transfer Conf. 5th Proc.Tokyo, Japan, Sept.3-7, V.3, ISME SCEJ, pap. $C_s1.5$, pp.235-240.

KOSKY, P.G. and STAUB, F.W. (1971) Local heat transfer coefficients in the annular flow regime. AICHE J., Vol.17, No.5, p.1037, Sept.

MOECK, E.O. and STACHIEWICZ, J.M. (1972) A droplet interchange model for annular dispersed, two-phase flow. Int. J.Heat and Mass Transfer, Vol.15, pp.637-653.

McCOY, D.D. and HANRATTY, J.J. (1977) Rate of deposition of droplets in annular two-phase flow. Int.J. Multiphase Flow, Vol.3, pp.319-331.

NARAYANA, V. and SARMA, P.K. (1972) Condensation heat transfer inside horizontal tubes. The Canadian J. of Chem Engng. V.50, pp.547-549.

PALEEV, I.I. and FILIPPOVICH, B.S. (1966) Phenomena of liquid transfer in two-phase dispersed annular flow. Int.J.Heat and Mass Transfer, Vol.9, p.1089.

PIMSNER, V. and TOMA, P. (1977) The wavy aspect of horizontal concurrent air-water film flow and transport phenomena. Int.J. Multiphase Flow, Vol.3, pp.273-283.

SMITH, S.L. (1969-70) Void fractions in two-phase flow : A correlation based upon equal velocity head model. Inst.of Mech.Engrs.London, 184, 647.

SOLIMAN, H.M. SCHUSTER, J.R. and BERENSON, P.J. (1968) A general heat transfer correlation for annular flow condensation. J.of Heat Transfer, Trans.ASME, p.267, May.

SOLIMAN, H.M. and AZER, N.Z. (1971) Flow patterns during condensation inside horizontal tube. ASHRAE Trans. 77, pt.1, p.210.

SOLIMAN, H.M. (1973) Experimental and analytical studies of flow patterns during condensation inside horizontal tubes. Ph.D. dissertation, Kansas State University.

SHAH, M.M. (1979) A general correlation for heat transfer during film condensation inside pipes. Int.J. Heat Mass Transfer, Vol.22, pp.547-556.

TELLES, A.S. and DUKLER, A.E. (1970) Statistical characteristics of thin, vertical, wavy liquid films. Ind.Eng.Chem. Fundam, Vol.9, No.3, pp.412-421.

TRAVISS, D.P., BARON, A.B. and ROHSENOW, M.W. (1971) Forced-convection condensation inside tubes. MIT Rep. No.DSR-72591-74.

TRAVISS, D.P. and ROHSENOW, W.N. (1973) Flow regimes in horizontal two-phase flow with condensation. ASHRAE Trans., V79, pt.II, p.31.

TRAVISS, D.P., ROHSENOW, W.N. and BARON, A.B. (1973) Forced convection inside tubes: A heat transfer equation for condenser design. ASHRAE Trans., V79, pt.I, p.157.

UEDA, T., AKIYOSHI, K. and MATSUI, T. (1972) Heat transfer and pressure drop for flow condensation inside a vertical tube. Bulletin JSME, Vol.15, p.1267.

UEDA, T., KUBO, T. and INOVE, M. (1974) Heat transfer for steam condensing inside a vertical tube. Int. Heat Transfer Conf.5th Proc., Tokyo, Japan, 3-7 Sept., V3, JSME SCEJ, Pap.C_s3.6, pp.304-308.

WEISMAN, J., DUNCAN, D., GIBSON, J. and CRAWFORD, T. (1979) Effects of fluid properties and pipe diameter on two-phase flow patterns in horizontal lines. Int.J. Multiphase Flow, Vol.5, pp.437-462.

WHALLEY, P.B., HUTCHINSON, P.and HEWITT, G.F. (1974) The calculation of critical heat flux in forced convection boiling. 5th Int.Heat Transfer Conf. Tokyo, Pap.B.6.11.

ZANELLY, S. and HANRATTY, J.J. (1973) Effect of entrainment on roll waves in air-liquid flow. Chem.Engng.Sci. Vol.28, pp.643-644.

ADDITIONAL REFERENCES

SCHLICHTING, H., Boundary Layer Theory, Sixth Edition, McGraw-Hill (1968)

1967 Steam Tables, The Electrical Research Association by Edward Arnold (Publisher) Ltd., London.

APPENDIX A

DIFFERENTIAL AREAS (SEE FIG. A-1)

The area of contact between the liquid and the wall of the tube is the product of the arc $\overline{BC}$ and the length $d\bar{z}$:

$$dA_W = \text{arc } \overline{BC}.\ d\bar{z} \tag{A1}$$

$$\text{arc } \overline{BC} = Rd\phi \tag{A2}$$

substituting (A2) into (A1) we obtain

$$dA_W = Rd\phi d\bar{z} \tag{A3}$$

Similarly, the interfacial area between the two phases is the product of the width of this area arc $\overline{AE}$ and the length $d\bar{z}/\cos\bar{\beta}$:

$$dA_I = \text{arc } \overline{AE}.\ \frac{d\bar{z}}{\cos\ \bar{\beta}} \tag{A4}$$

the arc $\overline{AE}$ is given by

$$\text{arc } \overline{AE} = \text{arc } \overline{AD}/\cos\bar{\gamma} \tag{A5}$$

$\cos\ \bar{\gamma}$ and $\cos\ \bar{\beta}$ are calculated as follows:

$$\cos\ \bar{\gamma} = \frac{(R-\delta)\ \frac{d\phi}{2}}{\frac{d\phi}{2}\sqrt{(R-\delta)^2+(\frac{\partial\delta}{\partial\phi})^2}} \sim 1 \tag{A6}$$

and

$$\cos\ \bar{\beta} = \frac{d\bar{z}}{d\bar{z}\sqrt{1+(\frac{\partial\delta}{\partial\bar{z}})^2}} \sim 1 \tag{A7}$$

the arc $\overline{AD}$ becomes

$$\text{arc } \overline{AD} = \left[(R-\delta) + \frac{\partial\delta}{\partial\phi}\ \frac{d\phi}{2}\right] d\phi \sim (R-\delta)d\phi \tag{A8}$$

therefore:

$$dA_I = (R-\delta)d\phi d\bar{z} \tag{A9}$$

Next are required the flow areas in the axial and circumferential directions. The flow area in the circumferential direction is the product of the film thickness and the length $d\bar{z}$

$$dA_{\phi} = \delta d\bar{z} \tag{A10}$$

The flow area in the axial direction is given by

$$dA_{\bar{z}} = \text{area OBCO} - \text{area OADO} + \text{area ADEA} \tag{A11}$$

$$= \tfrac{1}{2} R^2 d\phi - \tfrac{1}{2}\left[R-(\delta- \frac{\partial\delta}{\partial\phi}\frac{d\phi}{2})\right]^2 d\phi$$

$$+ \tfrac{1}{2}\left[R-(\delta- \frac{\partial\delta}{\partial\phi}\frac{d\phi}{2})\right]\left[(\delta+ \frac{\partial\delta}{\partial\phi}\frac{d\phi}{2})-(\delta- \frac{\partial\delta}{\partial\phi}\frac{d\phi}{2})\right] d\phi$$

$$= \tfrac{1}{2}\delta(2R-\delta)d\phi + (\frac{\partial\delta}{\partial\phi})^2(\frac{d\phi}{2})^3$$

$$\sim \tfrac{1}{2}\delta(2R-\delta)d\phi$$

Therefore:

$$dA_{\bar{z}} = \tfrac{1}{2}\delta(2R-\delta)d\phi \tag{A12}$$

In a similar manner the differential flow area for the vapour core is

$$dA_C = \text{area OAEO}$$

$$= \text{area OADO} - \text{area ADEA} \tag{A13}$$

$$= \tfrac{1}{2}\left[R-(\delta- \frac{\partial\delta}{\partial\phi}\frac{d\phi}{2})\right]^2 d\phi - \tfrac{1}{2}\left[R-(\delta- \frac{\partial\delta}{\partial\phi}\frac{d\phi}{2})\right]\frac{\partial\delta}{\partial\phi}(d\phi)^2$$

$$= \tfrac{1}{2}(R-\delta)^2 d\phi - (\frac{\partial\delta}{\partial\phi})^2(\frac{d\phi}{2})^3$$

$$\sim \tfrac{1}{2}(R-\delta)^2 d\phi$$

Therefore:

$$dA_C = \tfrac{1}{2}(R-\delta)^2 d\phi \tag{A14}$$

For the differential total flow area we have

$$dA_T = \text{area OBCO}$$

$$= \tfrac{1}{2} R^2 d\phi$$

therefore:

$$dA_T = \tfrac{1}{2} R^2 d\phi \qquad \text{(A15)}$$

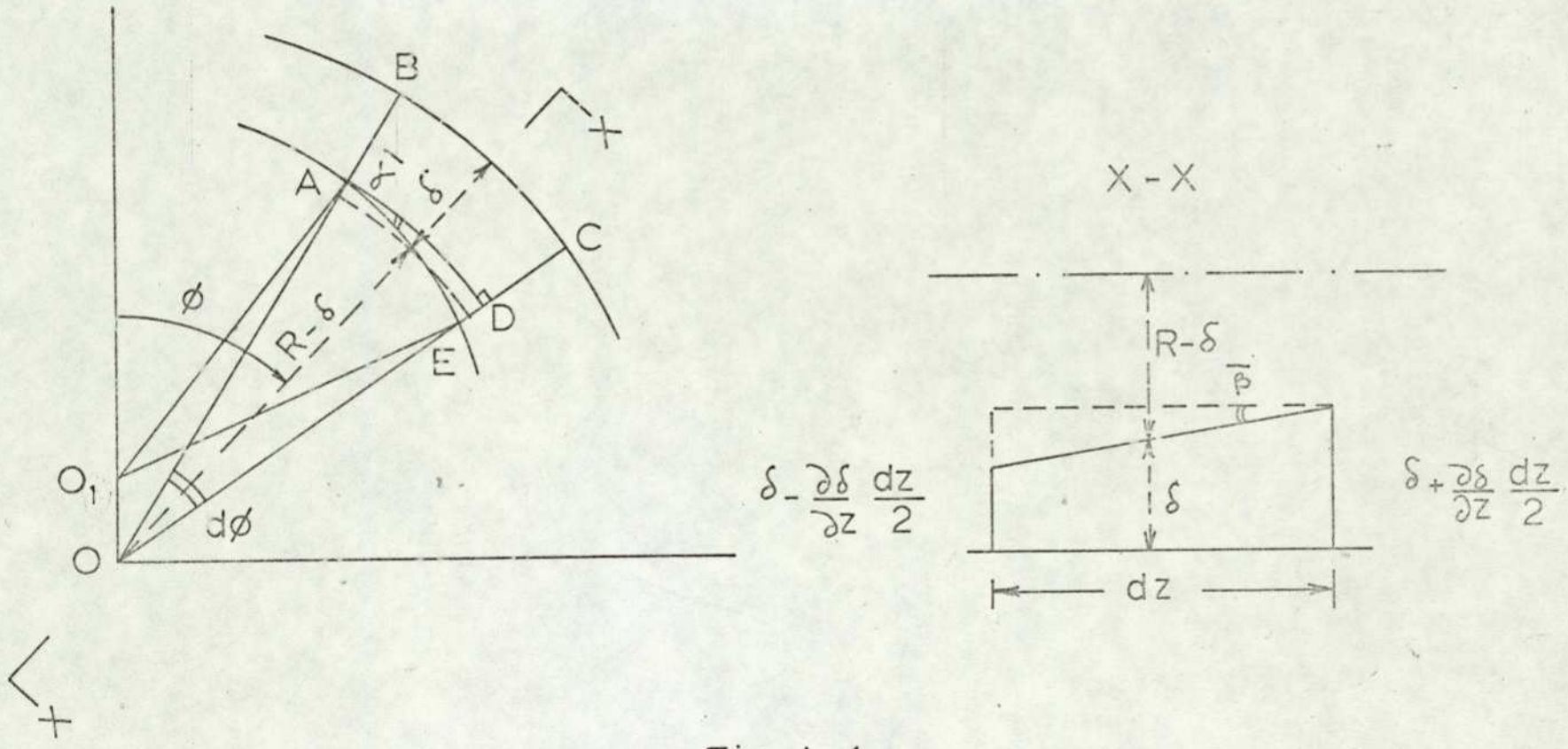

Fig. A-1

APPENDIX B

DATA REDUCTION ANALYSIS

For the experimental tests conducted on condensing steam inside a horizontal tube, the following data was recorded in most tests:

1. Local static pressure, p
2. Local cooling water temperature, T_{CW}
3. Local wall temperature, T_W
4. Total flow rate of steam, W_T
5. Total flow rate of cooling water, W_{CW}
6. Liquid film mass flow rate at exit, W_{LF}

From the above data the following information was computed for most tests:

1. Local heat transfer coefficient, h
2. Local liquid flow rate, W_L
3. Local vapour flow rate, W_G
4. Local steam quality, x
5. Local wall shear stress, τ_W
6. Local interfacial shear stress, τ_I
7. Local wall and interfacial friction factors, f_W and f_I

1. Local Heat Transfer Coefficient

The following steps were followed for the evaluation of the local heat transfer coefficient:

i) the measured axial cooling water temperature distribution $T_{CW}(Z)$ was approximated with a polynomial of order fifth or lower

ii) assuming that the total radial heat rate out of the two-phase flow stream was absorbed by the cooling water, a heat balance on the cooling water side from the inlet up to some position Z gives

$$Q(Z) = W_{CW} C_{pCW} \left(T_{CW}(Z) - T_{CW}(0)\right) \qquad (B1)$$

the above expression was differentiated to give

$$\frac{dQ(Z)}{dZ} = W_{CW} C_{pCW} \frac{dT_{CW}(Z)}{dZ} \qquad (B2)$$

The local heat flux at the inner wall of the condenser was calculated as follows:

$$q_i = \frac{W_{CW} C_{pCW}}{\pi D_i} \frac{dT_{CW}(Z)}{dZ} \qquad (B3)$$

where the numerator represents the increase in the enthalpy of the coolant and the denominator the area normal to the flow of heat. The slope of the coolant temperature profile $dT_{CW}(Z)/dZ$ was evaluated graphically by finding the tangent to the curve at a particular location.

The local condensing heat transfer coefficient was evaluated from

$$h_i = \frac{q_i}{T_S - T_{IW}} \qquad (B4)$$

where T_S is the saturation temperature corresponding to the measured pressure. T_{IW} is the inner wall temperature and was calculated from the relation for the radial heat flux in a cylinder:

$$q_i = \frac{K_w (T_{IW} - T_W)}{D_i \ln(D_j/D_i)} \qquad (B5)$$

Equation (B5) may be solved for the inner wall temperature in terms of the local heat flux q_i and measured T_W. The physical junction of the wall thermocouple was placed 3 mm from the outer wall. The diameter ratio of equation (B5) is the ratio of the diameter at which the wall temperature was measured to the inner diameter of the tube. The wall mean thermal conductivity was assumed constant over the temperature range encountered in the tests, and a value of $K_W = 0.0173$ kW/m^{o}K was used for stainless steel (Cr-Ni Steel 18% Cr, 8% Ni). Equation (B5) reduces to the following

expression after insertion of the constants:

$$T_{IW} = T_W + 1.14 \times 10^{-1} q_i \qquad (B6)$$

2. Local flow rates and quality

The local condensate flow was evaluated by heat balances over small increments of length (100 mm). The heat balance calculation was performed in the following manner. The total rate of heat transfer in the i^{th} increment Q_i is given by

$$Q_i = Q_{Ci} + Q_{\ell i} + Q_{Gi} \qquad (B7)$$

where Q_{Ci} is the heat released by the condensation process in the increment and is given by:

$$Q_{Ci} = \Delta W_{L_i} h_{fg} \qquad (B8)$$

$Q_{\ell i}$ represents the decrease in the enthalpy of the liquid in the increment. An average value of the liquid flow rate in the increment was used since the flow varies with length. The $Q_{\ell i}$ is represented by:

$$Q_{\ell i} = \left[\left(\tfrac{1}{2} \Delta W_{L_i} + \sum_{1}^{i-1} \Delta W_{L_i} \right) \right] C_{p_L} \Delta T_S \qquad (B9)$$

where the summation sign represents the quantity of liquid that was formed by condensation upstream of the increment. It was assumed that the change in temperature of the liquid from the beginning of the increment to the end of the increment was the same as the change in the saturation temperature. This temperature is represented by ΔT_S in equation (B9). The Q_{Gi} of equation (B7) represents the decrease in the enthalpy of the vapour in the increment and is given by:

$$Q_{Gi} = \left[W_T - \left(\tfrac{1}{2} \Delta W_{L_i} + \sum_{1}^{i-1} \Delta W_{L_i} \right) \right] C_{p_G} \Delta T_S \qquad (B10)$$

Substituting equations (B8),(B9) and (B10) into equation (B7), rearranging, and using the measured local heat flux, q, result in the following expression for the rate of liquid formation in the increment:

$$\Delta W_{L_i} = \frac{(\pi D_i \Delta Z) q_i - \Delta T_S \left[(C_{p_L} - C_{p_G}) \sum_{1}^{i-1} \Delta W_{L_i} + C_{p_G} W_T \right]}{h_{fg} + \frac{1}{2} \Delta T_S (C_{p_L} - C_{p_G})} \qquad \text{(B11)}$$

for small variation in the condensing pressure equation (B11) reduces to

$$\Delta W_{L_i} = (\pi D_i \Delta Z) q_i / h_{fg} \qquad \text{(B12)}$$

The local vapour flow rate was determined by subtracting the local condensate flow rate from the total measured flow rate as follows:

$$W_{G_i} = W_T - \sum_{1}^{i} \Delta W_{L_i} \qquad \text{(B13)}$$

The local steam quality was calculated as follows:

$$x_i = W_{G_i} / W_T \qquad \text{(B14)}$$

The local condensate flow rate is used to define a local condensate Reynolds number by

$$Re_{L_i} = \frac{4 W_{L_i}}{\pi D_i \mu_\ell} \qquad \text{(B15)}$$

It is important to point out that the above calculation procedure for local flow rates assumes that all the liquid flows in the annular film.

3. Local wall and interfacial shear stresses

The local wall and interfacial shear stresses were calculated from the momentum equations for the liquid phase and the steam phase as follows:

$$\tau_W = -\frac{R}{2}\left(\frac{dp}{dZ}\right)_{total} - \frac{1}{\pi D_i}\left(W_G \frac{dV_G}{dZ} + V_G \frac{dW_G}{dZ} + W_L \frac{dV_L}{dZ} + V_L \frac{dW_L}{dZ}\right) \quad \text{(B16)}$$

and

$$\tau_I = -\frac{R-\delta}{2}\left(\frac{dp}{dZ}\right)_{total} - \frac{1}{\pi(D_i-2\delta)}\left(W_G \frac{dV_G}{dZ} + V_G \frac{dW_G}{dZ} + 1.25 V_L \frac{dW_L}{dZ}\right) \quad \text{(B17)}$$

The term $(dp/dZ)_{total}$ was calculated from the measured pressure distribution along the tube length. It was assumed that the static pressure could be expressed as a fifth order function of Z, and constant for the function p(Z) were determined by applying the least square method to the eight static pressure data obtained in each test. Then $(dp/dZ)_{total}$ was obtained by differentiating p(Z).

In order to compute the momentum flux terms in equations (B16) and (B17) the average liquid and vapour velocities defined respectively by:

$$V_G = \frac{xW_T}{\rho_G \alpha A_T} \quad \text{(B18)}$$

and

$$V_L = \frac{(1-x)W_T}{\rho_L (1-\alpha) A_T} \quad \text{(B19)}$$

were required. All terms in equations B16, B17, B18 and B19 can be evaluated from known local quantities using the present method except for α. In order to obtain α in terms of known local quantities requires an empirical method. The empirical correlation for α of Smith (1969-70) was used as follows:

$$\alpha = \left\{1 + (\rho_G/\rho_L)\left(\frac{1-x}{x}\right)\left[0.4+0.6\sqrt{\frac{(\rho_L/\rho_G)+0.4(1-x)/x}{1+0.4(1-x)/x}}\right]\right\}^{-1} \quad \text{(B20)}$$

The value of liquid film thickness required in equation B17 was calculated from

$$\delta = R(1 - \sqrt{\alpha}) \quad \text{(B21)}$$

With the value of δ so calculated the Reynolds number for the vapour phase was defined as:

$$R_{e_G} = \frac{V_G(D_i - 2\delta)}{\nu_G} \qquad \text{(B22)}$$

The local wall and interfacial friction factors were defined as:

$$f_W = \tau_W / (\tfrac{1}{2}\rho_G V_G^2) \qquad \text{(B23)}$$

and

$$f_I = \tau_I / (\tfrac{1}{2}\rho_G V_G^2) \qquad \text{(B24)}$$

Once the wall shear stress has been computed it was of interest to calculate the Martinelli pressure parameters. These were computed from

$$X_{tt} = \left(\frac{W_L}{W_G}\right)^{0.9} \left(\frac{\mu_\ell}{\mu_G}\right)^{0.1} \left(\frac{\rho_G}{\rho_L}\right)^{0.5} \qquad \text{(B25)}$$

and

$$\phi_G = \sqrt{\tau_W/\tau_G} \qquad \text{(B26)}$$

where τ_G is the shear stress which would exist if the steam phase were assumed to flow alone. τ_G can be calculated according to Colburn's equation for a smooth tube as:

$$\tau_G = 0.023(D_i V_G/\nu_G)^{-0.2} \rho_G V_G^2 \qquad \text{(B27)}$$

APPENDIX C

Empirical equations for the transport and thermodynamic properties of saturated vapour and saturated liquid

For the two-phase system with condensing pure vapour, it was assumed that the two phases present are continuously in equilibrium at the saturation state of the respective phase.

Empirical functions may be used to represent the physical and thermodynamic properties of the pure saturated vapour and liquid over moderate pressure ranges. Some of the properties have been expressed by 8^{th} order logarithmic polynomial as a function of the saturation pressure as follows:

$$B^* = \sum_{K=0}^{K=8} A_K (\ell nP)^K \qquad (C1)$$

Table 1C shows the values of A_K for the corresponding properties and Figures 66 through 71 show typical results of the comparison between the calculated and tabulated values (1967 Steam Tables, The Electrical Research Association). Other properties have been expressed by a 5^{th} order polynomial as a function of the saturation pressure as follows:

$$D^* = \sum_{K=0}^{K=5} C_K P^K \qquad (C2)$$

Table 2C shows the values of C_K for the corresponding properties.

In addition, the viscosity of saturated liquid was calculated from

$$\mu_\ell \times 10^6 = 23.94 \times 10^{\left(\frac{248.37}{T_S + 133}\right)} \qquad (C3)$$

where T_S in ^oC and μ_ℓ in kg/m-s.

The surface tension was fitted to a second order polynomial as a function of the saturation temperature as follows

$$\sigma = 75.64 - 0.1391\ T_S - 0.0003\ T_S^2$$

where σ in N/m and T_S in ^oC.

T_S	h_L	h_{fg}
A_0 = 0.996327E 02	A_0 = 0.417516E 03	A_0 = 0.225792E 04
A_1 = 0.279568E 02	A_1 = 0.117906E 03	A_1 = -0.742758E 02
A_2 = 0.240251E 01	A_2 = 0.105898E 02	A_2 = -0.909945E 01
A_3 = 0.206036E 00	A_3 = 0.105940E 01	A_3 = -0.132658E 01
A_4 = 0.618418E-02	A_4 = 0.131209E 00	A_4 = -0.202712E 00
A_5 =-0.249131E-03	A_5 = 0.175151E-01	A_5 = -0.410571E-01
A_6 = 0.329173E-02	A_6 = -0.244458E-02	A_6 = -0.528206E-02
A_7 = 0.129126E-02	A_7 = -0.163587E-02	A_7 = 0.852176E-03
A_8 = 0.134748E-03	A_8 = -0.189092E-03	A_8 = 0.225853E-03

h_G	v_g	v_f
A_0 = 0.267542E 04	A_0 = 0.169361E 01	A_0 = 0.104336E-02
A_1 = 0.437071E 02	A_1 = -0.158541E 01	A_1 = 0.218518E-04
A_2 = 0.155794E 01	A_2 = 0.742383E 00	A_2 = 0.435857E-05
A_3 = -0.329715E 00	A_3 = -0.230492E 00	A_3 = 0.623349E-06
A_4 = -0.128900E 00	A_4 = 0.542381E-01	A_4 = 0.107910E-07
A_5 = -0.183520E-01	A_5 = -0.115617E-01	A_5 = -0.192049E-07
A_6 = 0.613253E-02	A_6 = 0.158872E-02	A_6 = 0.130490E-07
A_7 = 0.289520E-02	A_7 = 0.101415E-05	A_7 = 0.715115E-08
A_8 = 0.321030E-03	A_8 = 0.906249E-04	A_8 = 0.865755E-09

ρ_G	
A_0 = 0.590412E 00	
A_1 = 0.552436E 00	
A_2 = 0.258247E 00	
A_3 = 0.806075E-01	$0.02 < p < 5.0$ Bar
A_4 = 0.191524E-01	
A_5 = 0.384059E-02	
A_6 = 0.674333E-03	
A_7 = 0.876404E-04	
A_8 = 0.555125E-05	

TABLE 1C

C_{p_L}

C_0 = 0.417317E 01
C_1 = 0.655016E-01
C_2 =-0.315476E-01
C_3 = 0.143326E-01
C_4 = 0.320632E-02
C_5 = 0.263891E-03

C_{p_G}

C_0 = 0.187659E 01
C_1 = 0.183078E 00
C_2 = -0.781668E-01
C_3 = 0.323015E-01
C_4 = -0.704189E-02
C_5 = 0.600569E-03

$\mu_G \times 10^6$

C_0 = 9.88767
C_1 = 3.97708
C_2 = -2.90882
C_3 = 1.3102
C_4 = -0.292585
C_5 = 0.0248128

0.1574 < p < 4.155 Bar

TABLE 2C

APPENDIX D

CALIBRATION CURVES

CALIBRATION CURVE FOR
RA209212 ROTAMETER

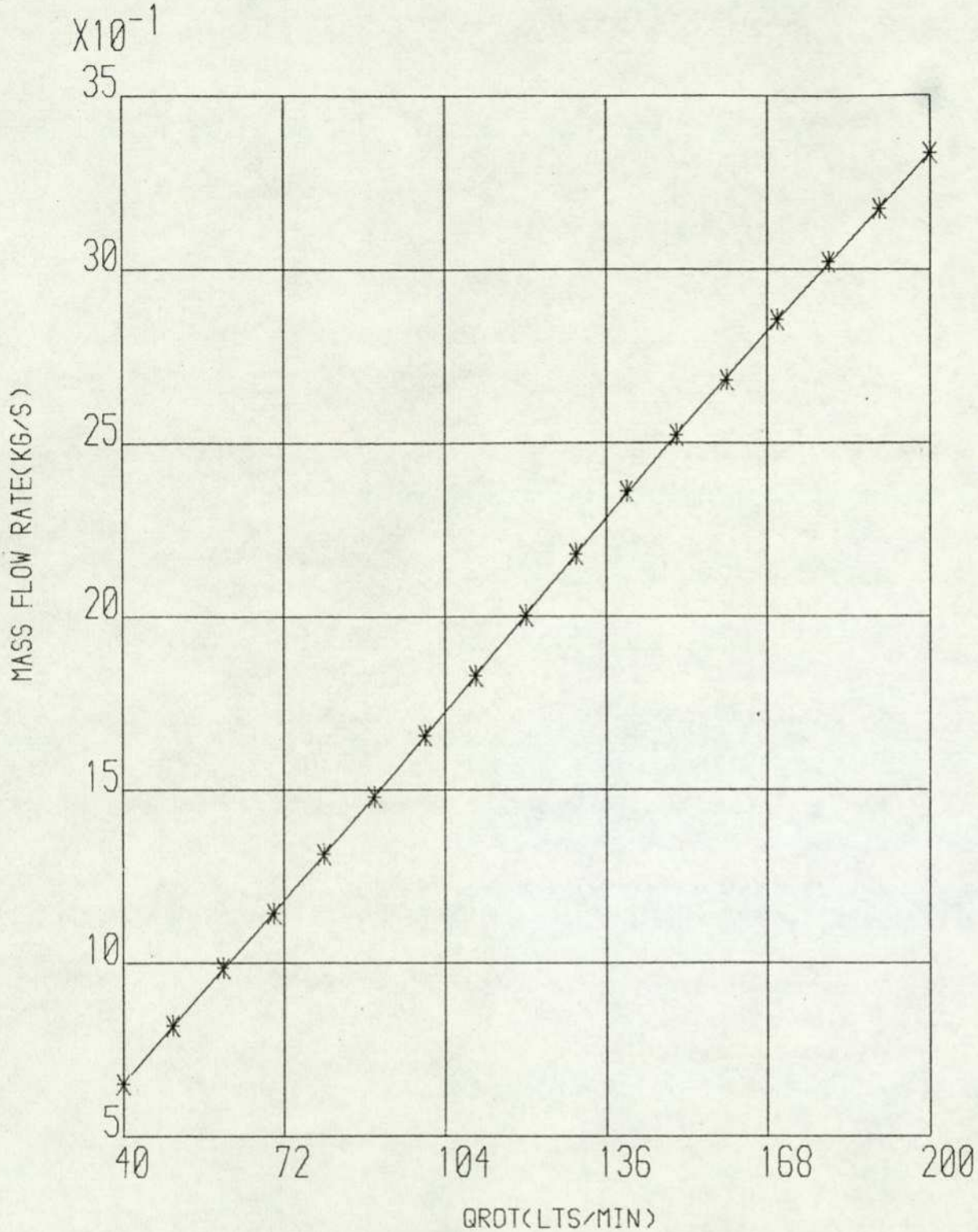

5th ORDER POLYNOMIAL COEFFICIENTS

A0= -.132570E 0
A1= .243320E -1
A2= -.182190E -3
A3= .191300E -5
A4= -.882530E -8
A5= .147090E-10

CALIBRATION CURVE FOR
11264-614 PRESSURE GAUGE

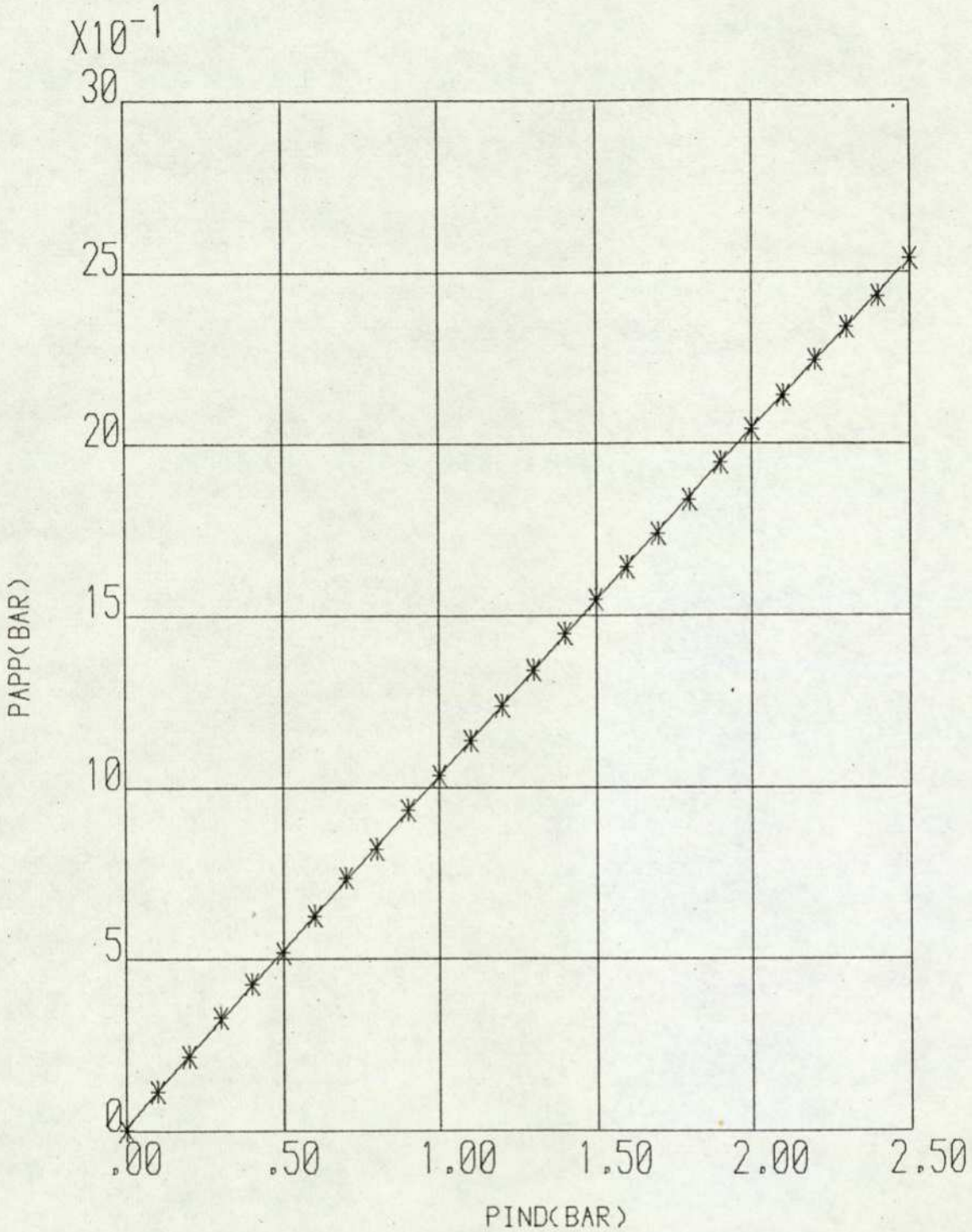

5th ORDER POLYNOMIAL COEFFICIENTS

A0= .745437E -2
A1= .107595E 1
A2= -.125112E 0
A3= .123974E 0
A4= -.552297E -1
A5= .862878E -2

CALIBRATION CURVE FOR
WALL TEMP 1 THERMOCOUPLE

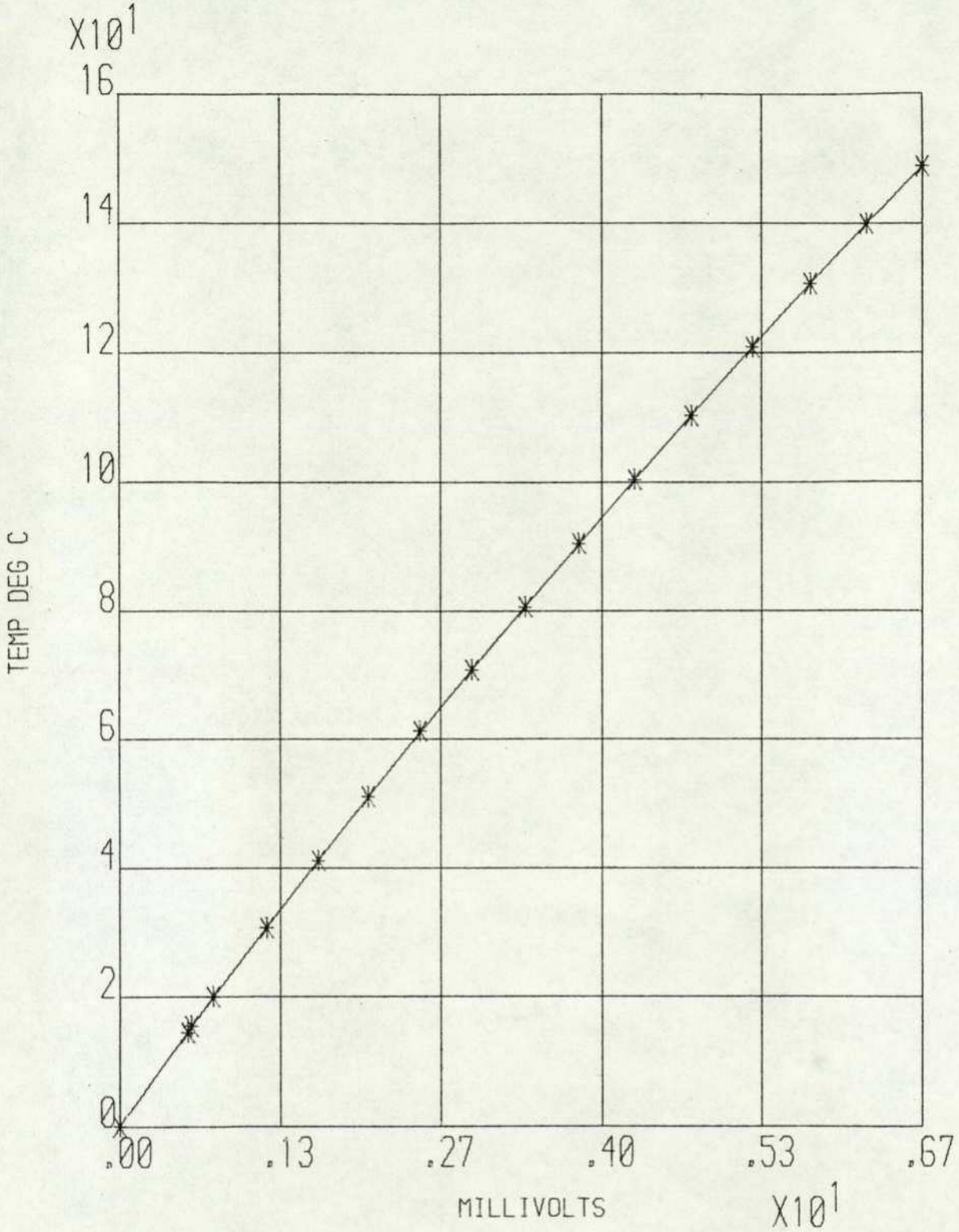

5th ORDER POLYNOMIAL COEFFICIENTS

A0= .198539E -1
A1= .260744E 2
A2= -.711029E 0
A3= .252387E -1
A4= .232162E -3
A5= -.102134E -3

TABLE 1. REDUCED EXPERIMENTAL DATA, RUN 1

AXIAL DISTANCE Z,M	STATIC PRESSURE P,BAR	SATURATION TEMPERATURE BASED ON P TS,C	COOLING WATER TEMPERATURE TCW,C	WALL TEMPERATURE TW,C	CONDITIONS
0.0	-	-	-	-	
0.04	1.3831	109.0	-	-	STEAM FLOW RATE
0.16	-	-	20.0	-	=487.0 KG/HR
0.31	-	-	-	77.5	MASS VELOCITY
0.4075	1.3778	108.8	-	-	=427120.0 KG/HR SQM
0.495	-	-	19.2	-	STEAM INLET VELOCITY
0.65	-	-	-	75.8	=137.0 M/S
0.77	1.3734	108.8	-	-	EXIT QUALITY
0.83	-	-	17.8	-	=0.6751
0.99	-	-	-	75.2	OVERALL PRESSURE DROP
1.0925	1.3669	108.6	-	-	=0.08210 BAR
1.165	-	-	16.6	-	COOLING WATER RATE
1.33	-	-	-	74.7	=5342.0 KG/HR
1.415	1.3592	108.4	-	-	HEAT BALANCE ERROR
1.5	-	-	15.9	-	= -2.1%
1.67	-	-	-	72.6	P IN TEST COND
1.835	-	-	14.3	-	=1.3831 BAR(ABS)
1.895	1.3475	108.2	-	-	TEMP IN CW
2.01	-	-	-	70.0	=11.0 C
2.17	-	-	12.6	-	TEMP RISE TEST COND
2.35	-	-	-	67.4	= 9.9 C
2.4275	1.3331	107.9	-	-	INLET QUALITY
2.505	-	-	11.5	-	=0.9200
2.69	-	-	-	69.8	
2.84	-	-	11.3	-	
2.96	1.3212	107.6	-	-	

TABLE 1. REDUCED EXPERIMENTAL DATA, RUN 2

AXIAL DISTANCE Z,M	STATIC PRESSURE P,BAR	SATURATION TEMPERATURE BASED ON P TS,C	COOLING WATER TEMPERATURE TCW,C	WALL TEMPERATURE TW,C	CONDITIONS
0.0	-	-	-	-	
0.04	1.3375	109.1	-	-	STEAM FLOW RATE
0.16	-	-	18.8	-	=501.4 KG/HR
0.31	-	-	-	76.1	MASS VELOCITY
0.4075	1.3328	109.0	-	-	=439783.0 KG/HR SQM
0.495	-	-	17.7	-	STEAM INLET VELOCITY
0.65	-	-	-	74.9	=137.0 M/S
0.77	1.3783	108.9	-	-	EXIT QUALITY
0.83	-	-	16.6	-	=0.6545
0.99	-	-	-	74.2	OVERALL PRESSURE DROP
1.0925	1.3720	108.7	-	-	=0.07310 BAR
1.165	-	-	15.3	-	COOLING WATER RATE
1.33	-	-	-	73.3	=7219.0 KG/HR
1.415	1.3642	108.6	-	-	HEAT BALANCE ERROR
1.5	-	-	14.5	-	= -2.1%
1.67	-	-	-	71.5	P IN TEST COND
1.835	-	-	14.3	-	=1.3875 BAR(ABS)
1.895	1.3524	108.3	-	-	TEMP IN CW
2.01	-	-	-	68.7	=11.0 C
2.17	-	-	13.3	-	TEMP RISE TEST COND
2.35	-	-	-	65.7	= 8.6 C
2.4275	1.3383	108.0	-	-	INLET QUALITY
2.505	-	-	12.3	-	=0.8900
2.69	-	-	-	69.2	
2.84	-	-	11.2	-	
2.96	1.3266	107.7	-	-	

TABLE 1. REDUCED EXPERIMENTAL DATA, RUN 3

AXIAL DISTANCE Z,M	STATIC PRESSURE P,BAR	SATURATION TEMPERATURE BASED ON P TS,C	COOLING WATER TEMPERATURE TCW,C	WALL TEMPERATURE TW,C	CONDITIONS
0.0	-	-	-	-	
0.04	1.3813	108.9	-	-	STEAM FLOW RATE
0.16	-	-	15.1	-	=495.4 KG/HR
0.31	-	-	-	74.0	MASS VELOCITY
0.4075	1.3767	108.8	-	-	=434502.0 KG/HR SQM
0.495	-	-	14.1	-	STEAM INLET VELOCITY
0.65	-	-	-	72.7	=132.0 M/S
0.77	1.3723	108.7	-	-	EXIT QUALITY
0.83	-	-	13.1	-	=0.6123
0.99	-	-	-	72.1	OVERALL PRESSURE DROP
1.0925	1.3660	108.6	-	-	=0.07450 BAR
1.165	-	-	12.4	-	COOLING WATER RATE
1.33	-	-	-	71.3	=9687.0 KG/HR
1.415	1.3581	108.4	-	-	HEAT BALANCE ERROR
1.5	-	-	11.8	-	= -2.8%
1.67	-	-	-	69.4	P IN TEST COND
1.835	-	-	11.5	-	=1.3813 BAR(ABS)
1.895	1.3466	108.2	-	-	TEMP IN CW
2.01	-	-	-	66.5	= 8.9 C
2.17	-	-	10.5	-	TEMP RISE TEST COND
2.35	-	-	-	63.8	= 6.9 C
2.4275	1.3328	107.9	-	-	INLET QUALITY
2.505	-	-	9.8	-	=0.8700
2.69	-	-	-	67.2	
2.84	-	-	9.1	-	
2.96	1.3215	107.6	-	-	

TABLE 1. REDUCED EXPERIMENTAL DATA, RUN 4

AXIAL DISTANCE Z,M	STATIC PRESSURE P,BAR	SATURATION TEMPERATURE BASED ON P TS,C	COOLING WATER TEMPERATURE TCW,C	WALL TEMPERATURE TW,C	CONDITIONS
0.0	-	-	-	-	
0.04	1.1806	104.3	-	-	STEAM FLOW RATE
0.16	-	-	15.6	-	=441.6 KG/HR
0.31	-	-	-	72.2	MASS VELOCITY
0.4075	1.1768	104.2	-	-	=387362.0 KG/HR SQM
0.495	-	-	14.4	-	STEAM INLET VELOCITY
0.65	-	-	-	71.4	=142.0 M/S
0.77	1.1729	104.2	-	-	EXIT QUALITY
0.83	-	-	13.8	-	=0.6630
0.99	-	-	-	70.1	OVERALL PRESSURE DROP
1.0925	1.1679	104.0	-	-	=0.06810 BAR
1.165	-	-	12.4	-	COOLING WATER RATE
1.33	-	-	-	69.6	=5342.0 KG/HR
1.415	1.1614	103.9	-	-	HEAT BALANCE ERROR
1.5	-	-	10.9	-	= 2.0%
1.67	-	-	-	67.0	P IN TEST COND
1.835	-	-	10.0	-	=1.1896 BAR(ABS)
1.895	1.1519	103.6	-	-	TEMP IN CW
2.01	-	-	-	65.2	= 5.8 C
2.17	-	-	8.8	-	TEMP RISE TEST COND
2.35	-	-	-	62.6	=11.3 C
2.4275	1.1403	103.3	-	-	INLET QUALITY
2.505	-	-	7.7	-	=0.9100
2.69	-	-	-	66.0	
2.84	-	-	6.6	-	
2.96	1.1307	103.1	-	-	

TABLE 1. REDUCED EXPERIMENTAL DATA, RUN 5

AXIAL DISTANCE Z,M	STATIC PRESSURE P,BAR	SATURATION TEMPERATURE BASED ON P TS,C	COOLING WATER TEMPERATURE TCW,C	WALL TEMPERATURE TW,C	CONDITIONS
0.0	-	-	-	-	
0.04	1.1769	104.3	-	-	STEAM FLOW RATE
0.16	-	-	14.1	-	=444.5 KG/HR
0.31	-	-	-	70.0	MASS VELOCITY
0.4075	1.1737	104.2	-	-	=389850.0 KG/HR SQM
0.495	-	-	13.0	-	STEAM INLET VELOCITY
0.65	-	-	-	69.4	=145.0 M/S
0.77	1.1701	104.1	-	-	EXIT QUALITY
0.83	-	-	12.4	-	=0.6545
0.99	-	-	-	68.4	OVERALL PRESSURE DROP
1.0925	1.1652	104.0	-	-	=0.06200 BAR
1.165	-	-	11.6	-	COOLING WATER RATE
1.33	-	-	-	68.1	=7219.0 KG/HR
1.415	1.1587	103.8	-	-	HEAT BALANCE ERROR
1.5	-	-	10.8	-	= -1.3%
1.67	-	-	-	66.1	P IN TEST COND
1.735	-	-	9.4	-	=1.1795 BAR(ABS)
1.895	1.1493	103.6	-	-	TEMP IN CW
2.01	-	-	-	63.7	= 6.6 C
2.17	-	-	8.5	-	TEMP RISE TEST COND
2.35	-	-	-	61.0	= 8.7 C
2.4275	1.1379	103.3	-	-	INLET QUALITY
2.505	-	-	7.7	-	=0.9200
2.69	-	-	-	64.0	
2.84	-	-	7.1	-	
2.96	1.1286	103.1	-	-	

TABLE 1. REDUCED EXPERIMENTAL DATA, RUN 6

AXIAL DISTANCE Z,M	STATIC PRESSURE P,BAR	SATURATION TEMPERATURE BASED ON P TS,C	COOLING WATER TEMPERATURE TCW,C	WALL TEMPERATURE TW,C	CONDITIONS
0.0	-	-	-	-	
0.04	1.1602	103.8	-	-	STEAM FLOW RATE
0.16	-	-	12.7	-	=445.0 KG/HR
0.31	-	-	-	69.2	MASS VELOCITY
0.4075	1.1572	103.8	-	-	=390314.0 KG/HR SQM
0.495	-	-	11.9	-	STEAM INLET VELOCITY
0.65	-	-	-	68.1	=144.0 M/S
0.77	1.1537	103.7	-	-	EXIT QUALITY
0.83	-	-	11.3	-	=0.6354
0.99	-	-	-	67.1	OVERALL PRESSURE DROP
1.0925	1.1490	103.6	-	-	=0.06420 BAR
1.165	-	-	10.6	-	COOLING WATER RATE
1.33	-	-	-	66.7	=9687.0 KG/HR
1.415	1.1426	103.4	-	-	HEAT BALANCE ERROR
1.5	-	-	10.0	-	= -2.3%
1.67	-	-	-	64.8	P IN TEST COND
1.835	-	-	9.4	-	=1.1640 BAR(ABS)
1.895	1.1333	103.2	-	-	TEMP IN CW
2.01	-	-	-	62.3	= 7.1 C
2.17	-	-	8.6	-	TEMP RISE TEST COND
2.35	-	-	-	59.6	= 6.4 C
2.4275	1.1223	102.9	-	-	INLET QUALITY
2.505	-	-	7.9	-	=0.9000
2.69	-	-	-	62.4	
2.84	-	-	7.3	-	
2.96	1.1133	102.7	-	-	

TABLE 1. REDUCED EXPERIMENTAL DATA, RUN 7

AXIAL DISTANCE Z,M	STATIC PRESSURE P,BAR	SATURATION TEMPERATURE BASED ON P TS,C	COOLING WATER TEMPERATURE TCW,C	WALL TEMPERATURE TW,C	CONDITIONS
0.0	-	-	-	-	
0.04	1.6103	113.5	-	-	STEAM FLOW RATE
0.16	-	-	16.3	-	=551.7 KG/HR
0.31	-	-	-	79.2	MASS VELOCITY
0.4075	1.6031	113.4	-	-	=483930.0 KG/HR SQM
0.495	-	-	14.9	-	STEAM INLET VELOCITY
0.65	-	-	-	77.7	=131.0 M/S
0.77	1.5964	113.3	-	-	EXIT QUALITY
0.83	-	-	13.8	-	=0.6540
0.99	-	-	-	77.4	OVERALL PRESSURE DROP
1.0925	1.5889	113.1	-	-	=0.09750 BAR
1.165	-	-	12.5	-	COOLING WATER RATE
1.33	-	-	-	76.6	=5342.0 KG/HR
1.415	1.5798	112.9	-	-	HEAT BALANCE ERROR
1.5	-	-	11.1	-	= -1.4%
1.67	-	-	-	74.3	P IN TEST COND
1.835	-	-	10.0	-	=1.5949 BAR(ABS)
1.895	1.5662	112.7	-	-	TEMP IN CW
2.01	-	-	-	71.8	= 5.8 C
2.17	-	-	8.6	-	TEMP RISE TEST COND
2.35	-	-	-	68.5	=11.8 C
2.4275	1.5500	112.4	-	-	INLET QUALITY
2.505	-	-	7.4	-	=0.8700
2.69	-	-	-	71.5	
2.84	-	-	6.3	-	
2.96	1.5361	112.1	-	-	

TABLE 1. REDUCED EXPERIMENTAL DATA, RUN 8

AXIAL DISTANCE Z,M	STATIC PRESSURE P,BAR	SATURATION TEMPERATURE BASED ON P TS,C	COOLING WATER TEMPERATURE TCW,C	WALL TEMPERATURE TW,C	CONDITIONS
0.0	-	-	-	-	
0.04	1.6373	114.0	-	-	STEAM FLOW RATE
0.16	-	-	14.5	-	=560.7 KG/HR
0.31	-	-	-	77.5	MASS VELOCITY
0.4075	1.6303	113.9	-	-	=491831.0 KG/HR SQM
0.495	-	-	13.4	-	STEAM INLET VELOCITY
0.65	-	-	-	77.0	=132.0 M/S
0.77	1.6236	113.8	-	-	EXIT QUALITY
0.83	-	-	12.5	-	=0.6620
0.99	-	-	-	76.0	OVERALL PRESSURE DROP
1.0925	1.6160	113.6	-	-	=0.10590 BAR
1.165	-	-	11.5	-	COOLING WATER RATE
1.33	-	-	-	75.2	=7219.0 KG/HR
1.415	1.6068	113.5	-	-	HEAT BALANCE ERROR
1.5	-	-	10.2	-	= 0.3%
1.67	-	-	-	72.8	P IN TEST COND
1.835	-	-	9.4	-	=1.6540 BAR(ABS)
1.895	1.5933	113.2	-	-	TEMP IN CW
2.01	-	-	-	70.2	= 5.8 C
2.17	-	-	8.3	-	TEMP RISE TEST COND
2.35	-	-	-	66.6	= 9.5 C
2.4275	1.5771	112.9	-	-	INLET QUALITY
2.505	-	-	7.1	-	=0.8900
2.69	-	-	-	70.1	
2.84	-	-	6.3	-	
2.96	1.5633	112.6	-	-	

TABLE 1. REDUCED EXPERIMENTAL DATA, RUN 9

AXIAL DISTANCE Z,M	STATIC PRESSURE P,BAR	SATURATION TEMPERATURE BASED ON P TS,C	COOLING WATER TEMPERATURE TCW,C	WALL TEMPERATURE TW,C	CONDITIONS
0.0	-	-	-	-	
0.04	1.6232	113.8	-	-	STEAM FLOW RATE
0.16	-	-	12.6	-	=563.5 KG/HR
0.31	-	-	-	75.9	MASS VELOCITY
0.4075	1.6162	113.6	-	-	=498687.0 KG/HR SQM
0.495	-	-	11.6	-	STEAM INLET VELOCITY
0.65	-	-	-	75.1	=131.5 M/S
0.77	1.6095	113.5	-	-	EXIT QUALITY
0.83	-	-	11.1	-	=0.6436
0.99	-	-	-	74.3	OVERALL PRESSURE DROP
1.0925	1.6018	113.4	-	-	=0.10020 BAR
1.165	-	-	10.2	-	COOLING WATER RATE
1.33	-	-	-	73.5	=9687.0 KG/HR
1.415	1.5927	113.2	-	-	HEAT BALANCE ERROR
1.5	-	-	9.2	-	= 0.7%
1.67	-	-	-	71.1	P IN TEST COND
1.835	-	-	8.6	-	=1.6489 BAR(ABS)
1.895	1.5792	112.9	-	-	TEMP IN CW
2.01	-	-	-	68.5	= 5.8 C
2.17	-	-	7.7	-	TEMP RISE TEST COND
2.35	-	-	-	65.0	= 7.5 C
2.4275	1.5628	112.6	-	-	INLET QUALITY
2.505	-	-	6.8	-	=0.8800
2.69	-	-	-	68.6	
2.84	-	-	6.2	-	
2.96	1.5490	112.3	-	-	

TABLE 1. REDUCED EXPERIMENTAL DATA, RUN 10

AXIAL DISTANCE Z,M	STATIC PRESSURE P,BAR	SATURATION TEMPERATURE BASED ON P TS,C	COOLING WATER TEMPERATURE TCW,C	WALL TEMPERATURE TW,C	CONDITIONS
0.0	-	-	-	-	
0.04	1.5603	112.6	-	-	STEAM FLOW RATE
0.16	-	-	18.0	-	=539.6 KG/HR
0.31	-	-	-	79.2	MASS VELOCITY
0.4075	1.5537	112.4	-	-	=473326.0 KG/HR SQM
0.495	-	-	16.9	-	STEAM INLET VELOCITY
0.65	-	-	-	77.9	=119.4 M/S
0.77	1.5480	112.3	-	-	EXIT QUALITY
0.83	-	-	15.6	-	=0.5936
0.99	-	-	-	76.9	OVERALL PRESSURE DROP
1.0925	1.5409	112.2	-	-	=0.08480 BAR
1.165	-	-	13.9	-	COOLING WATER RATE
1.33	-	-	-	76.0	=5342.0 KG/HR
1.415	1.5321	112.0	-	-	HEAT BALANCE ERROR
1.5	-	-	12.5	-	= 0. %
1.67	-	-	-	74.4	P IN TEST COND
1.835	-	-	12.2	-	=1.5668 BAR(ABS)
1.895	1.5190	111.8	-	-	TEMP IN CW
2.01	-	-	-	71.9	= 7.6 C
2.17	-	-	10.5	-	TEMP RISE TEST COND
2.35	-	-	-	69.0	=11.7 C
2.4275	1.5031	111.4	-	-	INLET QUALITY
2.505	-	-	9.2	-	=0.8100
2.69	-	-	-	72.3	
2.84	-	-	8.1	-	
2.96	1.4895	111.2	-	-	

TABLE 1. REDUCED EXPERIMENTAL DATA, RUN 11

AXIAL DISTANCE Z,M	STATIC PRESSURE P,BAR	SATURATION TEMPERATURE BASED ON P TS,C	COOLING WATER TEMPERATURE TCW,C	WALL TEMPERATURE TW,C	CONDITIONS
0.0	-	-	-	-	
0.04	1.5478	112.3	-	-	STEAM FLOW RATE
0.16	-	-	15.8	-	=544.6 KG/HR
0.31	-	-	-	75.4	MASS VELOCITY
0.4075	1.5419	112.2	-	-	=477713.0 KG/HR SQM
0.495	-	-	14.8	-	STEAM INLET VELOCITY
0.65	-	-	-	75.1	=120.0 M/S
0.77	1.5364	112.1	-	-	EXIT QUALITY
0.83	-	-	14.0	-	=0.5630
0.99	-	-	-	74.3	OVERALL PRESSURE DROP
1.0925	1.5294	112.0	-	-	=0.08280 BAR
1.165	-	-	13.1	-	COOLING WATER RATE
1.33	-	-	-	73.5	=9687.0 KG/HR
1.415	1.5206	111.8	-	-	HEAT BALANCE ERROR
1.5	-	-	12.3	-	= 0. %
1.67	-	-	-	71.3	P IN TEST COND
1.835	-	-	12.0	-	=1.5497 BAR(ABS)
1.895	1.5080	111.5	-	-	TEMP IN CW
2.01	-	-	-	68.9	= 9.2 C
2.17	-	-	10.8	-	TEMP RISE TEST COND
2.35	-	-	-	66.0	= 7.1 C
2.4275	1.4928	111.2	-	-	INLET QUALITY
2.505	-	-	10.1	-	=0.8000
2.69	-	-	-	69.3	
2.84	-	-	9.4	-	
2.96	1.4799	111.0	-	-	

TABLE 1. REDUCED EXPERIMENTAL DATA, RUN 12

AXIAL DISTANCE Z,M	STATIC PRESSURE P,BAR	SATURATION TEMPERATURE BASED ON P TS,C	COOLING WATER TEMPERATURE TCW,C	WALL TEMPERATURE TW,C	CONDITIONS
0.0	-	-	-	-	
0.04	0.7914	93.2	-	-	STEAM FLOW RATE
0.16	-	-	13.7	-	=323.9 KG/HR
0.31	-	-	-	64.4	MASS VELOCITY
0.4075	0.7889	93.1	-	-	=284109.0 KG/HR SQM
0.495	-	-	12.4	-	STEAM INLET VELOCITY
0.65	-	-	-	63.1	=143.3 M/S
0.77	0.7877	93.1	-	-	EXIT QUALITY
0.83	-	-	11.5	-	=0.5664
0.99	-	-	-	62.2	OVERALL PRESSURE DROP
1.1925	0.7851	93.0	-	-	=0.04790 BAR
1.165	-	-	10.4	-	COOLING WATER RATE
1.33	-	-	-	61.8	=5342.0 KG/HR
1.415	0.7812	92.9	-	-	HEAT BALANCE ERROR
1.5	-	-	9.5	-	= -5.5%
1.67	-	-	-	59.4	P IN TEST COND
1.835	-	-	8.0	-	=0.7952 BAR(ABS)
1.895	0.7749	92.7	-	-	TEMP IN CW
2.01	-	-	-	57.6	= 5.3 C
2.17	-	-	6.6	-	TEMP RISE TEST COND
2.35	-	-	-	55.4	= 9.5 C
2.4275	0.7674	92.4	-	-	INLET QUALITY
2.505	-	-	5.7	-	=0.8600
2.69	-	-	-	58.1	
2.84	-	-	5.5	-	
2.96	0.7595	92.1	-	-	

TABLE 1. REDUCED EXPERIMENTAL DATA, RUN 13

AXIAL DISTANCE Z,M	STATIC PRESSURE P,BAR	SATURATION TEMPERATURE BASED ON P TS,C	COOLING WATER TEMPERATURE TCW,C	WALL TEMPERATURE TW,C	CONDITIONS
0.0	-	-	-	-	
0.04	0.7366	93.1	-	-	STEAM FLOW RATE
0.16	-	-	10.8	-	=328.4 KG/HR
0.31	-	-	-	61.5	MASS VELOCITY
0.4075	0.7643	93.0	-	-	=288039.0 KG/HR SQM
0.495	-	-	9.9	-	STEAM INLET VELOCITY
0.65	-	-	-	60.1	=150.3 M/S
0.77	0.7840	93.0	-	-	EXIT QUALITY
0.83	-	-	9.3	-	=0.5471
0.99	-	-	-	59.7	OVERALL PRESSURE DROP
1.0925	0.7814	92.9	-	-	=0.04620 BAR
1.165	-	-	8.5	-	COOLING WATER RATE
1.33	-	-	-	58.5	=9687.0 KG/HR
1.415	0.7773	92.8	-	-	HEAT BALANCE ERROR
1.5	-	-	7.7	-	= -1.0%
1.67	-	-	-	56.8	P IN TEST COND
1.835	-	-	7.6	-	=0.7891 BAR(ABS)
1.895	0.7713	92.5	-	-	TEMP IN CW
2.01	-	-	-	54.7	= 5.3 C
2.17	-	-	7.0	-	TEMP RISE TEST COND
2.35	-	-	-	52.9	= 6.2 C
2.4275	0.7639	92.3	-	-	INLET QUALITY
2.505	-	-	6.2	-	=0.8850
2.69	-	-	-	55.2	
2.84	-	-	5.5	-	
2.96	0.7560	92.0	-	-	

TABLE 1. REDUCED EXPERIMENTAL DATA, RUN 14

AXIAL DISTANCE Z,M	STATIC PRESSURE P,BAR	SATURATION TEMPERATURE BASED ON P TS,C	COOLING WATER TEMPERATURE TCW,C	WALL TEMPERATURE TW,C	CONDITIONS
0.0	-	-	-	-	
0.04	0.5699	84.6	-	-	STEAM FLOW RATE
0.16	-	-	12.1	-	=252.7 KG/HR
0.31	-	-	-	57.8	MASS VELOCITY
0.4075	0.5632	84.6	-	-	=221618.0 KG/HR SQM
0.495	-	-	11.1	-	STEAM INLET VELOCITY
0.65	-	-	-	56.4	=176.0 M/S
0.77	0.5686	84.6	-	-	EXIT QUALITY
0.83	-	-	10.2	-	=0.6785
0.99	-	-	-	56.0	OVERALL PRESSURE DROP
1.0925	0.5674	84.5	-	-	=0.03590 BAR
1.165	-	-	9.2	-	COOLING WATER RATE
1.33	-	-	-	54.9	=5342.0 KG/HR
1.415	0.5653	84.4	-	-	HEAT BALANCE ERROR
1.5	-	-	8.0	-	= 1.5%
1.67	-	-	-	53.5	P IN TEST COND
1.835	-	-	7.9	-	=0.5711 BAR(ABS)
1.895	0.5612	84.3	-	-	TEMP IN CW
2.01	-	-	-	51.3	= 4.5 C
2.17	-	-	6.7	-	TEMP RISE TEST COND
2.35	-	-	-	49.7	= 8.5 C
2.4275	0.5573	84.1	-	-	INLET QUALITY
2.505	-	-	5.8	-	=1.0000
2.69	-	-	-	51.3	
2.84	-	-	5.0	-	
2.96	0.5515	83.8	-	-	

TABLE 1. REDUCED EXPERIMENTAL DATA, RUN 15

AXIAL DISTANCE Z,M	STATIC PRESSURE P,BAR	SATURATION TEMPERATURE BASED ON P TS,C	COOLING WATER TEMPERATURE TCW,C	WALL TEMPERATURE TW,C	CONDITIONS
0.0	-	-	-	-	
0.04	0.5615	84.3	-	-	STEAM FLOW RATE
0.16	-	-	10.3	-	=255.3 KG/HR
0.31	-	-	-	56.4	MASS VELOCITY
0.4075	0.5610	84.2	-	-	=223968.0 KG/HR SQM
0.495	-	-	9.4	-	STEAM INLET VELOCITY
0.65	-	-	-	55.0	=181.0 M/S
0.77	0.5615	84.3	-	-	EXIT QUALITY
0.83	-	-	8.9	-	=0.6517
0.99	-	-	-	54.6	OVERALL PRESSURE DROP
1.0925	0.5604	84.2	-	-	=0.03330 BAR
1.165	-	-	8.0	-	COOLING WATER RATE
1.33	-	-	-	53.7	=7219.0 KG/HR
1.415	0.5586	84.1	-	-	HEAT BALANCE ERROR
1.5	-	-	7.1	-	= -1.0%
1.67	-	-	-	52.0	P IN TEST COND
1.835	-	-	6.9	-	=0.5615 BAR(ABS)
1.895	0.5553	84.0	-	-	TEMP IN CW
2.01	-	-	-	49.6	= 4.5 C
2.17	-	-	6.0	-	TEMP RISE TEST COND
2.35	-	-	-	48.0	= 6.7 C
2.4275	0.5513	83.9	-	-	INLET QUALITY
2.505	-	-	5.3	-	=1.0000
2.69	-	-	-	49.8	
2.84	-	-	4.7	-	
2.96	0.5459	83.5	-	-	

TABLE 1. REDUCED EXPERIMENTAL DATA, RUN 16

AXIAL DISTANCE Z,M	STATIC PRESSURE P,BAR	SATURATION TEMPERATURE BASED ON P TS,C	COOLING WATER TEMPERATURE TCW,C	WALL TEMPERATURE TW,C	CONDITIONS
0.0	-	-	-	-	
0.04	0.5395	83.2	-	-	STEAM FLOW RATE
0.16	-	-	9.1	-	=252.7 KG/HR
0.31	-	-	-	54.5	MASS VELOCITY
0.4075	0.5389	83.2	-	-	=221655.0 KG/HR SQM
0.495	-	-	8.4	-	STEAM INLET VELOCITY
0.65	-	-	-	53.0	=186.0 M/S
0.77	0.5395	83.2	-	-	EXIT QUALITY
0.83	-	-	8.0	-	=0.6388
0.99	-	-	-	52.8	OVERALL PRESSURE DROP
1.0925	0.5388	83.2	-	-	=0.04880 BAR
1.165	-	-	7.2	-	COOLING WATER RATE
1.33	-	-	-	51.5	=9687.0 KG/HR
1.415	0.5371	83.1	-	-	HEAT BALANCE ERROR
1.5	-	-	6.4	-	= -5.7%
1.67	-	-	-	50.0	P IN TEST COND
1.835	-	-	6.3	-	=0.5601 BAR(ABS)
1.895	0.5342	83.0	-	-	TEMP IN CW
2.01	-	-	-	47.8	= 4.8 C
2.17	-	-	6.0	-	TEMP RISE TEST COND
2.35	-	-	-	46.1	= 4.9 C
2.4275	0.5303	82.8	-	-	INLET QUALITY
2.505	-	-	5.3	-	=1.0000
2.69	-	-	-	48.0	
2.84	-	-	4.7	-	
2.96	0.5242	82.5	-	-	

TABLE 1. REDUCED EXPERIMENTAL DATA, RUN 17

AXIAL DISTANCE Z,M	STATIC PRESSURE P,BAR	SATURATION TEMPERATURE BASED ON P TS,C	COOLING WATER TEMPERATURE TCW,C	WALL TEMPERATURE TW,C	CONDITIONS
0.0	-	-	-	-	
0.04	0.3354	71.7	-	-	STEAM FLOW RATE
0.16	-	-	11.8	-	=157.6 KG/HR
0.31	-	-	-	48.6	MASS VELOCITY
0.4075	0.3361	71.8	-	-	=138234.0 KG/HR SQM
0.495	-	-	11.1	-	STEAM INLET VELOCITY
0.65	-	-	-	46.5	=181.0 M/S
0.77	0.3369	71.8	-	-	EXIT QUALITY
0.83	-	-	10.3	-	=0.5705
0.99	-	-	-	46.0	OVERALL PRESSURE DROP
1.0925	0.3364	71.8	-	-	=0.01670 BAR
1.165	-	-	9.8	-	COOLING WATER RATE
1.33	-	-	-	45.2	=7219.0 KG/HR
1.415	0.3367	71.8	-	-	HEAT BALANCE ERROR
1.5	-	-	9.3	-	= -1.7%
1.67	-	-	-	44.0	P IN TEST COND
1.835	-	-	9.1	-	=0.3400 BAR(ABS)
1.895	0.3370	71.8	-	-	TEMP IN CW
2.01	-	-	-	42.3	= 7.4 C
2.17	-	-	8.8	-	TEMP RISE TEST COND
2.35	-	-	-	40.6	= 5.1 C
2.4275	0.3376	71.9	-	-	INLET QUALITY
2.505	-	-	8.3	-	=1.0000
2.69	-	-	-	41.7	
2.84	-	-	7.7	-	
2.96	0.3329	71.5	-	-	

TABLE 1. REDUCED EXPERIMENTAL DATA, RUN 18

AXIAL DISTANCE Z,M	STATIC PRESSURE P,BAR	SATURATION TEMPERATURE BASED ON P TS,C	COOLING WATER TEMPERATURE TCW,C	WALL TEMPERATURE TW,C	CONDITIONS
0.0	-	-	-	-	
0.04	0.3294	71.3	-	-	STEAM FLOW RATE
0.16	-	-	12.7	-	=153.0 KG/HR
0.31	-	-	-	48.4	MASS VELOCITY
0.4075	0.3301	71.3	-	-	=134200.0 KG/HR SQM
0.495	-	-	12.0	-	STEAM INLET VELOCITY
0.65	-	-	-	46.4	=178.6 M/S
0.77	0.3310	71.4	-	-	EXIT QUALITY
0.83	-	-	11.6	-	=0.5232
0.99	-	-	-	45.9	OVERALL PRESSURE DROP
1.0925	0.3313	71.4	-	-	=0.01930 BAR
1.165	-	-	11.1	-	COOLING WATER RATE
1.33	-	-	-	45.2	=9687.0 KG/HR
1.415	0.3316	71.4	-	-	HEAT BALANCE ERROR
1.5	-	-	10.8	-	= -2.5%
1.67	-	-	-	43.8	P IN TEST COND
1.835	-	-	10.7	-	=0.3487 BAR(ABS)
1.895	0.3320	71.5	-	-	TEMP IN CW
2.01	-	-	-	42.3	= 9.2 C
2.17	-	-	10.2	-	TEMP RISE TEST COND
2.35	-	-	-	40.7	= 4.1 C
2.4275	0.3325	71.5	-	-	INLET QUALITY
2.505	-	-	9.7	-	=1.0000
2.69	-	-	-	41.9	
2.84	-	-	9.3	-	
2.96	0.3279	71.2	-	-	

TABLE 1. REDUCED EXPERIMENTAL DATA, RUN 19

AXIAL DISTANCE Z,M	STATIC PRESSURE P,BAR	SATURATION TEMPERATURE BASED ON P TS,C	COOLING WATER TEMPERATURE TCW,C	WALL TEMPERATURE TW,C	CONDITIONS
0.0	-	-	-	-	
0.04	0.3924	75.4	-	-	STEAM FLOW RATE
0.16	-	-	11.5	-	=261.0 KG/HR
0.31	-	-	-	49.2	MASS VELOCITY
0.4075	0.3904	75.3	-	-	=228929.0 KG/HR SQM
0.495	-	-	10.8	-	STEAM INLET VELOCITY
0.65	-	-	-	48.2	=179.0 M/S
0.77	0.3391	75.2	-	-	EXIT QUALITY
0.83	-	-	10.3	-	=0.4112
0.99	-	-	-	47.5	OVERALL PRESSURE DROP
1.0925	0.3380	75.1	-	-	=0.02050 BAR
1.165	-	-	9.8	-	COOLING WATER RATE
1.33	-	-	-	46.9	=8471.0 KG/HR
1.415	0.3368	75.1	-	-	HEAT BALANCE ERROR
1.5	-	-	9.3	-	= -3.7%
1.67	-	-	-	45.4	P IN TEST COND
1.835	-	-	9.0	-	=0.3924 BAR(ABS)
1.895	0.3858	75.0	-	-	TEMP IN CW
2.01	-	-	-	43.4	= 7.4 C
2.17	-	-	8.5	-	TEMP RISE TEST COND
2.35	-	-	-	41.6	= 4.6 C
2.4275	0.3856	75.0	-	-	INLET QUALITY
2.505	-	-	7.9	-	=0.6900
2.69	-	-	-	42.9	
2.84	-	-	7.5	-	
2.96	0.3814	74.7	-	-	

TABLE 1. REDUCED EXPERIMENTAL DATA, RUN 20

AXIAL DISTANCE Z,M	STATIC PRESSURE P,BAR	SATURATION TEMPERATURE BASED ON P TS,C	COOLING WATER TEMPERATURE TCW,C	WALL TEMPERATURE TW,C	CONDITIONS
0.0	-	-	-	-	
0.04	0.3963	75.7	-	-	STEAM FLOW RATE
0.16	-	-	11.9	-	=258.0 KG/HR
0.31	-	-	-	49.7	MASS VELOCITY
0.4075	0.3943	75.5	-	-	=226298.0 KG/HR SQM
0.495	-	-	11.1	-	STEAM INLET VELOCITY
0.65	-	-	-	48.6	=176.5 M/S
0.77	0.3930	75.5	-	-	EXIT QUALITY
0.83	-	-	10.6	-	=0.4306
0.99	-	-	-	47.8	OVERALL PRESSURE DROP
1.0925	0.3917	75.4	-	-	=0.02310 BAR
1.165	-	-	10.1	-	COOLING WATER RATE
1.33	-	-	-	47.2	=7219.0 KG/HR
1.415	0.3905	75.3	-	-	HEAT BALANCE ERROR
1.5	-	-	9.5	-	= -2.5%
1.67	-	-	-	46.0	P IN TEST COND
1.835	-	-	9.4	-	=0.3963 BAR(ABS)
1.895	0.3895	75.2	-	-	TEMP IN CW
2.01	-	-	-	44.0	= 7.4 C
2.17	-	-	8.6	-	TEMP RISE TEST COND
2.35	-	-	-	42.3	= 5.1 C
2.4275	0.3890	75.2	-	-	INLET QUALITY
2.505	-	-	8.2	-	=0.6950
2.69	-	-	-	43.6	
2.84	-	-	7.5	-	
2.96	0.3847	74.9	-	-	

TABLE 1. REDUCED EXPERIMENTAL DATA, RUN 21

AXIAL DISTANCE Z,M	STATIC PRESSURE P,BAR	SATURATION TEMPERATURE BASED ON P TS,C	COOLING WATER TEMPERATURE TCW,C	WALL TEMPERATURE TW,C	CONDITIONS
0.0	-	-	-	-	
0.04	1.1684	104.0	-	-	STEAM FLOW RATE
0.16	-	-	17.7	-	=487.7 KG/HR
0.31	-	-	-	71.0	MASS VELOCITY
0.4075	1.1612	103.9	-	-	=427754.0 KG/HR SQM
0.495	-	-	16.5	-	STEAM INLET VELOCITY
0.65	-	-	-	69.4	= 97.0 M/S
0.77	1.1557	103.7	-	-	EXIT QUALITY
0.83	-	-	15.7	-	=0.3377
0.99	-	-	-	69.1	OVERALL PRESSURE DROP
1.0925	1.1506	103.6	-	-	=0.06540 BAR
1.165	-	-	14.7	-	COOLING WATER RATE
1.33	-	-	-	68.2	=7219.0 KG/HR
1.415	1.1454	103.5	-	-	HEAT BALANCE ERROR
1.5	-	-	13.8	-	= 0.2%
1.67	-	-	-	66.3	P IN TEST COND
1.835	-	-	13.5	-	=1.1684 BAR(ABS)
1.895	1.1385	103.3	-	-	TEMP IN CW
2.01	-	-	-	63.6	=10.5 C
2.17	-	-	12.5	-	TEMP RISE TEST COND
2.35	-	-	-	61.6	= 7.9 C
2.4275	1.1314	103.1	-	-	INLET QUALITY
2.505	-	-	11.5	-	=0.5500
2.69	-	-	-	63.9	
2.84	-	-	10.8	-	
2.96	1.1270	103.0	-	-	

TABLE 1. REDUCED EXPERIMENTAL DATA, RUN 22

AXIAL DISTANCE Z,M	STATIC PRESSURE P,BAR	SATURATION TEMPERATURE BASED ON P TS,C	COOLING WATER TEMPERATURE TCW,C	WALL TEMPERATURE TW,C	CONDITIONS
0.0	-	-	-	-	
0.04	1.1629	103.9	-	-	STEAM FLOW RATE
0.16	-	-	16.6	-	=482.2 KG/HR
0.31	-	-	-	70.2	MASS VELOCITY
0.4075	1.1557	103.7	-	-	=422989.0 KG/HR SQM
0.495	-	-	15.7	-	STEAM INLET VELOCITY
0.65	-	-	-	68.9	= 98.0 M/S
0.77	1.1503	103.6	-	-	EXIT QUALITY
0.83	-	-	15.0	-	=0.3343
0.99	-	-	-	68.2	OVERALL PRESSURE DROP
1.0925	1.1452	103.5	-	-	=0.06290 BAR
1.165	-	-	14.4	-	COOLING WATER RATE
1.33	-	-	-	67.7	=8471.0 KG/HR
1.415	1.1399	103.3	-	-	HEAT BALANCE ERROR
1.5	-	-	13.3	-	= -1.2%
1.67	-	-	-	65.7	P IN TEST COND
1.835	-	-	12.9	-	=1.1654 BAR(ABS)
1.895	1.1331	103.2	-	-	TEMP IN CW
2.01	-	-	-	63.1	=10.5 C
2.17	-	-	12.1	-	TEMP RISE TEST COND
2.35	-	-	-	61.0	= 6.9 C
2.4275	1.1262	103.0	-	-	INLET QUALITY
2.505	-	-	11.3	-	=0.5600
2.69	-	-	-	63.2	
2.84	-	-	10.7	-	
2.96	1.1221	102.9	-	-	

TABLE 1. REDUCED EXPERIMENTAL DATA, RUN 23

AXIAL DISTANCE Z,M	STATIC PRESSURE P,BAR	SATURATION TEMPERATURE BASED ON P TS,C	COOLING WATER TEMPERATURE TCW,C	WALL TEMPERATURE TW,C	CONDITIONS
0.0	-	-	-	-	
0.04	1.1587	103.8	-	-	STEAM FLOW RATE
0.16	-	-	12.2	-	=533.2 KG/HR
0.31	-	-	-	69.7	MASS VELOCITY
0.4075	1.1481	103.5	-	-	=467722.0 KG/HR SQM
0.495	-	-	11.3	-	STEAM INLET VELOCITY
0.65	-	-	-	68.5	=127.0 M/S
0.77	1.1398	103.3	-	-	EXIT QUALITY
0.83	-	-	10.7	-	=0.4408
0.99	-	-	-	68.0	OVERALL PRESSURE DROP
1.0925	1.1322	103.1	-	-	=0.08730 BAR
1.165	-	-	9.8	-	COOLING WATER RATE
1.33	-	-	-	67.1	=7219.0 KG/HR
1.415	1.1241	102.9	-	-	HEAT BALANCE ERROR
1.5	-	-	8.4	-	= 0.1%
1.67	-	-	-	64.5	P IN TEST COND
1.835	-	-	7.6	-	=1.1676 BAR(ABS)
1.895	1.1131	102.7	-	-	TEMP IN CW
2.01	-	-	-	62.1	= 4.2 C
2.17	-	-	6.7	-	TEMP RISE TEST COND
2.35	-	-	-	59.7	= 8.8 C
2.4275	1.1012	102.4	-	-	INLET QUALITY
2.505	-	-	5.8	-	=0.6600
2.69	-	-	-	62.5	
2.84	-	-	4.7	-	
2.96	1.0926	102.1	-	-	

TABLE 1. REDUCED EXPERIMENTAL DATA, RUN 24

AXIAL DISTANCE Z,M	STATIC PRESSURE P,BAR	SATURATION TEMPERATURE BASED ON P TS,C	COOLING WATER TEMPERATURE TCW,C	WALL TEMPERATURE TW,C	CONDITIONS
0.0	-	-	-	-	
0.04	1.1327	104.4	-	-	STEAM FLOW RATE
0.16	-	-	12.3	-	=578.0 KG/HR
0.31	-	-	-	71.2	MASS VELOCITY
0.4075	1.1724	104.3	-	-	=506965.0 KG/HR SQM
0.495	-	-	11.7	-	STEAM INLET VELOCITY
0.65	-	-	-	70.1	=128.0 M/S
0.77	1.1741	104.2	-	-	EXIT QUALITY
0.83	-	-	11.2	-	=0.4310
0.99	-	-	-	69.7	OVERALL PRESSURE DROP
1.0925	1.1676	104.0	-	-	=0.09630 BAR
1.165	-	-	10.1	-	COOLING WATER RATE
1.33	-	-	-	68.8	=7219.0 KG/HR
1.415	1.1613	103.9	-	-	HEAT BALANCE ERROR
1.5	-	-	9.0	-	= -0.4%
1.67	-	-	-	66.5	P IN TEST COND
1.835	-	-	8.5	-	=1.2174 BAR(ABS)
1.895	1.1512	103.6	-	-	TEMP IN CW
2.01	-	-	-	63.7	= 5.0 C
2.17	-	-	7.3	-	TEMP RISE TEST COND
2.35	-	-	-	61.4	= 8.3 C
2.4275	1.1392	103.3	-	-	INLET QUALITY
2.505	-	-	6.4	-	=0.6200
2.69	-	-	-	64.4	
2.84	-	-	5.4	-	
2.96	1.1296	103.1	-	-	

TABLE 1. REDUCED EXPERIMENTAL DATA, RUN 25

AXIAL DISTANCE Z,M	STATIC PRESSURE P,BAR	SATURATION TEMPERATURE BASED ON P TS,C	COOLING WATER TEMPERATURE TCW,C	WALL TEMPERATURE TW,C	CONDITIONS
0.0	-	-	-	-	
0.04	1.1622	103.9	-	-	STEAM FLOW RATE
0.16	-	-	13.1	-	=527.1 KG/HR
0.31	-	-	-	69.8	MASS VELOCITY
0.4075	1.1516	103.6	-	-	=462312.0 KG/HR SQM
0.495	-	-	12.1	-	STEAM INLET VELOCITY
0.65	-	-	-	68.3	=127.0 M/S
0.77	1.1435	103.4	-	-	EXIT QUALITY
0.83	-	-	11.2	-	=0.4521
0.99	-	-	-	68.0	OVERALL PRESSURE DROP
1.0925	1.1357	103.2	-	-	=0.08730 BAR
1.165	-	-	10.3	-	COOLING WATER RATE
1.33	-	-	-	67.1	=8471.0 KG/HR
1.415	1.1275	103.0	-	-	HEAT BALANCE ERROR
1.5	-	-	9.5	-	= 6.4%
1.67	-	-	-	64.6	P IN TEST COND
1.835	-	-	9.4	-	=1.1712 BAR(ABS)
1.895	1.1164	102.7	-	-	TEMP IN CW
2.01	-	-	-	62.1	= 6.1 C
2.17	-	-	8.3	-	TEMP RISE TEST COND
2.35	-	-	-	60.0	= 7.7 C
2.4275	1.1045	102.4	-	-	INLET QUALITY
2.505	-	-	7.7	-	=0.6650
2.69	-	-	-	62.8	
2.84	-	-	6.8	-	
2.96	1.0960	102.2	-	-	

TABLE 1. REDUCED EXPERIMENTAL DATA, RUN 26

AXIAL DISTANCE Z,M	STATIC PRESSURE P,BAR	SATURATION TEMPERATURE BASED ON P TS,C	COOLING WATER TEMPERATURE TCW,C	WALL TEMPERATURE TW,C	CONDITIONS
0.0	-	-	-	-	
0.04	1.1548	103.7	-	-	STEAM FLOW RATE
0.16	-	-	13.1	-	=521.4 KG/HR
0.31	-	-	-	70.2	MASS VELOCITY
0.4075	1.1445	103.4	-	-	=457330.0 KG/HR SQM
0.495	-	-	12.4	-	STEAM INLET VELOCITY
0.65	-	-	-	68.4	=126.0 M/S
0.77	1.1363	103.2	-	-	EXIT QUALITY
0.83	-	-	11.6	-	=0.4457
0.99	-	-	-	68.0	OVERALL PRESSURE DROP
1.0925	1.1286	103.1	-	-	=0.08730 BAR
1.165	-	-	10.7	-	COOLING WATER RATE
1.33	-	-	-	67.3	=8471.0 KG/HR
1.415	1.1204	102.8	-	-	HEAT BALANCE ERROR
1.5	-	-	9.7	-	= 1.6%
1.67	-	-	-	64.7	P IN TEST COND
1.835	-	-	9.3	-	=1.2922 BAR(ABS)
1.895	1.1093	102.6	-	-	TEMP IN CW
2.01	-	-	-	62.1	= 6.3 C
2.17	-	-	8.4	-	TEMP RISE TEST COND
2.35	-	-	-	59.9	= 7.5 C
2.4275	1.0974	102.3	-	-	INLET QUALITY
2.505	-	-	7.5	-	=0.6650
2.69	-	-	-	62.7	
2.84	-	-	6.8	-	
2.96	1.0887	102.0	-	-	

TABLE 1. REDUCED EXPERIMENTAL DATA, RUN 27

AXIAL DISTANCE Z,M	STATIC PRESSURE P,BAR	SATURATION TEMPERATURE BASED ON P TS,C	COOLING WATER TEMPERATURE TCW,C	WALL TEMPERATURE TW,C	CONDITIONS
0.0	-	-	-	-	
0.04	1.3689	108.7	-	-	STEAM FLOW RATE
0.16	-	-	11.3	-	=594.7 KG/HR
0.31	-	-	-	73.3	MASS VELOCITY
0.4075	1.3568	108.4	-	-	=521622.0 KG/HR SQM
0.495	-	-	10.3	-	STEAM INLET VELOCITY
0.65	-	-	-	72.1	=126.0 M/S
0.77	1.3474	108.2	-	-	EXIT QUALITY
0.83	-	-	9.2	-	=0.4773
0.99	-	-	-	71.5	OVERALL PRESSURE DROP
1.0925	1.3385	108.0	-	-	=0.09750 BAR
1.165	-	-	8.2	-	COOLING WATER RATE
1.33	-	-	-	70.8	=7219.0 KG/HR
1.415	1.3294	107.8	-	-	HEAT BALANCE ERROR
1.5	-	-	7.0	-	= -2.0%
1.67	-	-	-	63.0	P IN TEST COND
1.835	-	-	6.3	-	=1.3804 BAR(ABS)
1.895	1.3166	107.5	-	-	TEMP IN CW
2.01	-	-	-	65.3	= 2.9 C
2.17	-	-	5.4	-	TEMP RISE TEST COND
2.35	-	-	-	62.8	= 9.1 C
2.4275	1.3027	107.2	-	-	INLET QUALITY
2.505	-	-	4.3	-	=0.6850
2.69	-	-	-	65.7	
2.84	-	-	3.3	-	
2.96	1.2924	107.0	-	-	

TABLE 1. REDUCED EXPERIMENTAL DATA, RUN 28

AXIAL DISTANCE Z,M	STATIC PRESSURE P,BAR	SATURATION TEMPERATURE BASED ON P TS,C	COOLING WATER TEMPERATURE TCW,C	WALL TEMPERATURE TW,C	CONDITIONS
0.0	-	-	-	-	
0.04	1.4204	109.7	-	-	STEAM FLOW RATE
0.16	-	-	11.0	-	=596.8 KG/HR
0.31	-	-	-	73.8	MASS VELOCITY
0.4075	1.4083	109.5	-	-	=523502.0 KG/HR SQM
0.495	-	-	9.9	-	STEAM INLET VELOCITY
0.65	-	-	-	72.6	=120.0 M/S
0.77	1.3988	109.3	-	-	EXIT QUALITY
0.83	-	-	9.2	-	=0.4709
0.99	-	-	-	71.7	OVERALL PRESSURE DROP
1.0925	1.3898	109.1	-	-	=0.10010 BAR
1.165	-	-	8.1	-	COOLING WATER RATE
1.33	-	-	-	71.4	=7219.0 KG/HR
1.415	1.3805	108.9	-	-	HEAT BALANCE ERROR
1.5	-	-	7.3	-	= -0.4%
1.67	-	-	-	68.9	P IN TEST COND
1.835	-	-	6.3	-	=1.4281 BAR(ABS)
1.895	1.3677	108.6	-	-	TEMP IN CW
2.01	-	-	-	66.0	= 3.2 C
2.17	-	-	5.4	-	TEMP RISE TEST COND
2.35	-	-	-	63.3	= 8.8 C
2.4275	1.3537	108.3	-	-	INLET QUALITY
2.505	-	-	4.4	-	=0.6690
2.69	-	-	-	66.0	
2.84	-	-	3.7	-	
2.96	1.3434	108.1	-	-	

TABLE 1. REDUCED EXPERIMENTAL DATA, RUN 29

AXIAL DISTANCE Z,M	STATIC PRESSURE P,BAR	SATURATION TEMPERATURE BASED ON P TS,C	COOLING WATER TEMPERATURE TCW,C	WALL TEMPERATURE TW,C	CONDITIONS
0.0	-	-	-	-	
0.04	1.3914	109.1	-	-	STEAM FLOW RATE
0.16	-	-	8.8	-	=603.8 KG/HR
0.31	-	-	-	72.2	MASS VELOCITY
0.4075	1.3791	108.9	-	-	=529574.0 KG/HR SQM
0.495	-	-	7.9	-	STEAM INLET VELOCITY
0.65	-	-	-	71.2	=128.0 M/S
0.77	1.3697	108.7	-	-	EXIT QUALITY
0.83	-	-	7.1	-	=0.4887
0.99	-	-	-	70.4	OVERALL PRESSURE DROP
1.0925	1.3607	108.5	-	-	=0.10010 BAR
1.165	-	-	6.2	-	COOLING WATER RATE
1.33	-	-	-	69.7	=8471.0 KG/HR
1.415	1.3513	108.3	-	-	HEAT BALANCE ERROR
1.5	-	-	5.3	-	= 0.6%
1.67	-	-	-	67.1	P IN TEST COND
1.335	-	-	4.6	-	=1.4042 BAR(ABS)
1.895	1.3336	108.0	-	-	TEMP IN CW
2.01	-	-	-	64.2	= 1.6 C
2.17	-	-	3.7	-	TEMP RISE TEST COND
2.35	-	-	-	61.7	= 8.1 C
2.4275	1.3247	107.7	-	-	INLET QUALITY
2.505	-	-	2.9	-	=0.7000
2.69	-	-	-	64.4	
2.84	-	-	2.1	-	
2.96	1.3149	107.5	-	-	

TABLE 1. REDUCED EXPERIMENTAL DATA, RUN 30

AXIAL DISTANCE Z,M	STATIC PRESSURE P,BAR	SATURATION TEMPERATURE BASED ON P TS,C	COOLING WATER TEMPERATURE TCW,C	WALL TEMPERATURE TW,C	CONDITIONS
0.0	-	-	-	-	
0.04	1.4040	109.4	-	-	STEAM FLOW RATE
0.16	-	-	9.1	-	=606.3 KG/HR
0.31	-	-	-	72.1	MASS VELOCITY
0.4075	1.3919	109.1	-	-	=531772.0 KG/HR SQM
0.495	-	-	8.1	-	STEAM INLET VELOCITY
0.65	-	-	-	70.9	=126.0 M/S
0.77	1.3826	108.9	-	-	EXIT QUALITY
0.83	-	-	6.9	-	=0.4731
0.99	-	-	-	70.3	OVERALL PRESSURE DROP
1.0925	1.3736	108.8	-	-	=0.09490 BAR
1.165	-	-	6.3	-	COOLING WATER RATE
1.33	-	-	-	69.9	=8471.0 KG/HR
1.415	1.3644	108.6	-	-	HEAT BALANCE ERROR
1.5	-	-	5.3	-	= -1.7%
1.67	-	-	-	67.0	P IN TEST COND
1.735	-	-	4.7	-	=1.4052 BAR(ABS)
1.895	1.3515	108.3	-	-	TEMP IN CW
2.01	-	-	-	64.1	= 2.0 C
2.17	-	-	3.8	-	TEMP RISE TEST COND
2.35	-	-	-	61.6	= 8.1 C
2.4275	1.3381	108.0	-	-	INLET QUALITY
2.505	-	-	2.9	-	=0.6860
2.69	-	-	-	64.5	
2.84	-	-	2.2	-	
2.96	1.3283	107.8	-	-	

TABLE 1. REDUCED EXPERIMENTAL DATA, RUN 31

AXIAL DISTANCE Z,M	STATIC PRESSURE P,BAR	SATURATION TEMPERATURE BASED ON P TS,C	COOLING WATER TEMPERATURE TCW,C	WALL TEMPERATURE TW,C	CONDITIONS
0.0	-	-	-	-	
0.04	1.6253	113.8	-	-	STEAM FLOW RATE
0.16	-	-	10.1	-	=697.0 KG/HR
0.31	-	-	-	75.8	MASS VELOCITY
0.4075	1.6120	113.6	-	-	=611388.0 KG/HR SQM
0.495	-	-	8.7	-	STEAM INLET VELOCITY
0.65	-	-	-	74.4	=107.2 M/S
0.77	1.6017	113.4	-	-	EXIT QUALITY
0.83	-	-	7.5	-	=0.3829
0.99	-	-	-	73.4	OVERALL PRESSURE DROP
1.0925	1.5916	113.2	-	-	=0.11550 BAR
1.165	-	-	6.6	-	COOLING WATER RATE
1.33	-	-	-	73.2	=7219.0 KG/HR
1.415	1.5812	113.0	-	-	HEAT BALANCE ERROR
1.5	-	-	7.7	-	= -1.3%
1.67	-	-	-	70.4	P IN TEST COND
1.835	-	-	5.0	-	=1.6412 BAR(ABS)
1.895	1.5668	112.7	-	-	TEMP IN CW
2.01	-	-	-	67.7	= 1.0 C
2.17	-	-	3.8	-	TEMP RISE TEST COND
2.35	-	-	-	64.4	=10.2 C
2.4275	1.5509	112.4	-	-	INLET QUALITY
2.505	-	-	2.7	-	=0.5808
2.69	-	-	-	68.5	
2.84	-	-	1.3	-	
2.96	1.5393	112.2	-	-	

TABLE 1. REDUCED EXPERIMENTAL DATA, RUN 32

AXIAL DISTANCE Z,M	STATIC PRESSURE P,BAR	SATURATION TEMPERATURE BASED ON P TS,C	COOLING WATER TEMPERATURE TCW,C	WALL TEMPERATURE TW,C	CONDITIONS
0.0	-	-	-	-	
0.04	1.6131	113.6	-	-	STEAM FLOW RATE
0.16	-	-	10.1	-	=707.4 KG/HR
0.31	-	-	-	75.2	MASS VELOCITY
0.4075	1.5991	113.3	-	-	=620497.0 KG/HR SQM
0.495	-	-	8.7	-	STEAM INLET VELOCITY
0.65	-	-	-	73.9	=106.0 M/S
0.77	1.5889	113.1	-	-	EXIT QUALITY
0.83	-	-	7.7	-	=0.3844
0.99	-	-	-	72.9	OVERALL PRESSURE DROP
1.0925	1.5791	112.9	-	-	=0.10270 BAR
1.165	-	-	6.4	-	COOLING WATER RATE
1.33	-	-	-	72.3	=7219.0 KG/HR
1.415	1.5688	112.7	-	-	HEAT BALANCE ERROR
1.5	-	-	5.5	-	= -1.1%
1.67	-	-	-	69.8	P IN TEST COND
1.835	-	-	5.0	-	=1.6310 BAR(ABS)
1.895	1.5547	112.5	-	-	TEMP IN CW
2.01	-	-	-	67.0	= 1.1 C
2.17	-	-	4.0	-	TEMP RISE TEST COND
2.35	-	-	-	63.9	= 9.9 C
2.4275	1.5391	112.2	-	-	INLET QUALITY
2.505	-	-	2.7	-	=0.5740
2.69	-	-	-	68.0	
2.84	-	-	1.4	-	
2.96	1.5278	111.9	-	-	

TABLE 1. REDUCED EXPERIMENTAL DATA, RUN 33

AXIAL DISTANCE Z,M	STATIC PRESSURE P,BAR	SATURATION TEMPERATURE BASED ON P TS,C	COOLING WATER TEMPERATURE TCW,C	WALL TEMPERATURE TW,C	CONDITIONS
0.0	-	-	-	-	
0.04	0.7596	92.1	-	-	STEAM FLOW RATE
0.16	-	-	13.3	-	=397.7 KG/HR
0.31	-	-	-	61.3	MASS VELOCITY
0.4075	0.7521	91.9	-	-	=348832.0 KG/HR SQM
0.495	-	-	12.5	-	STEAM INLET VELOCITY
0.65	-	-	-	60.5	=162.0 M/S
0.77	0.7464	91.7	-	-	EXIT QUALITY
0.83	-	-	12.1	-	=0.5157
0.99	-	-	-	59.9	OVERALL PRESSURE DROP
1.0925	0.7407	91.5	-	-	=0.06160 BAR
1.165	-	-	11.3	-	COOLING WATER RATE
1.33	-	-	-	58.8	=8471.0 KG/HR
1.415	0.7352	91.3	-	-	HEAT BALANCE ERROR
1.5	-	-	10.4	-	= 1.8%
1.67	-	-	-	57.3	P IN TEST COND
1.835	-	-	10.4	-	=0.7634 BAR(ABS)
1.895	0.7281	91.0	-	-	TEMP IN CW
2.01	-	-	-	55.1	= 7.6 C
2.17	-	-	9.7	-	TEMP RISE TEST COND
2.35	-	-	-	53.2	= 6.4 C
2.4275	0.7206	90.7	-	-	INLET QUALITY
2.505	-	-	8.8	-	=0.7600
2.69	-	-	-	55.4	
2.84	-	-	8.1	-	
2.96	0.7163	90.6	-	-	

TABLE 1. REDUCED EXPERIMENTAL DATA, RUN 34

AXIAL DISTANCE Z,M	STATIC PRESSURE P,BAR	SATURATION TEMPERATURE BASED ON P TS,C	COOLING WATER TEMPERATURE TCW,C	WALL TEMPERATURE TW,C	CONDITIONS
0.0	-	-	-	-	
0.04	0.7536	91.9	-	-	STEAM FLOW RATE
0.16	-	-	14.7	-	=391.1 KG/HR
0.31	-	-	-	62.4	MASS VELOCITY
0.4075	0.7463	91.7	-	-	=343074.0 KG/HR SQM
0.495	-	-	14.0	-	STEAM INLET VELOCITY
0.65	-	-	-	61.3	=159.4 M/S
0.77	0.7407	91.5	-	-	EXIT QUALITY
0.83	-	-	13.3	-	=0.5316
0.99	-	-	-	60.6	OVERALL PRESSURE DROP
1.0925	0.7353	91.3	-	-	=0.06160 BAR
1.165	-	-	12.2	-	COOLING WATER RATE
1.33	-	-	-	59.8	=7219.0 KG/HR
1.415	0.7299	91.1	-	-	HEAT BALANCE ERROR
1.5	-	-	11.4	-	= 3.2%
1.67	-	-	-	58.2	P IN TEST COND
1.835	-	-	11.3	-	=0.7549 BAR(ABS)
1.995	0.7223	90.8	-	-	TEMP IN CW
2.01	-	-	-	55.8	= 8.4 C
2.17	-	-	10.5	-	TEMP RISE TEST COND
2.35	-	-	-	53.2	= 6.9 C
2.4275	0.7153	90.5	-	-	INLET QUALITY
2.505	-	-	9.6	-	=0.7550
2.69	-	-	-	56.1	
2.84	-	-	8.9	-	
2.96	0.7108	90.4	-	-	

TABLE 1. REDUCED EXPERIMENTAL DATA, RUN 35

AXIAL DISTANCE Z,M	STATIC PRESSURE P,BAR	SATURATION TEMPERATURE BASED ON P TS,C	COOLING WATER TEMPERATURE TCW,C	WALL TEMPERATURE TW,C	CONDITIONS
0.0	-	-	-	-	
0.04	0.7585	92.1	-	-	STEAM FLOW RATE
0.16	-	-	13.7	-	=373.3 KG/HR
0.31	-	-	-	62.0	MASS VELOCITY
0.4075	0.7508	91.8	-	-	=327423.0 KG/HR SQM
0.495	-	-	12.5	-	STEAM INLET VELOCITY
0.65	-	-	-	60.5	=126.8 M/S
0.77	0.7452	91.6	-	-	EXIT QUALITY
0.83	-	-	11.2	-	=0.3692
0.99	-	-	-	60.2	OVERALL PRESSURE DROP
1.0925	0.7397	91.4	-	-	=0.06160 BAR
1.165	-	-	10.4	-	COOLING WATER RATE
1.33	-	-	-	59.2	=7219.0 KG/HR
1.415	0.7341	91.2	-	-	HEAT BALANCE ERROR
1.5	-	-	9.9	-	= -3.8%
1.67	-	-	-	57.0	P IN TEST COND
1.835	-	-	9.5	-	=0.7624 BAR(ABS)
1.895	0.7267	90.9	-	-	TEMP IN CW
2.01	-	-	-	55.3	= 6.8 C
2.17	-	-	8.6	-	TEMP RISE TEST COND
2.35	-	-	-	52.8	= 7.4 C
2.4275	0.7188	90.7	-	-	INLET QUALITY
2.505	-	-	7.9	-	=0.6300
2.69	-	-	-	55.5	
2.84	-	-	7.2	-	
2.96	0.7103	90.3	-	-	

TABLE 1. REDUCED EXPERIMENTAL DATA, RUN 36

AXIAL DISTANCE Z,M	STATIC PRESSURE P,BAR	SATURATION TEMPERATURE BASED ON P TS,C	COOLING WATER TEMPERATURE TCW,C	WALL TEMPERATURE TW,C	CONDITIONS
0.0	-	-	-	-	
0.04	0.7518	91.3	-	-	STEAM FLOW RATE
0.16	-	-	13.2	-	=394.1 KG/HR
0.31	-	-	-	61.3	MASS VELOCITY
0.4075	0.7444	91.6	-	-	=345635.0 KG/HR SQM
0.495	-	-	12.1	-	STEAM INLET VELOCITY
0.65	-	-	-	59.9	=121.0 M/S
0.77	0.7383	91.4	-	-	EXIT QUALITY
0.83	-	-	11.3	-	=0.3085
0.99	-	-	-	59.6	OVERALL PRESSURE DROP
1.0925	0.7334	91.2	-	-	=0.06160 BAR
1.165	-	-	10.3	-	COOLING WATER RATE
1.33	-	-	-	58.8	=8471.0 KG/HR
1.415	0.7278	91.0	-	-	HEAT BALANCE ERROR
1.5	-	-	9.9	-	= -2.8%
1.67	-	-	-	56.8	P IN TEST COND
1.835	-	-	9.8	-	=0.7570 BAR(ABS)
1.895	0.7204	90.7	-	-	TEMP IN CW
2.01	-	-	-	54.7	= 7.4 C
2.17	-	-	9.0	-	TEMP RISE TEST COND
2.35	-	-	-	52.3	= 6.4 C
2.4275	0.7129	90.4	-	-	INLET QUALITY
2.505	-	-	8.3	-	=0.5660
2.69	-	-	-	55.0	
2.84	-	-	7.5	-	
2.96	0.7051	90.1	-	-	

TABLE 1. REDUCED EXPERIMENTAL DATA, RUN 37

AXIAL DISTANCE Z,M	STATIC PRESSURE P,BAR	SATURATION TEMPERATURE BASED ON P TS,C	COOLING WATER TEMPERATURE TCW,C	WALL TEMPERATURE TW,C	CONDITIONS
0.0	-	-	-	-	
0.04	0.5573	84.1	-	-	STEAM FLOW RATE
0.16	-	-	11.8	-	=328.0 KG/HR
0.31	-	-	-	55.9	MASS VELOCITY
0.4075	0.5543	83.9	-	-	=287725.0 KG/HR SQM
0.495	-	-	11.1	-	STEAM INLET VELOCITY
0.65	-	-	-	54.9	=170.0 M/S
0.77	0.5490	83.7	-	-	EXIT QUALITY
0.83	-	-	11.3	-	=0.4066
0.99	-	-	-	54.2	OVERALL PRESSURE DROP
1.0925	0.5453	83.5	-	-	=0.04880 BAR
1.165	-	-	10.1	-	COOLING WATER RATE
1.33	-	-	-	53.0	=7219.0 KG/HR
1.415	0.5416	83.3	-	-	HEAT BALANCE ERROR
1.5	-	-	9.0	-	= 24.0%
1.67	-	-	-	51.4	P IN TEST COND
1.335	-	-	9.4	-	=0.5604 BAR(ABS)
1.895	0.5373	83.1	-	-	TEMP IN CW
2.01	-	-	-	49.5	= 6.6 C
2.17	-	-	8.5	-	TEMP RISE TEST COND
2.35	-	-	-	47.6	= 6.4 C
2.4275	0.5335	83.0	-	-	INLET QUALITY
2.505	-	-	7.9	-	=0.7240
2.69	-	-	-	49.7	
2.84	-	-	6.8	-	
2.96	0.5263	82.6	-	-	

TABLE 1. REDUCED EXPERIMENTAL DATA, RUN 38

AXIAL DISTANCE Z,M	STATIC PRESSURE P,BAR	SATURATION TEMPERATURE BASED ON P TS,C	COOLING WATER TEMPERATURE TCW,C	WALL TEMPERATURE TW,C	CONDITIONS
0.0	-	-	-	-	
0.04	0.5569	84.1	-	-	STEAM FLOW RATE
0.16	-	-	11.5	-	=331.7 KG/HR
0.31	-	-	-	55.2	MASS VELOCITY
0.4075	0.5519	83.8	-	-	=290937.0 KG/HR SQM
0.495	-	-	10.4	-	STEAM INLET VELOCITY
0.65	-	-	-	53.4	=172.0 M/S
0.77	0.5482	83.7	-	-	EXIT QUALITY
0.83	-	-	9.4	-	=0.4100
0.99	-	-	-	53.1	OVERALL PRESSURE DROP
1.0925	0.5445	83.5	-	-	=0.04240 BAR
1.165	-	-	8.5	-	COOLING WATER RATE
1.33	-	-	-	52.1	=8471.0 KG/HR
1.415	0.5410	83.3	-	-	HEAT BALANCE ERROR
1.5	-	-	8.1	-	=-17.0%
1.67	-	-	-	50.2	P IN TEST COND
1.835	-	-	8.4	-	=0.5621 BAR(ABS)
1.895	0.5368	83.1	-	-	TEMP IN CW
2.01	-	-	-	48.6	= 5.8 C
2.17	-	-	7.7	-	TEMP RISE TEST COND
2.35	-	-	-	46.4	= 5.9 C
2.4275	0.5329	82.9	-	-	INLET QUALITY
2.505	-	-	7.0	-	=0.7250
2.69	-	-	-	43.9	
2.84	-	-	5.9	-	
2.96	0.5257	82.6	-	-	

TABLE 1. REDUCED EXPERIMENTAL DATA, RUN 39

AXIAL DISTANCE Z,M	STATIC PRESSURE P,BAR	SATURATION TEMPERATURE BASED ON P TS,C	COOLING WATER TEMPERATURE TCW,C	WALL TEMPERATURE TW,C	CONDITIONS
0.0	-	-	-	-	
0.04	0.5386	83.2	-	-	STEAM FLOW RATE
0.16	-	-	16.6	-	=309.8 KG/HR
0.31	-	-	-	56.9	MASS VELOCITY
0.4075	0.5340	83.0	-	-	=271688.0 KG/HR SQM
0.495	-	-	16.3	-	STEAM INLET VELOCITY
0.65	-	-	-	55.7	=154.6 M/S
0.77	0.5307	82.8	-	-	EXIT QUALITY
0.83	-	-	15.3	-	=0.4211
0.99	-	-	-	55.6	OVERALL PRESSURE DROP
1.0925	0.5273	82.7	-	-	=0.04110 BAR
1.165	-	-	14.5	-	COOLING WATER RATE
1.33	-	-	-	54.1	=7219.0 KG/HR
1.415	0.5239	82.5	-	-	HEAT BALANCE ERROR
1.5	-	-	13.7	-	= -3.6%
1.67	-	-	-	53.0	P IN TEST COND
1.835	-	-	13.1	-	=0.5424 BAR(ABS)
1.895	0.5198	82.3	-	-	TEMP IN CW
2.01	-	-	-	50.9	=11.2 C
2.17	-	-	12.3	-	TEMP RISE TEST COND
2.35	-	-	-	49.2	= 5.8 C
2.4275	0.5158	82.1	-	-	INLET QUALITY
2.505	-	-	11.5	-	=0.6750
2.69	-	-	-	50.8	
2.84	-	-	11.3	-	
2.96	0.5108	81.9	-	-	

TABLE 1. REDUCED EXPERIMENTAL DATA, RUN 40

AXIAL DISTANCE Z,M	STATIC PRESSURE P,BAR	SATURATION TEMPERATURE BASED ON P TS,C	COOLING WATER TEMPERATURE TCW,C	WALL TEMPERATURE TW,C	CONDITIONS
0.0	-	-	-	-	
0.04	0.5391	83.2	-	-	STEAM FLOW RATE
0.16	-	-	15.9	-	=312.4 KG/HR
0.31	-	-	-	56.1	MASS VELOCITY
0.4075	0.5343	83.0	-	-	=273971.0 KG/HR SQM
0.495	-	-	15.1	-	STEAM INLET VELOCITY
0.65	-	-	-	55.0	=156.2 M/S
0.77	0.5314	82.9	-	-	EXIT QUALITY
0.83	-	-	14.5	-	=0.4112
0.99	-	-	-	54.4	OVERALL PRESSURE DROP
1.0925	0.5281	82.7	-	-	=0.08730 BAR
1.165	-	-	13.9	-	COOLING WATER RATE
1.33	-	-	-	53.5	=8471.0 KG/HR
1.415	0.5248	82.6	-	-	HEAT BALANCE ERROR
1.5	-	-	13.6	-	= -3.2%
1.67	-	-	-	53.0	P IN TEST COND
1.835	-	-	13.1	-	=0.5430 BAR(ABS)
1.895	0.5197	82.3	-	-	TEMP IN CW
2.01	-	-	-	50.5	=11.0 C
2.17	-	-	12.5	-	TEMP RISE TEST COND
2.35	-	-	-	48.8	= 5.3 C
2.4275	0.5160	82.1	-	-	INLET QUALITY
2.505	-	-	11.9	-	=0.6770
2.69	-	-	-	50.3	
2.84	-	-	11.2	-	
2.96	0.5116	81.9	-	-	

TABLE 2. COMPUTED DATA

AXIAL DISTANCE Z,M	INNER WALL TEMPERATURE TIW,C	LOCAL HEAT FLUX Q,KW/SQM	LOCAL HEAT TRANS COEFF HZ KW/SQM-K	NUSSELT NUMBER NUZ
		RUN 1		
0.31	92.5	131.6	8.1	454.6
0.65	99.8	210.5	23.8	1332.3
0.99	97.6	195.8	17.7	987.7
1.33	87.4	111.1	5.3	296.8
1.67	100.4	243.7	30.8	1722.8
2.01	99.1	254.8	28.4	1589.1
2.35	87.2	173.4	8.4	473.2
2.69	73.0	28.6	0.8	47.7
		RUN 2		
0.31	102.4	230.6	37.3	2082.1
0.65	101.5	233.2	32.4	1811.5
0.99	104.5	265.5	62.7	3495.8
1.33	93.5	177.1	11.7	657.3
1.67	75.7	36.9	1.1	64.1
2.01	92.7	210.5	13.6	764.3
2.35	89.4	207.5	11.2	630.0
2.69	95.0	226.2	20.3	1136.6

TABLE 2. COMPUTED DATA

AXIAL DISTANCE Z,M	INNER WALL TEMPERATURE TIW,C	LOCAL HEAT FLUX Q,KW/SQM	LOCAL HEAT TRANS COEFF HZ KW/SQM-K	NUSSELT NUMBER NUZ
		RUN 3		
0.31	105.3	274.0	100.9	5629.1
0.65	105.0	283.1	80.9	4514.9
0.99	96.7	215.6	18.0	1010.4
1.33	90.3	166.2	9.1	513.2
1.67	79.4	87.8	3.0	172.0
2.01	90.7	211.9	12.2	684.6
2.35	91.5	242.3	14.9	835.9
2.69	89.8	198.1	11.8	663.4
		RUN 4		
0.31	93.9	190.5	18.6	1045.7
0.65	82.4	96.5	4.4	251.2
0.99	95.0	217.8	23.9	1340.8
1.33	96.0	230.8	29.0	1627.9
1.67	81.7	128.5	5.8	329.4
2.01	87.7	197.4	12.5	702.6
2.35	82.4	173.1	8.3	467.5
2.69	85.6	171.4	10.3	582.7

TABLE 2. COMPUTED DATA

AXIAL DISTANCE Z,M	INNER WALL TEMPERATURE TIW,C	LOCAL HEAT FLUX Q,KW/SQM	LOCAL HEAT TRANS COEFF HZ KW/SQM-K	NUSSELT NUMBER NUZ
		RUN 5		
0.31	96.3	230.9	30.8	1726.3
0.65	84.4	132.1	6.7	380.0
0.99	86.7	161.0	9.3	525.4
1.33	88.3	177.4	11.4	644.0
1.67	98.3	282.1	53.0	2965.5
2.01	85.0	185.9	10.1	567.1
2.35	81.5	179.5	8.2	466.2
2.69	78.0	123.0	5.0	285.0
		RUN 6		
0.31	96.3	237.5	33.0	1847.1
0.65	84.5	143.6	7.5	423.6
0.99	91.8	216.6	18.3	1030.3
1.33	85.6	165.7	9.3	524.5
1.67	83.3	162.2	8.1	459.7
2.01	86.6	213.2	12.9	728.5
2.35	83.0	204.7	10.3	581.2
2.69	81.2	164.7	7.8	443.0

TABLE 2. COMPUTED DATA

AXIAL DISTANCE Z,M	INNER WALL TEMPERATURE TIW,C	LOCAL HEAT FLUX Q,KW/SQM	LOCAL HEAT TRANS COEFF HZ KW/SQM-K	NUSSELT NUMBER NUZ
		RUN 7		
0.31	103.2	210.2	20.9	1165.0
0.65	97.7	175.0	11.3	629.3
0.99	100.0	198.0	15.0	838.7
1.33	100.7	210.7	17.2	958.1
1.67	93.5	168.4	8.7	489.1
2.01	96.6	217.5	13.7	765.2
2.35	90.5	193.1	8.8	496.2
2.69	91.4	171.6	8.8	492.3
		RUN 8		
0.31	103.8	230.8	23.1	1290.4
0.65	98.1	185.2	11.9	664.8
0.99	100.5	214.7	16.3	909.9
1.33	104.6	258.0	29.2	1625.8
1.67	92.7	174.7	8.5	475.8
2.01	97.6	240.2	15.5	867.7
2.35	93.2	233.7	11.9	667.0
2.69	90.4	177.9	8.4	470.0

TABLE 2. COMPUTED DATA

AXIAL DISTANCE Z,M	INNER WALL TEMPERATURE TIW,C	LOCAL HEAT FLUX Q,KW/SQM	LOCAL HEAT TRANS COEFF HZ KW/SQM-K	NUSSELT NUMBER NUZ
		RUN 9		
0.31	107.1	273.3	42.5	2368.4
0.65	91.5	144.2	6.6	368.5
0.99	103.2	253.0	24.8	1381.2
1.33	104.8	273.9	32.4	1806.8
1.67	89.7	163.3	7.0	393.4
2.01	97.0	250.1	15.9	887.4
2.35	96.5	276.6	17.3	967.2
2.69	87.6	166.4	6.9	388.7
		RUN 10		
0.31	98.7	170.8	12.5	699.3
0.65	102.2	212.4	21.1	1179.3
0.99	106.2	256.2	42.5	2366.9
1.33	100.0	210.3	17.5	976.9
1.67	79.9	48.0	1.5	84.7
2.01	103.3	276.0	33.6	1875.9
2.35	91.1	193.4	9.5	534.3
2.69	91.7	169.8	9.0	506.7

TABLE 2. COMPUTED DATA

AXIAL DISTANCE Z,M	INNER WALL TEMPERATURE TIW,C	LOCAL HEAT FLUX Q,KW/SQM	LOCAL HEAT TRANS COEFF HZ KW/SQM-K	NUSSELT NUMBER NUZ
		RUN 11		
0.31	106.7	274.2	50.0	2784.0
0.65	99.1	210.2	16.3	909.5
0.99	102.9	251.0	27.8	1550.7
1.33	100.6	238.0	21.2	1185.9
1.67	81.3	87.3	2.9	162.4
2.01	105.4	320.0	53.9	3005.7
2.35	89.6	206.2	9.5	535.2
2.69	91.9	197.8	10.8	603.4
		RUN 12		
0.31	88.4	210.2	47.8	2695.5
0.65	78.9	138.2	9.8	553.5
0.99	80.3	159.3	12.5	711.0
1.33	79.1	151.1	10.9	619.4
1.67	85.7	230.2	33.0	1866.6
2.01	82.6	219.0	21.9	1242.0
2.35	70.4	131.6	6.0	342.9
2.69	61.7	32.2	1.1	61.6

TABLE 2. COMPUTED DATA

AXIAL DISTANCE Z,M	INNER WALL TEMPERATURE TIW,C	LOCAL HEAT FLUX Q,KW/SQM	LOCAL HEAT TRANS COEFF HZ KW/SQM-K	NUSSELT NUMBER NUZ
		RUN 13		
0.31	88.5	236.4	59.9	3374.1
0.65	81.1	184.0	15.6	884.5
0.99	84.5	217.9	26.0	1471.3
1.33	85.6	237.0	33.0	1863.0
1.67	59.1	19.9	0.6	34.3
2.01	75.0	178.0	10.2	580.7
2.35	76.1	203.0	12.6	714.1
2.69	78.5	204.0	16.1	911.4
		RUN 14		
0.31	75.0	150.7	15.8	902.3
0.65	72.4	139.8	11.5	657.9
0.99	74.2	159.9	15.5	884.0
1.33	74.4	171.0	17.1	974.7
1.67	57.0	30.7	1.1	65.2
2.01	71.7	178.7	14.4	822.0
2.35	64.8	131.9	6.9	394.4
2.69	66.5	133.0	8.0	462.0

TABLE 2. COMPUTED DATA

AXIAL DISTANCE Z,M	INNER WALL TEMPERATURE TIW,C	LOCAL HEAT FLUX Q,KW/SQM	LOCAL HEAT TRANS COEFF HZ KW/SQM-K	NUSSELT NUMBER NUZ
		RUN 15		
0.31	76.4	175.9	23.0	1310.0
0.65	67.7	111.0	6.7	385.6
0.99	76.3	189.7	23.9	1360.6
1.33	73.8	176.4	17.0	973.2
1.67	56.8	42.5	1.6	90.7
2.01	71.0	187.6	14.6	837.3
2.35	65.1	150.4	8.1	464.3
2.69	64.2	125.9	6.7	386.5
		RUN 16		
0.31	77.1	198.8	34.5	1966.3
0.65	66.2	115.1	6.8	389.2
0.99	77.7	218.6	39.8	2264.0
1.33	78.4	236.1	50.3	2862.2
1.67	52.5	21.7	0.7	41.3
2.01	55.7	69.1	2.5	147.3
2.35	69.1	201.3	14.7	844.6
2.69	67.3	169.4	11.6	667.9

TABLE 2. COMPUTED DATA

AXIAL DISTANCE Z,M	INNER WALL TEMPERATURE TIW,C	LOCAL HEAT FLUX Q,KW/SQM	LOCAL HEAT TRANS COEFF HZ KW/SQM-K	NUSSELT NUMBER NUZ
		RUN 17		
0.31	65.7	150.0	25.3	1462.7
0.65	65.0	162.0	24.5	1417.4
0.99	58.3	107.9	8.0	466.8
1.33	56.3	96.2	6.2	360.3
1.67	45.5	13.6	0.5	30.5
2.01	57.3	131.8	9.1	529.0
2.35	51.9	98.8	5.0	290.4
2.69	55.7	122.2	7.9	458.2
		RUN 18		
0.31	71.4	201.7		
0.65	58.7	107.3	8.5	495.5
0.99	62.4	144.3	16.1	930.4
1.33	55.9	93.8	6.1	353.3
1.67	45.7	16.5	0.6	37.8
2.01	58.3	139.9	10.6	615.9
2.35	56.0	133.6	8.6	501.6
2.69	56.2	125.9	8.6	500.4

TABLE 2. COMPUTED DATA

AXIAL DISTANCE Z,M	INNER WALL TEMPERATURE TIW,C	LOCAL HEAT FLUX Q,KW/SQM	LOCAL HEAT TRANS COEFF HZ KW/SQM-K	NUSSELT NUMBER NUZ
		RUN 19		
0.31	69.2	175.7	29.3	1682.3
0.65	62.8	127.5	10.2	591.9
0.99	62.0	126.6	9.6	556.4
1.33	59.8	112.9	7.4	427.5
1.67	54.5	79.2	3.9	225.1
2.01	57.4	123.0	7.0	406.3
2.35	58.4	147.5	8.9	517.9
2.69	55.6	111.9	6.0	348.3
		RUN 20		
0.31	69.9	176.8	31.7	1821.4
0.65	60.9	108.1	7.4	430.6
0.99	60.1	107.8	7.1	409.9
1.33	61.3	123.3	8.8	510.3
1.67	47.5	13.2	0.5	28.1
2.01	62.1	158.9	12.2	703.3
2.35	53.5	98.8	4.6	266.3
2.69	60.7	149.3	11.0	636.7

TABLE 2. COMPUTED DATA

AXIAL DISTANCE Z,M	INNER WALL TEMPERATURE TIW,C	LOCAL HEAT FLUX Q,KW/SQM	LOCAL HEAT TRANS COEFF HZ KW/SQM-K	NUSSELT NUMBER NUZ
		RUN 21		
0.31	97.3	230.9	36.1	2019.0
0.65	90.1	181.3	13.3	748.4
0.99	93.4	212.8	20.8	1164.6
1.33	88.4	177.2	11.8	662.0
1.67	73.6	64.1	2.1	122.2
2.01	87.7	210.8	13.6	764.3
2.35	85.3	207.5	11.7	659.2
2.69	80.6	146.3	6.7	380.5
		RUN 22		
0.31	97.5	239.9	39.8	2227.4
0.65	86.1	151.4	8.7	488.7
0.99	86.0	156.3	8.9	504.1
1.33	98.6	270.6	57.0	3192.0
1.67	77.9	107.0	4.2	239.2
2.01	84.2	184.7	9.8	551.4
2.35	85.2	212.2	11.9	672.5
2.69	79.2	140.1	6.1	345.5

TABLE 2. COMPUTED DATA

AXIAL DISTANCE Z,M	INNER WALL TEMPERATURE TIW,C	LOCAL HEAT FLUX Q,KW/SQM	LOCAL HEAT TRANS COEFF HZ KW/SQM-K	NUSSELT NUMBER NUZ
		RUN 23		
0.31	89.8	177.0	13.0	728.9
0.65	83.8	134.7	6.9	388.9
0.99	89.5	188.7	13.8	778.9
1.33	99.7	285.0	86.8	4857.6
1.67	84.7	176.9	9.8	551.8
2.01	83.5	187.1	9.8	554.4
2.35	80.1	178.3	8.0	453.2
2.69	89.2	234.4	20.6	1160.1
		RUN 24		
0.31	85.3	123.5	6.5	366.4
0.65	82.3	107.2	4.9	277.0
0.99	97.3	242.4	36.2	2025.4
1.33	95.1	231.1	26.5	1486.6
1.67	77.3	94.9	3.6	203.7
2.01	91.2	240.9	19.6	1103.9
2.35	84.9	206.0	11.2	632.7
2.69	87.9	206.3	14.9	839.3

TABLE 2. COMPUTED DATA

AXIAL DISTANCE Z,M	INNER WALL TEMPERATURE TIW,C	LOCAL HEAT FLUX Q,KW/SQM	LOCAL HEAT TRANS COEFF HZ KW/SQM-K	NUSSELT NUMBER NUZ
		RUN 25		
0.31	97.1	239.3	37.6	2105.3
0.65	93.4	219.7	21.8	1224.8
0.99	93.2	221.1	22.1	1238.3
1.33	90.8	208.0	17.0	953.4
1.67	66.4	15.5	0.4	24.3
2.01	94.3	281.9	34.0	1909.3
2.35	76.8	147.2	5.8	326.2
2.69	86.5	207.9	14.2	799.4
		RUN 26		
0.31	90.4	176.7	13.5	758.8
0.65	89.8	187.7	14.0	785.5
0.99	93.2	220.9	22.3	1249.2
1.33	94.6	239.6	29.1	1634.6
1.67	77.3	110.4	4.3	246.3
2.01	87.0	218.3	14.1	796.2
2.35	83.9	211.0	11.5	651.0
2.69	82.7	176.0	9.6	541.2

TABLE 2. COMPUTED DATA

AXIAL DISTANCE Z,M	INNER WALL TEMPERATURE TIW,C	LOCAL HEAT FLUX Q,KW/SQM	LOCAL HEAT TRANS COEFF HZ KW/SQM-K	NUSSELT NUMBER NUZ
		RUN 27		
0.31	96.5	203.3	17.2	963.1
0.65	100.0	244.5	29.8	1668.2
0.99	93.1	189.5	12.7	713.0
1.33	100.2	257.9	33.8	1887.1
1.67	85.2	151.5	6.8	381.4
2.01	86.7	188.1	9.1	513.1
2.35	89.2	231.2	12.9	725.9
2.69	89.6	209.8	13.3	746.8
		RUN 28		
0.31	100.0	229.9	24.5	1371.4
0.65	91.4	164.2	9.2	513.9
0.99	96.5	216.6	17.1	955.2
1.33	91.6	176.6	10.2	571.0
1.67	92.3	205.6	12.5	703.4
2.01	87.5	188.1	9.0	503.4
2.35	86.6	203.8	9.4	527.9
2.69	83.7	154.9	6.6	371.4

TABLE 2. COMPUTED DATA

AXIAL DISTANCE Z,M	INNER WALL TEMPERATURE TIW,C	LOCAL HEAT FLUX Q,KW/SQM	LOCAL HEAT TRANS COEFF HZ KW/SQM-K	NUSSELT NUMBER NUZ
		RUN 29		
0.31	99.3	236.8	24.9	1393.5
0.65	93.8	197.6	13.2	742.8
0.99	95.9	223.7	17.7	993.0
1.33	93.2	205.7	13.6	763.1
1.67	87.7	180.9	8.9	499.7
2.01	89.6	222.6	12.2	684.7
2.35	85.0	204.1	9.0	508.1
2.69	85.6	185.2	8.9	499.3
		RUN 30		
0.31	99.2	237.2	24.1	1347.2
0.65	104.3	292.4	63.7	3554.9
0.99	88.5	159.8	7.9	442.3
1.33	97.0	237.6	20.5	1149.7
1.67	84.0	148.8	6.1	344.1
2.01	89.5	222.4	11.9	671.1
2.35	88.6	236.4	12.3	688.8
2.69	82.0	152.8	6.1	346.8

TABLE 2. COMPUTED DATA

AXIAL DISTANCE Z,M	INNER WALL TEMPERATURE TIW,C	LOCAL HEAT FLUX Q,KW/SQM	LOCAL HEAT TRANS COEFF HZ KW/SQM-K	NUSSELT NUMBER NUZ
		RUN 31		
0.31	111.2	310.0	181.6	10099.2
0.65	102.7	248.2	23.4	1305.6
0.99	95.1	190.4	10.5	588.3
1.33	93.2	175.7	8.9	497.6
1.67	88.0	153.4	6.2	347.2
2.01	95.6	244.2	14.4	806.4
2.35	90.6	229.0	10.6	593.4
2.69	102.2	295.8	43.6	2433.7
		RUN 32		
0.31	110.5	310.0	131.5	7319.0
0.65	96.0	193.9	11.4	635.8
0.99	103.9	272.0	30.2	1684.4
1.33	95.4	202.8	11.7	654.3
1.67	81.1	99.1	3.1	177.6
2.01	91.7	216.7	10.5	589.4
2.35	93.1	256.5	13.6	764.2
2.69	98.6	268.3	23.7	1322.0

TABLE 2. COMPUTED DATA

AXIAL DISTANCE Z,M	INNER WALL TEMPERATURE TIW,C	LOCAL HEAT FLUX Q,KW/SQM	LOCAL HEAT TRANS COEFF HZ KW/SQM-K	NUSSELT NUMBER NUZ
		RUN 33		
0.31	85.1	207.8	30.9	1747.5
0.65	71.2	93.1	4.5	259.0
0.99	81.4	189.0	18.7	1061.8
1.33	86.2	239.6	46.8	2645.0
1.67	59.2	16.8	0.5	30.4
2.01	76.3	185.8	12.8	727.3
2.35	77.3	211.5	15.9	901.6
2.69	75.3	174.5	12.3	702.5
		RUN 34		
0.31	79.7	151.1	12.6	715.4
0.65	79.3	157.7	13.0	737.0
0.99	85.0	214.2	34.2	1932.4
1.33	80.1	177.5	16.1	912.2
1.67	59.5	11.8	0.4	21.7
2.01	76.9	184.9	13.4	764.6
2.35	73.8	180.5	10.9	618.8
2.69	73.0	147.9	9.0	511.7

TABLE 2. COMPUTED DATA

AXIAL DISTANCE Z,M	INNER WALL TEMPERATURE TIW,C	LOCAL HEAT FLUX Q,KW/SQM	LOCAL HEAT TRANS COEFF HZ KW/SQM-K	NUSSELT NUMBER NUZ
		RUN 35		
0.31	91.3	257.3		
0.65	91.0	267.3		
0.99	78.6	161.5	12.6	714.2
1.33	73.3	123.5	6.9	392.6
1.67	64.6	66.9	2.5	145.4
2.01	76.5	185.9	12.9	735.7
2.35	70.2	152.6	7.5	427.2
2.69	72.6	149.9	8.8	503.6
		RUN 36		
0.31	92.2	270.5		
0.65	81.4	188.2	18.8	1062.7
0.99	88.4	252.7	89.9	5071.1
1.33	71.7	113.1	5.8	333.6
1.67	58.6	15.3	0.5	27.4
2.01	75.9	186.2	12.7	721.8
2.35	72.8	179.4	10.2	582.0
2.69	78.6	207.0	20.1	1139.5

TABLE 2. COMPUTED DATA

AXIAL DISTANCE Z,M	INNER WALL TEMPERATURE TIW,C	LOCAL HEAT FLUX Q,KW/SQM	LOCAL HEAT TRANS COEFF HZ KW/SQM-K	NUSSELT NUMBER NUZ
		RUN 37		
0.31	73.0	150.0	13.8	786.6
0.65	61.0	53.3	2.3	135.3
0.99	84.9	269.3		
1.33	79.3	231.1	57.3	3260.5
1.67	62.2	94.5	4.5	259.1
2.01	70.7	186.0	15.1	863.8
2.35	61.9	125.4	6.0	344.4
2.69	76.1	231.4	65.7	3738.2
		RUN 38		
0.31	86.0	270.1		
0.65	82.5	254.7	242.7	13768.7
0.99	78.5	222.2	44.3	2517.8
1.33	64.9	112.0	6.1	348.7
1.67	59.2	78.4	3.3	188.7
2.01	66.3	155.2	9.3	534.3
2.35	66.7	178.0	11.0	630.3
2.69	80.0	273.3	50.1	2855.2

TABLE 2. COMPUTED DATA

AXIAL DISTANCE Z,M	INNER WALL TEMPERATURE TIW,C	LOCAL HEAT FLUX Q,KW/SQM	LOCAL HEAT TRANS COEFF HZ KW/SQM-K	NUSSELT NUMBER NUZ
		RUN 39		
0.31	65.1	72.1	4.0	232.2
0.65	79.5	208.2	62.4	3548.9
0.99	73.9	159.8	18.0	1030.3
1.33	74.3	177.2	21.6	1234.9
1.67	66.4	117.6	7.3	422.1
2.01	71.9	184.2	17.9	1026.7
2.35	66.8	153.9	10.4	577.4
2.69	55.3	38.7	1.5	85.7
		RUN 40		
0.31	77.0	183.7	31.1	1769.4
0.65	71.6	145.9	12.9	740.6
0.99	72.2	156.4	14.8	847.5
1.33	63.0	82.8	4.2	244.0
1.67	65.2	106.7	6.2	357.1
2.01	68.0	153.2	10.8	618.0
2.35	65.9	149.2	9.2	529.1
2.69	69.9	171.2	15.4	881.6

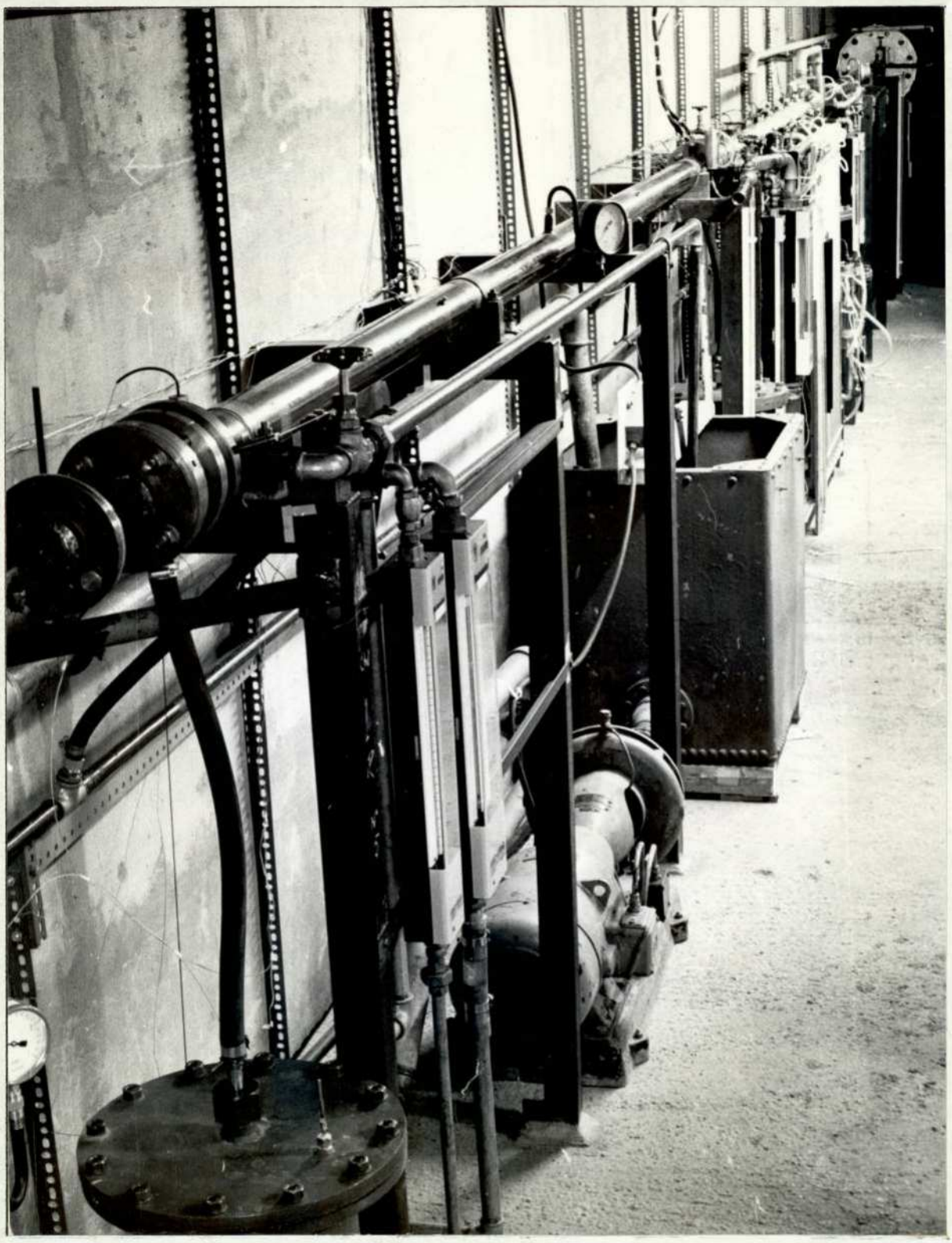

FIG.1 EXPERIMENTAL RIG

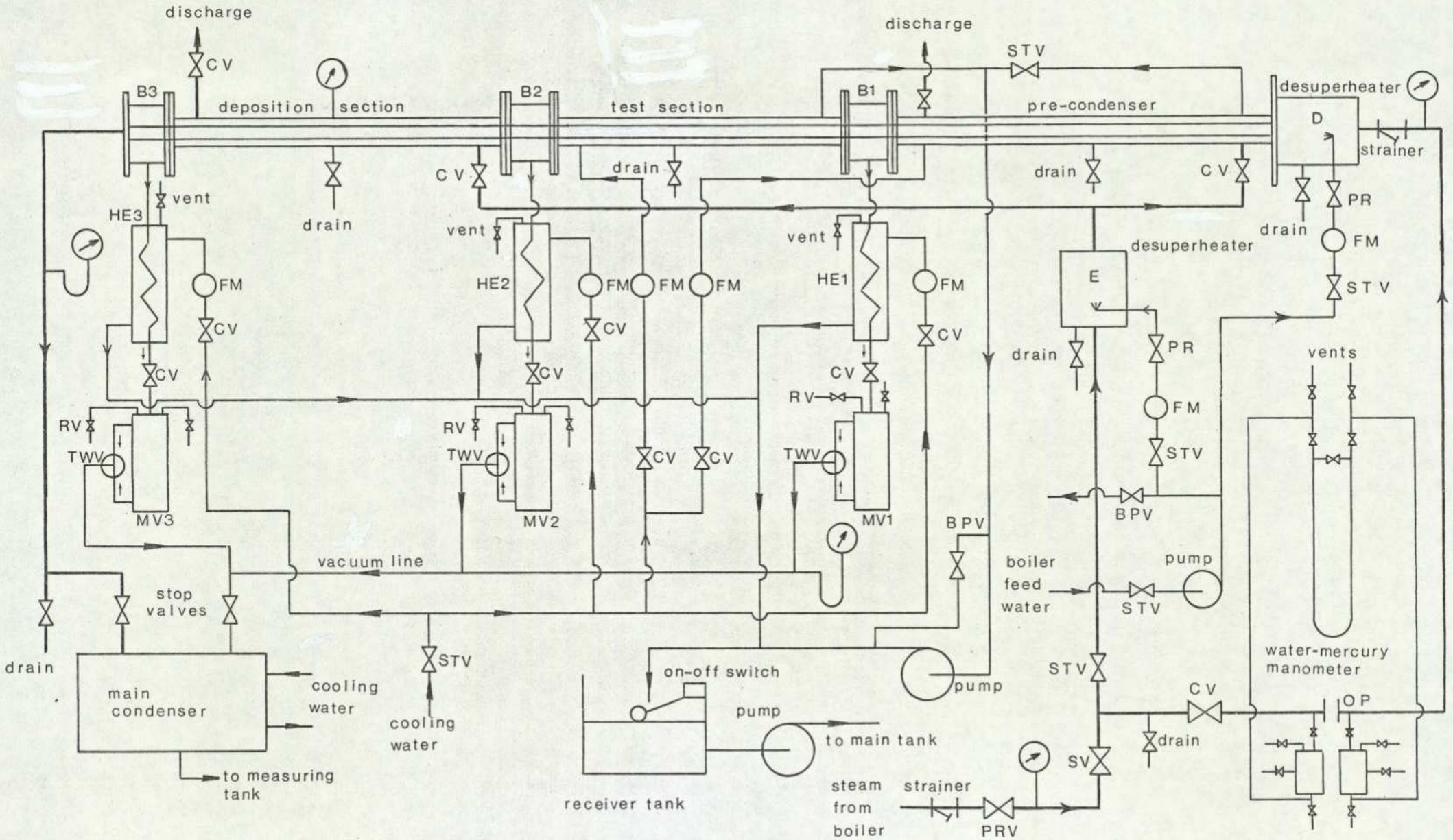

FIG. 2 FLOW DIAGRAM OF EXPERIMENTAL RIG

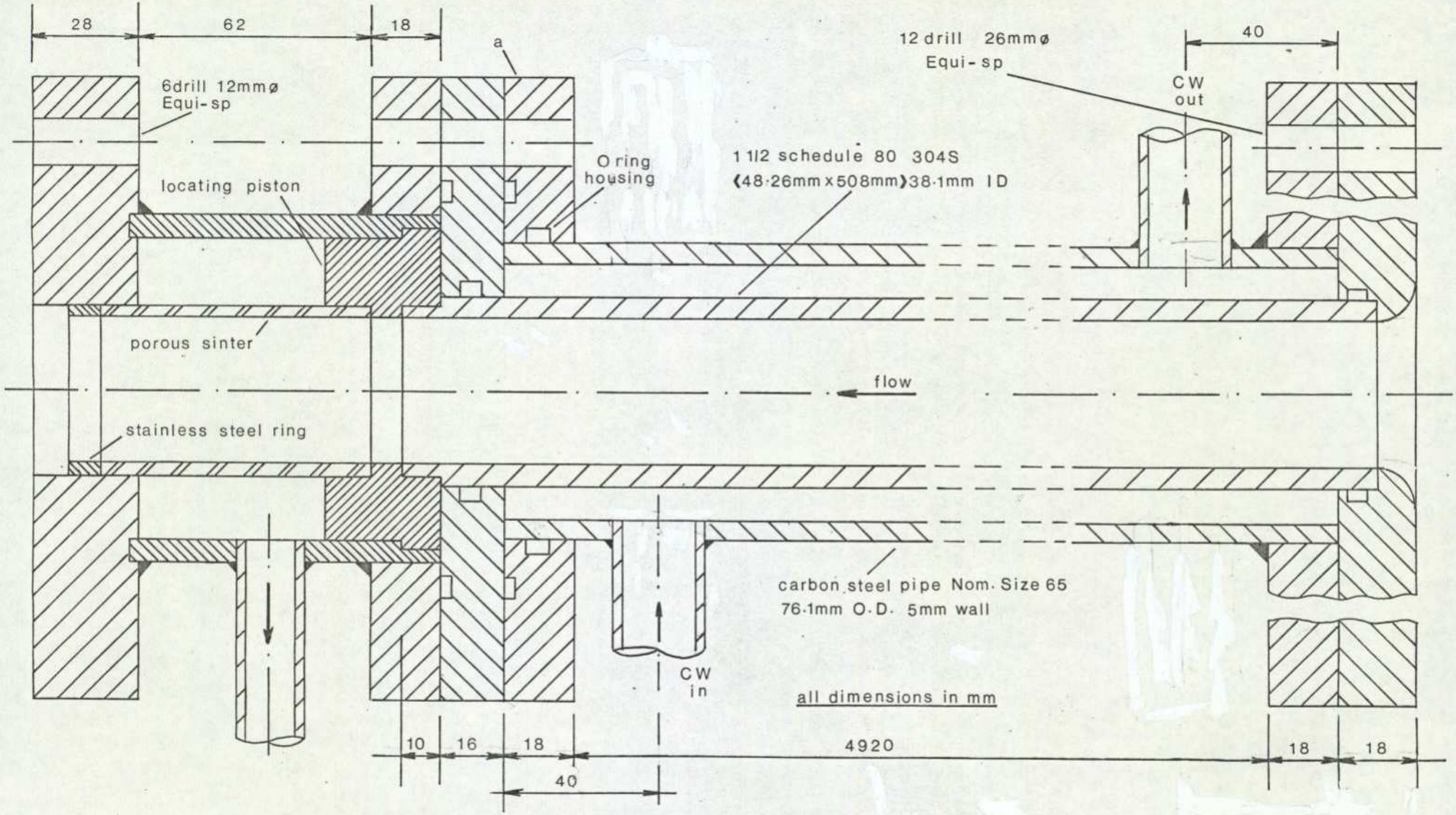

FIG. 3 PRE CONDENSER AND FILM REMOVAL UNIT ARRANGEMENT

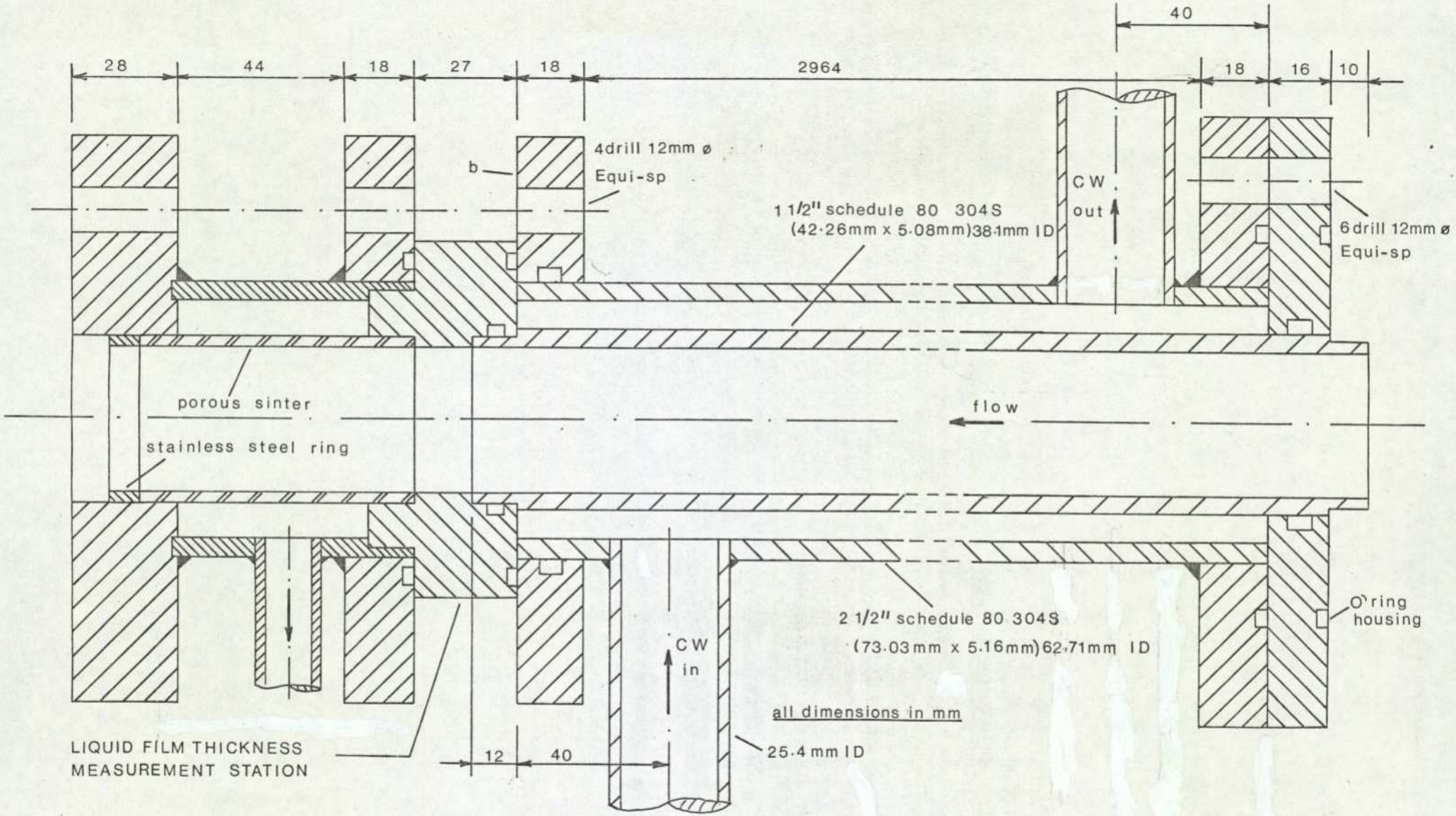

FIG. 4 TEST CONDENSER AND FILM REMOVAL UNIT ARRANGEMENT

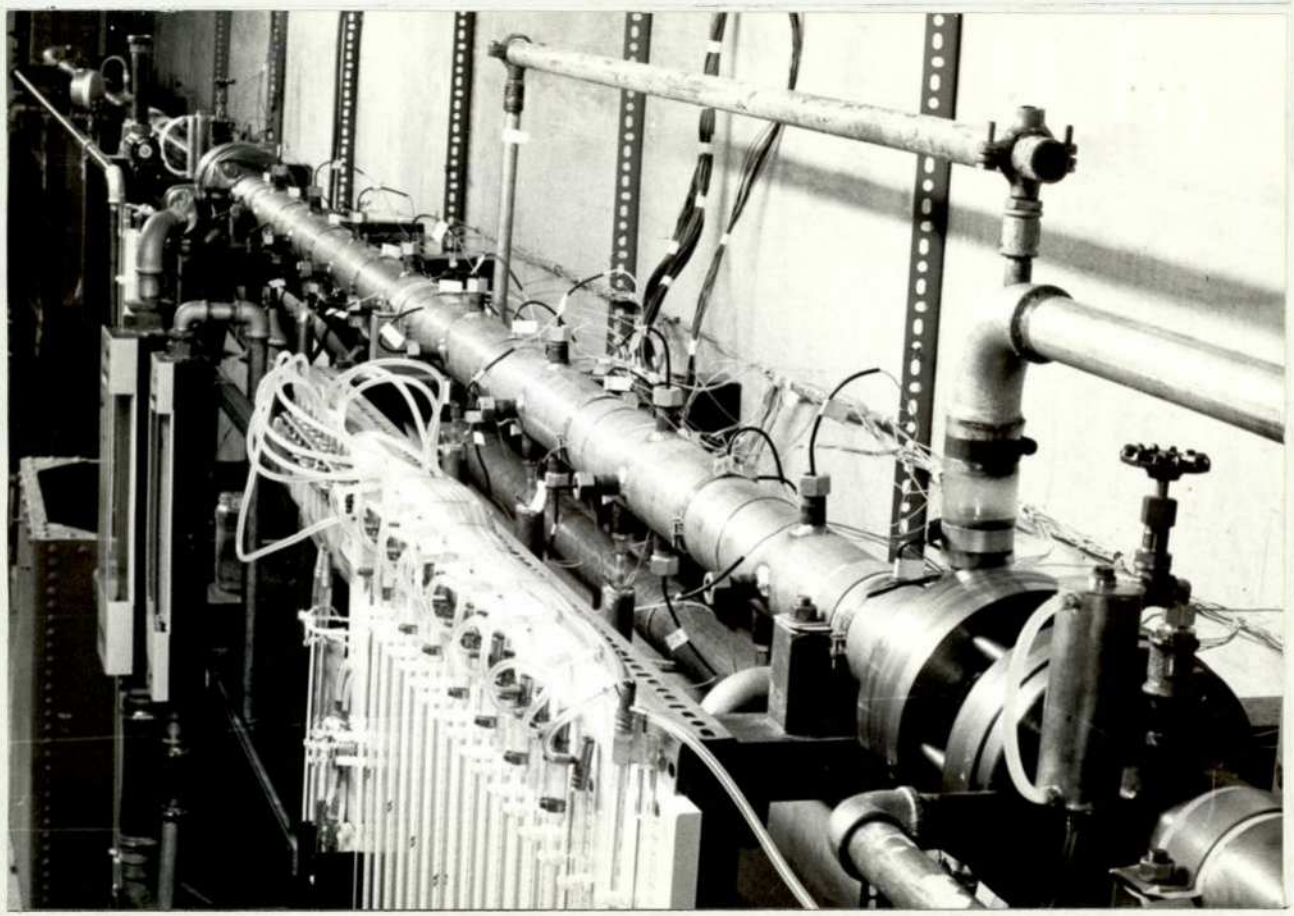

FIG. 5 TEST CONDENSER

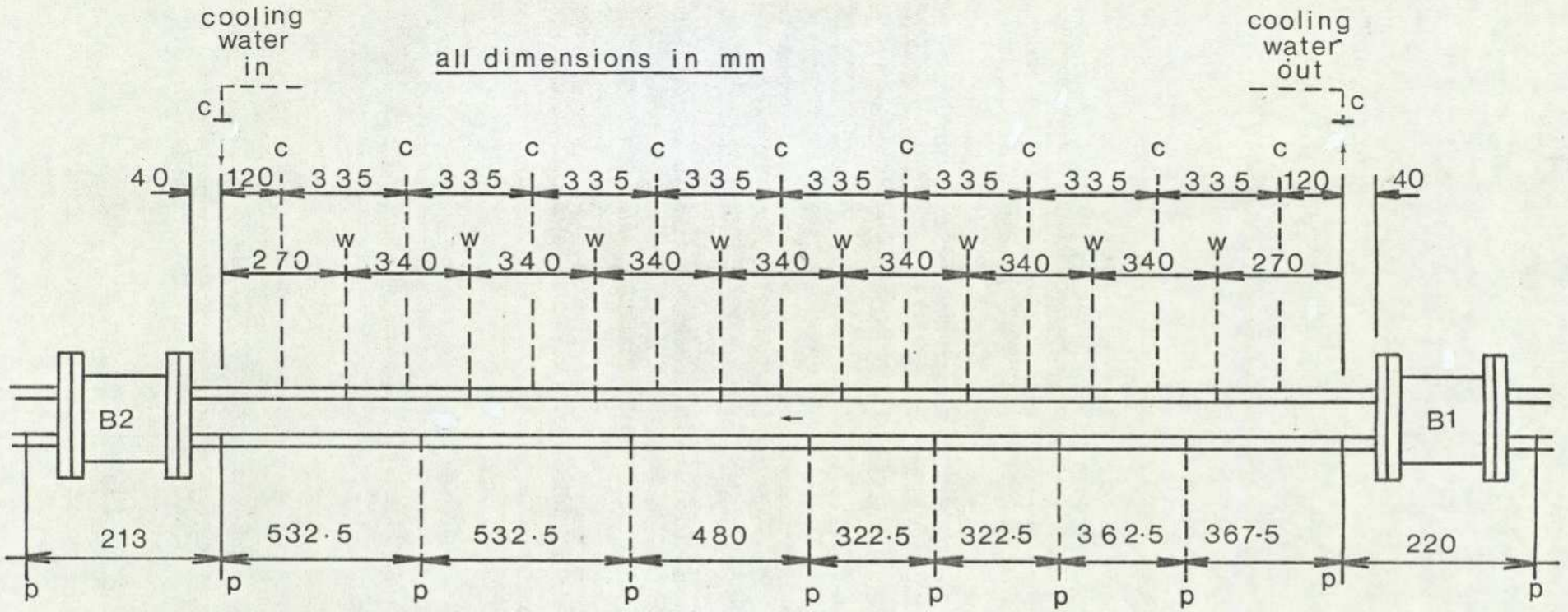

c = Cooling water thermocouple
w = Wall thermocouple
p = Pressure tap
B_1, B_2 = Porous sinter bush

FIG. 6 THERMOCOUPLE AND PRESSURE TAPS LAYOUT ON TEST CONDENSER

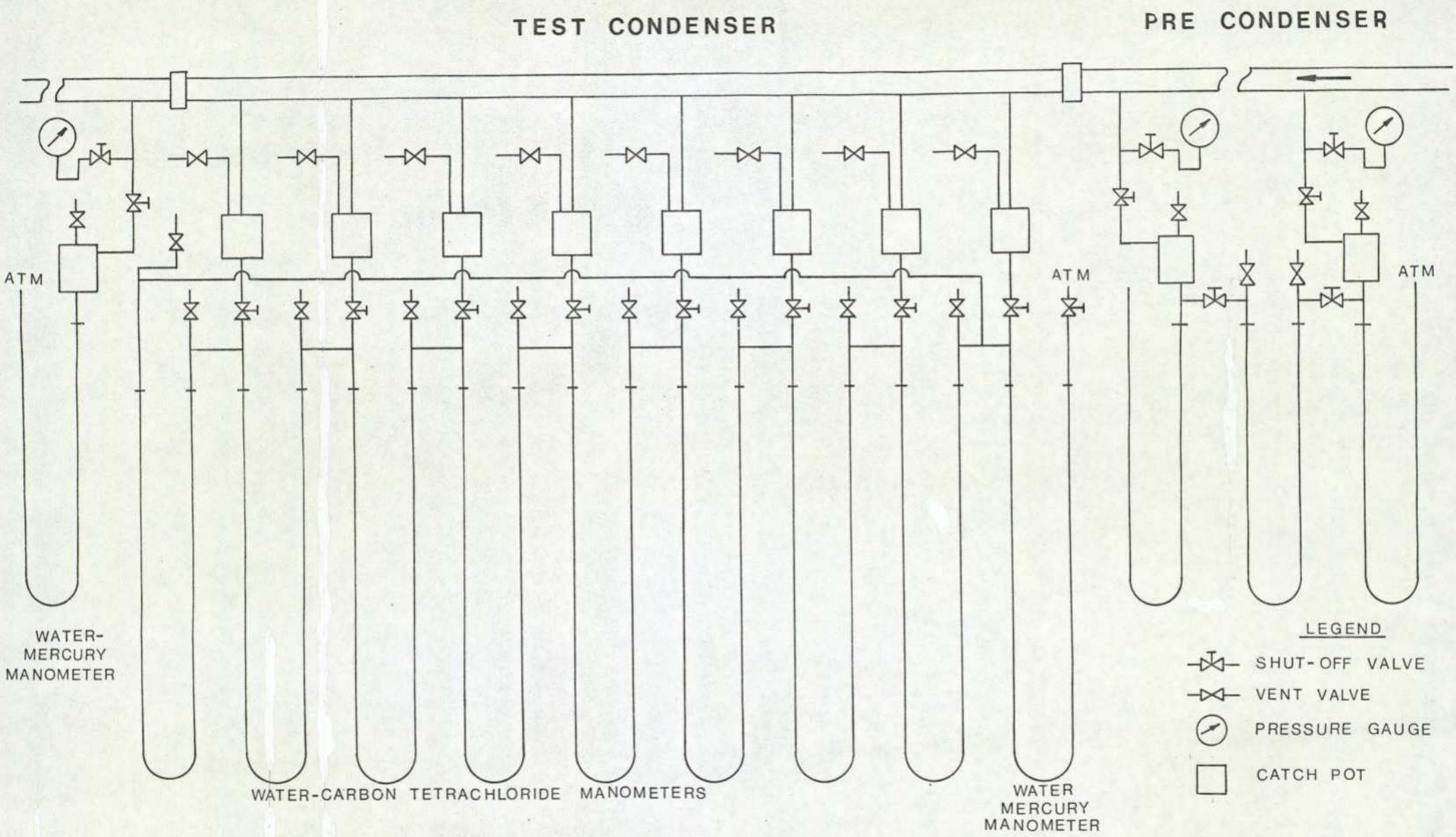

FIG. 7 SCHEMATIC DIAGRAM FOR PRESSURE DROP MEASUREMENT

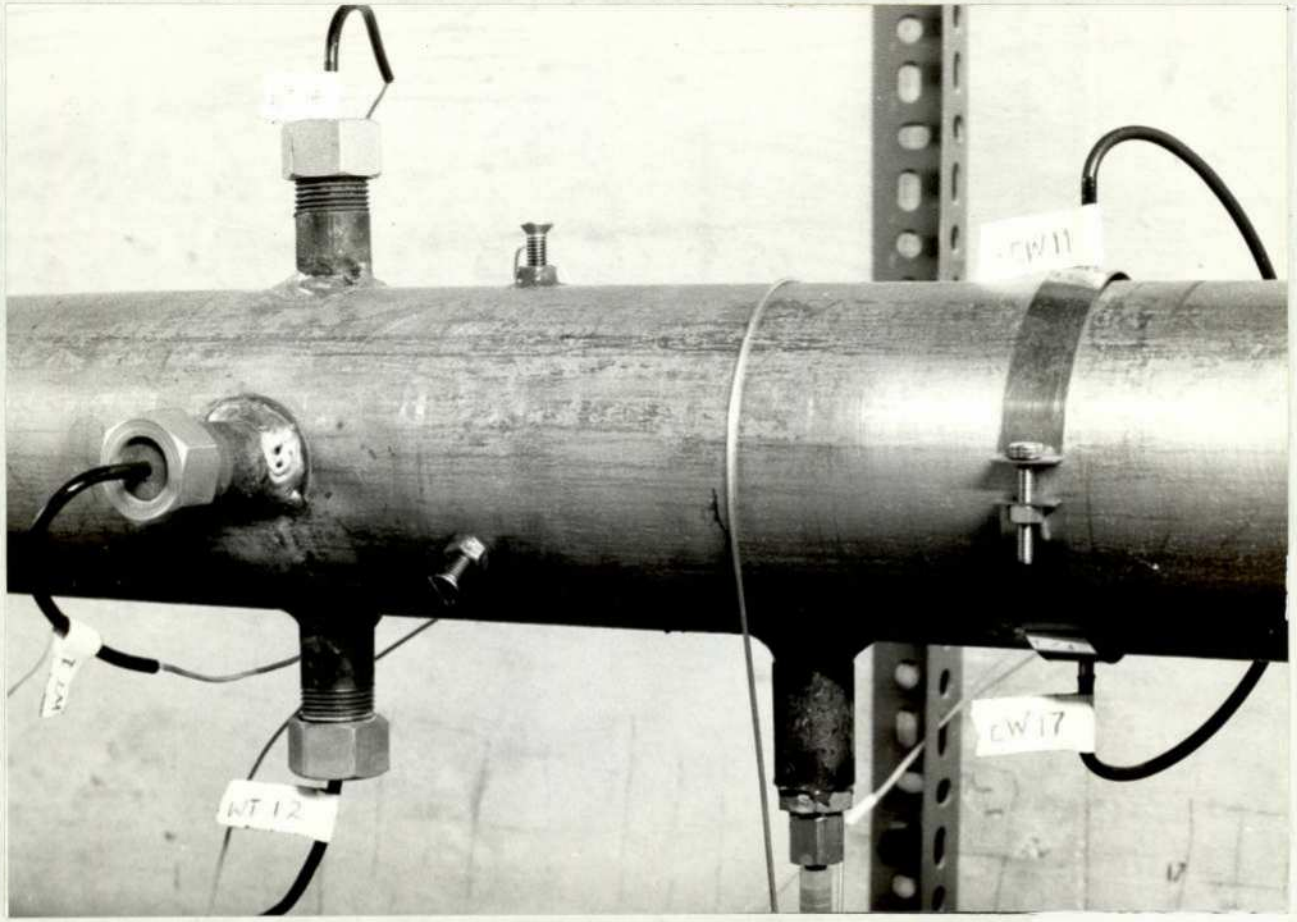

FIG. 8 TEST CONDENSER MEASUREMENT STATIONS

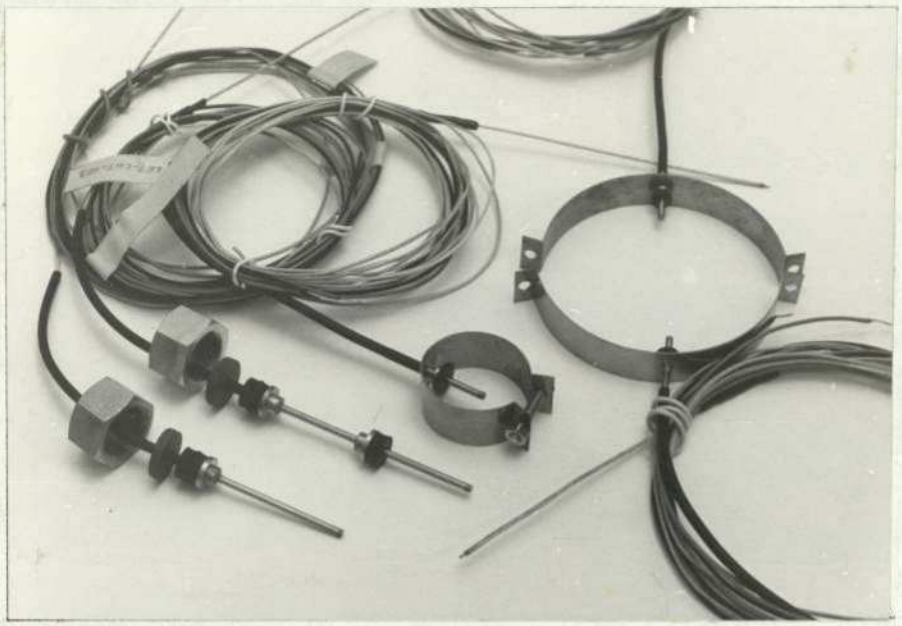

FIG. 9 DIFFERENT THERMOCOUPLE ARRANGEMENTS

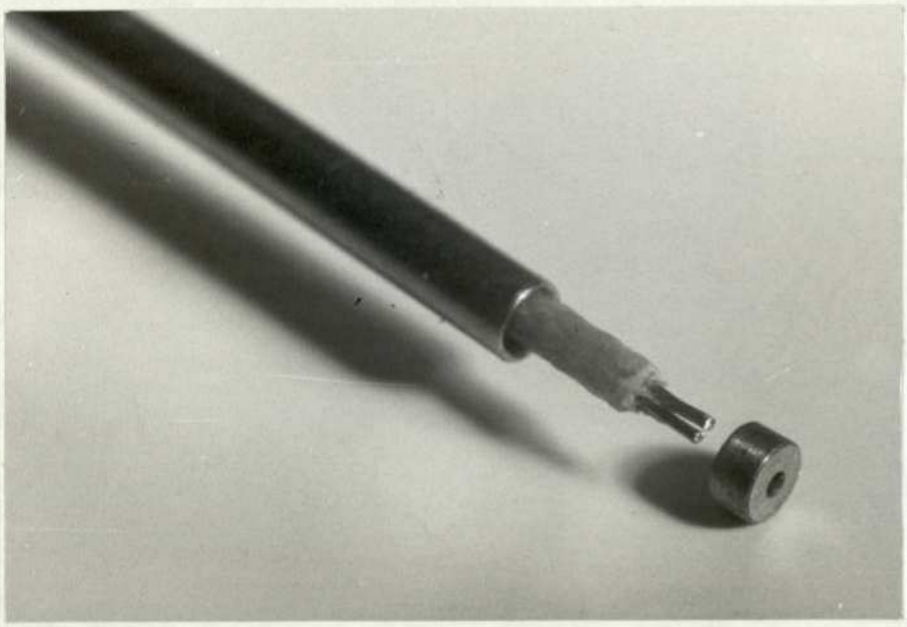

FIG. 10 THERMOCOUPLE ASSEMBLE DETAILS

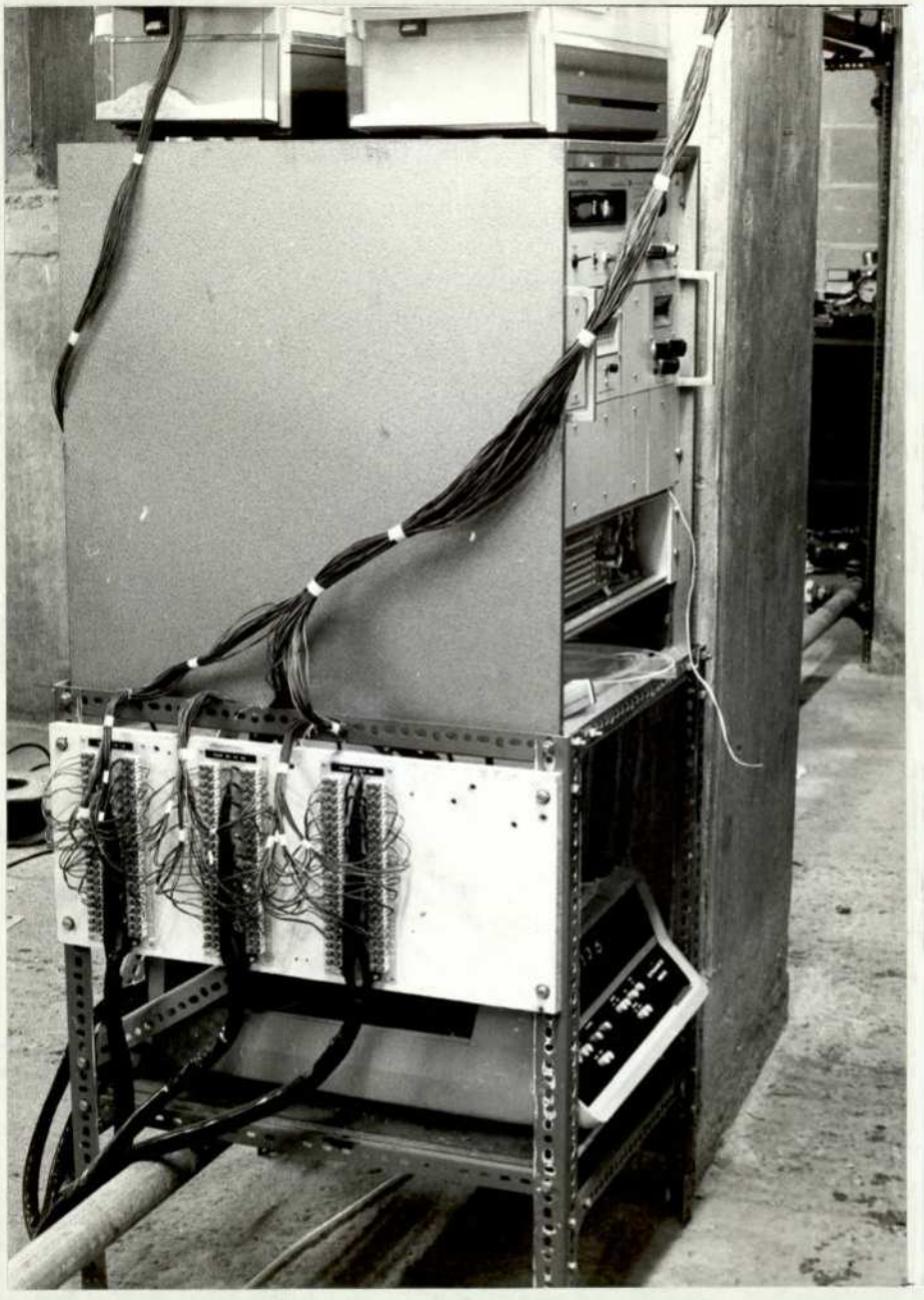

FIG. 11 THERMOCOUPLE OUTPUT MEASURING DEVICE

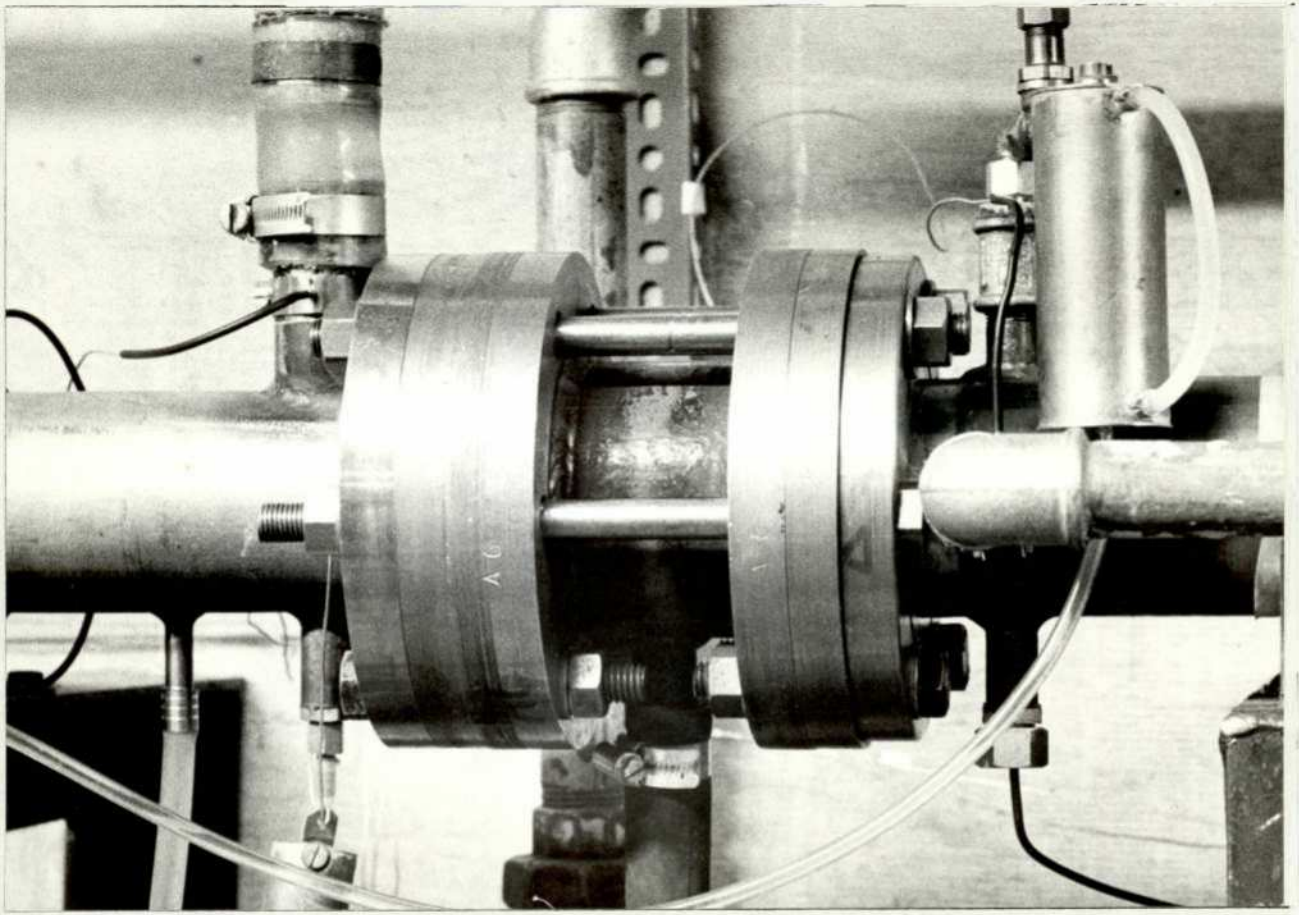

FIG.12 POROUS WALL FILM REMOVAL DEVICE

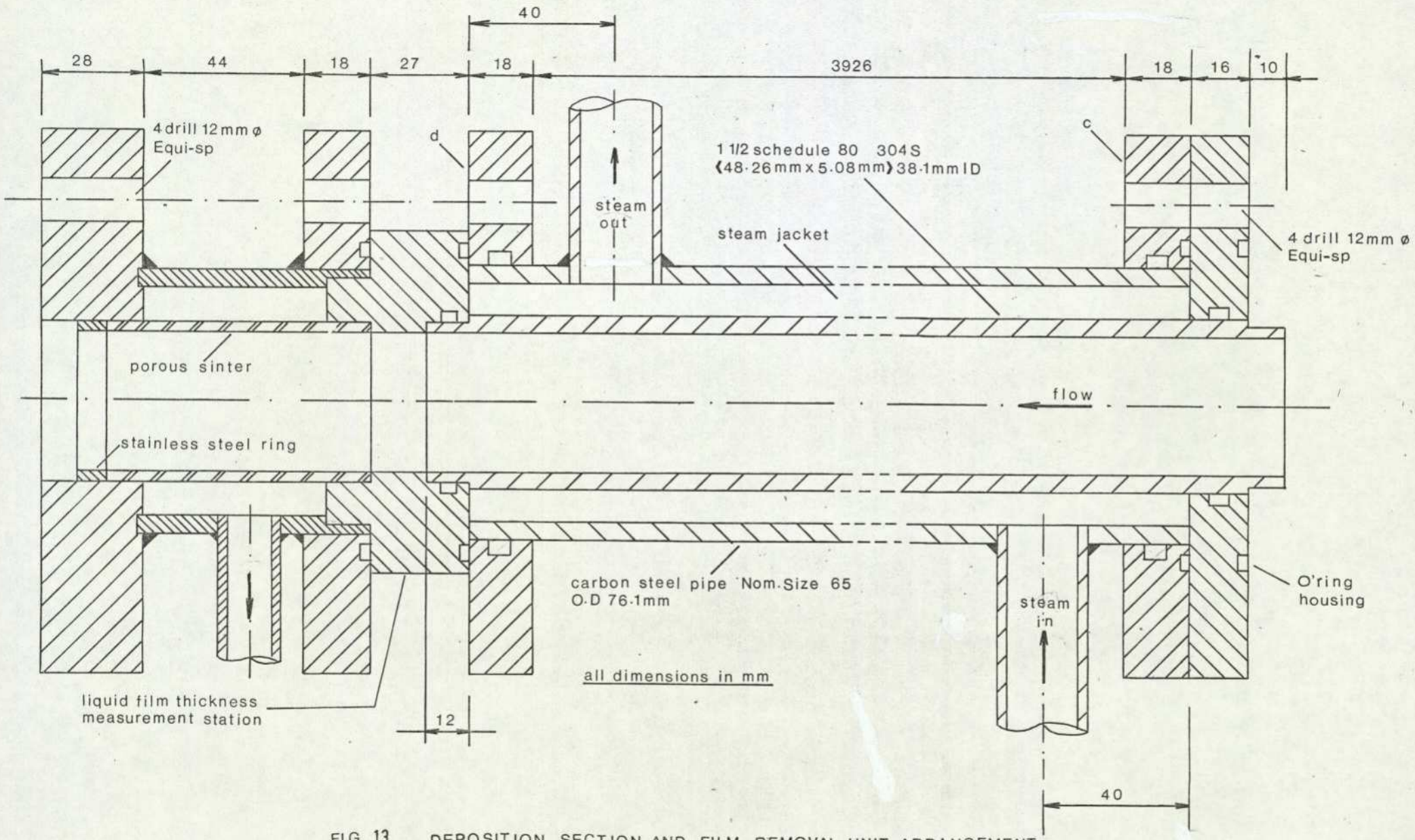

FIG. 13 DEPOSITION SECTION AND FILM REMOVAL UNIT ARRANGEMENT

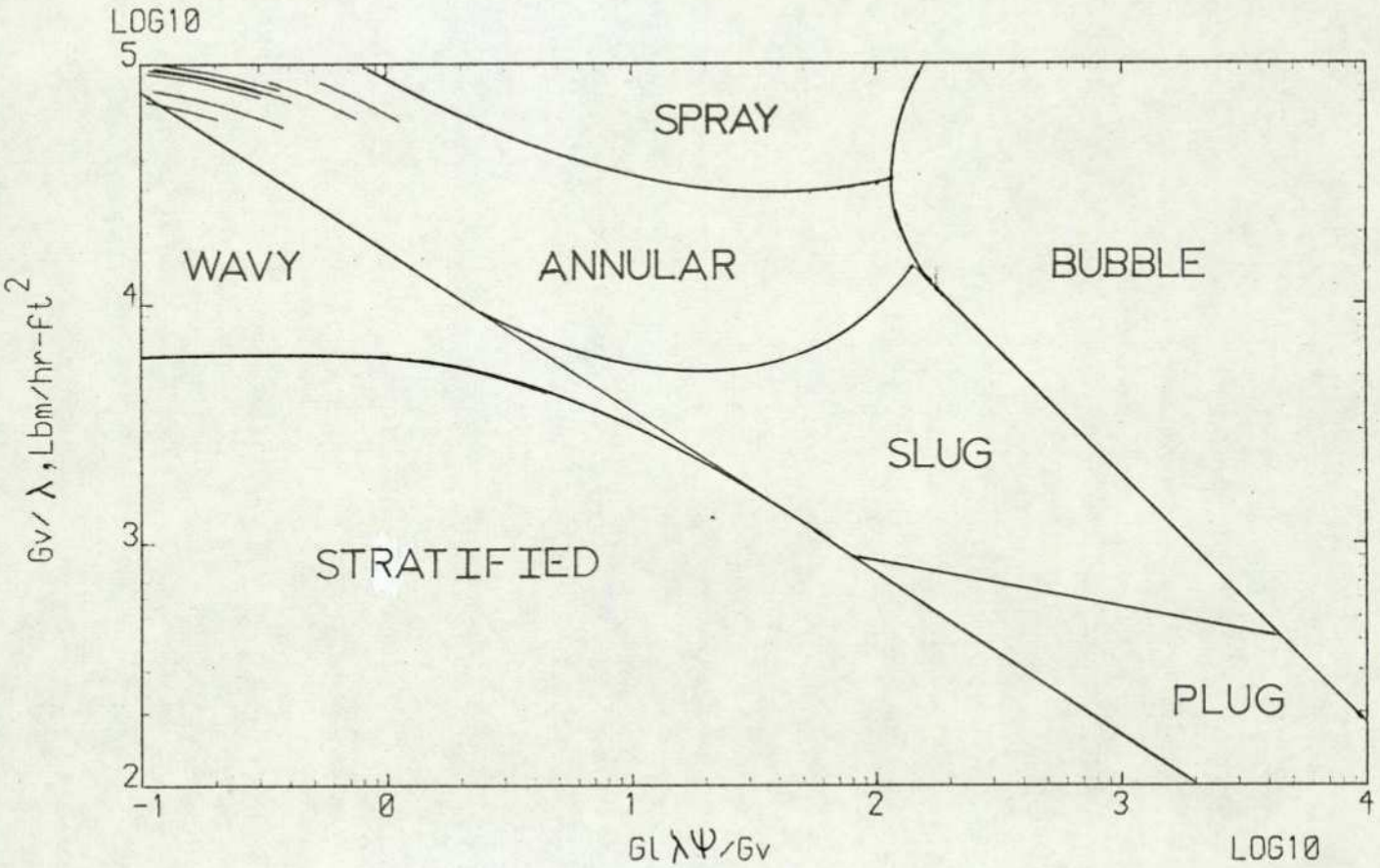

FIG.14 LOCATION OF RUNS ON THE BAKER'S MAP

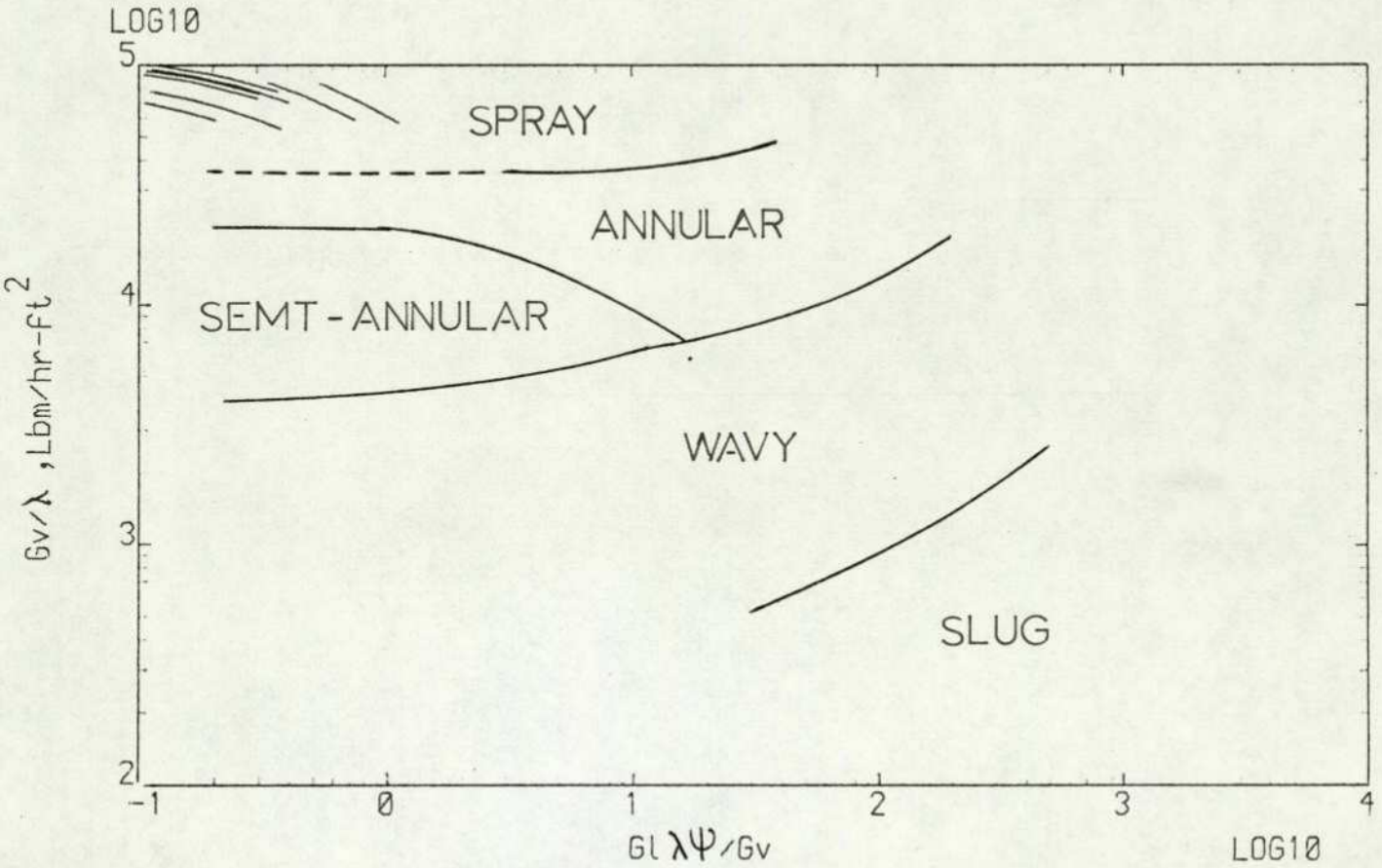

FIG.15 LOCATION OF RUNS ON THE MODIFIED BAKER'S MAP(SOLIMAN,1973)

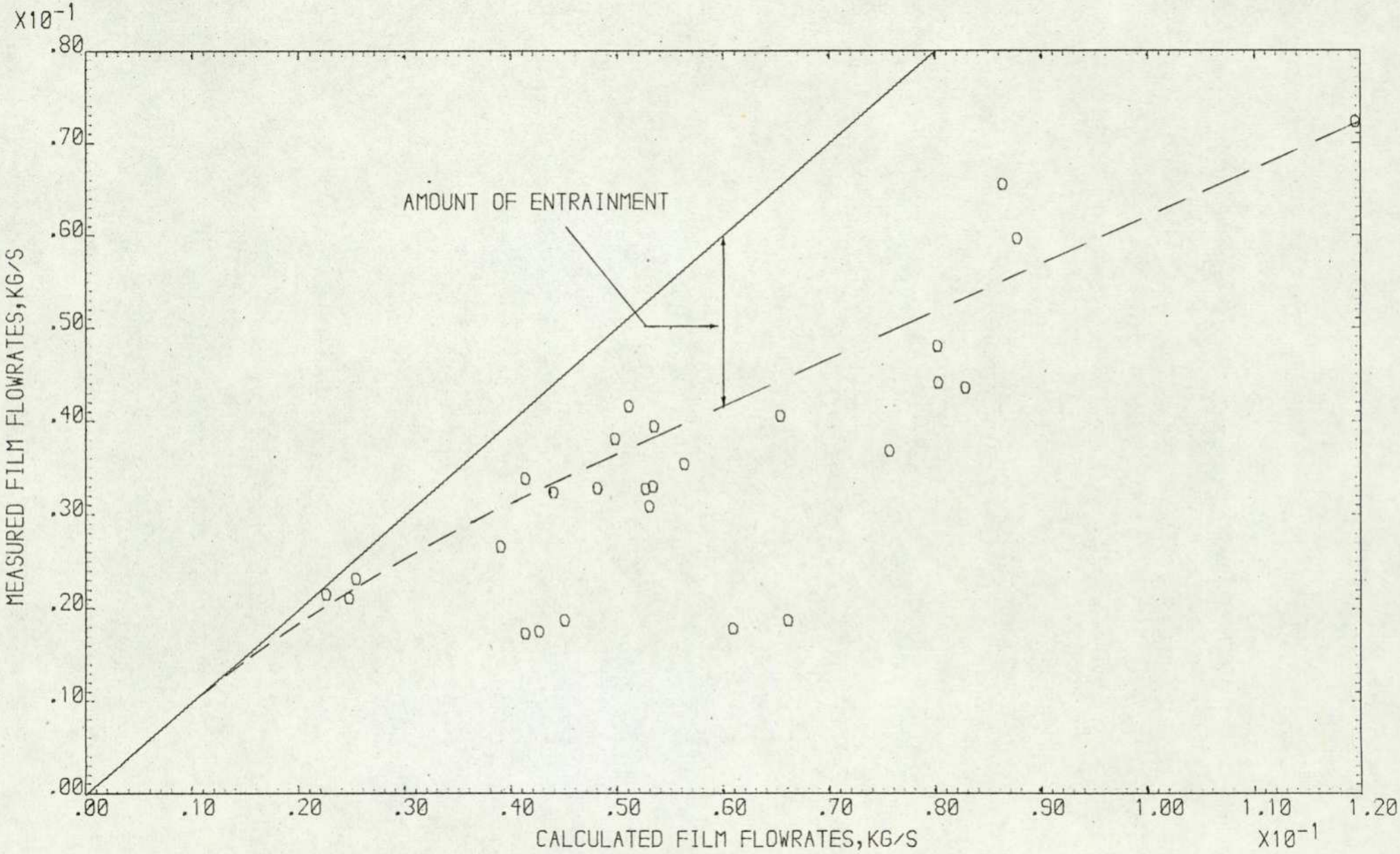

FIG.16 COMPARISON OF MEASURED AND CALCULATED FILM FLOWRATES

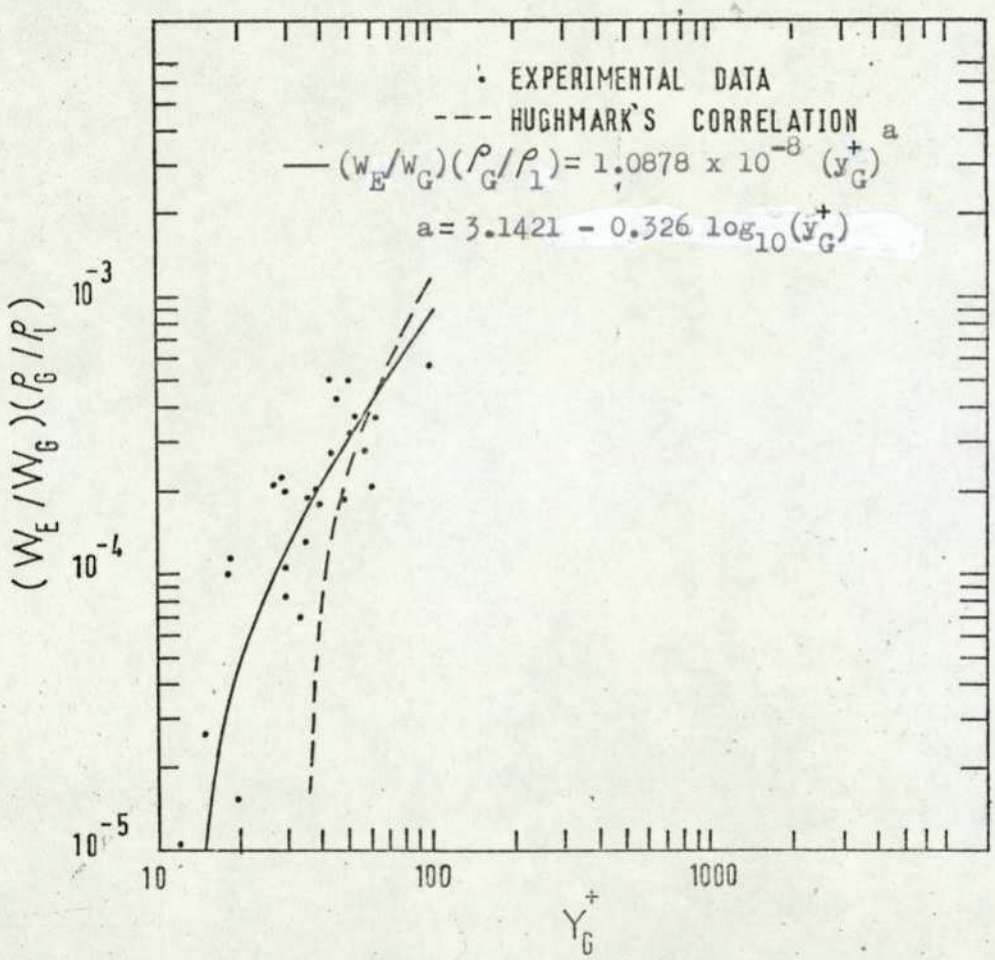

FTG. 17 ENTRAINMENT CORRELATION OF HUGHMARK.

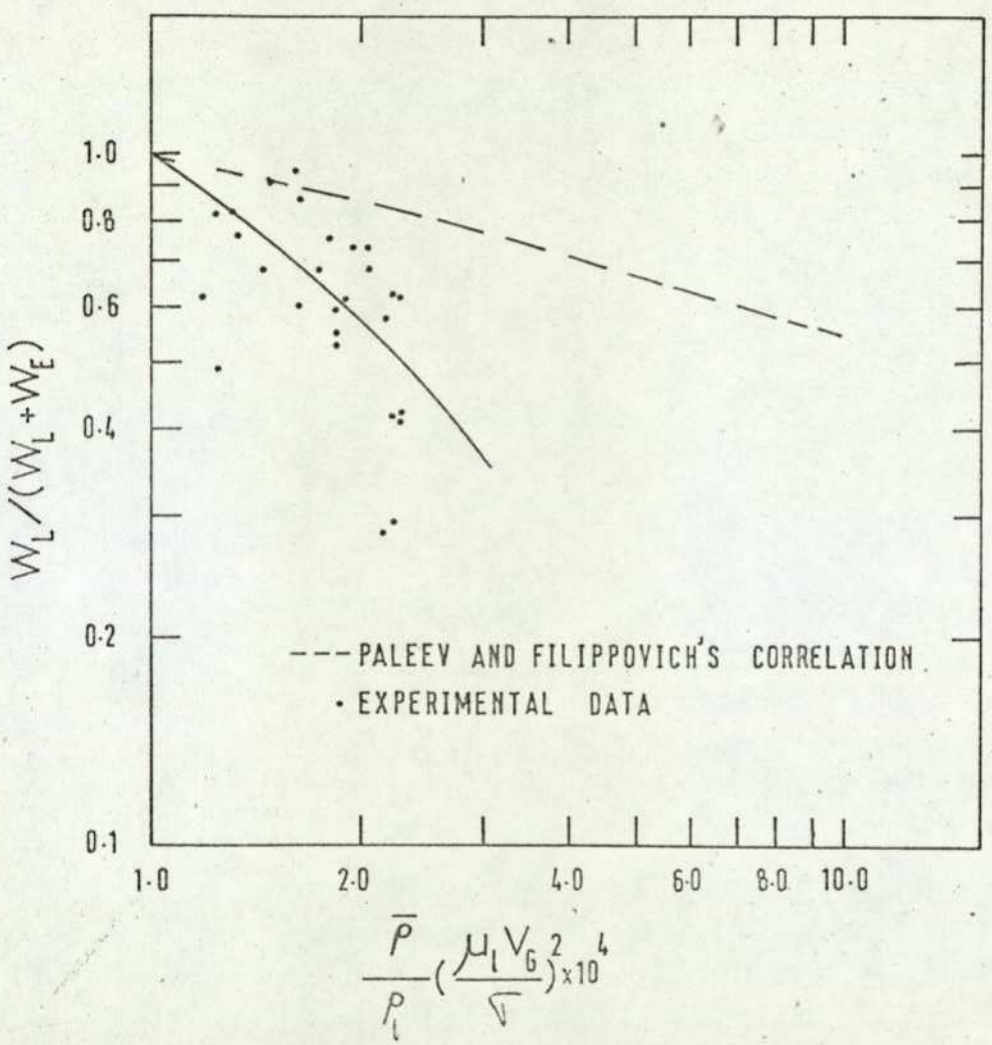

FIG·18 ENTRAINMENT CORRELATION OF PALEEV AND FTLIPPOVICH

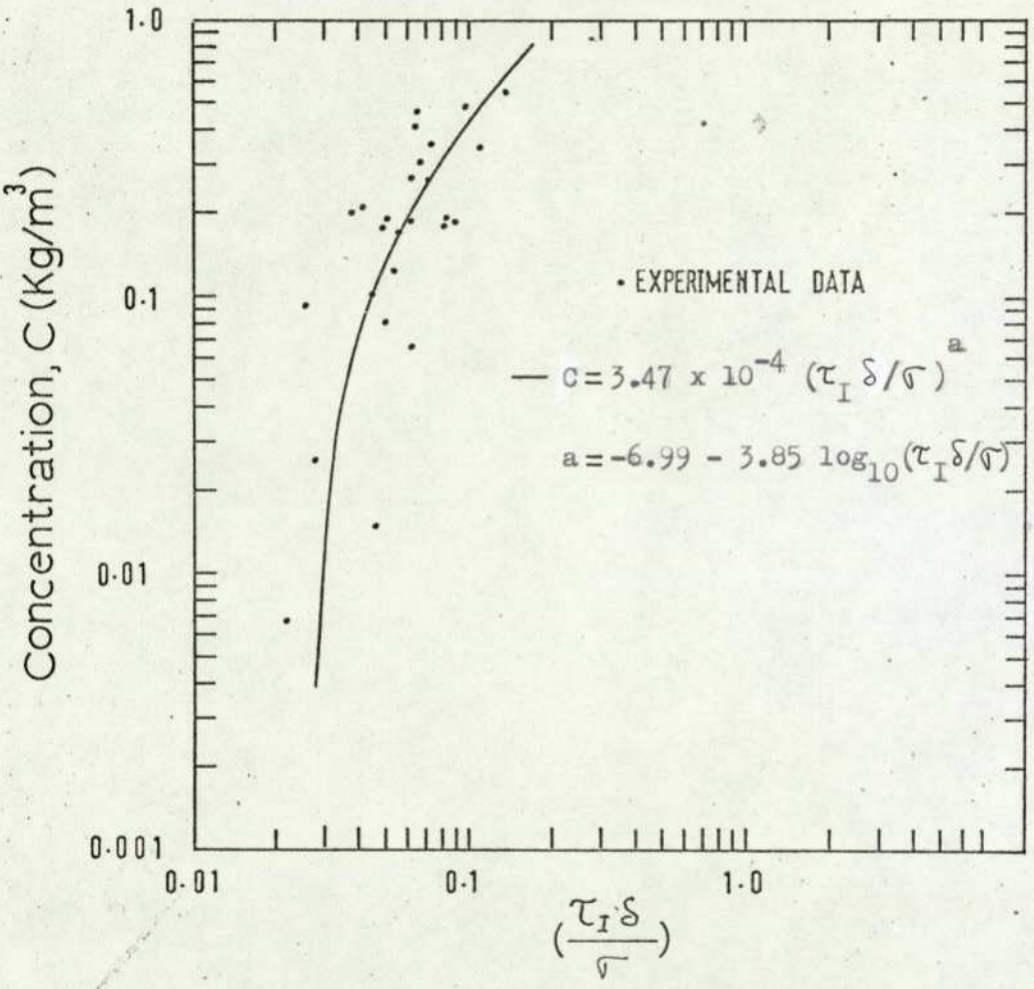

FTG·19 ENTRAINMENT CORRELATION OF WHALLEY et al

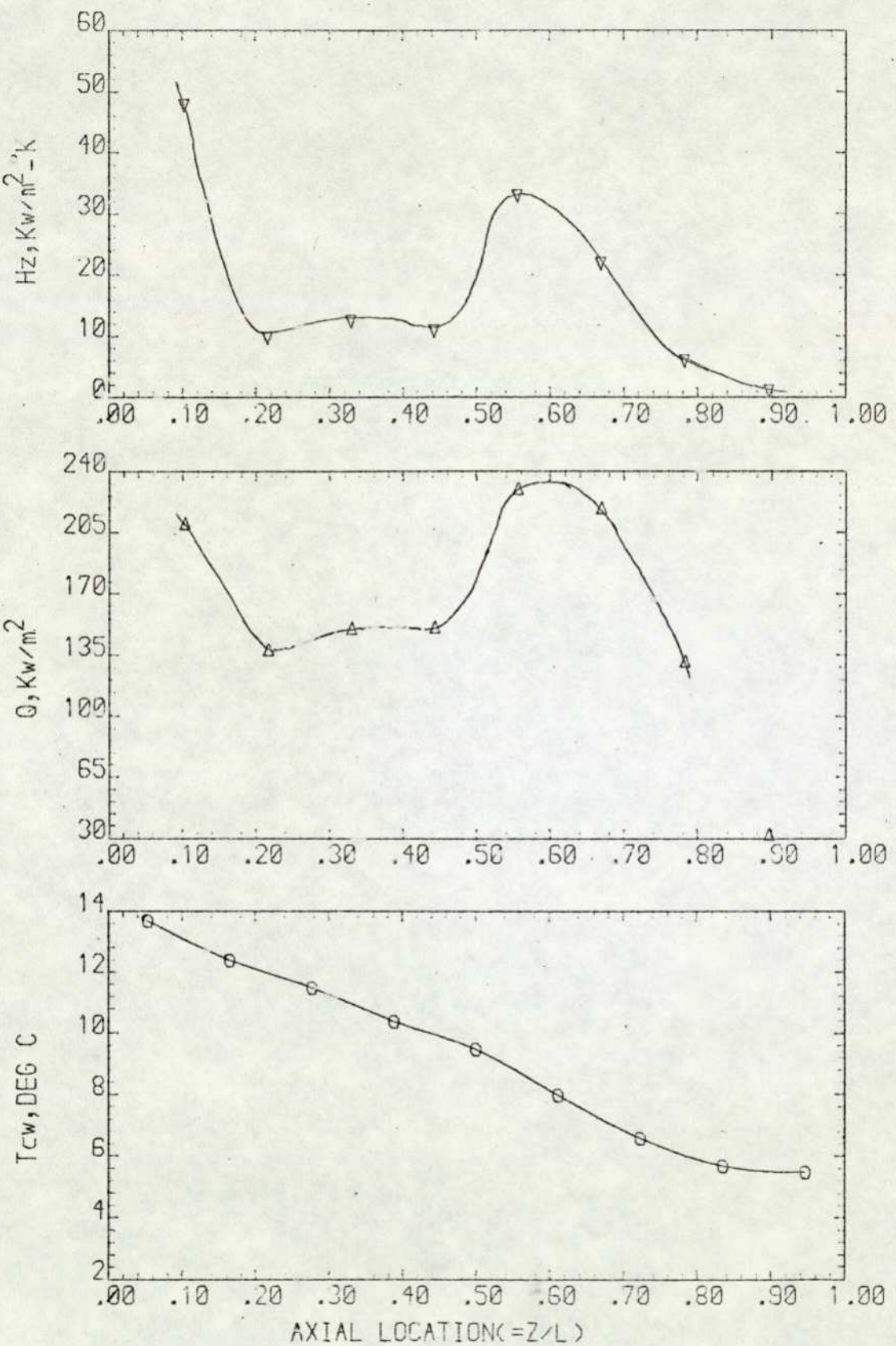

FIG. 20 VARIATION OF LOCAL HEAT TRANSFER COEFFICIENT, LOCAL HEAT FLUX AND COOLING WATER TEMPERATURE RUN 12

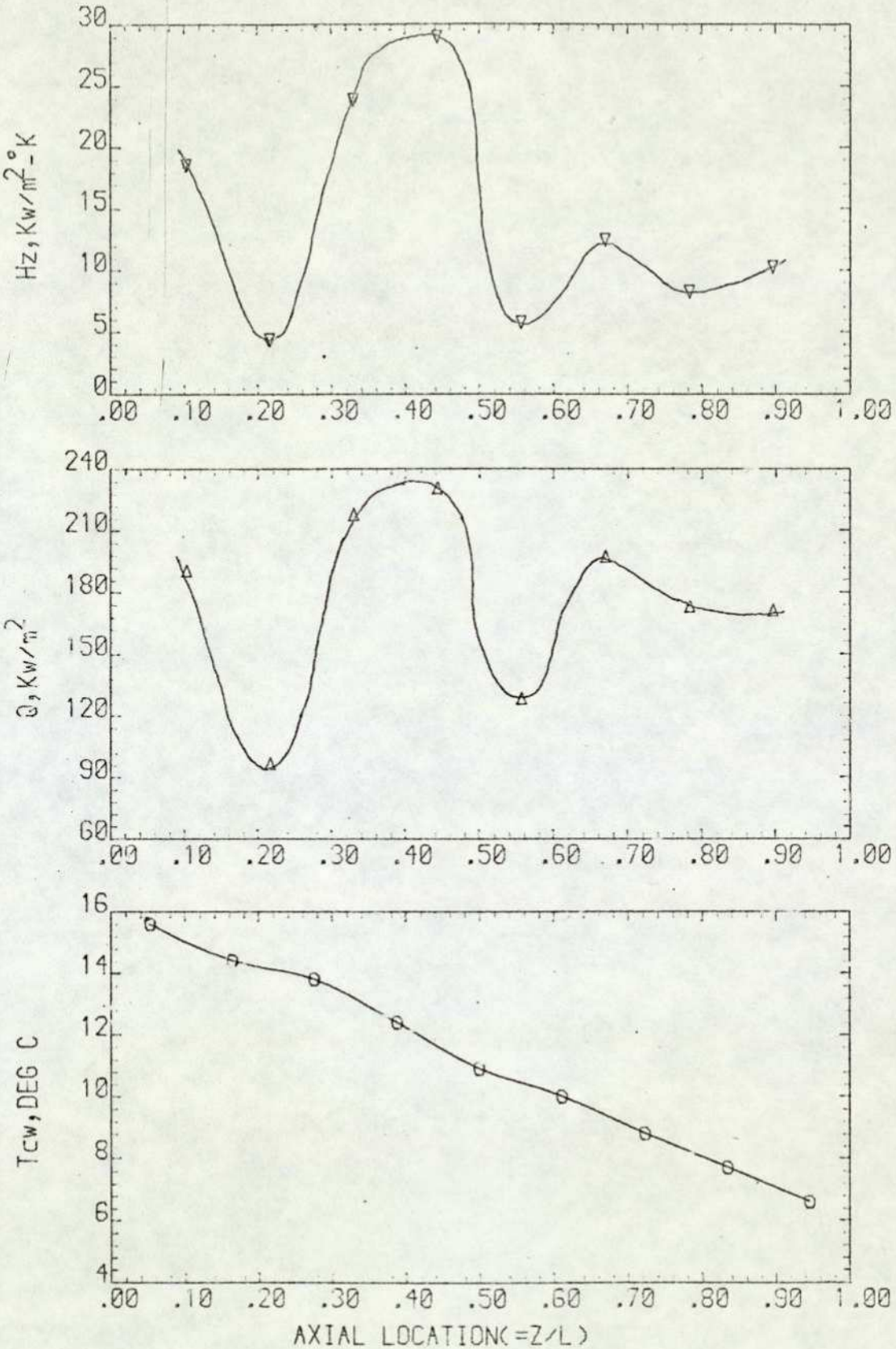

FIG.21 VARIATION OF LOCAL HEAT TRANSFER COEFFICIENT, LOCAL HEAT FLUX AND COOLING WATER TEMPERATURE RUN 4

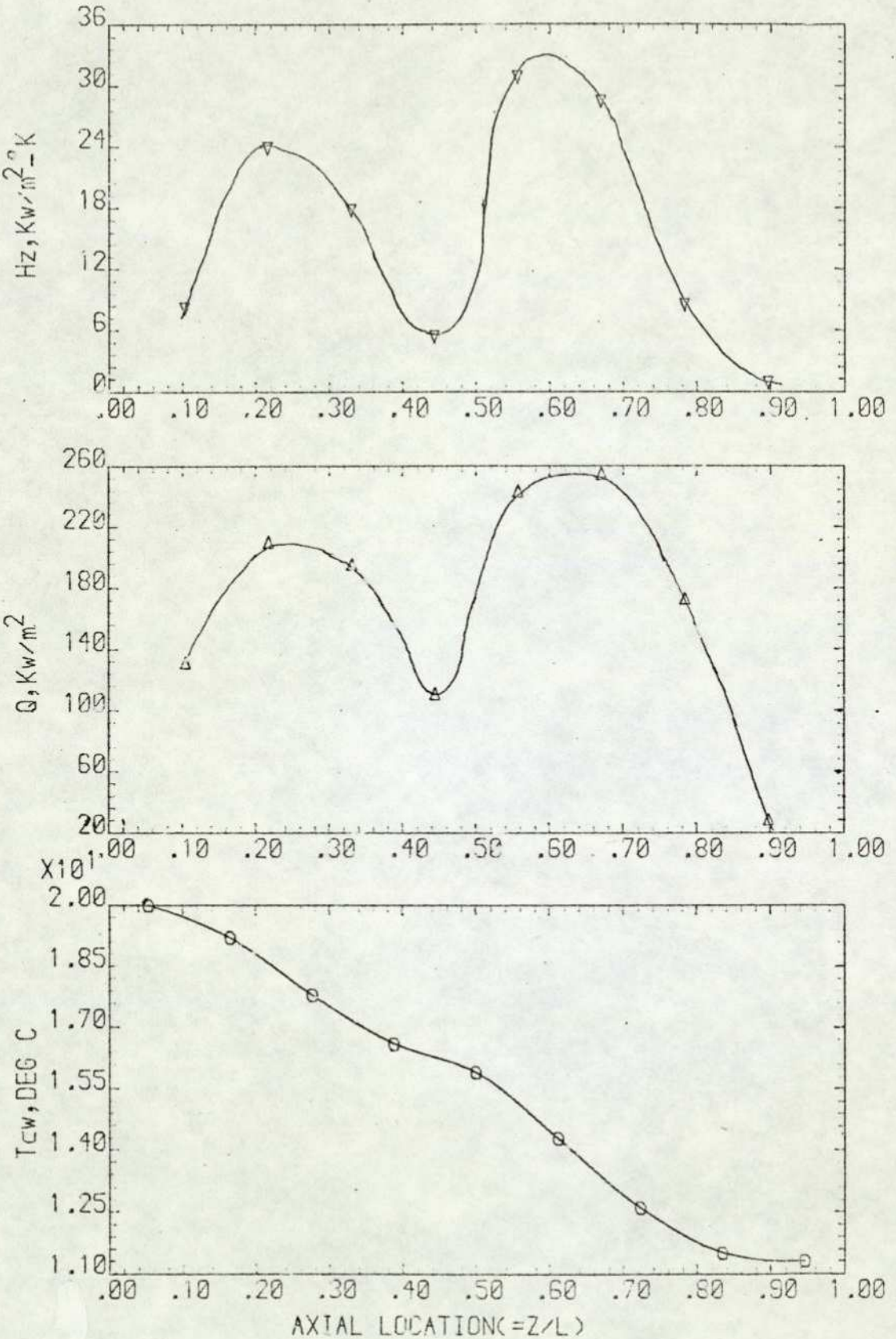

FIG.23 VARIATION OF LOCAL HEAT TRANSFER COEFFICIENT, LOCAL HEAT FLUX AND COOLING WATER TEMPERATURE RUN 1

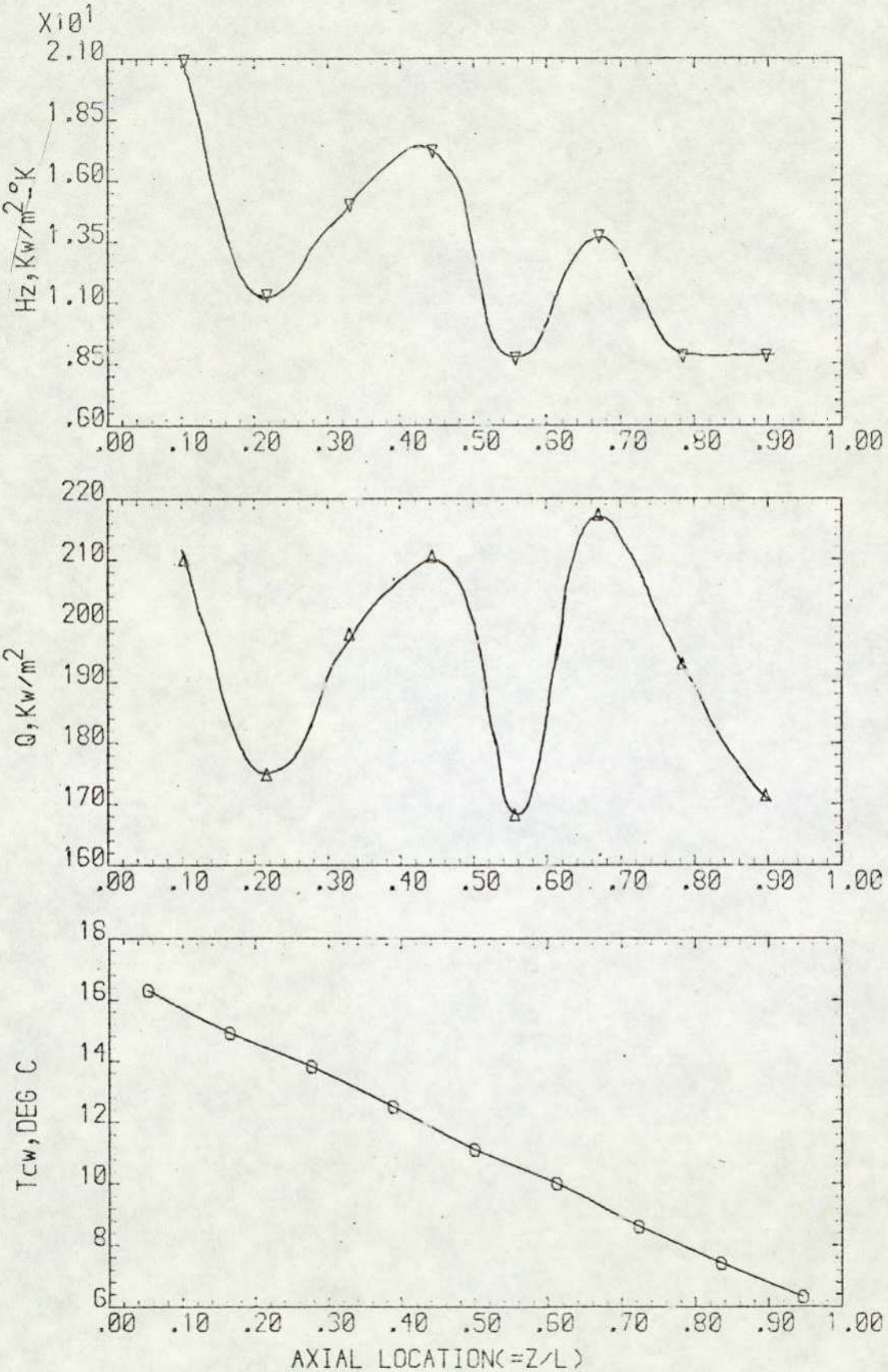

FIG. 24 VARIATION OF LOCAL HEAT TRANSFER COEFFICIENT, LOCAL HEAT FLUX AND COOLING WATER TEMPERATURE RUN 7

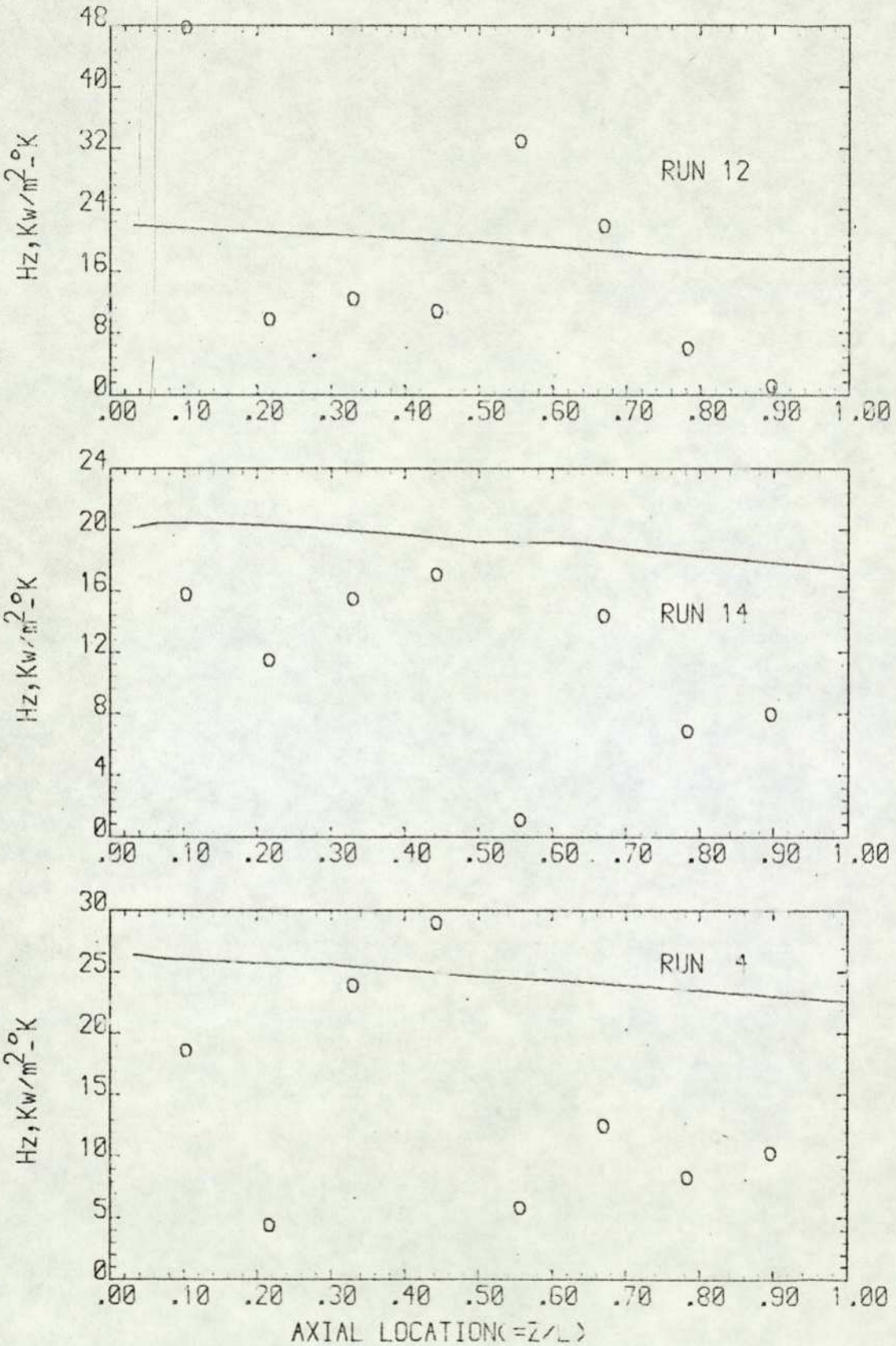

FIG. 25 COMPARISON BETWEEN EXPERIMENTAL AND CALCULATED LOCAL HEAT TRANSFER COEFFICIENT USING SHAH'S CORRELATION(SHAH, 1979)

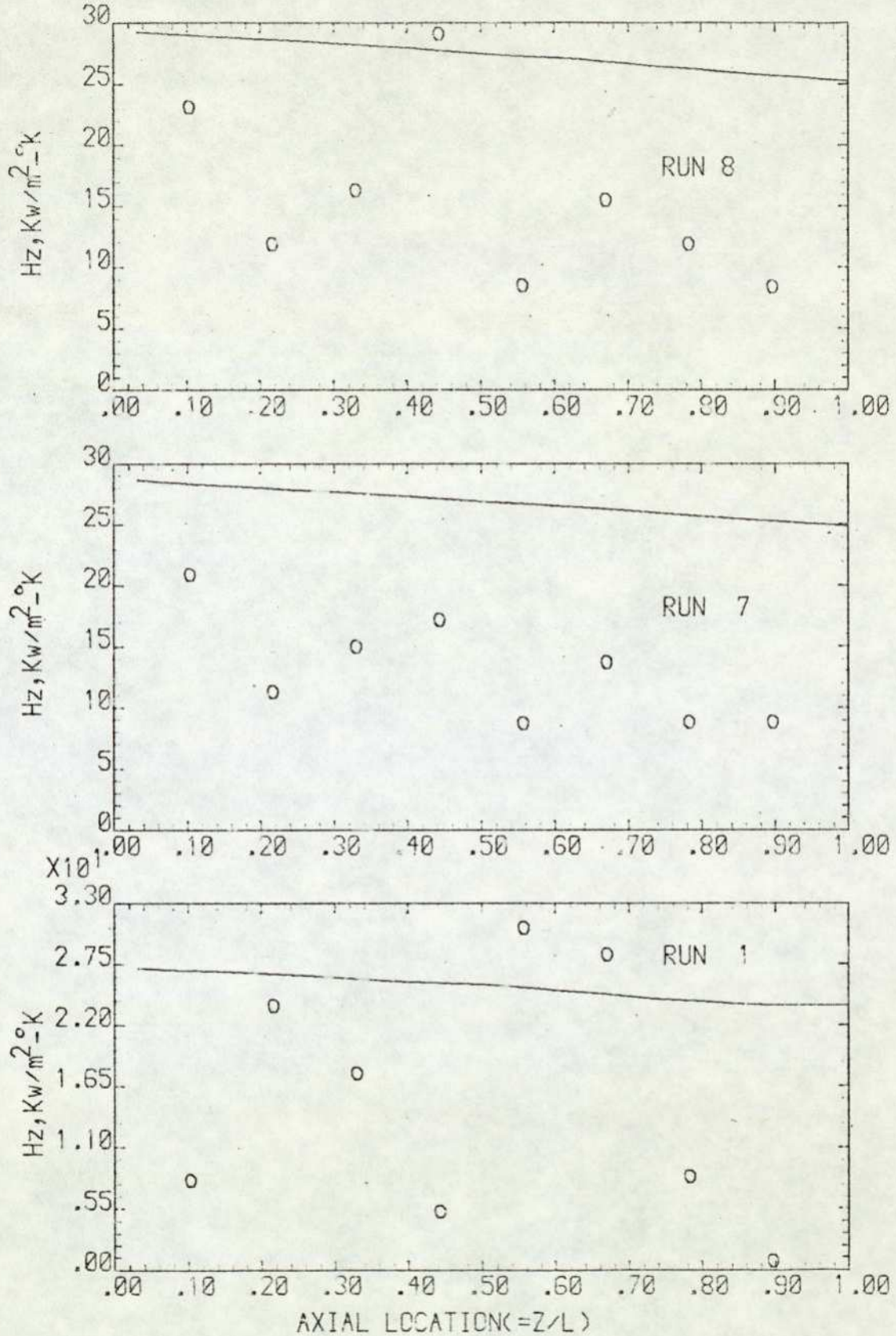

FIG. 26 COMPARISON BETWEEN EXPERIMENTAL AND CALCULATED LOCAL HEAT TRANSFER COEFFICIENT USING SHAH'S CORRELATION(SHAH, 1979)

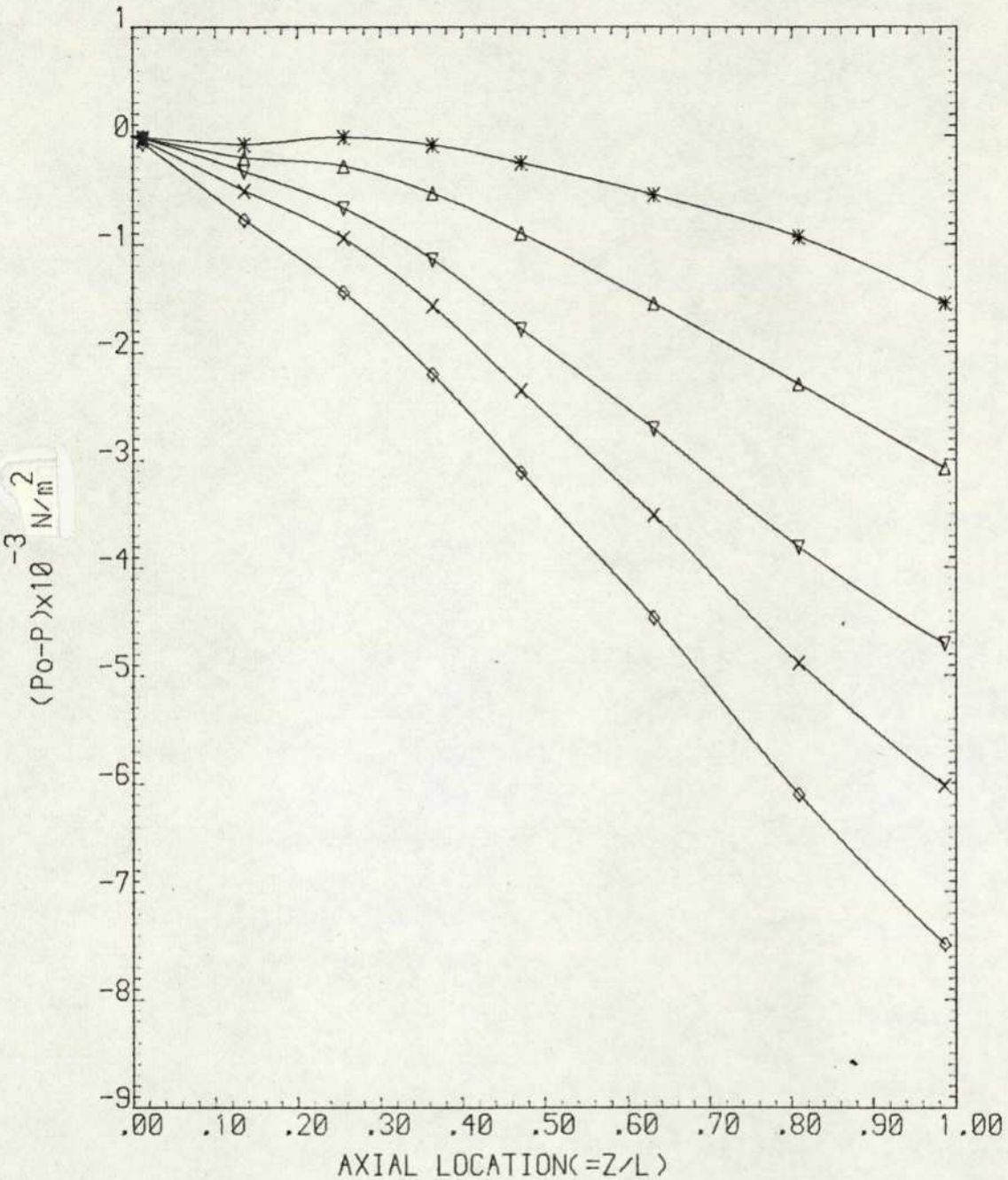

FIG.27 EFFECT OF THE INLET STATIC PRESSURE ON THE AXIAL STATIC PRESSURE DISTRIBUTION

	RUN	Po(BAR ABS)	Wcw KG/HR
*	16	0.6	9687.0
△	13	0.8	9687.0
▽	6	1.2	9687.0
×	3	1.4	9687.0
◇	9	1.6	9687.0

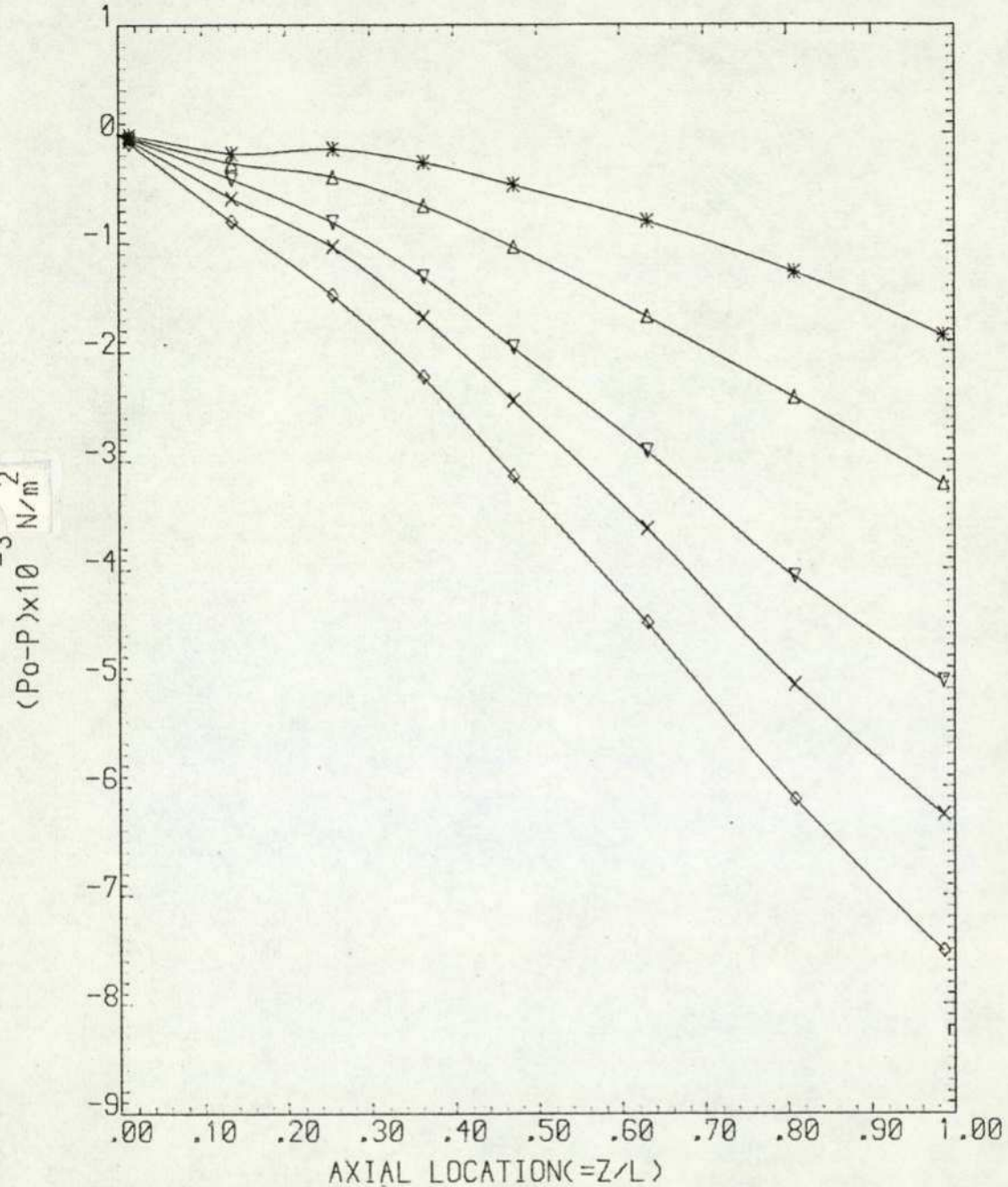

FIG. 28 EFFECT OF THE INLET STATIC PRESSURE ON THE AXIAL STATIC PRESSURE DISTRIBUTION

	RUN	Po(BAR ABS)	Wcw KG/HR
*	14	0.6	5342.3
△	12	0.8	5342.3
▽	4	1.2	5342.3
×	1	1.4	5342.3
◇	7	1.6	5342.3

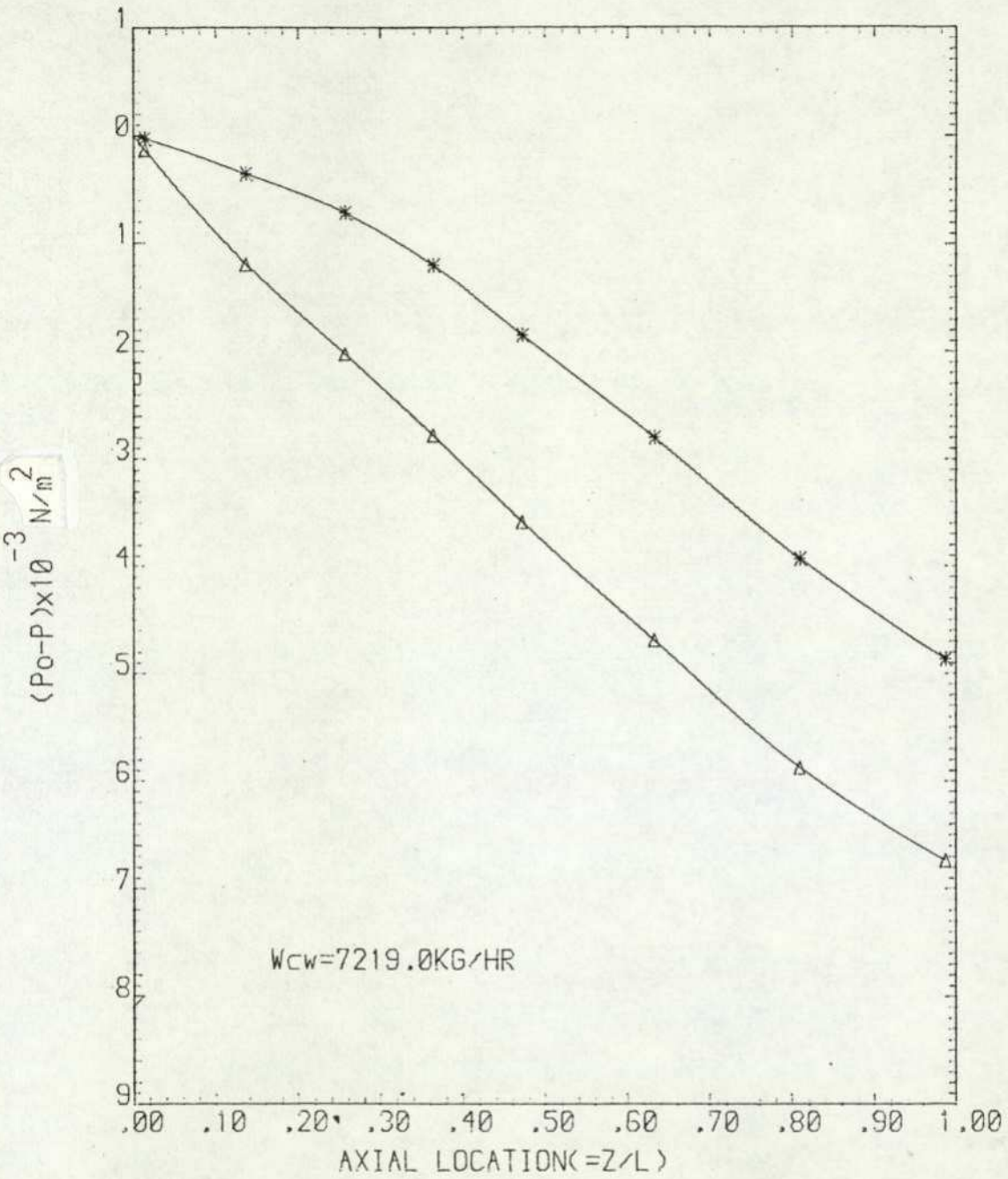

FIG. 29 EFFECT OF THE INLET QUALITY (=WG/WT) ON THE AXIAL STATIC PRESSURE DISTRIBUTION

	RUN	Po(BAR ABS)	X_1
*	5	1.2	0.920
Δ	23	1.2	0.659

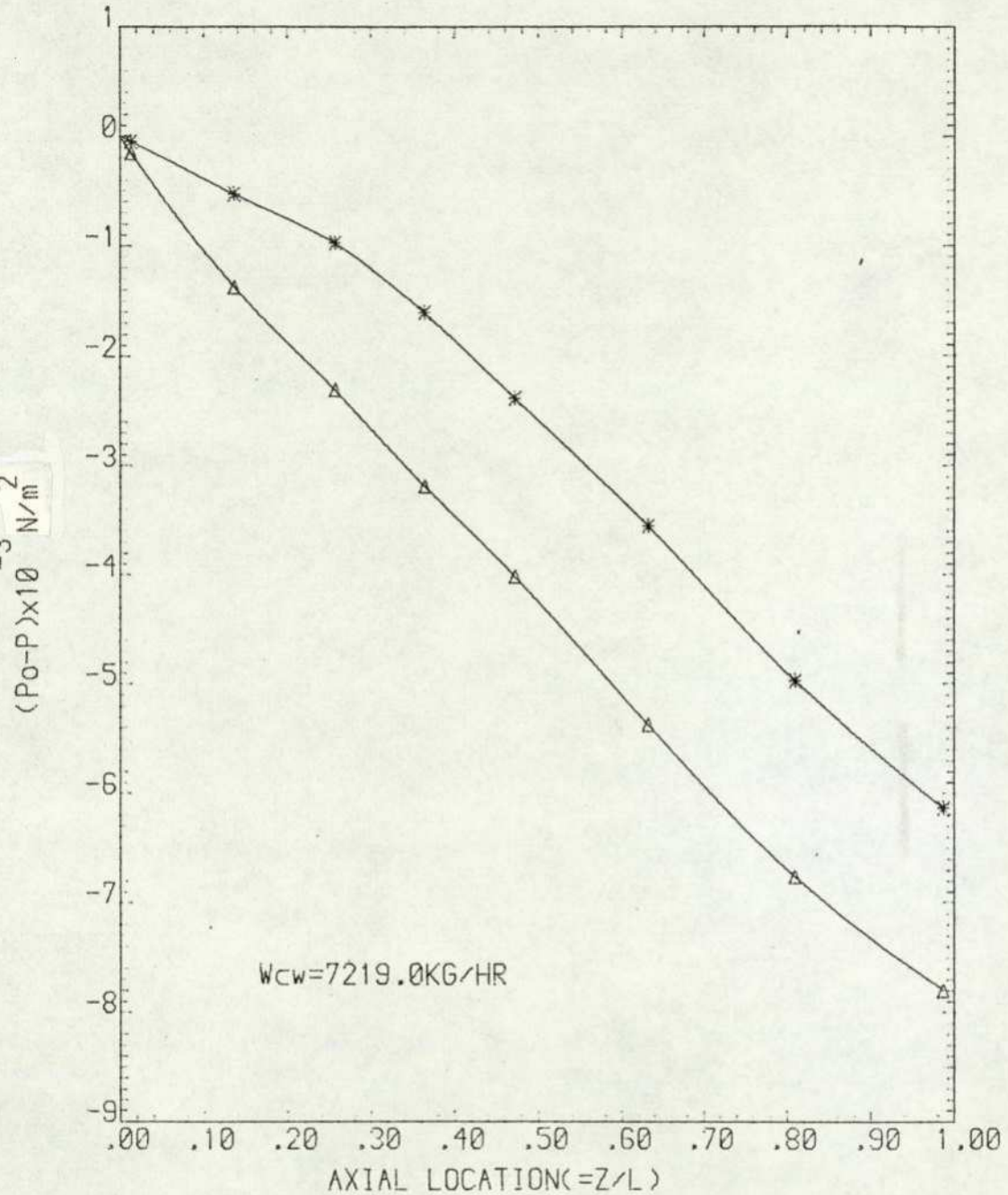

FIG. 30 EFFECT OF THE INLET QUALITY (=WG/WT) ON THE AXIAL STATIC PRESSURE DISTRIBUTION

	RUN	Po(BAR ABS)	X1
*	2	1.4	0.900
Δ	27	1.4	0.685

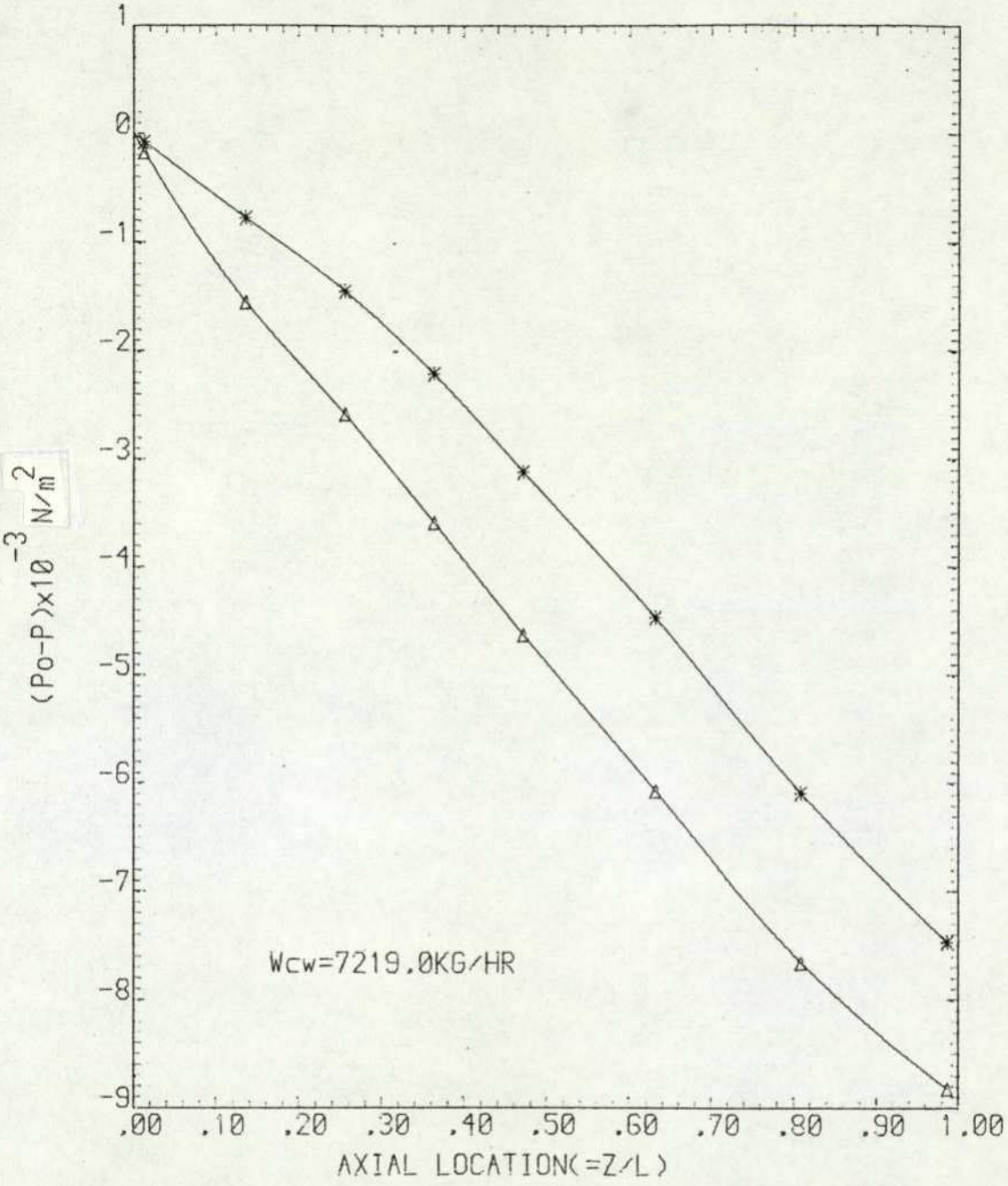

FIG. 31 EFFECT OF THE INLET QUALITY (=WG/WT) ON THE AXIAL STATIC PRESSURE DISTRIBUTION

	RUN	Po(BAR ABS)	X_1
*	8	1.6	0.900
Δ	31	1.6	0.567

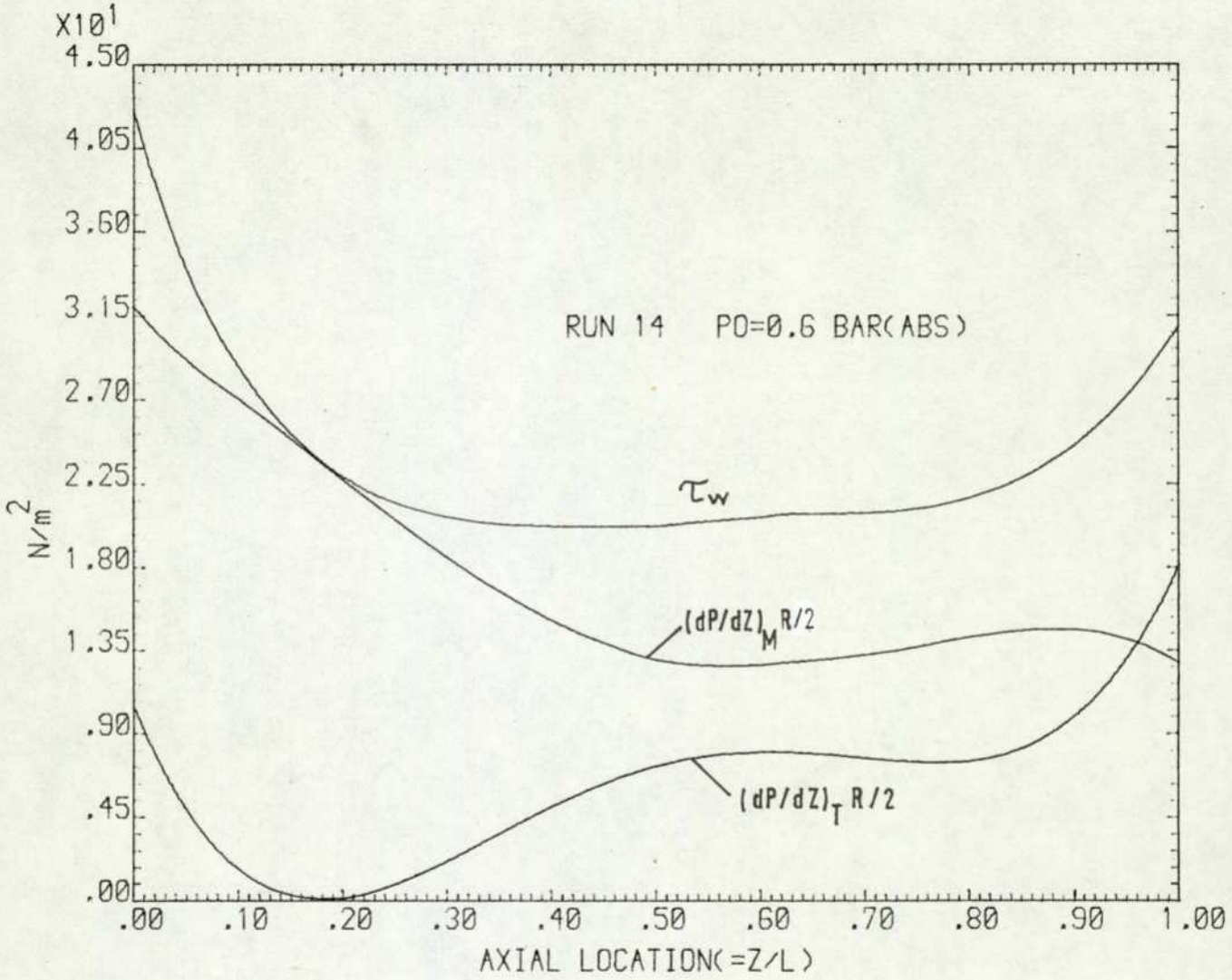

FIG.32 WALL SHEAR STRESS AND COMPONENTS

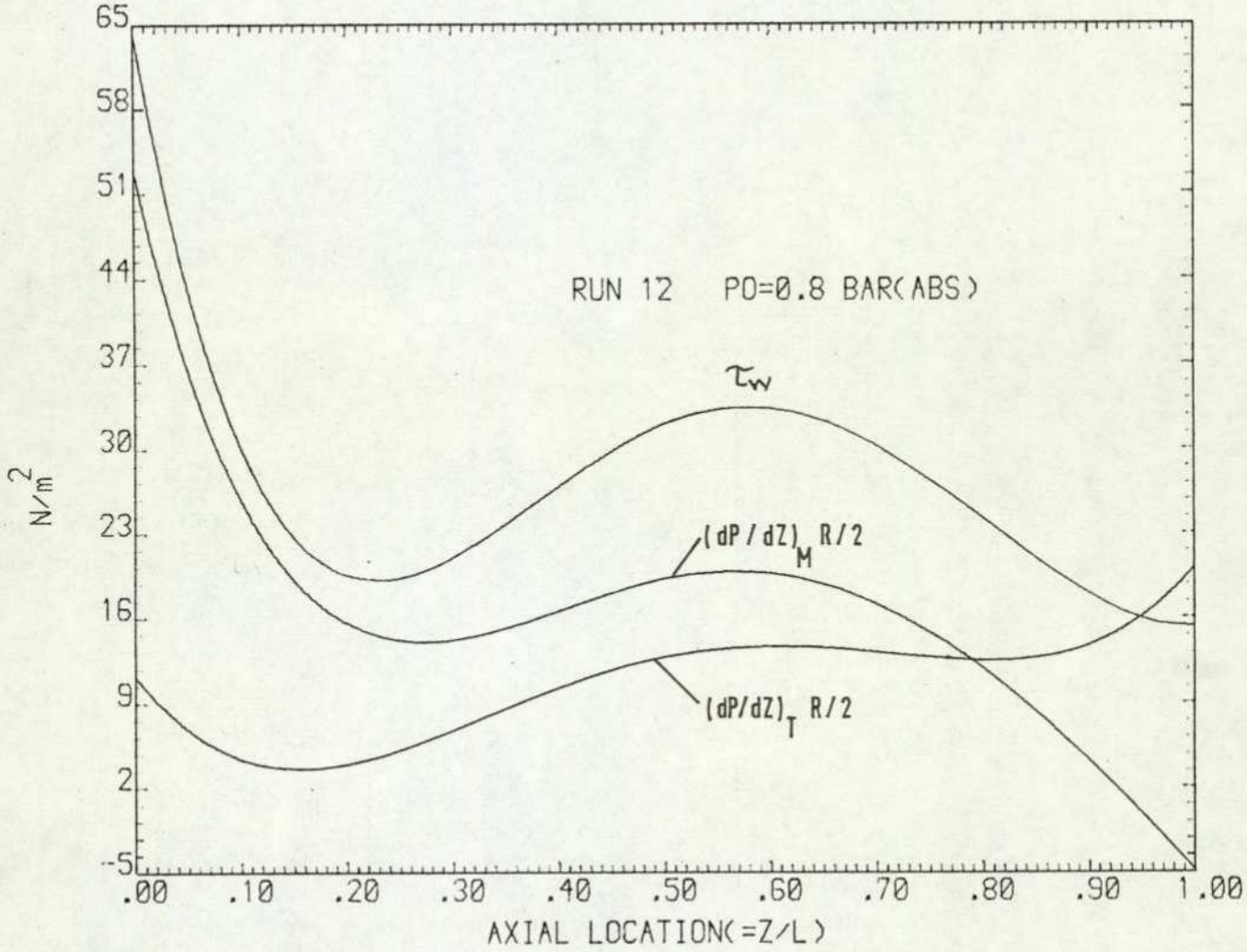

FIG.33 WALL SHEAR STRESS AND COMPONENTS

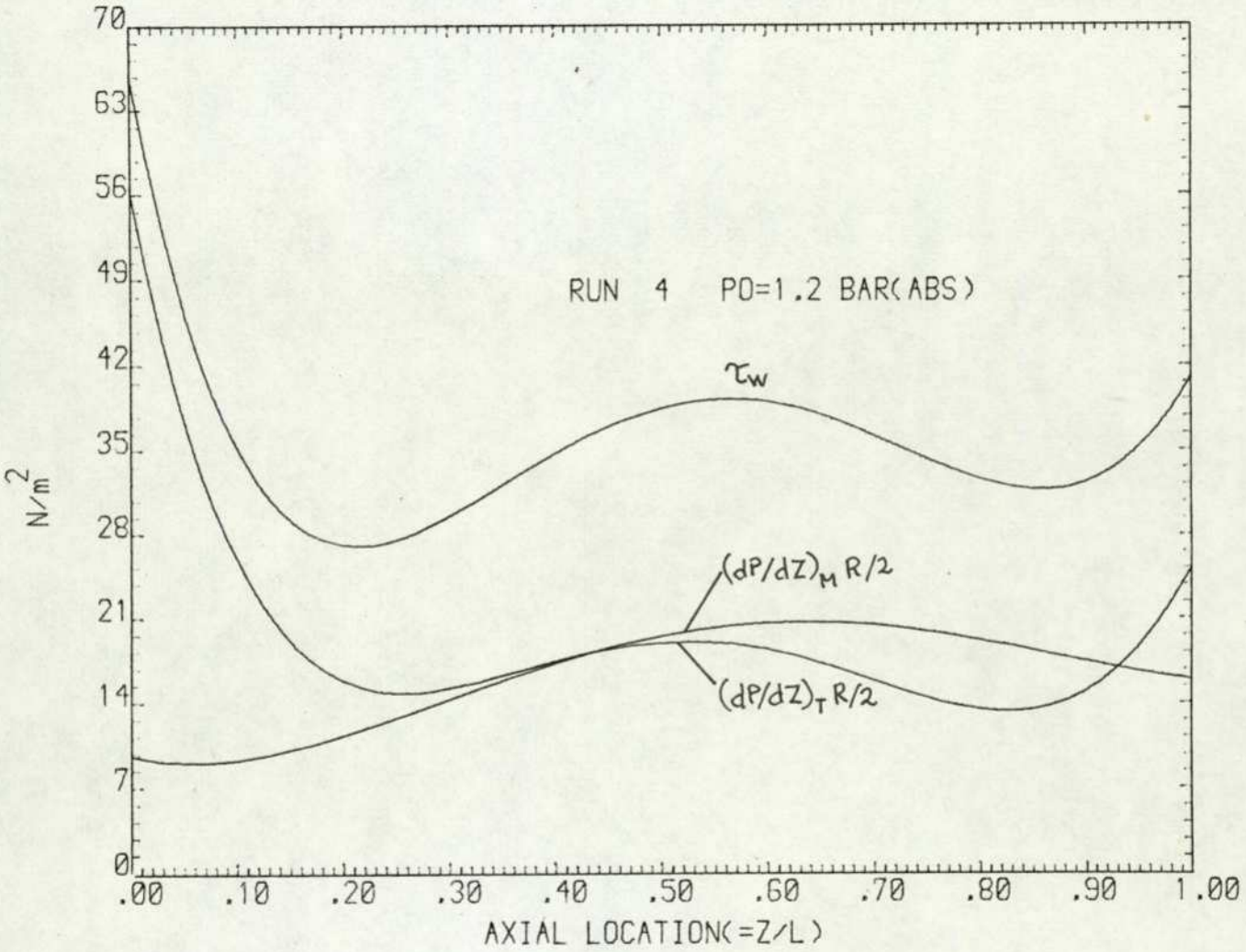

FIG.34 WALL SHEAR STRESS AND COMPONENTS

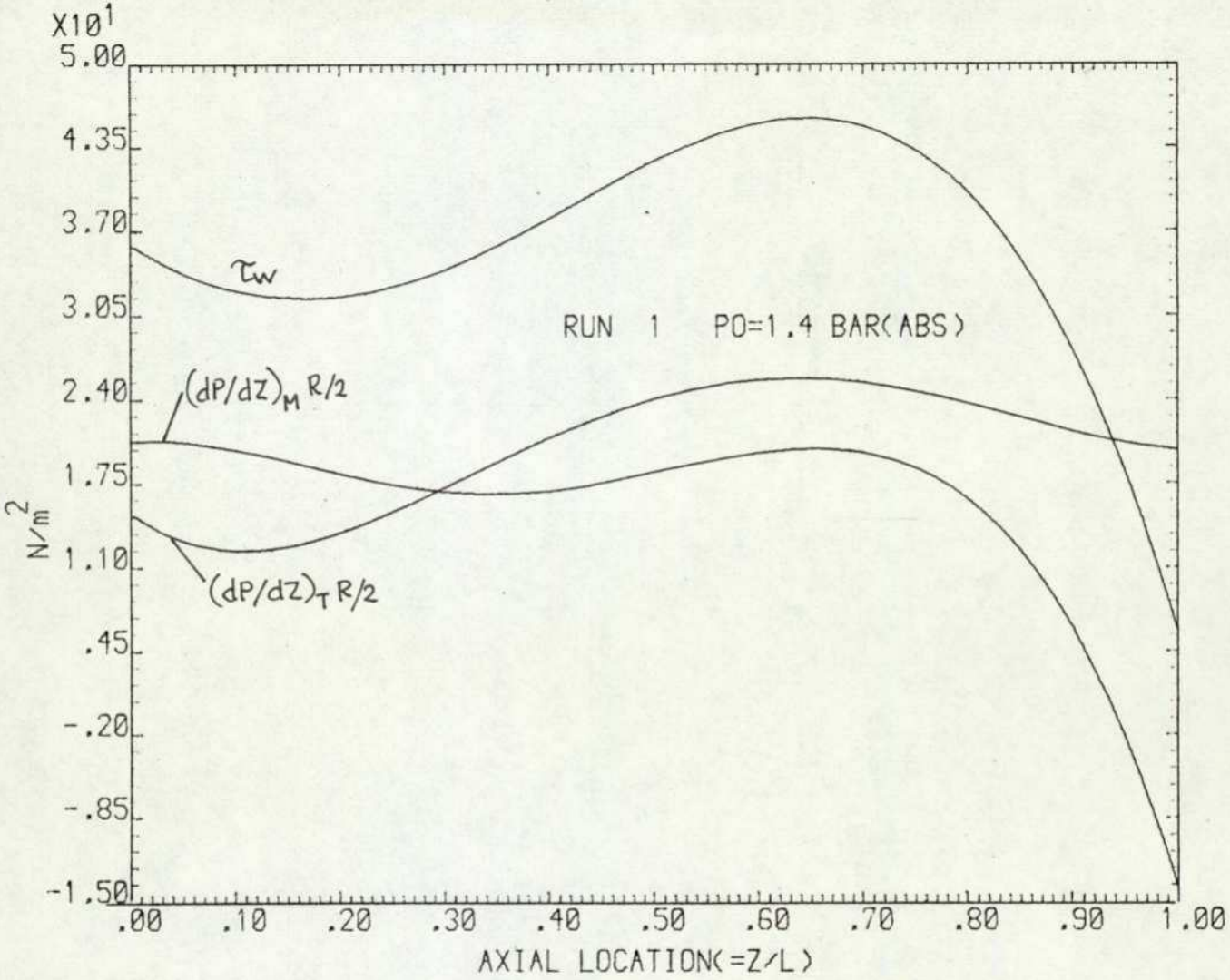

FIG.35 WALL SHEAR STRESS AND COMPONENTS

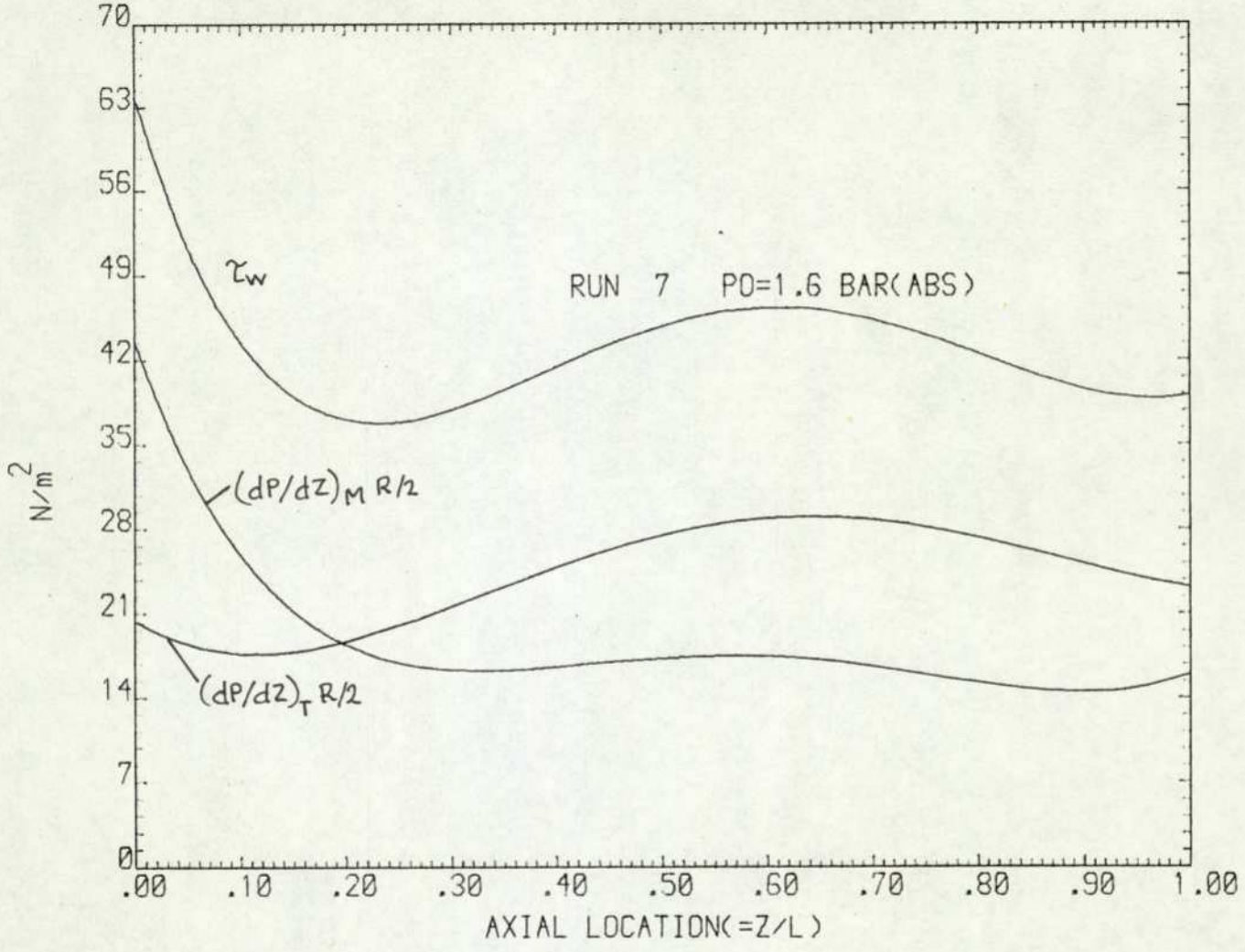

FIG. 36 WALL SHEAR STRESS AND COMPONENTS

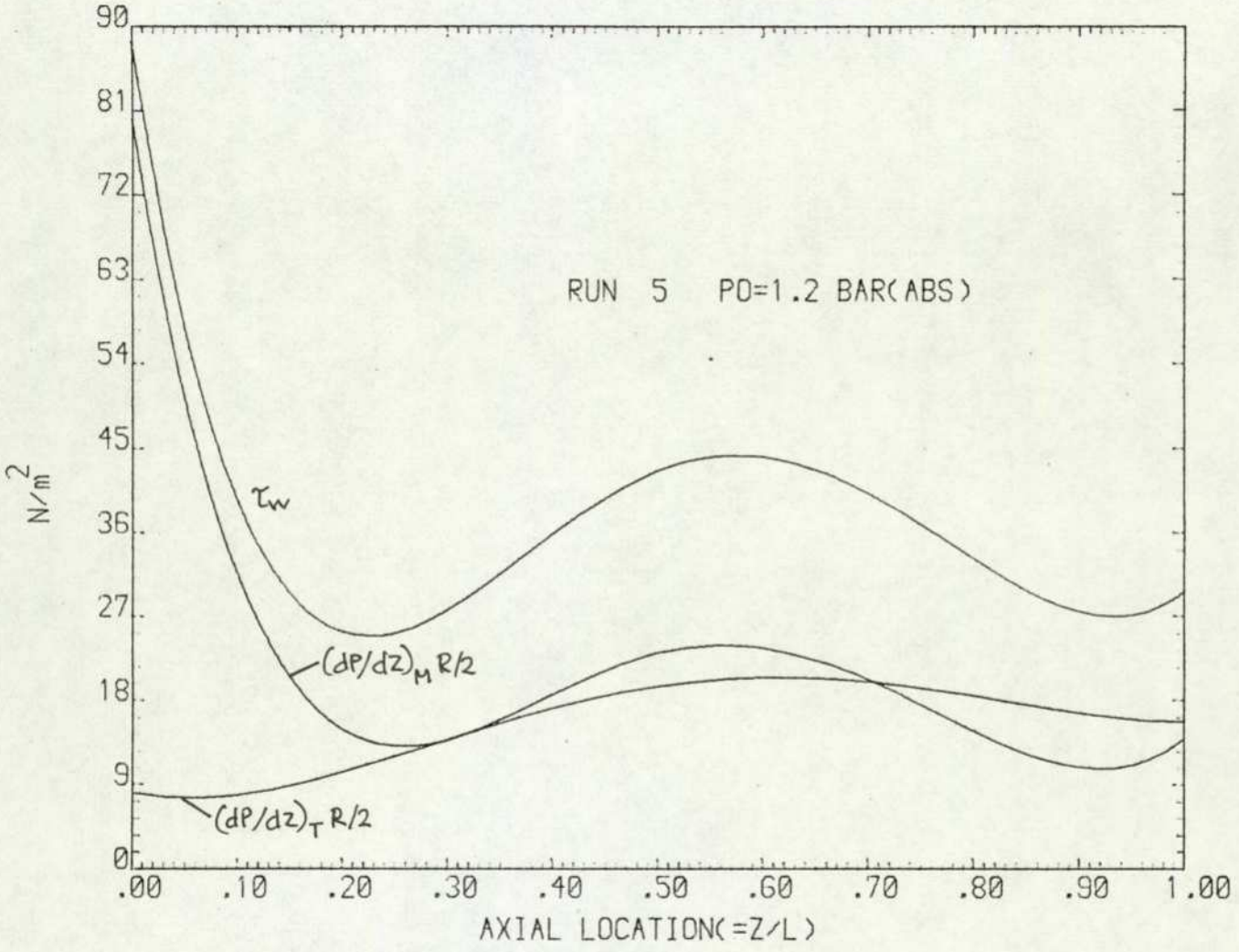

FIG.37 WALL SHEAR STRESS AND COMPONENTS

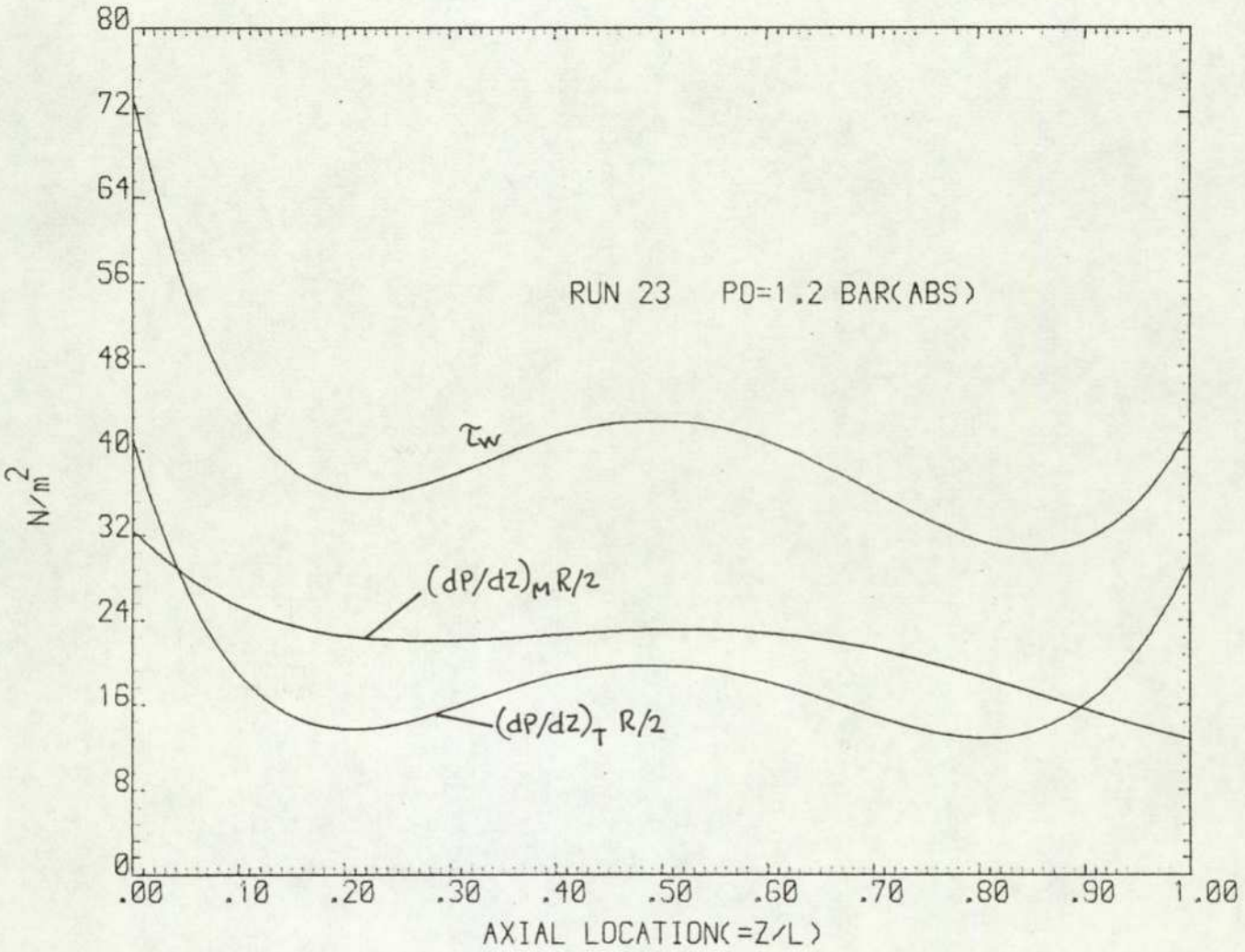

FIG.38 WALL SHEAR STRESS AND COMPONENTS

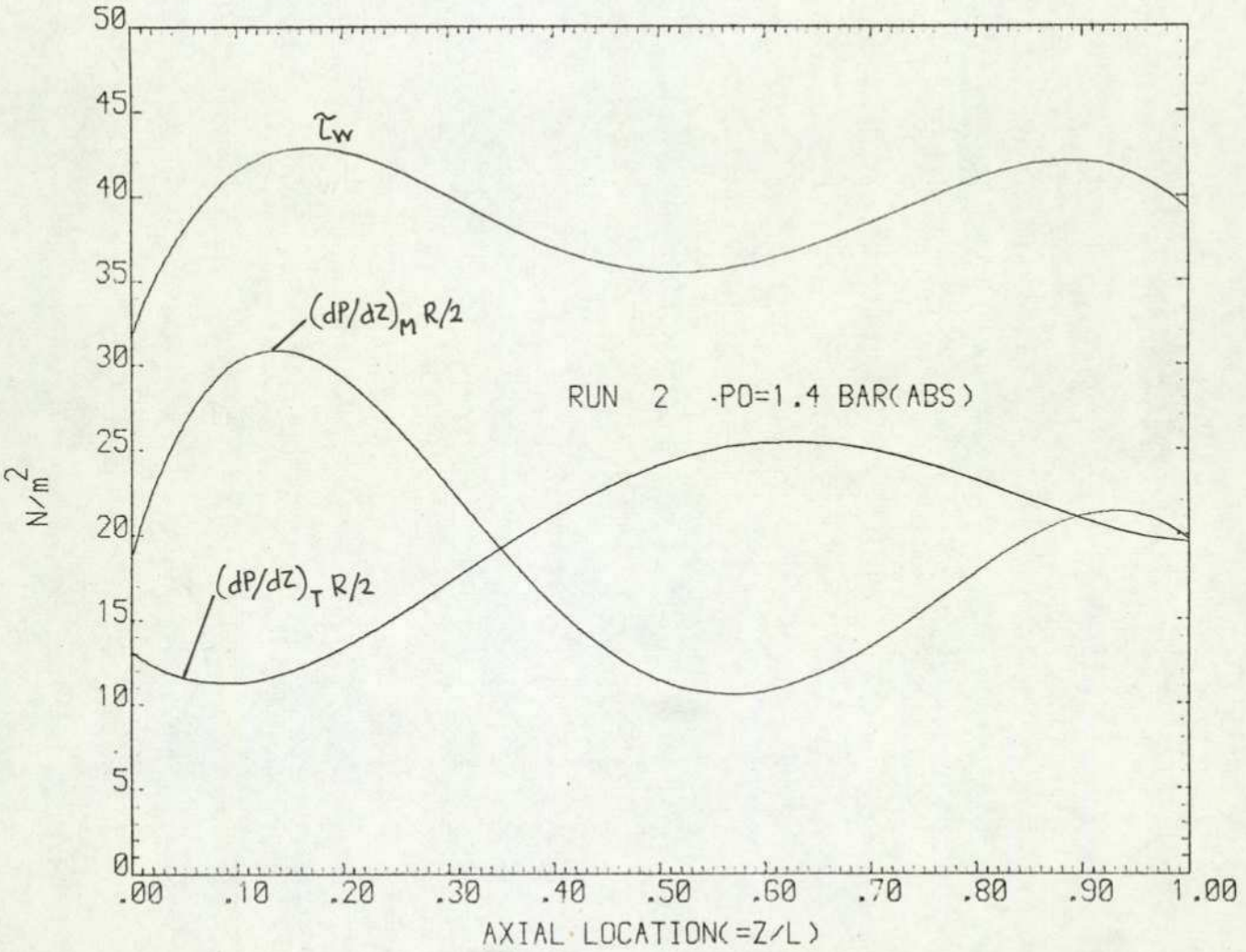

FIG. 39 WALL SHEAR STRESS AND COMPONENTS

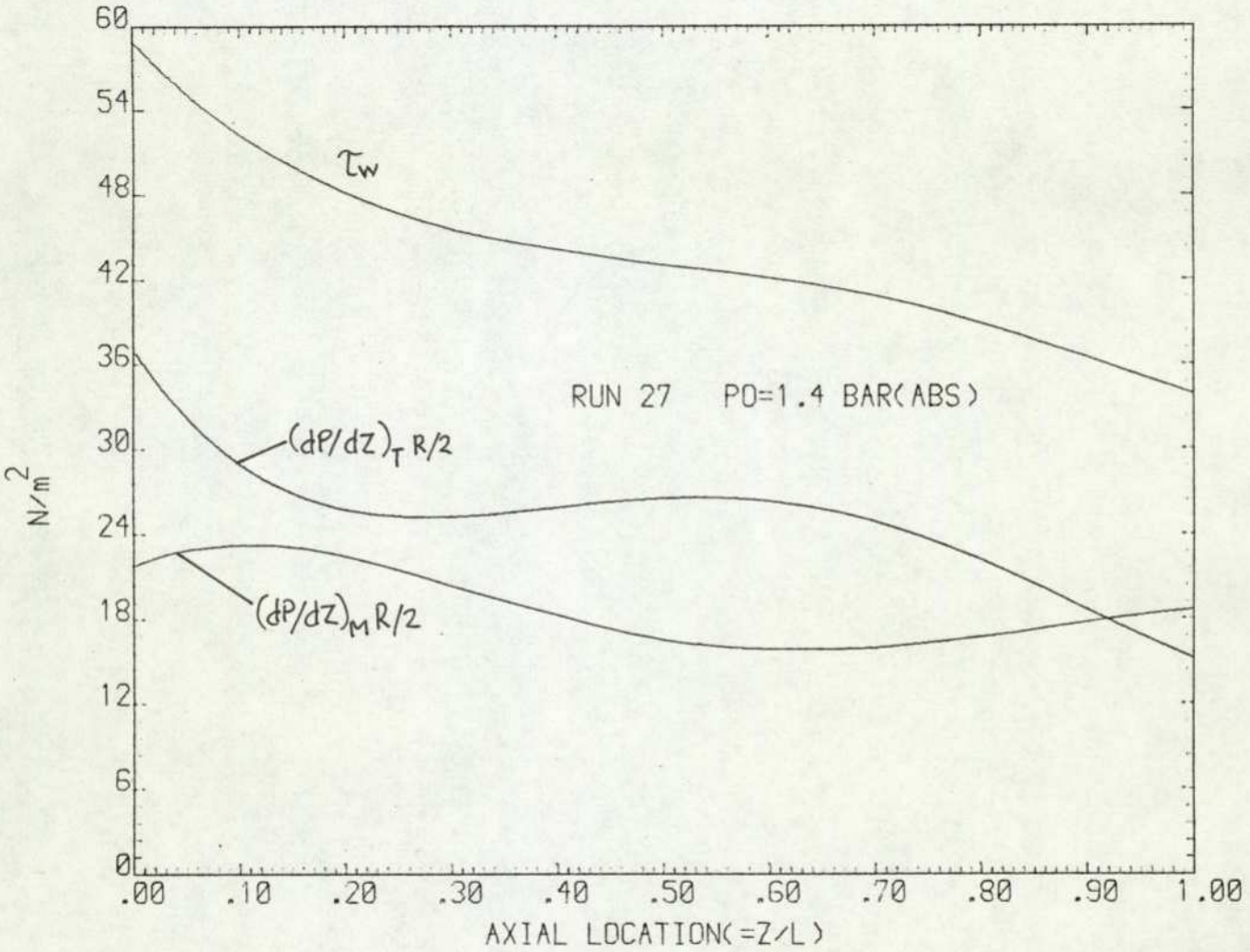

FIG.40 WALL SHEAR STRESS AND COMPONENTS

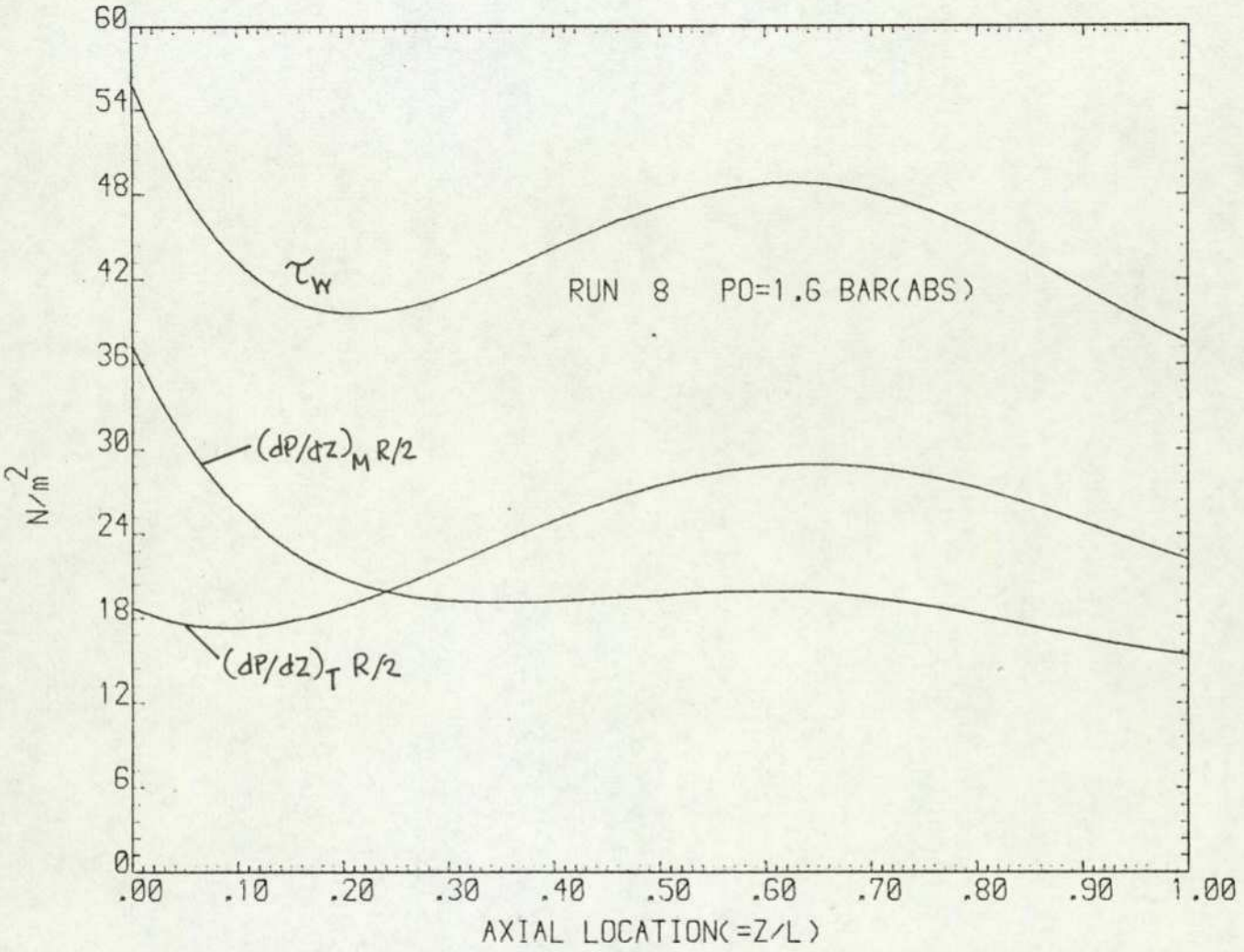

FIG. 41 WALL SHEAR STRESS AND COMPONENTS

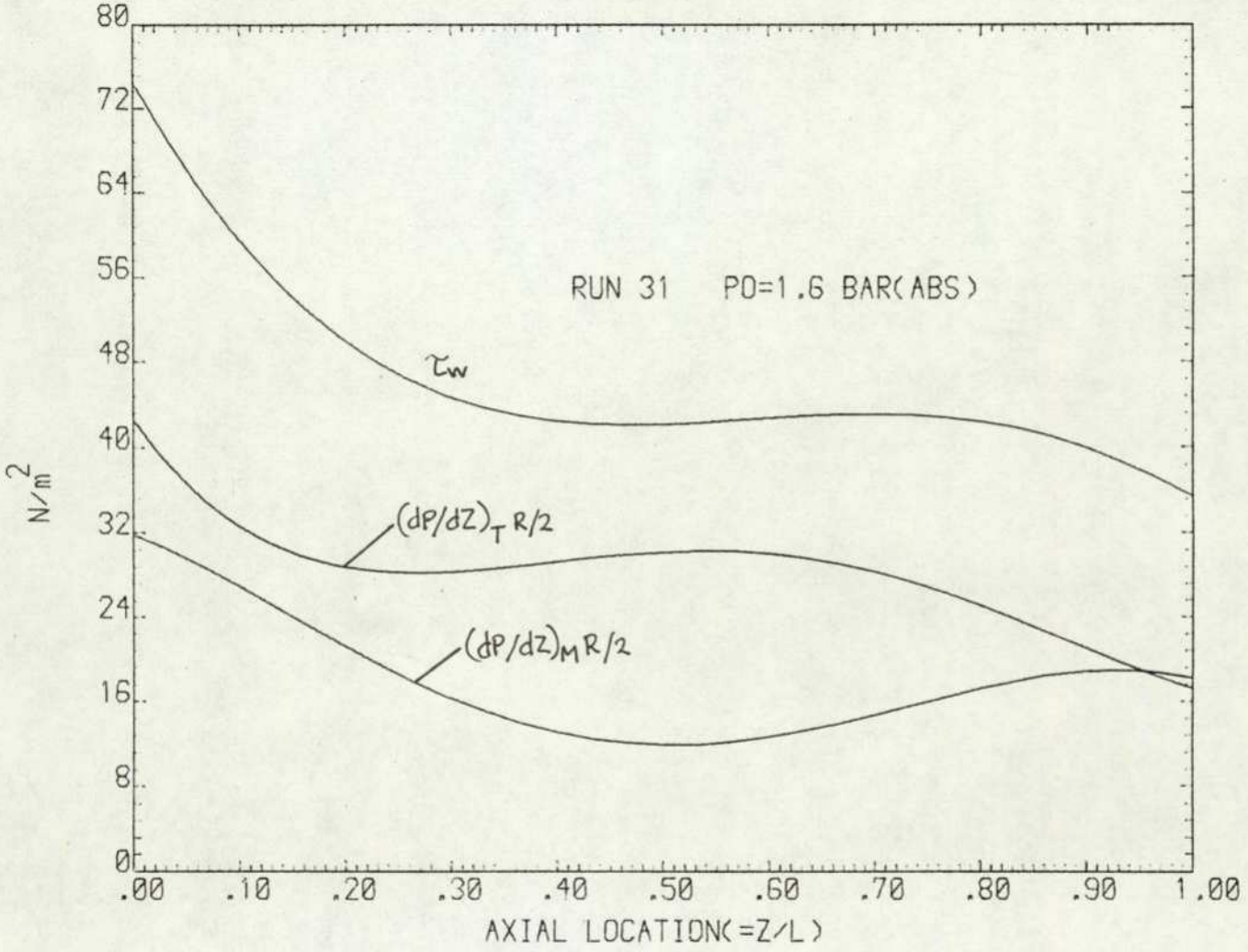

FIG.42 WALL SHEAR STRESS AND COMPONENTS

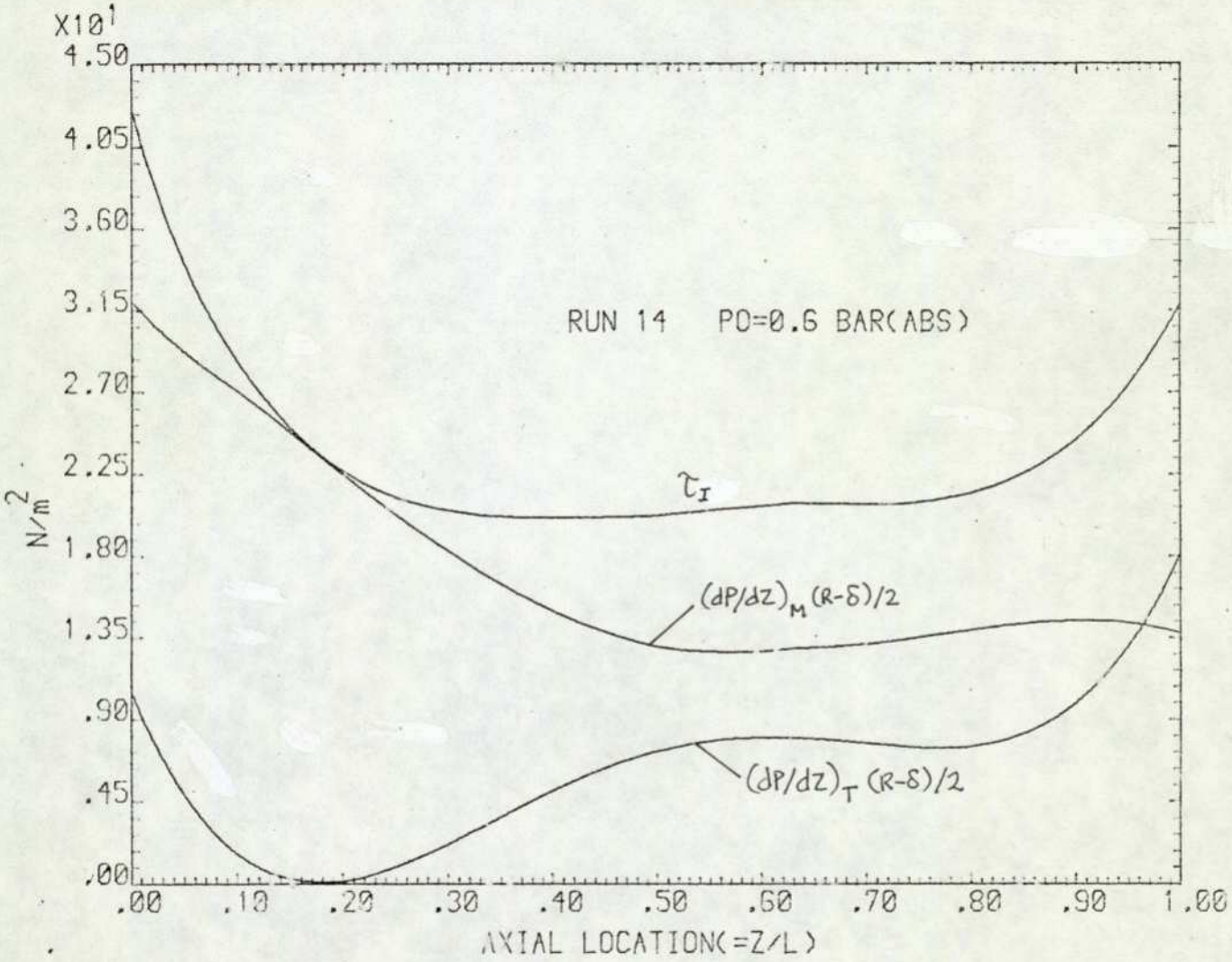

FIG. 43 INTERFACIAL SHEAR STRESS AND COMPONENTES

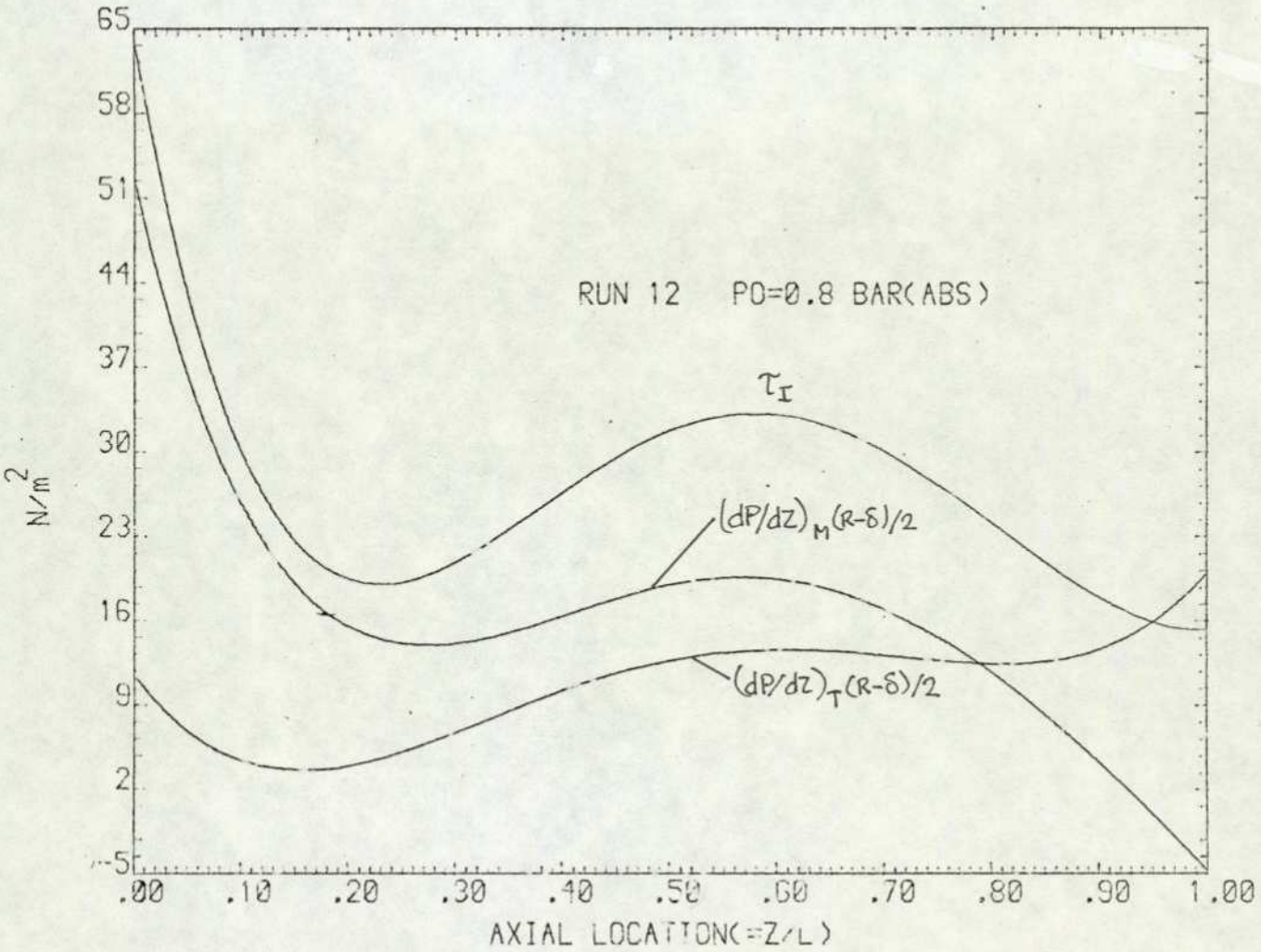

FIG.44 INTERFACIAL SHEAR STRESS AND COMPONENTES

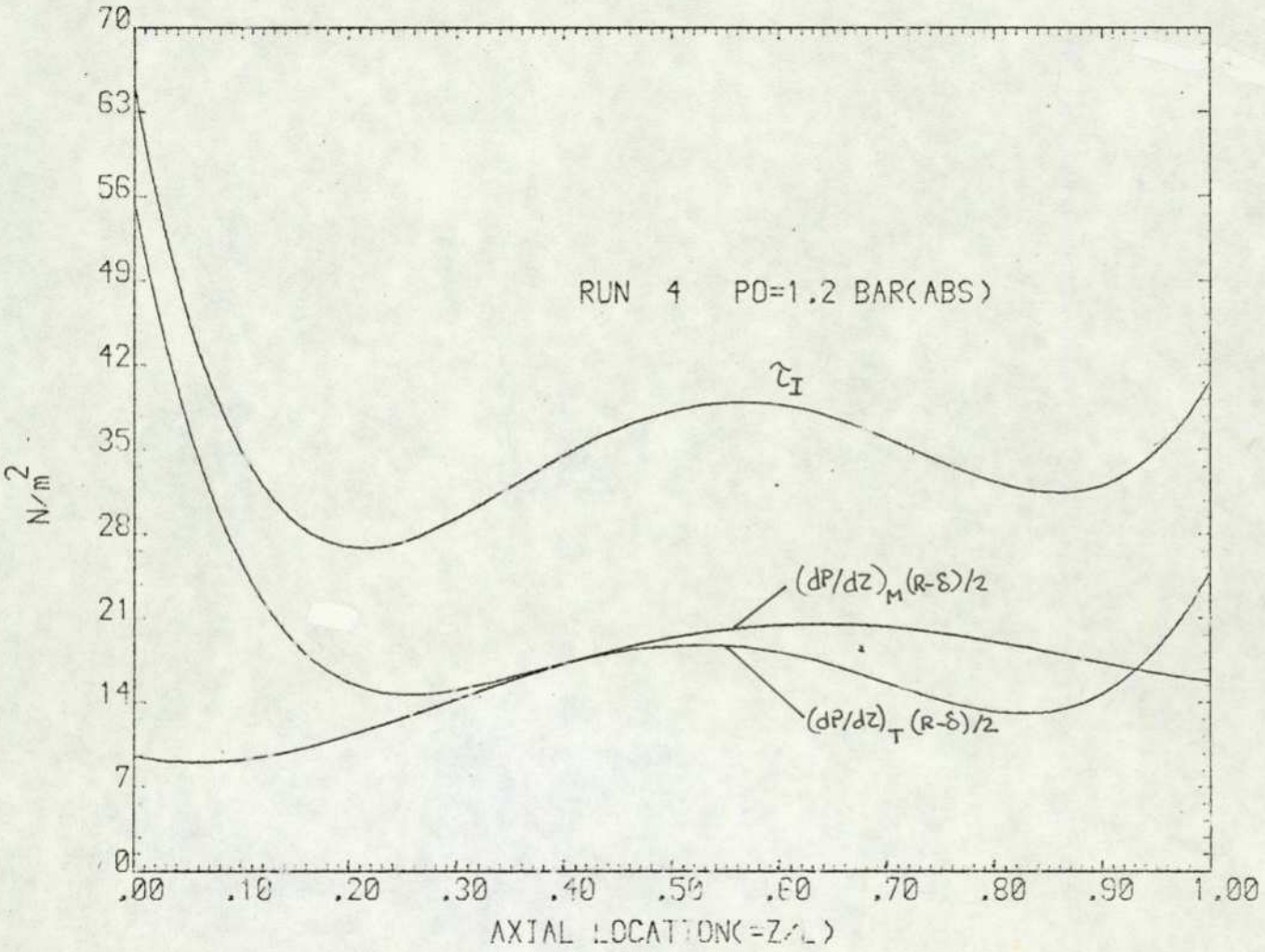

FIG. 45 INTERFACIAL SHEAR STRESS AND COMPONENTES

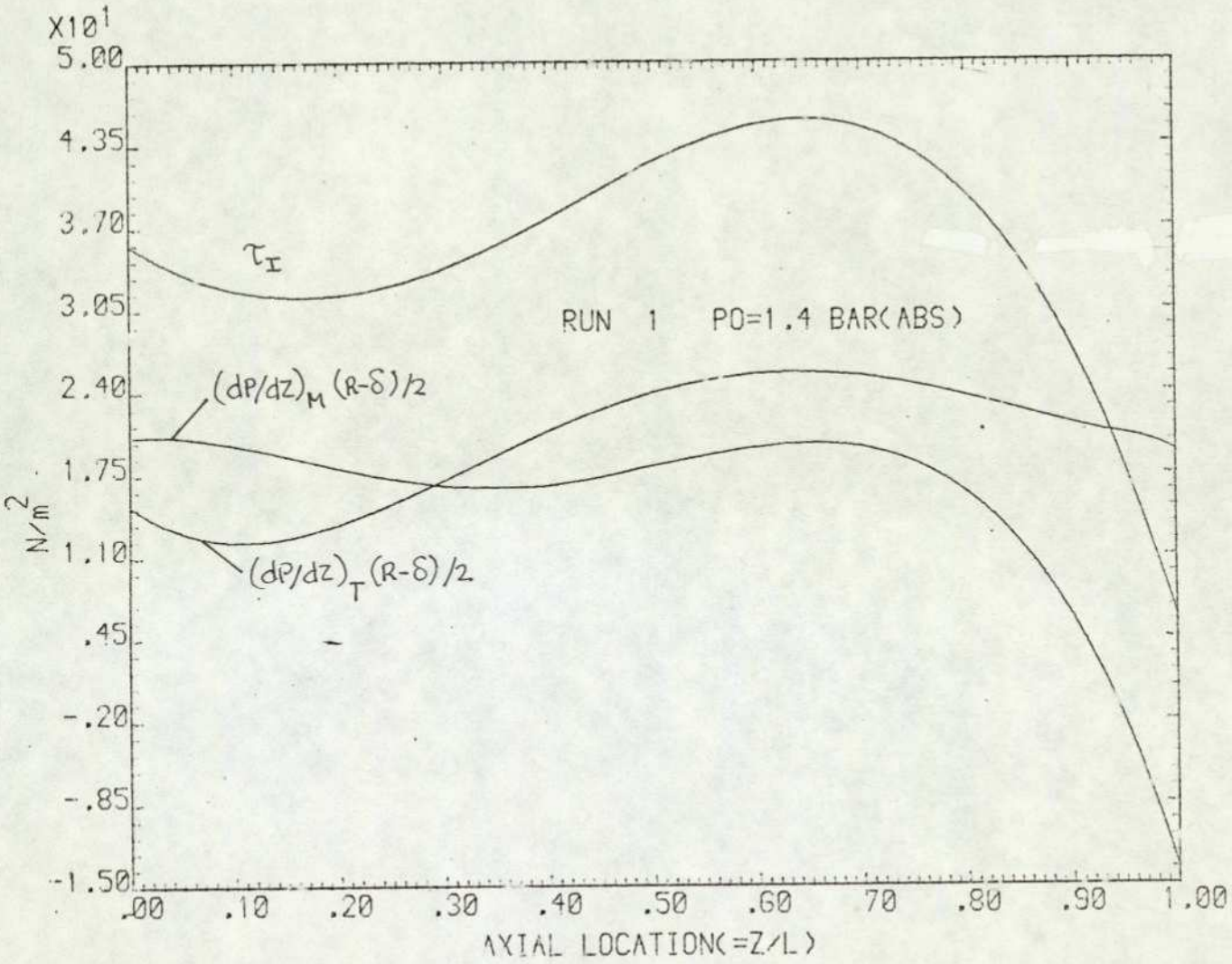

FIG. 46 INTERFACIAL SHEAR STRESS AND COMPONENTES

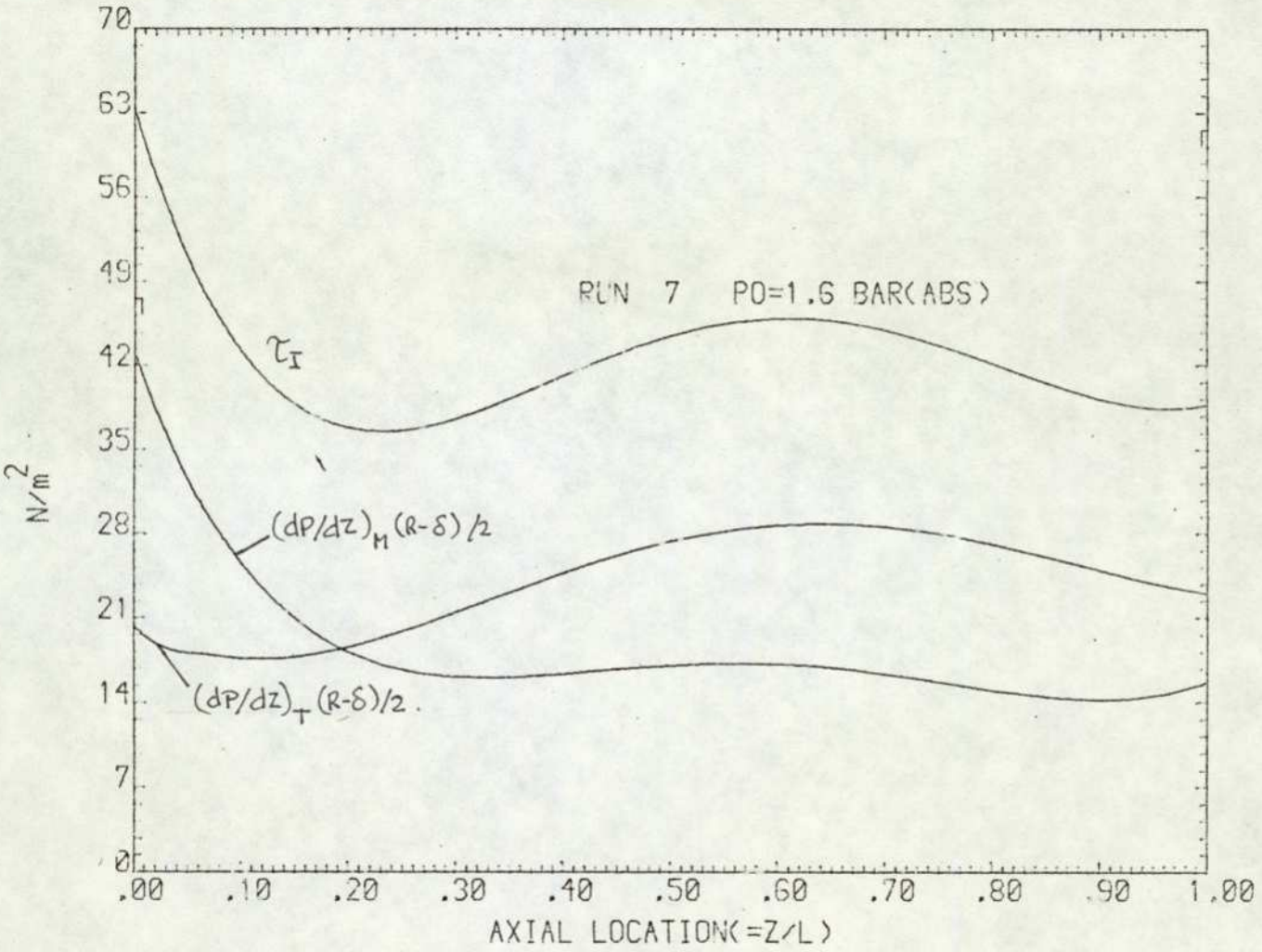

FIG. 47 INTERFACIAL SHEAR STRESS AND COMPONENTES

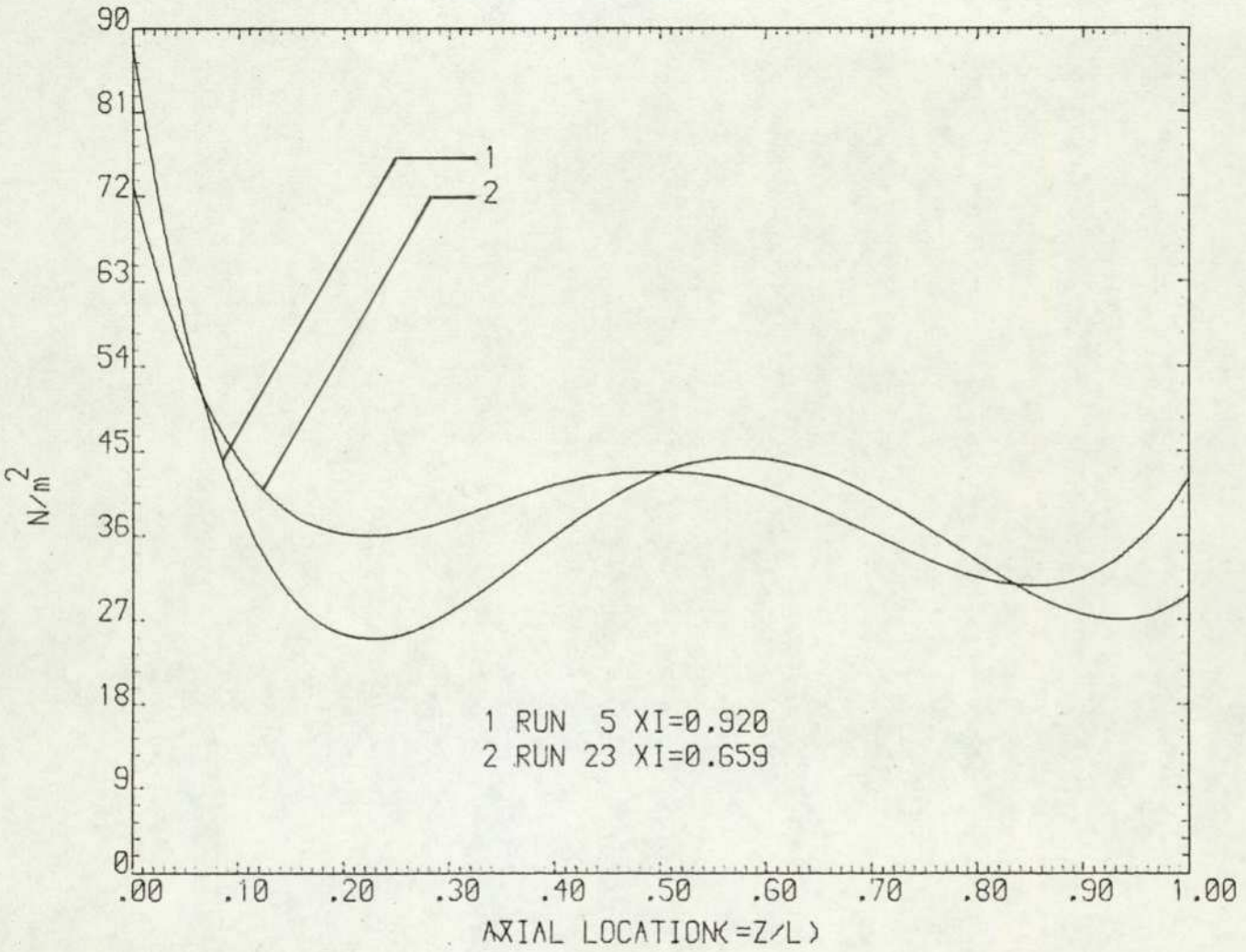

FIG. 48 EFFECT OF THE INLET QUALITY ON THE WALL SHEAR STRESS

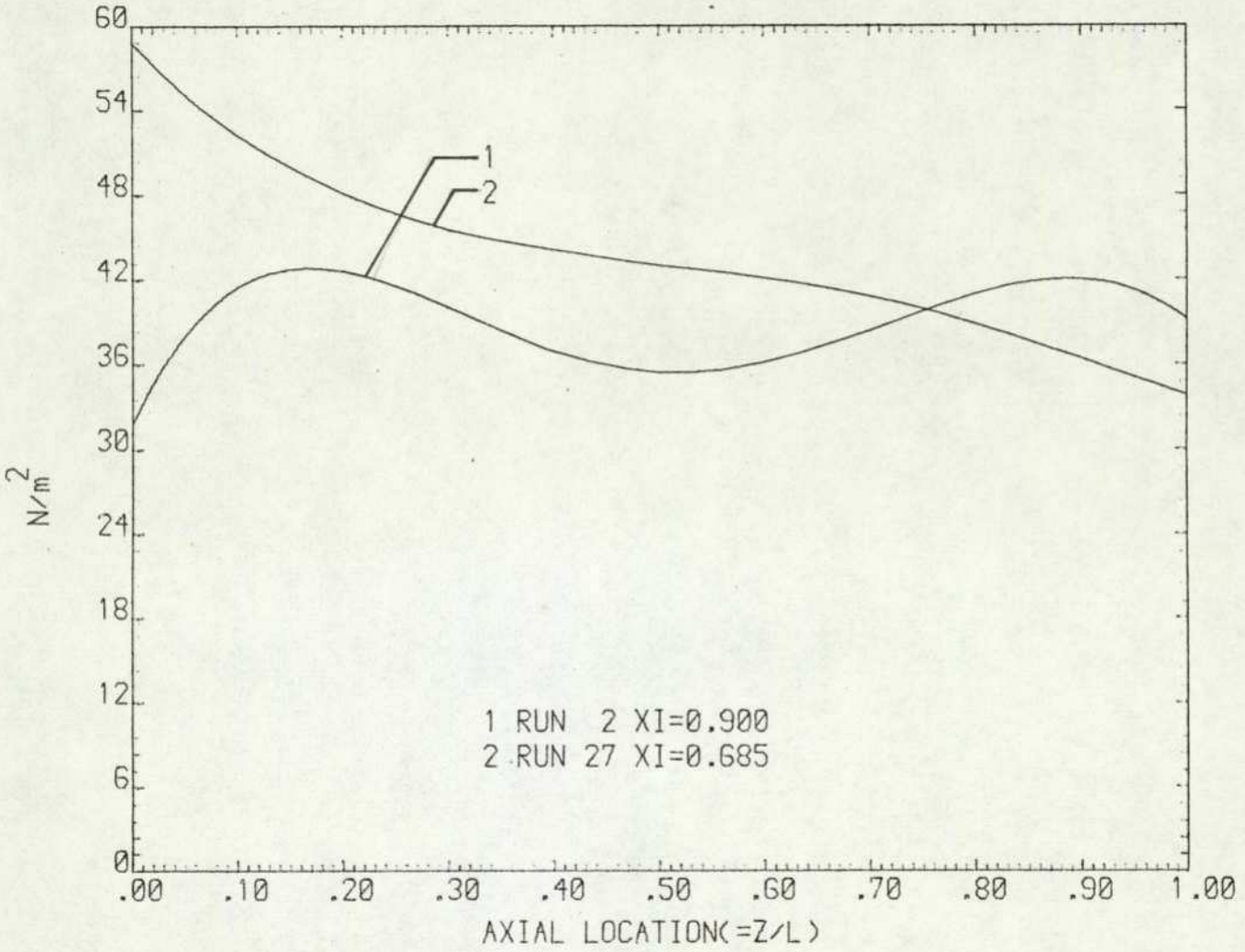

FIG. 49 EFFECT OF THE INLET QUALITY ON THE WALL SHEAR STRESS

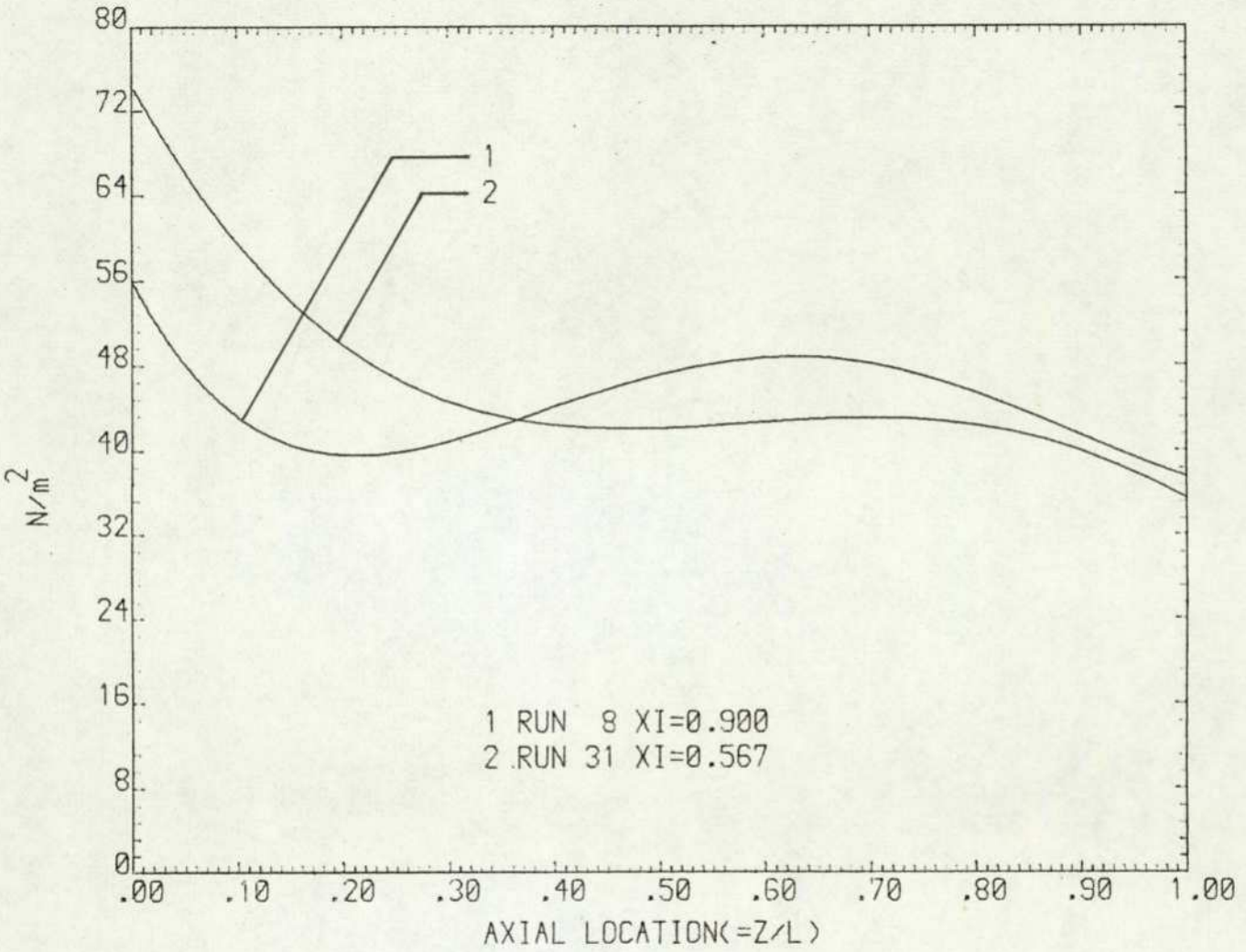

FIG. 50 EFFECT OF THE INLET QUALITY ON THE WALL SHEAR STRESS

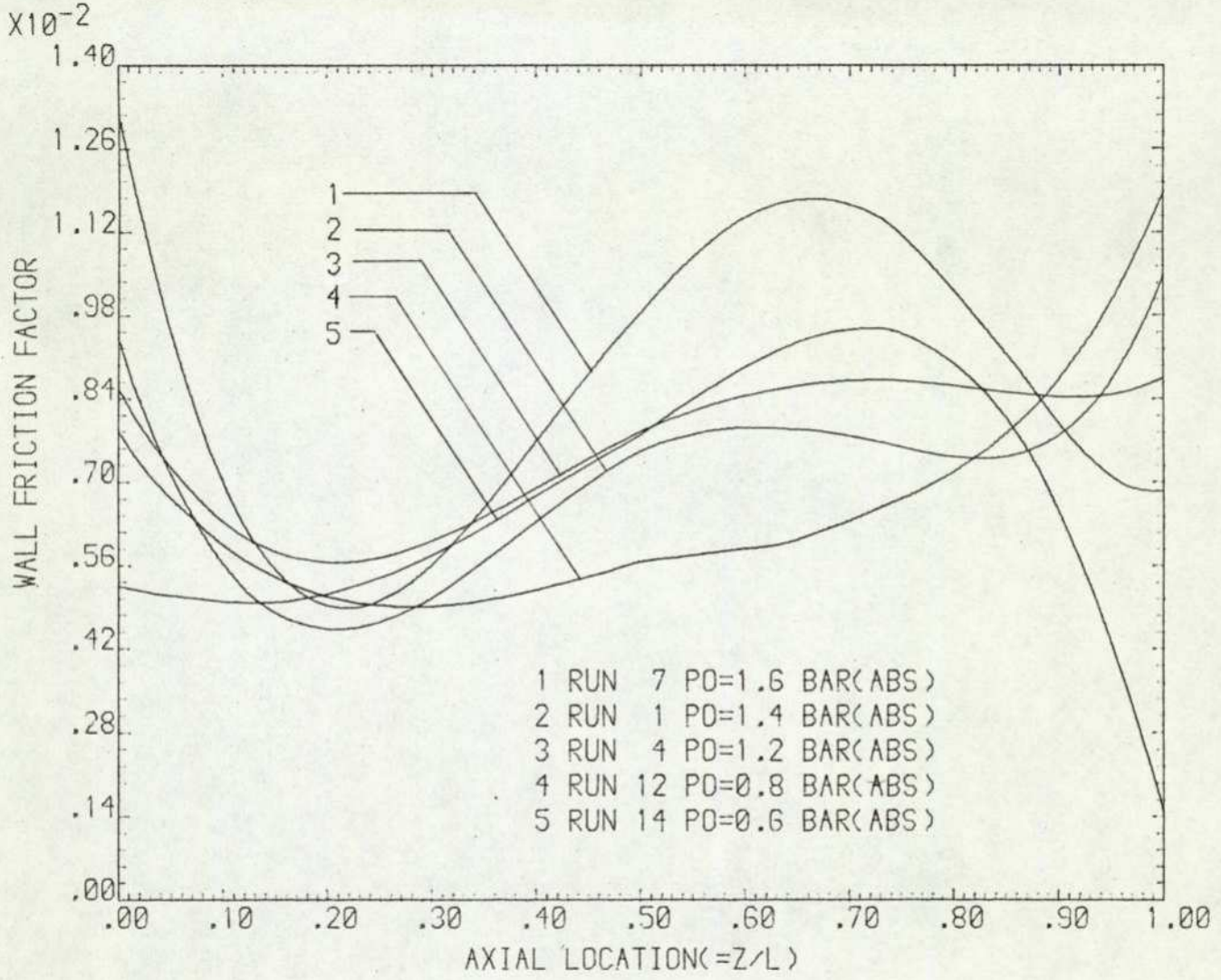

FIG. 51 EFFECT OF THE INLET STATIC PRESSURE ON THE WALL FRICTION FACTOR

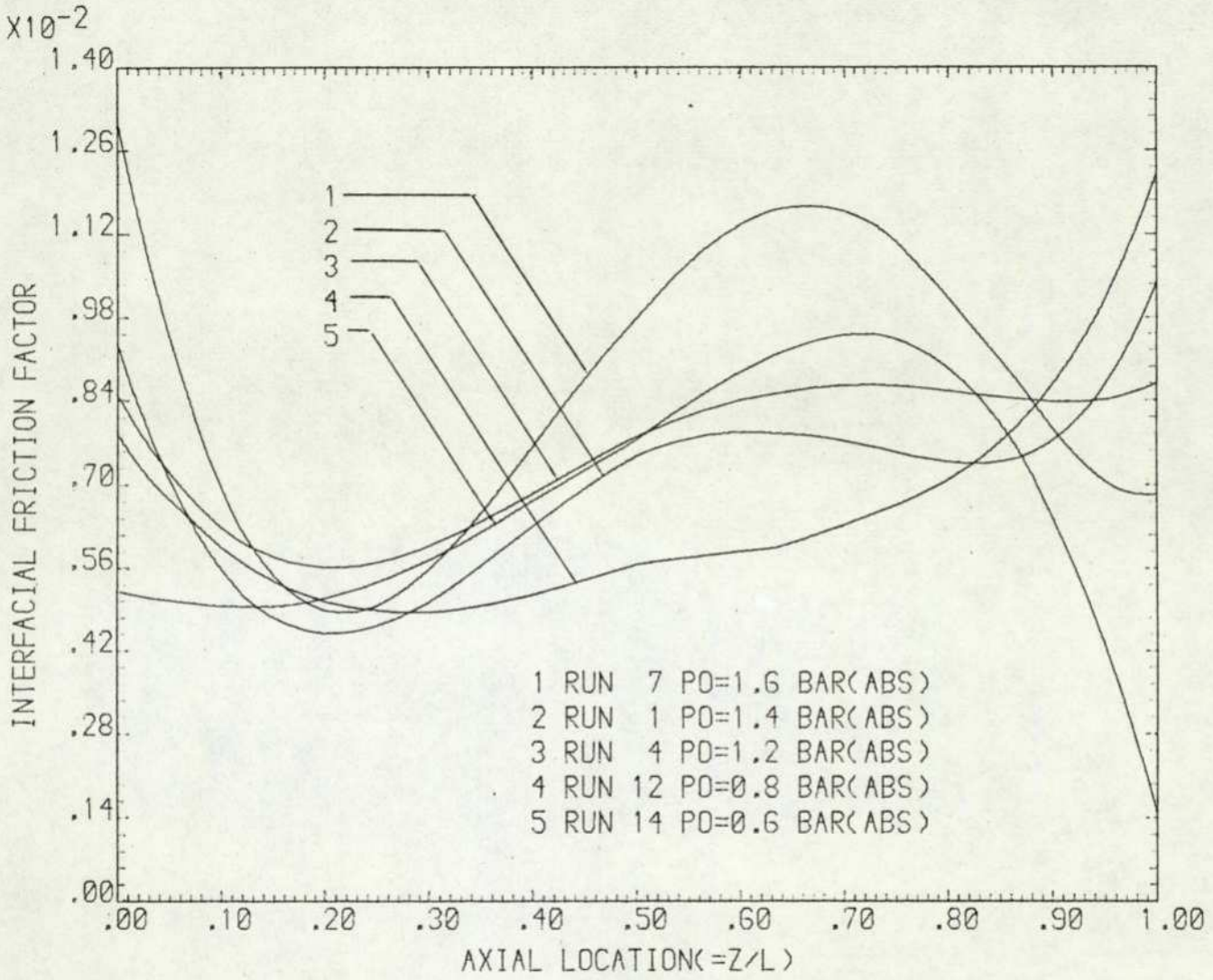

FIG. 52 EFFECT OF THE INLET STATIC PRESSURE ON THE INTERFACIAL FRICTION FACTOR

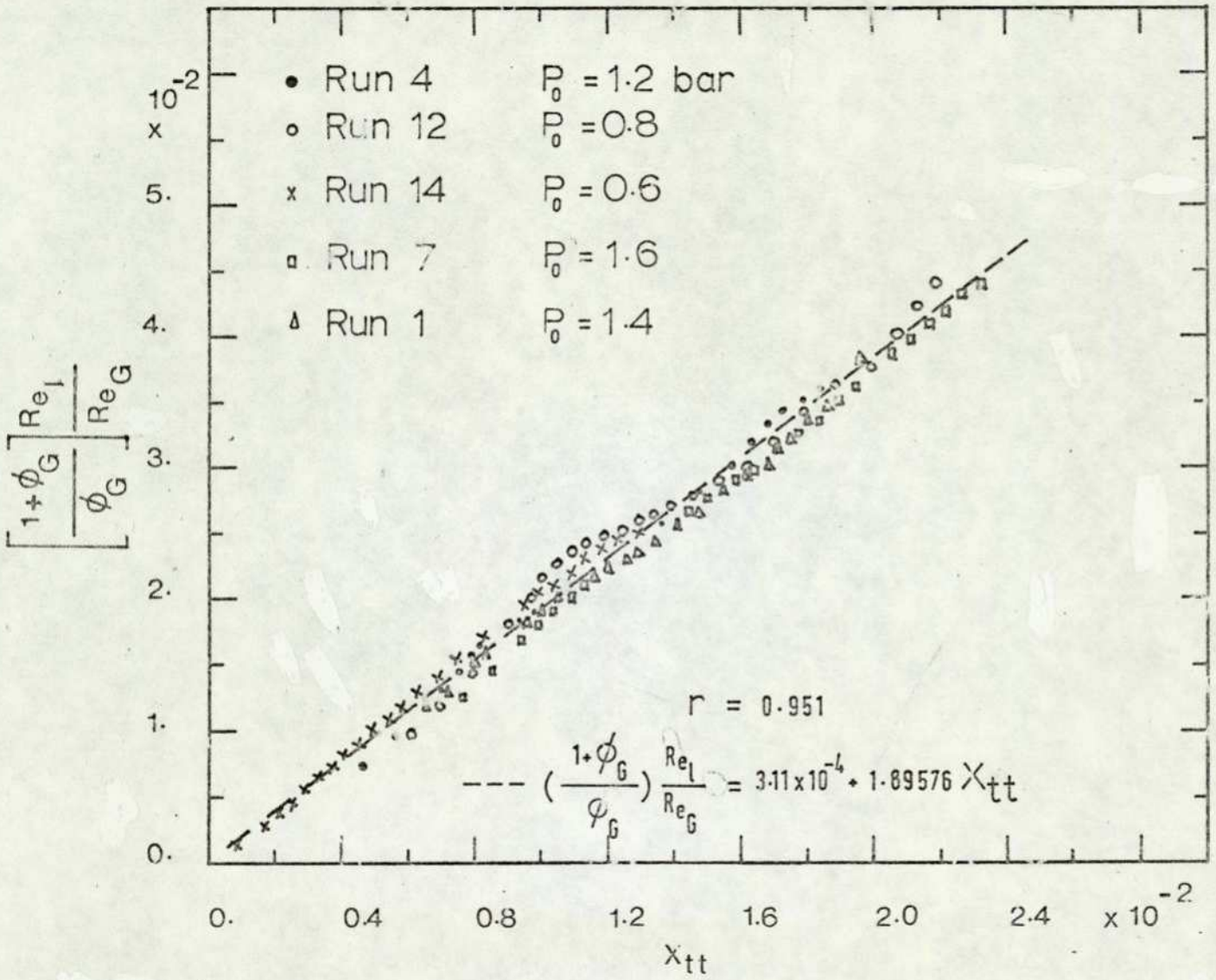

FIG. 53 PRESSURE DROP CORRELATION

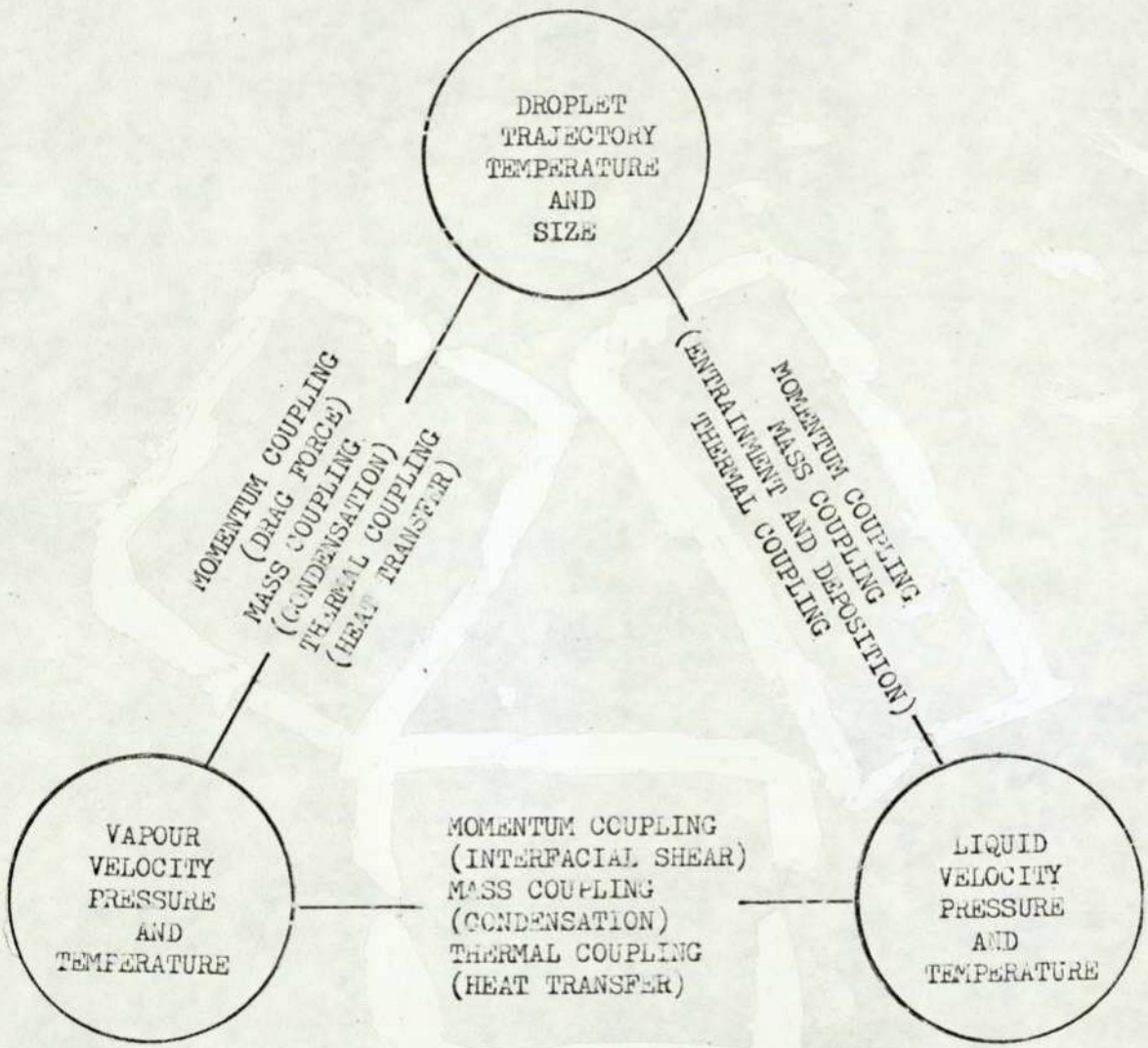

FTG. 54 COUPLING PHENOMENA IN VAPOUR-DROPLET-LIQUID FILM FLOW

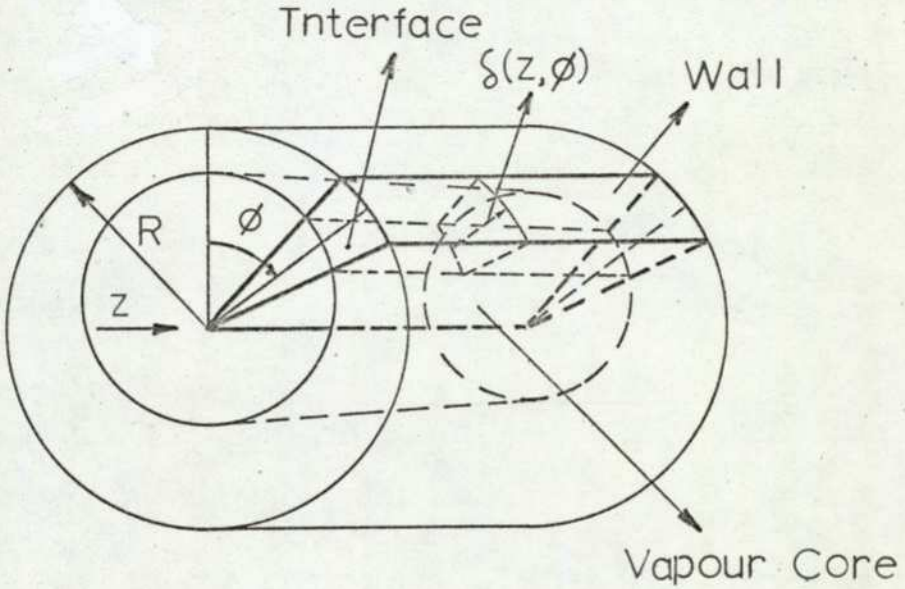

FTG. 55 MODEL FOR CONDENSING ANNULAR FLOW

INSIDE TUBE

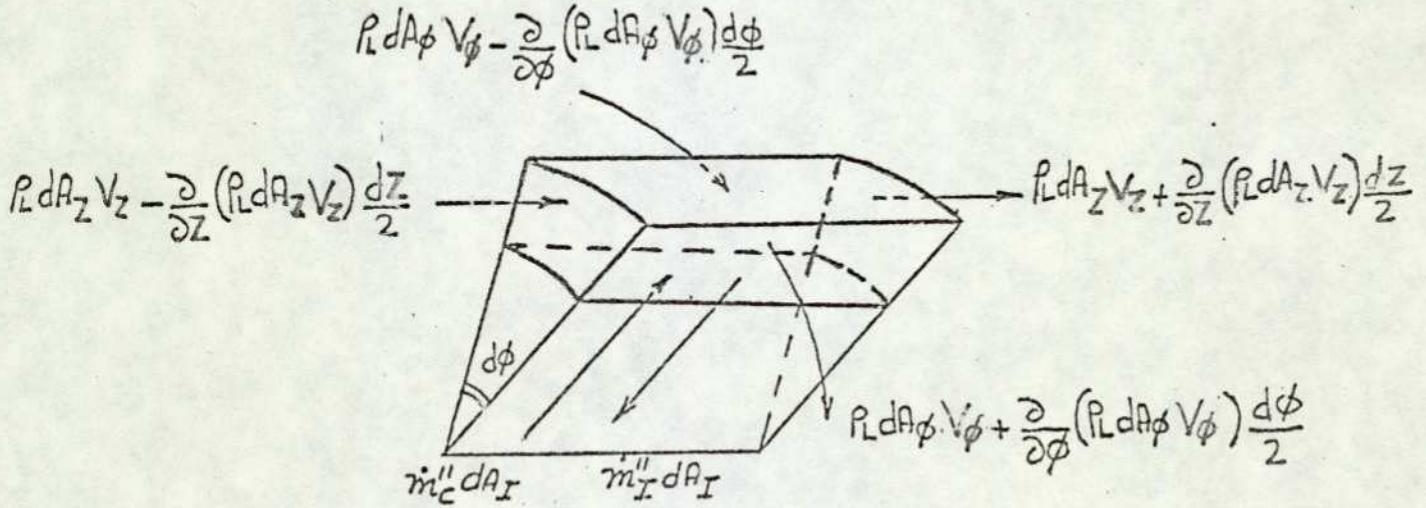

FIG. 56 LIQUID FILM DIFFERENTIAL ELEMENT

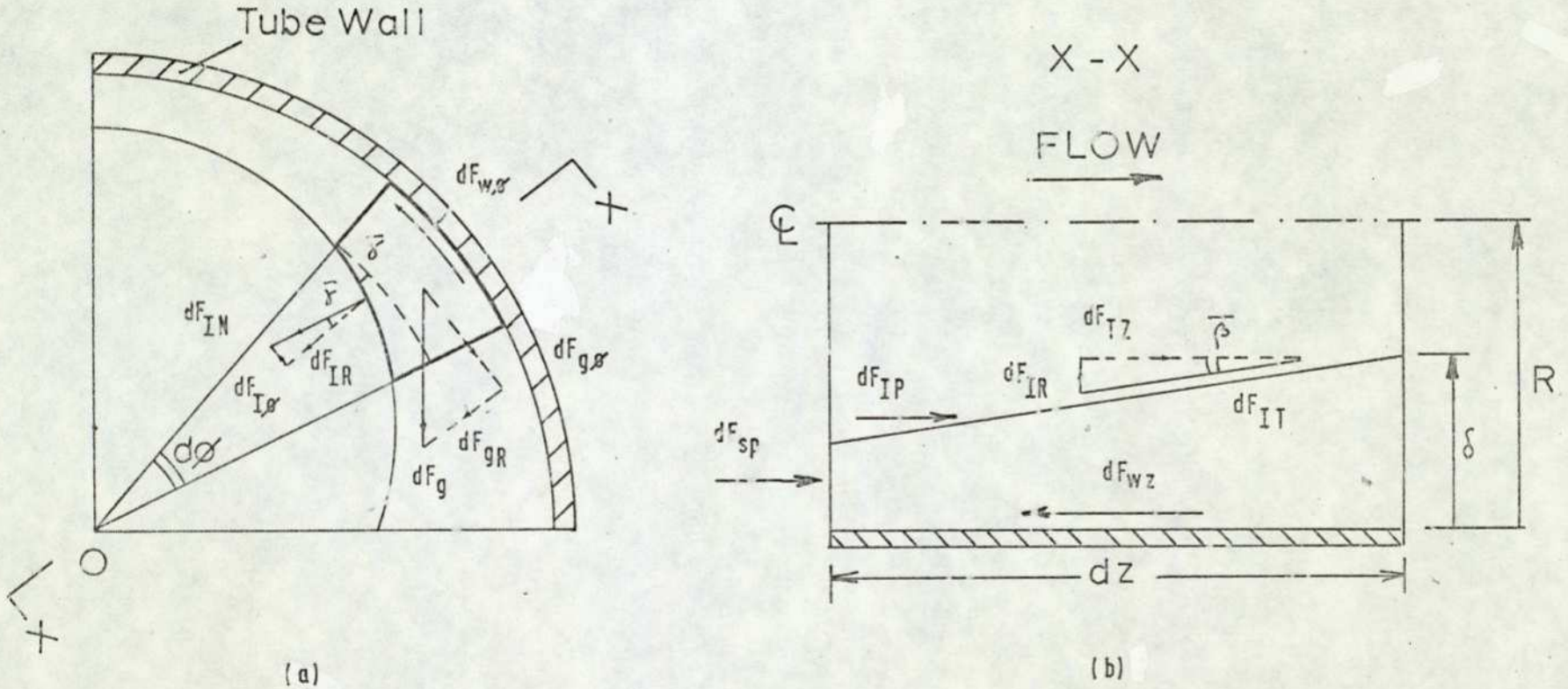

FTG. 57 FORCES ACTING ON THE LIQUID FILM DIFFERENTIAL ELEMENT

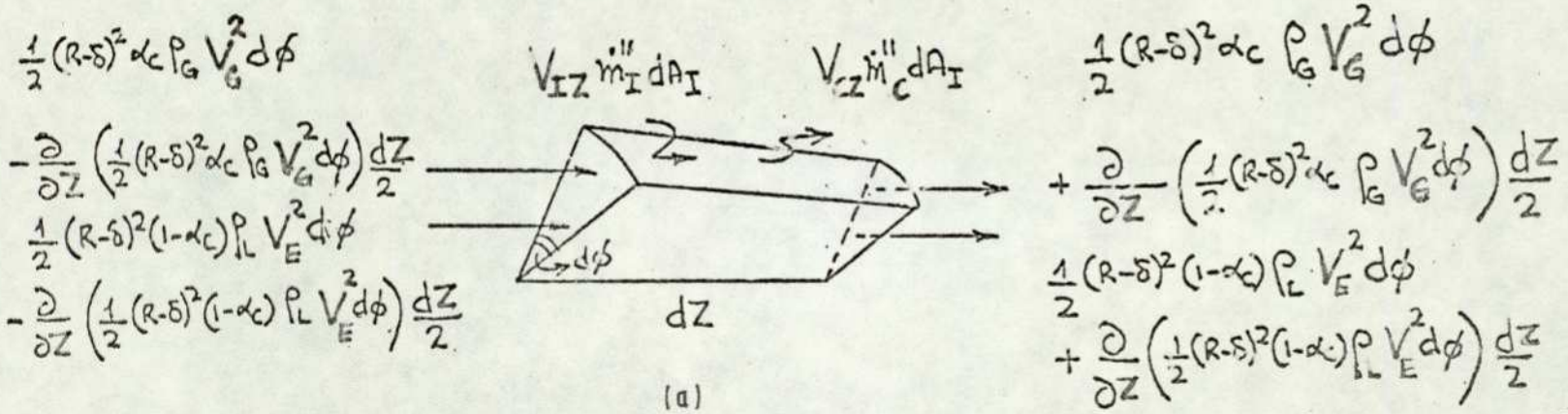

FIG. 58 VAPOUR CORE DIFFERENTIAL ELEMENT

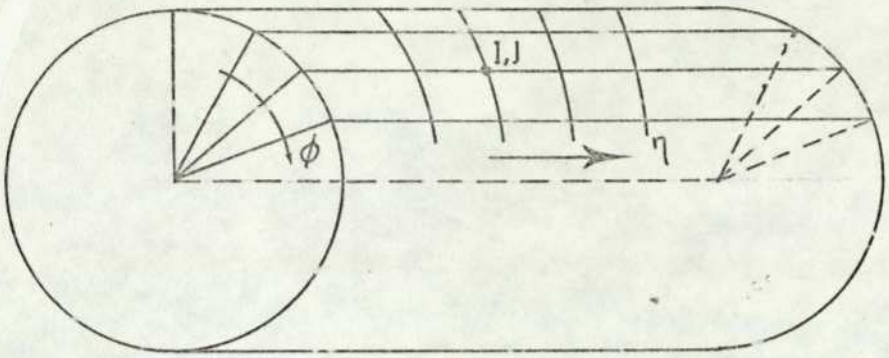

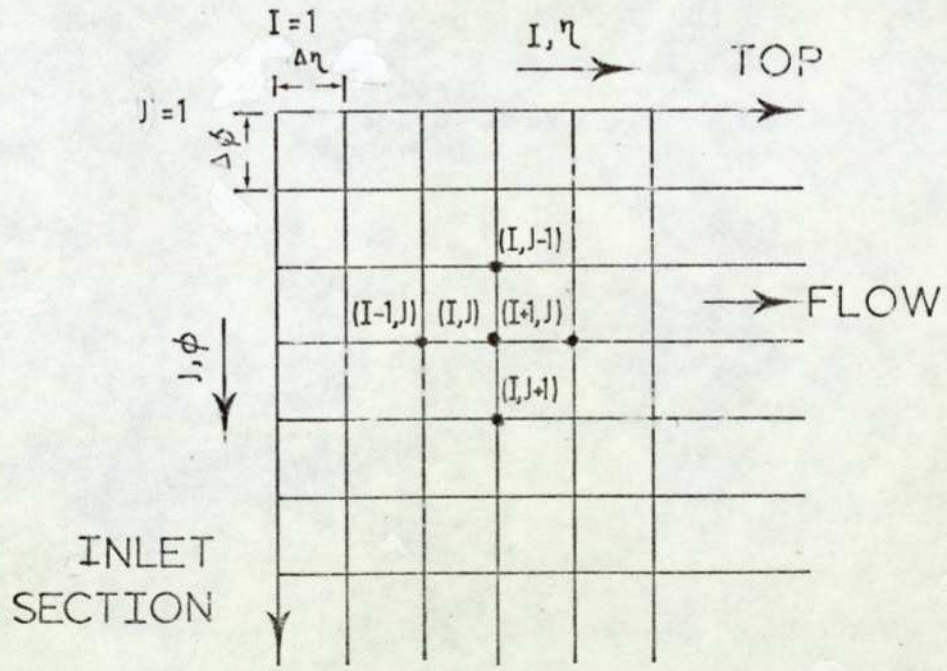

FTG. 59 RECTANGULAR MESH

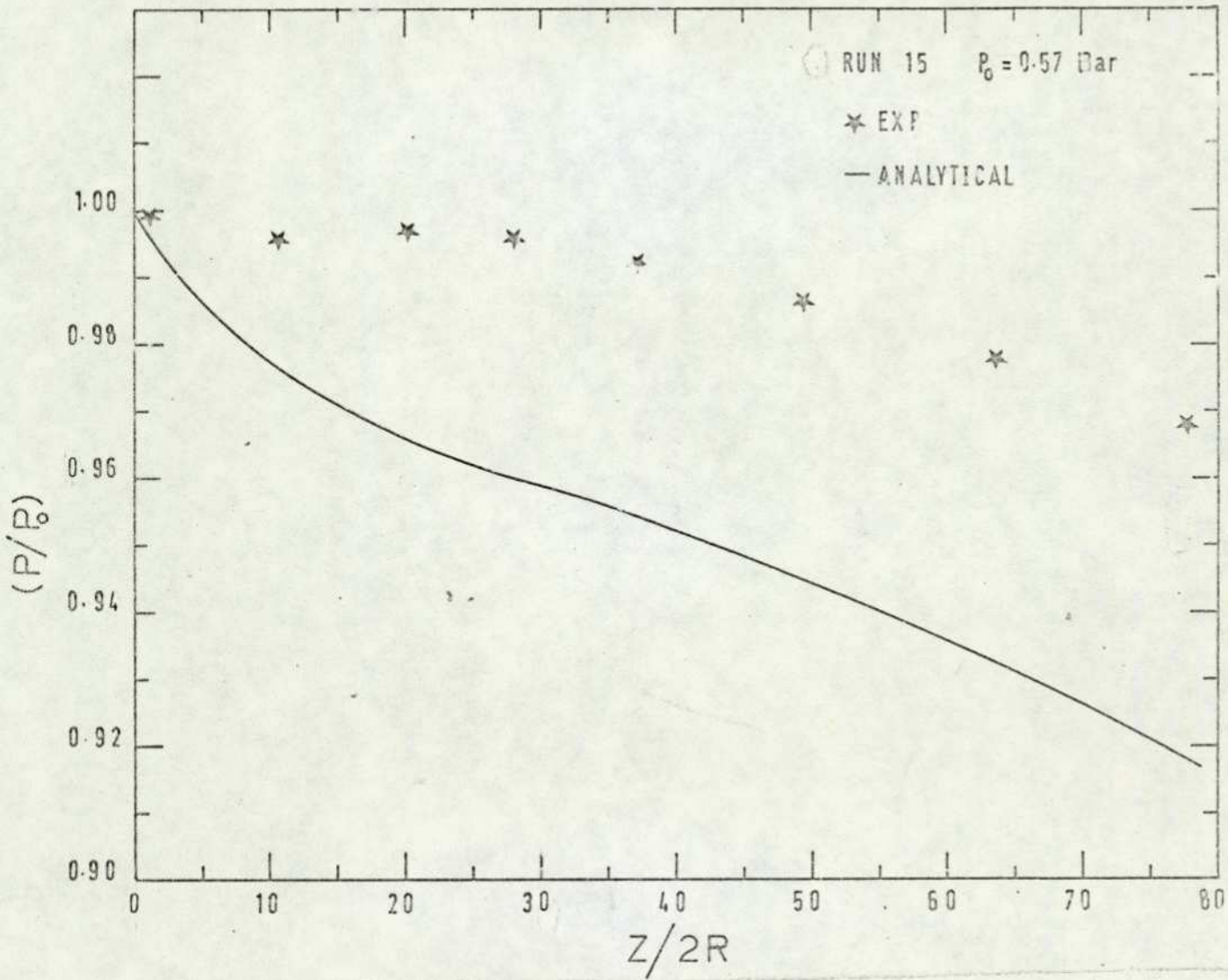

Figure 60 Comparison between the experimental and predicted axial pressure distribution, RUN 15 P_o=0 57 bar (abs)

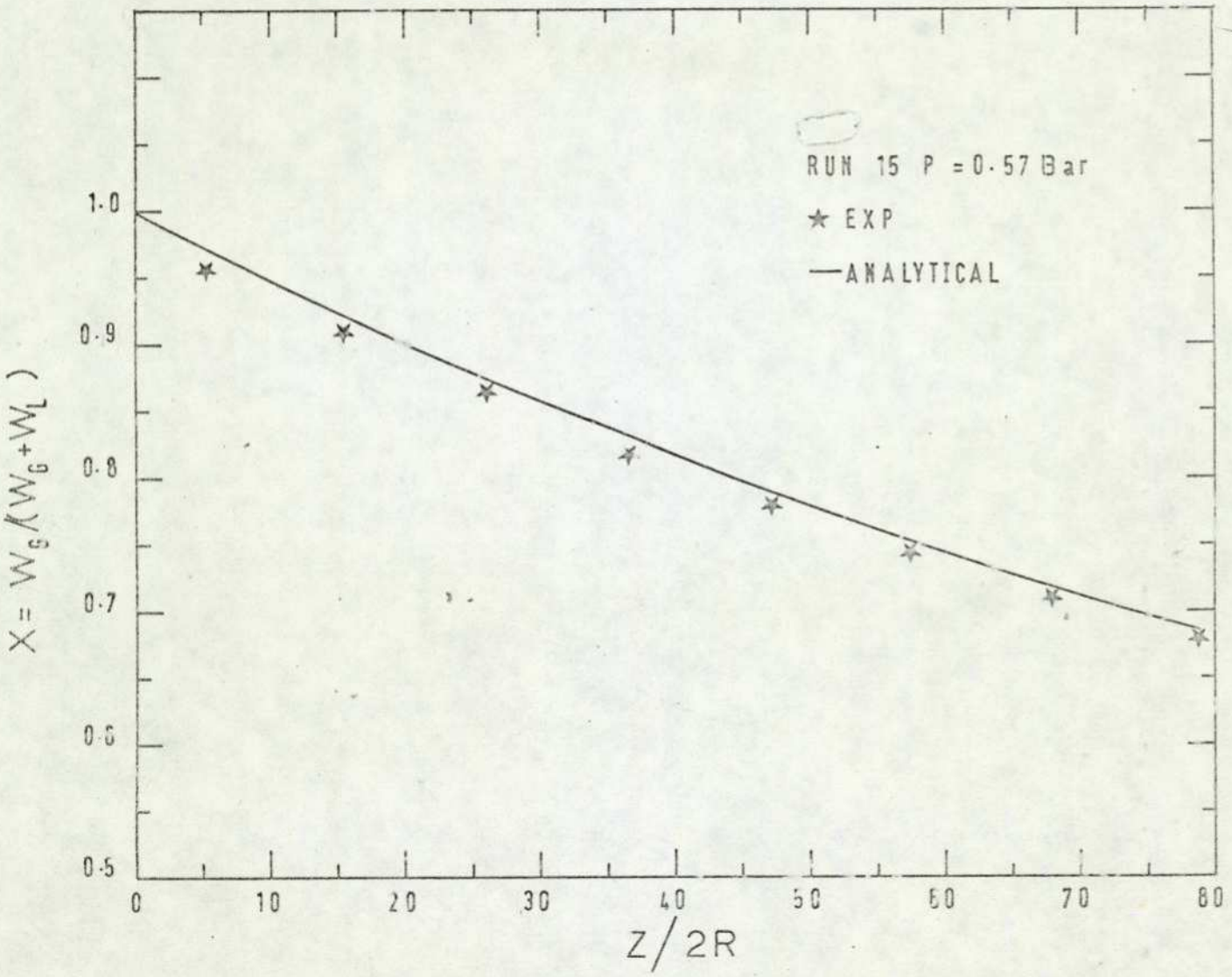

Figure 61 Comparison between the epxerimental and predicted vapour quality, RUN 15, Po = 0.57 bar (abs).

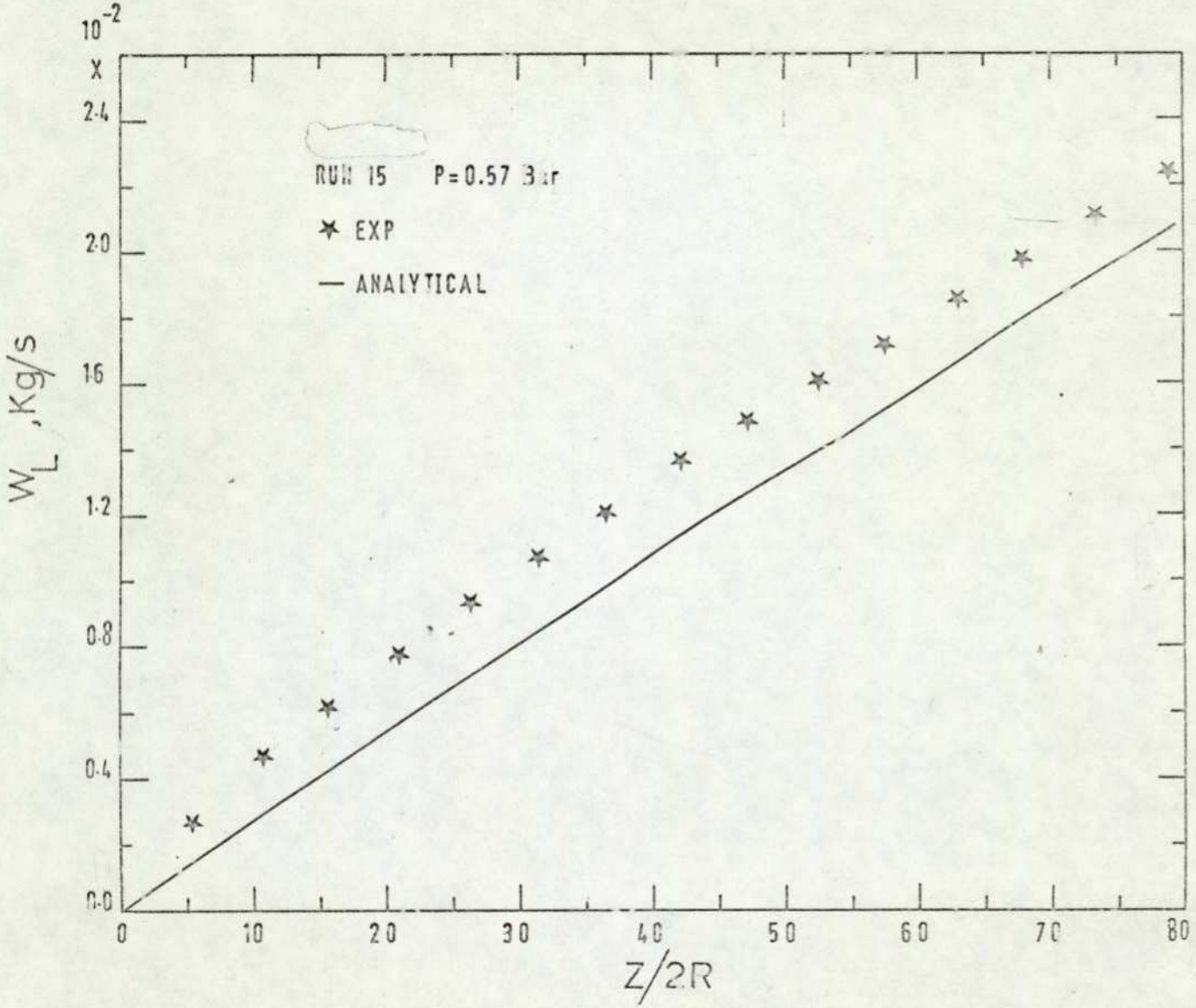

Figure 62 Comparison between the experimental and predicted liquid film flow rate, RUN 15 P_o = 0.57 bar (abs).

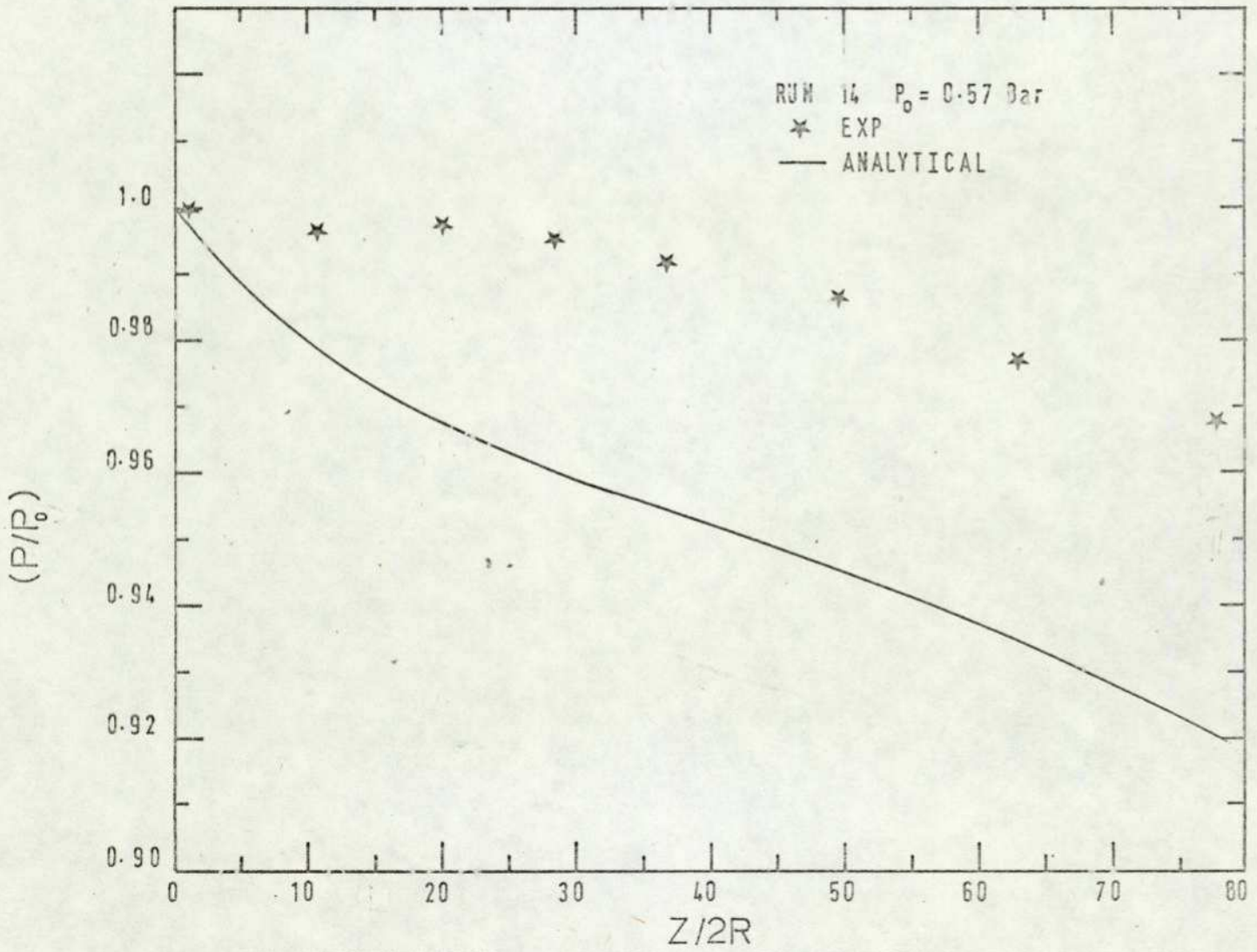

Figure 63 Comparison between the experimental and predicted axial pressure distribution, RUN 14 P_o=0.57 bar (abs).

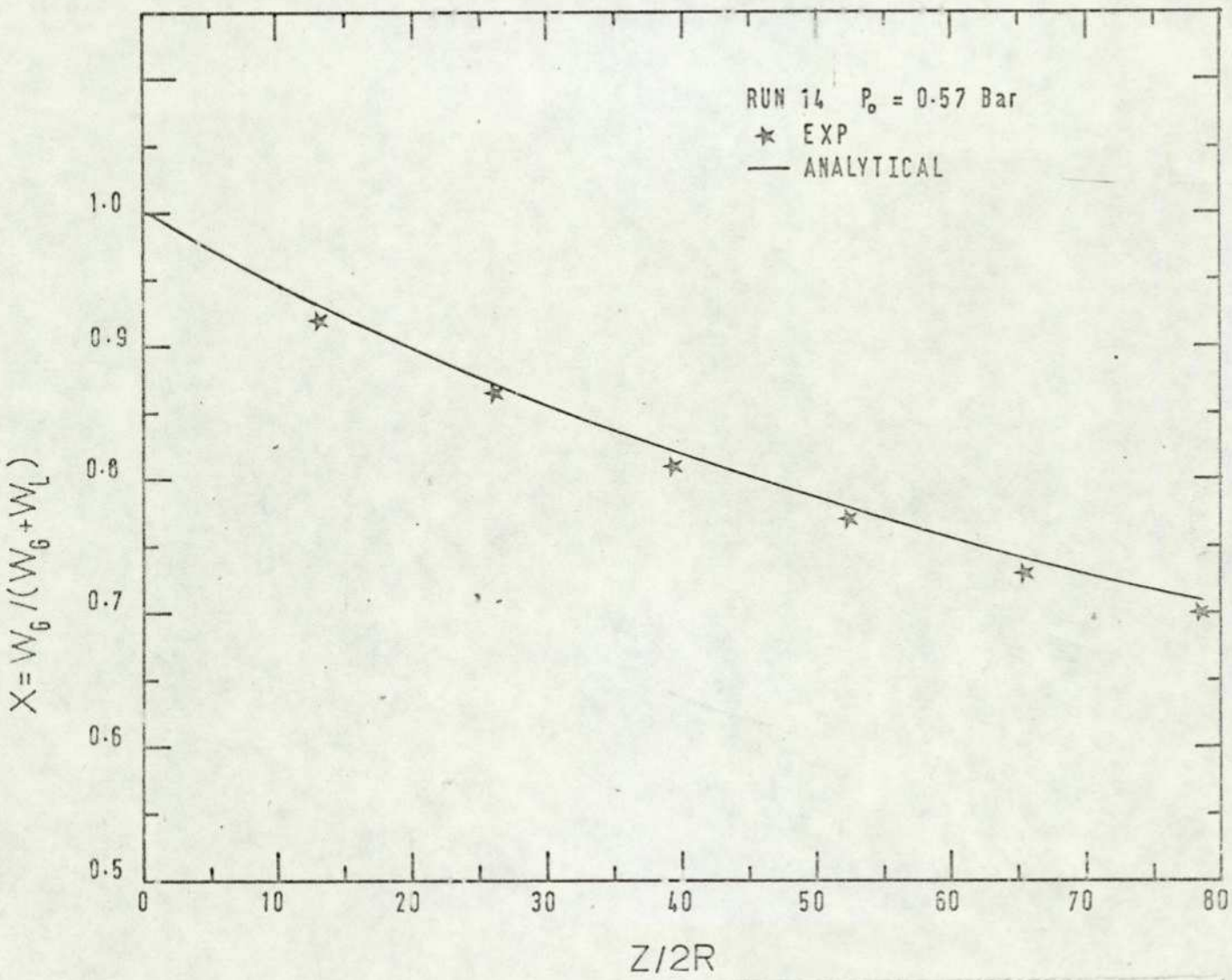

Figure 64 Comparison between the experimental and predicted vapour quality, RUN 14 P_o = 057 bar (abs).

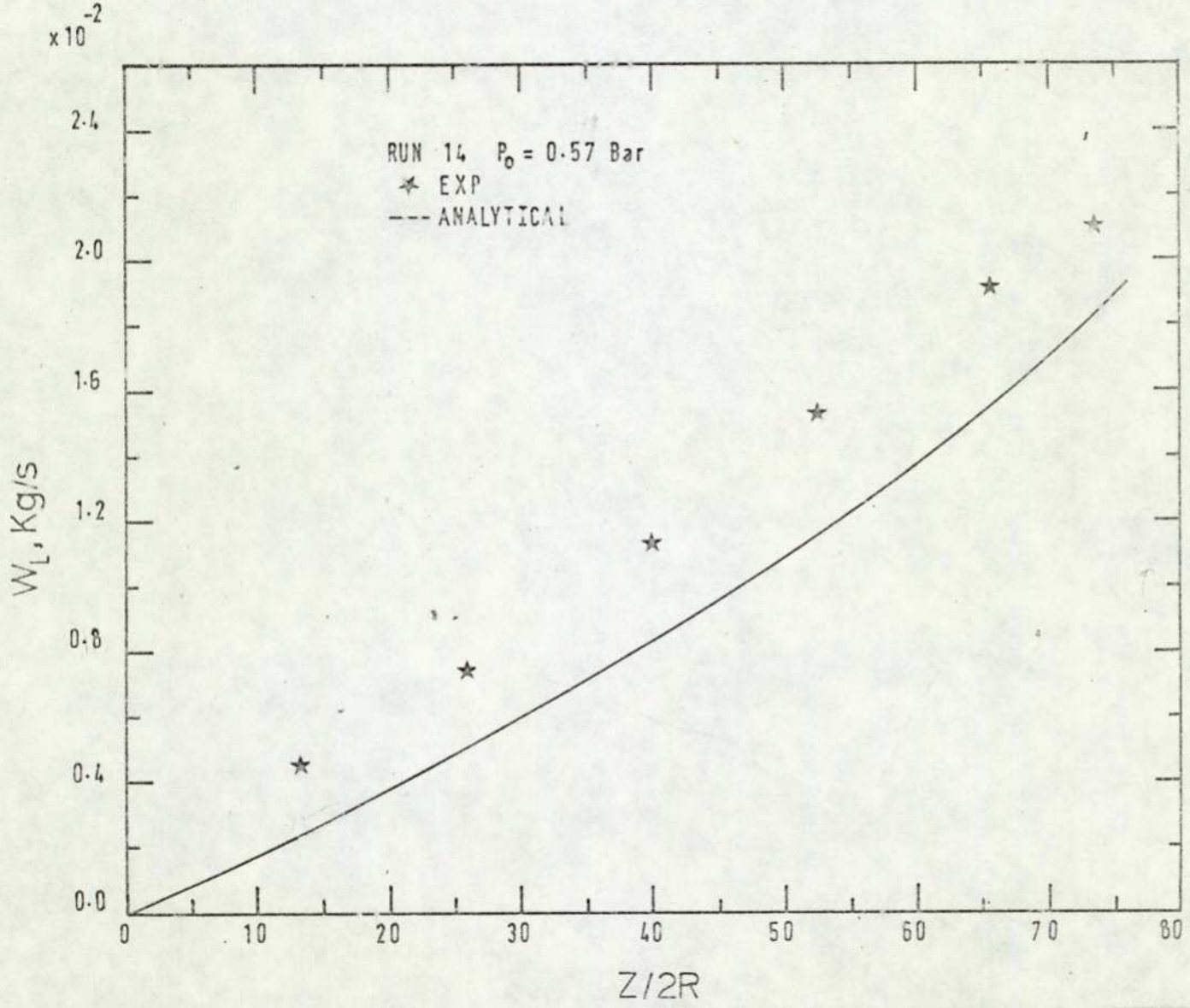

Figure 65 Comparison between the experimental and predicted liquid film flow rate, RUN 14 P_o = 0.57 bar (abs).

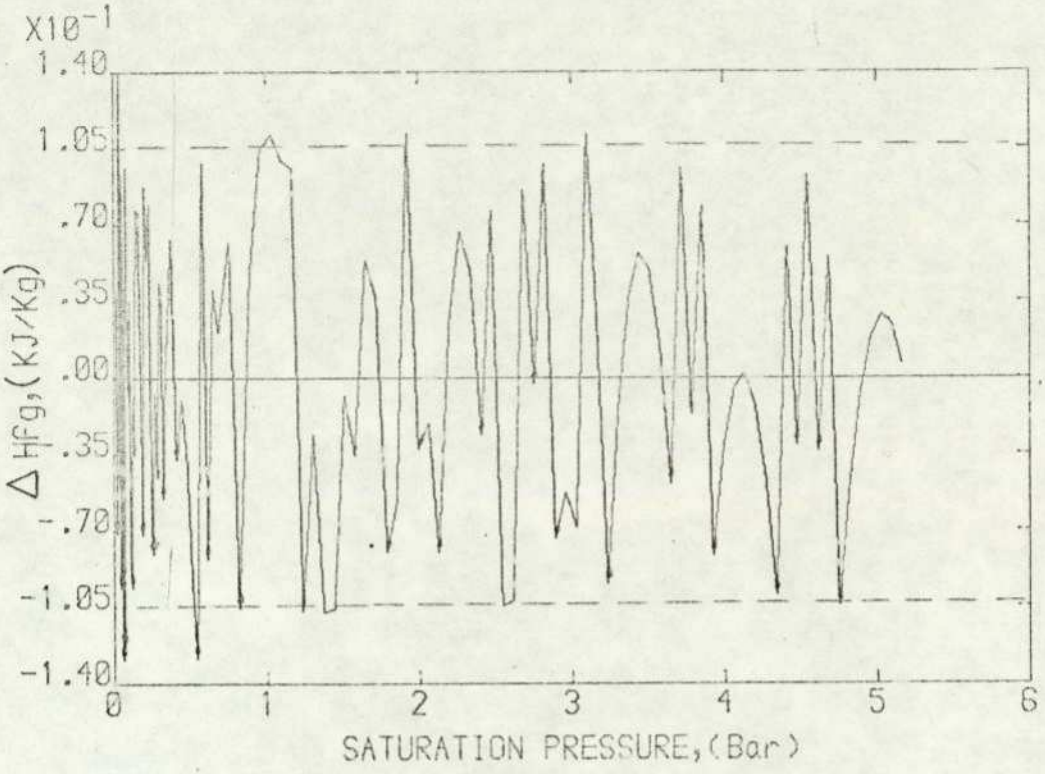

FIG.66 DIFFERENCE BETWEEN CALCULATED AND TABULATED VALUES FOR Hfg

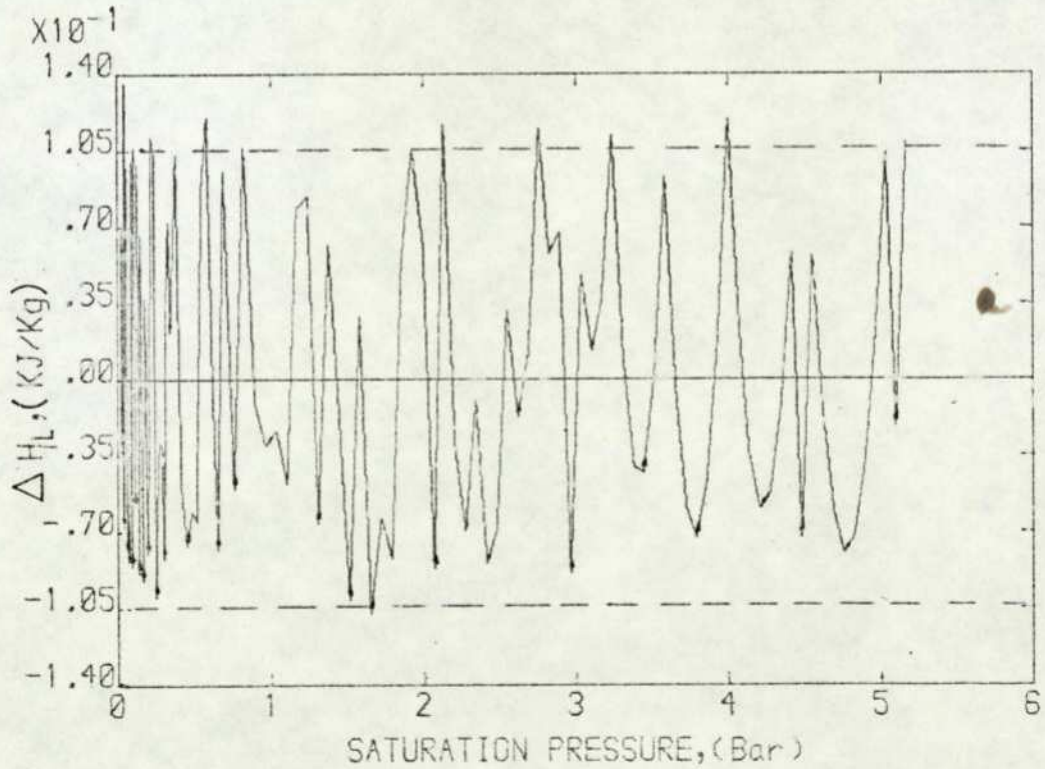

FIG.67 DIFFERENCE BETWEEN CALCULATED AND TABULATED VALUES FOR H_L

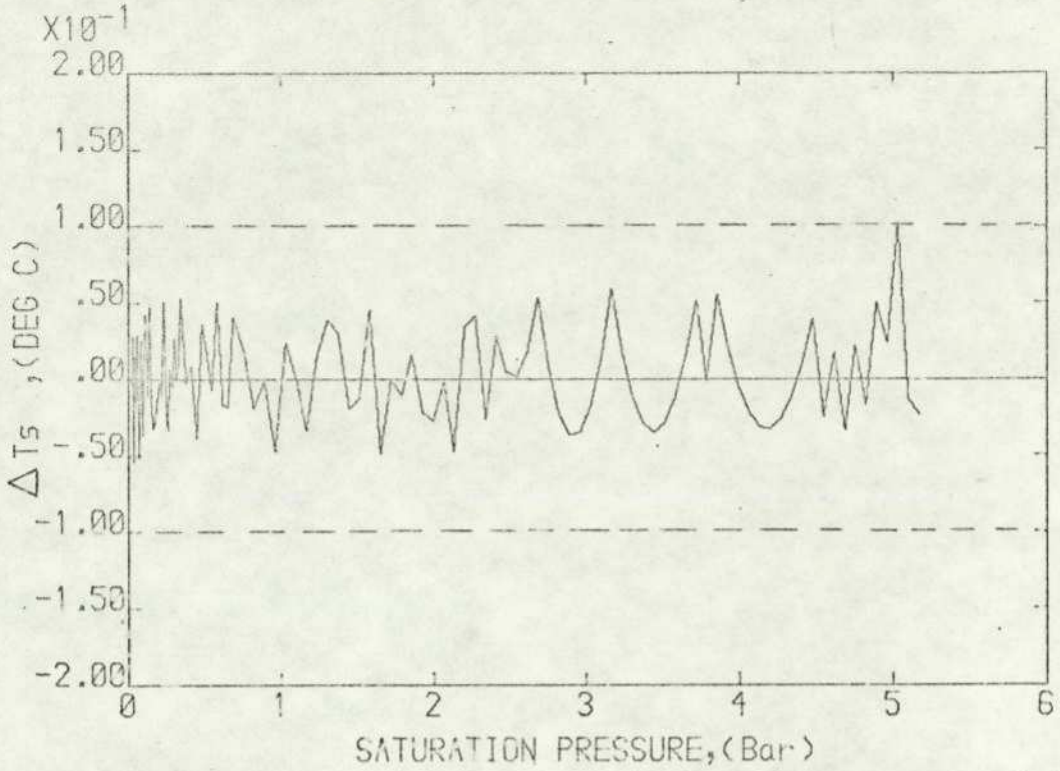

FIG.68 DIFFERENCE BETWEEN CALCULATED AND TABULATED VALUES FOR Ts

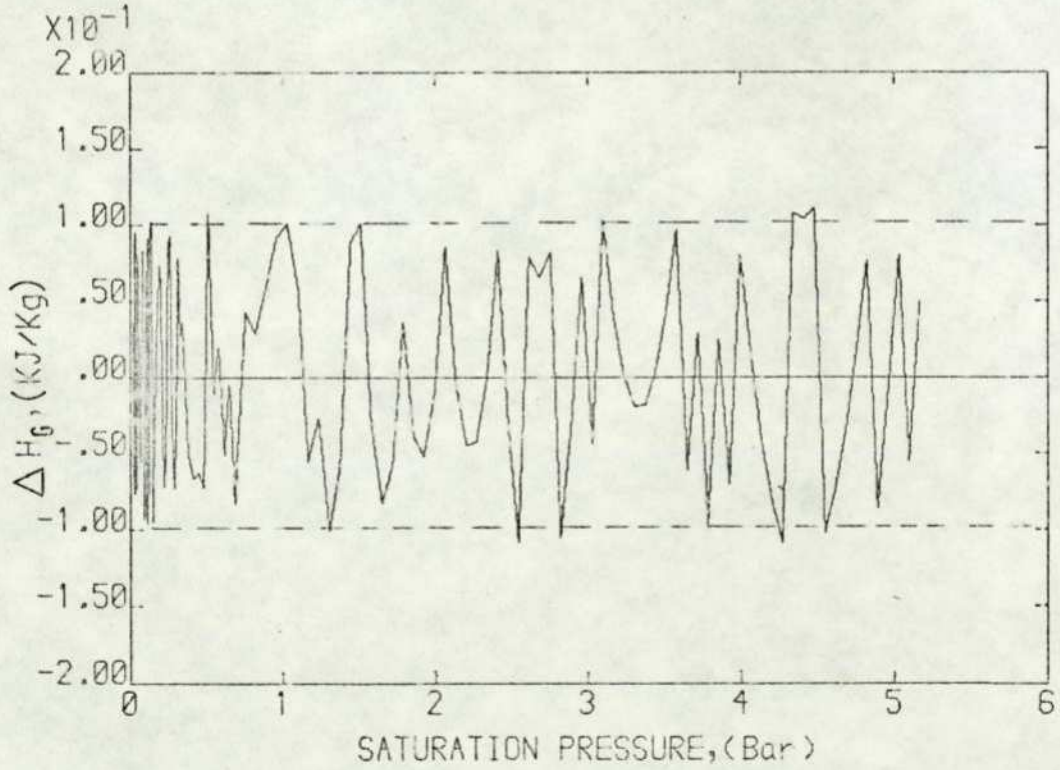

FIG.69 DIFFERENCE BETWEEN CALCULATED AND TABULATED VALUES FOR H_G

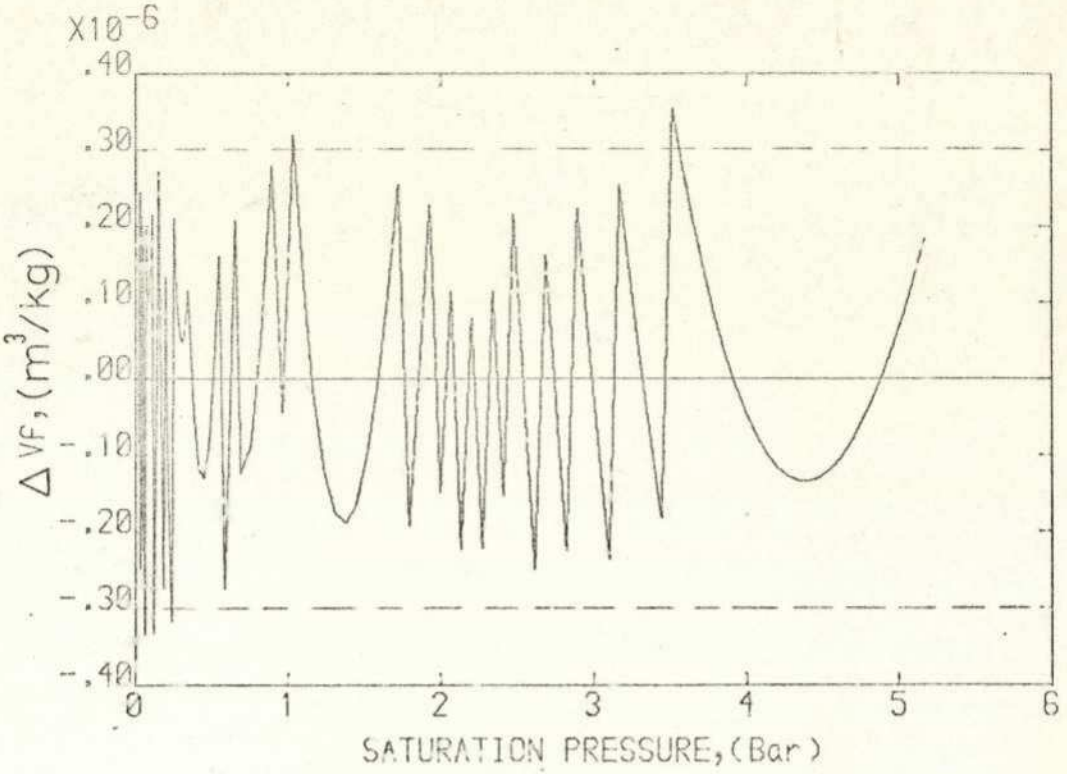

FIG. 70 DIFFERENCE BETWEEN CALCULATED AND TABULATED VALUES FOR VF

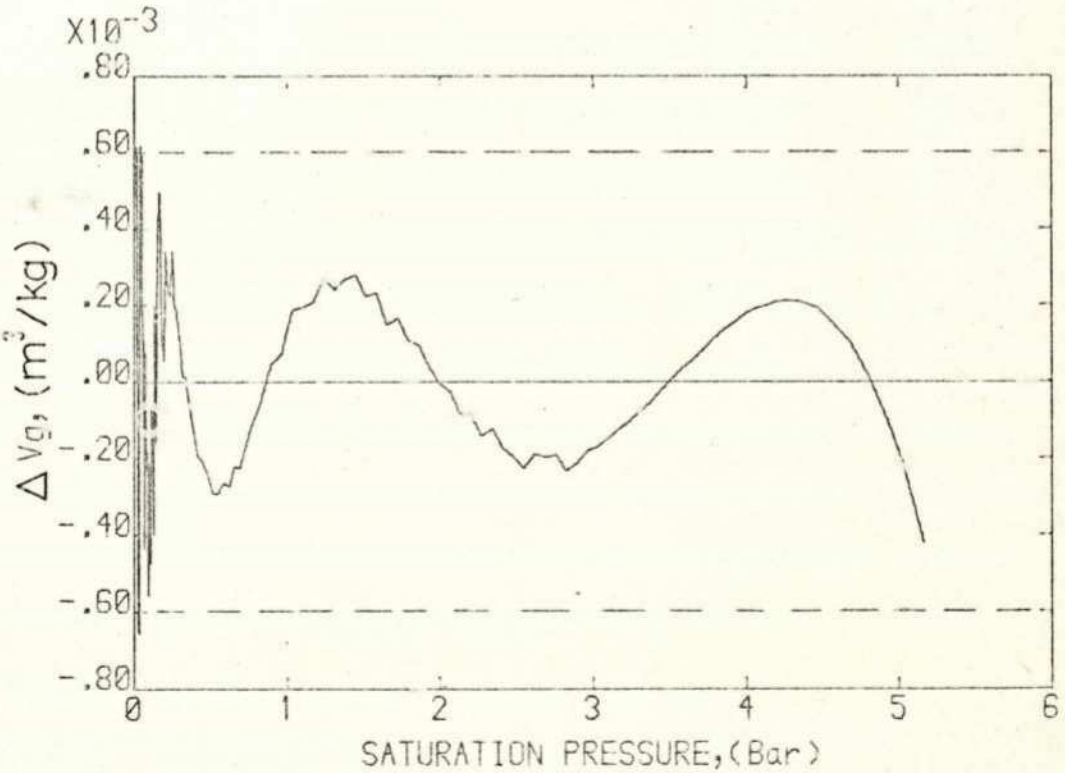

FIG. 71 DIFFERENCE BETWEEN CALCULATED AND TABULATED VALUES FOR Vg